Dysfunction of the Endosomal Na^+/H^+ Exchanger 6 (NHE6) in Cellular Models of Corticobasal Syndrome

Dissertation

der Mathematisch-Naturwissenschaftlichen Fakultät

der Eberhard Karls Universität Tübingen

zur Erlangung des Grades eines

Doktors der Naturwissenschaften

(Dr. rer. nat.)

vorgelegt von

Katharina Stegen

aus Lüneburg

Tübingen

2018

Gedruckt mit Genehmigung der Mathematisch-Naturwissenschaftlichen Fakultät der Eberhard Karls Universität Tübingen.

Tag der mündlichen Qualifikation:	19.05.2020
Dekan:	Prof. Dr. Wolfgang Rosenstiel
1. Berichterstatter:	Prof. Dr. Rejko Krüger
2. Berichterstatter:	Prof. Dr. Tassula Proikas-Cezanne

Erklärung

Ich erkläre hiermit, dass ich die zur Promotion eingereichte Arbeit mit dem Titel:

Dysfunction of the Endosomal Na^+/H^+ Exchanger 6 (NHE6) in Cellular Models of Corticobasal Syndrome

selbständig ohne unzulässige Hilfe Dritter und ohne Benutzung anderer als der angegebenen Hilfsmittel angefertigt habe; die aus fremden Quellen direkt oder indirekt übernommenen Gedanken sind als solche kenntlich gemacht. Ich versichere an Eides statt, dass diese Angaben wahr sind und dass ich nichts verschwiegen habe. Mir ist bekannt, dass die falsche Abgabe einer Versicherung an Eides statt mit einer Freiheitsstrafe bis zu drei Jahren oder mit einer Geldstrafe bestraft wird.

Tübingen, im Feburar 2019

Index

1. Summary

The endosomal-lysosomal system plays an important role for a variety of cellular processes, from receptor and nutrient uptake to protein recycling and organelle degradation. All of these processes depend on a fine tuning of the endosomal pH, regulated by the Na^+/H^+ exchanger 6 (NHE6) of the early endosome which alkalises the endosomal lumen. *SLC9A6*, the gene coding for NHE6, has been found to be mutated in male patients with Christianson syndrome (CS), a form of X-linked mental retardation with ataxia, epilepsy and progressive loss of motor functions. In 2013, Riess and colleagues described a T insertion in exon 12 of the gene, leading to an amino acid exchange, frame shift and premature stop codon (c.1464_1465insT, p. T489YfsX23). The grandmother of the index patient and the grandmother's mother were diagnosed with corticobasal syndrome (CBS), an atypical parkinsonism, where the underlying pathology with aggregated hyperphosphorylated tau in most cases is corticobasal degeneration (CBD). In a targeted screen for *SLC9A6* in CBS and CBD patients, the c.G1703A/p.R568Q variant (rs146263125) was found in two patients from a family with CBS and CBD, respectively. The variant has previously been reported in schizophrenia and X-linked mental retardation but was also found in healthy controls.

In this work, the functional consequences of the T489Yfs mutation and R568Q variant were assessed using fibroblasts from one T489Yfs carrier, cDNA overexpression models and brain samples from the two R568Q patients. Furthermore, an inducible NHE6 knockdown (k.d.) model was generated in M17 neuroblastoma cells in order to delineate the involvement in neurodegeneration, and fibroblasts from the T489Yfs carrier were reprogrammed into induced pluripotent stem cells (iPSCs) that were further differentiated into neuronal precursor cells (NPCs).

Results from T489Yfs fibroblasts showed reduced levels of full-length protein in the patient, and the overexpression model indicated proteasomal removal of the protein and a multimerisation defect of T489Yfs NHE6. While the overexpressed R568Q variant did not cause changes from wildtype (WT) protein in removal or multimerisation, both the T489Yfs mutation and the R568Q variant resulted in

increased protein levels of the chaperone BiP involved in the unfolded protein response, indicating potential misfolding of both proteins.

In the M17 NHE6 k.d. model, markers of the endosomal pathway were misregulated, with endocytosis and late endosomal markers reduced and levels of early and recycling endosomal markers increased.

Investigation of T489Yfs fibroblasts with the pH-sensitive dye LysoTracker revealed a non-significant increase in signal, and perinuclear clustering of LysoTracker-positive vesicles. In the M17 NHE6 k.d. model, there was a significant increase in signal in LysoTracker fluorescence caused by enlarged vesicles that were also increased in number, but not because of a decreased pH in lysosomes.

Overexpression of WT or R568Q NHE6 decreased LysoTracker fluorescence, while overexpression of T489Yfs NHE6 resulted in an increase, indicative of increased acidity in the endosomal-lysosomal system.

In autophagy, LC3-I is lipidated into LC3-II. Levels of both forms of the protein are reduced under baseline conditions and under amino acid starvation in NHE6 k.d. cells, but LC3-II accumulates after lysosomal degradation is inhibited by BafA1 treatment. In fibroblasts, results for LC3 lipidation either showed an increase in LC3-II in T489Yfs fibroblasts compared to controls under baseline, starved and BafA1-treated conditions, or a lack of accumulation after BafA1 treatment, overall indicating reduced autophagic flux.

A loss of NHE6 in M17 neuroblastoma cells led to an increase in the mitochondrial protein TOM22 and in cytosolic oxidative stress, even though there is no significant increase in oxidative damage to proteins.

In M17 cells, k.d. of NHE6 caused accumulation of the hyperphosphorylated tau, a finding similar to that previously described for Christianson syndrome patients and connected to CBS, which is predominantly caused by tau-related pathologies, and CBD, a tauopathy.

Insoluble tau in the brain of a CBD patient carrying the R568Q variant lacked CBD-related posttranslational modifications and might predominantly be the 3-repeat isoform, instead of 4-repeat tau found in other CBD patients.

Despite the phenotype observed in the endosomal-lysosomal system, neither early apoptosis in M17 NHE6 k.d. cells measured by Annexin V binding in untreated cells, nor cell death in T489Yfs fibroblasts measured by LDH release under baseline conditions are significantly elevated. Overexpression of all three NHE6 cDNA

constructs elevated cell death in an LDH release assay compared to a transfection control, but the difference between WT, R568Q and T489Yfs NHE6 was not significant.

Taken together, this work relates a mutation in *SLC9A6*/NHE6 to CBS for the first time and shows that an experimental loss of NHE6 leads to increases in acidification in the endosomal-lysosomal system, impacts several steps of the system including autophagy, and causes accumulation of hyperphosphorylated tau. Together with previous evidence of endosomal-lysosomal dysfunction in neurodegenerative diseases, further research and the development of compounds targeting pH regulation in the endosomal-lysosomal system are therefore a promising path for new therapies against these devastating diseases.

2. Introduction

Age-related neurodegenerative diseases such as Alzheimer's disease (AD) and Parkinson's disease (PD) are becoming increasingly common as the general population ages. These diseases place a high burden both on patients and families and on society as economic costs for care rise. Causative treatments are currently not available for most neurodegenerative diseases as the underlying causes remain not fully understood.

One of the cellular processes thought to be involved in neurodegeneration is the endosomal-lysosomal system because it is crucial for the turnover of dysfunctional organelles and misfolded or aggregated proteins that are found in almost all neurodegenerative diseases. It is equally important for synaptic transmission because of the recycling and movement of vesicles. Involvement of the endosomal-lysosomal system has been shown in common neurodegenerative diseases like AD and PD but has also been linked to rare diseases such as corticobasal syndrome (CBS) and corticobasal degeneration (CBD), where accumulation of the microtubule-binding protein tau can occur, therefore histologically overlapping with another group of neurodegenerative diseases termed tauopathies.

2.1 Corticobasal Syndrome (CBS) and Corticobasal Degeneration (CBD)

Corticobasal syndrome and corticobasal degeneration are rare diseases of the central nervous system (CNS) with an incidence of 1:100,000 per year[1] and a prevalence of ≈6 cases in 100,000 people[2].

CBS and CBD were originally described by Rebeiz et al. in 1968 as one entity under the name corticodentatonigral degeneration with neuronal achromasia[3]. In the paper, the authors reported three patients with progressive asymmetric motor symptoms, an abnormal posture with flexed limbs, tremor and involuntary movements in connection with 'alien limb syndrome', where patients could no longer control the actions of a certain limb and lost proprioception. Autopsies showed a similar pathology for all three cases with pronounced cell loss in the outer three cortical layers and misplaced neurons, 'swollen' cell bodies that could not be stained, and lipid granules in the

deeper layers. They also noted diffuse neuronal and pigmentation loss in the substantia nigra (SN) and gliosis in the highly affected frontoparietal regions and the SN.[3]

Later it was proposed to separate the clinical description of CBS from the pathological findings of CBD, as a number of pathologies were found to cause CBS and CBD, and these resulted in various clinical presentations.[4, 5]

2.1.1 Corticobasal syndrome

The term corticobasal syndrome describes a cluster of symptoms, the most common being levodopa-resistant parkinsonism (tremor, rigidity, bradykinesia, postural instability), limb apraxia, dystonia, myoclonus, cortical sensory loss and alien limb syndrome.[4, 6] Several other symptoms like aphasia/language disturbances and late, but not early dementia have been proposed as well;[1] however, the frequent overlap with other neurodegenerative diseases makes diagnosis difficult.[1, 5, 6]

A number of underlying pathologies have been found to cause CBS. While CBD is the most common one (35–56% of cases),[7-9] AD, progressive supranuclear palsy (PSP), and several forms of frontotemporal lobar degeneration (FTLD)[10, 11] as well as mixed or unspecified degenerative changes can result in the clinical presentation of CBS.[12, 13] There are no specific symptoms that allow for a prediction of the underlying pathology; but a large proportion of them are tauopathies.[14]

The heterogenicity of the pathological findings contributes to the fact that not much is known about the causes of CBS. A number of genes have been implicated in the disease, but not all studies differentiate clearly between CBS and CBD. One study described a mutation in the *MAPT* gene coding for the microtubule-associated protein tau that leads to an amino acid exchange (G389R) in CBS, but the same mutation has also been found in FTDP-17 (Frontotemporal dementia and parkinsonism linked to chromosome 17).[15] Similarly, the *MAPT* haplotype H1 is overrepresented in PSP and CBS cases.[16]

Mutations and a single nucleotide polymorphism (SNP) in the *GRN* gene coding for Progranulin have been reported in CBS,[17-19] and mutations in the same gene are involved in a large percentage of frontotemporal dementia (FTD) cases.[20, 21] Also, the G2019S mutation in leucine-rich repeat kinase 2 (*LRRK2*) that is frequent in familial PD might be a cause for CBS.[22]

2.1.2 Corticobasal degeneration

Corticobasal degeneration describes a pathology that typically occurs in the 6–7th decade of life with a reported mean age of onset of ≈64 years.[6, 23] The mean survival after onset of symptoms is 7–8 years.[6, 23]

CBD is a tauopathy in which mainly hyperphosphorylated insoluble tau[24] with four microtubule binding domains (4R-tau) accumulates.[25] Biochemical analysis showed that insoluble tau in CBD differs from that found in AD, PSP or Pick's disease (PiD) in banding patterns when analysed by Western blotting, influenced by different isoforms and posttranslational modifications and proteolytic cleavage.[25, 26] Also, twisted filaments in CBD can be distinguished from those observed in AD on electron microscopy pictures by a longer periodicity and broader width.[27]

CBD is marked by asymmetric atrophy of parietal and, in part, frontal cerebral areas[28] as well as neuronal loss in SN and globus pallidus, and astrocytosis.[27]

Tau positive lesions are one of the histopathological hallmarks with neuronal inclusions (Fig. 1A) in the cortex, basal ganglia (namely corpus striatum, globus pallidus, SN, and subthalamic nucleus), thalamus, basal nucleus of Meynert and locus coeruleus. Another finding are tau-positive neurofibrillary inclusions named corticobasal bodies (Fig. 1B and 1C). Furthermore, threads (Fig. 1D) and coiled bodies (Fig. 1E) can be observed in both white and grey matter, especially the most affected regions in cortex, basal ganglia, thalamus, brainstem and cerebellum. Astrocytic plaques are a distinguishing hallmark in CBD (Fig. 1F), while the presence of ballooned (Fig. 1G and 1H) or achromatic neurons found in the cortex and sometimes the basal ganglia has a high diagnostic value.[27]

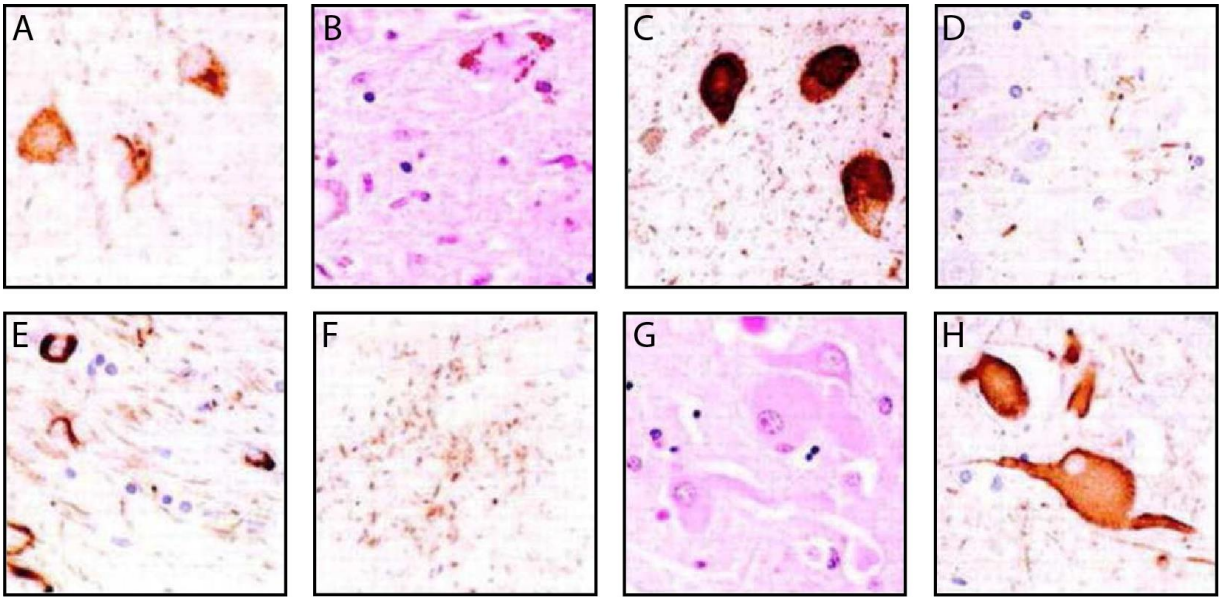

Fig. 1: Pathological findings in corticobasal degeneration. **A**: Tau-positive neuronal inclusions (cortex) **B**: Neurofibrillary inclusions (corticobasal bodies) in substantia nigra (H&E staining). **C**: Corticobasal bodies in substantia nigra (tau staining). **D**: Tau-positive thread-like structures in pons **E**: Thread-like processes and coiled bodies in white matter (tau staining). **F**: Astrocytic plaques in the cortex (tau staining). **G**: Ballooned neurons in cortex (H&E staining). **H**: Ballooned neurons in cortex (neurofilament staining). Modified from Dickson, D. W., et al. (2002). "Office of Rare Diseases neuropathologic criteria for corticobasal degeneration." J Neuropathol Exp Neurol 61(11): 935-946.[27]

While diagnosis of CBD during life is difficult,[7] retrospective studies of autopsy-confirmed cases allow the definition of common clinical presentations. Early symptoms can vary, with half of the patients presenting with motor dysfunction, mostly limb rigidity, bradykinesia, postural instability, falls and abnormal gait.[6] Tremor is only present in 20% of the cases at first presentation.[23] Early cortical symptoms include cognitive impairment, behavioural changes, and aphasia.[6] During the course of the disease, motor findings become more common, with abnormal gait, postural instability, bradykinesia and limb rigidity found in 70-85% of patients.[23] Similarly, ≈70% of patients have cognitive impairment at the end of their life and about half present with behavioural changes, limb apraxia, aphasia and depression. Cortical sensory loss and alien limb syndrome affect between 25% and 30% of patients.[7, 23]
Based on these symptoms, 25-56% of cases are diagnosed with CBS, but frontal behavioural-spatial syndrome, progressive nonfluent aphasia,[12] FTD[29] and PSP[1, 30] are also common diagnoses.
Like in CBS, underlying causes of CBD are largely unknown, but some genetic connection to *MAPT* exists. Some mutations in *MAPT* have been linked to CBD,[29]

including P301S[28] and N410H,[31] but the P301S mutation was found in a case of FTLD as well;[28] also, the *MAPT* H1 haplotype is overrepresented in CBD.[32]

A genome-wide association study (GWAS) in CBD cases identified genetic variants in the *MAPT* gene and in a regulatory region for *MAPT*. The study further connected the pathology to variants in *MOBP* (myelin-associated oligodendrocyte basic protein) involved in myelination, *KIF13B* (kinesin family member 13B) important for vesicle transport on microtubules (MT) and *SOS1* (Son of sevenless homolog 1), a guanine nucleotide exchange factor important for intracellular signaling[31]. However, GWAS studies on rare diseases are often difficult to interpret because of the low number of cases.

Taken together, the etiology of both CBS and CBD remains unsolved, even though there is evidence for an involvement of the microtubule-associated protein tau.

2.2 The microtubule-associated protein tau

Tau was first isolated by Weingarten in 1975 as a factor necessary for the assembly of the α-/β-tubulin dimer into rings[33] and subsequently MTs. Later, its involvement in MT elongation was shown.[34]

Tau is alternatively spliced, with six isoforms found in the brain[35] and a 'big tau' isoform that contains an additional 300 amino acids expressed exclusively in the peripheral nervous system.[36]

The *MAPT* gene on chromosome 17 coding for tau consists of 16 exons.[35] Exon 2 and 3 are alternatively spliced, giving rise to tau that contains either none (0N), one (1N containing exon 2) or two (2N containing exons 2 and 3) N-terminal inserts.[37] Furthermore, alternative splicing of exon 10 leads to three or four repeats of the MT-binding domain (3R and 4R), with the second repeat being included or spliced out.[38] The majority (54%) of tau in the brain contains one insert (3R1N and 4R1N), while 2N tau (3R2N and 4R2N) is the least abundant (9%).[39] The majority of pathological tau mutations is found in the repeat region (see Fig. 2).

3R tau binds MTs less strongly than 4R tau[39] and at different sites,[40] leading to different effects on velocity and number of kinesin motor proteins transporting cargo along the MTs.[41] Tau expression is developmentally regulated by an upregulation

together with tubulin and a shift to higher-molecular weight isoforms and axonal localisation during neuronal maturation.[42, 43]

Because of a large number of polar amino acids residues, tau is a mostly hydrophilic protein and has little secondary structure, leading to a highly dynamic conformation.[44, 45] When bound to MTs, the N-terminal (projection domain) containing the first 150 amino acids extends away from the MTs,[46] influencing the distance to neighbouring MTs and other cellular components.[47] Furthermore, it is involved in interactions with the plasma membrane (PM) and dynactin, thereby mediating dynactin-dynein interaction and dynein-dependent transport.[48]

The C-terminal repeat domain binds to MTs and is important for MT assembly, hence it is also called 'assembly domain'.[49]

Apart from the different isoforms, tau function is also influenced by several posttranslational modifications.

2.2.1 Posttranslational modifications of tau

A large number of posttranslational modifications of tau, often in a pathological setting, have been reported. Because hyperphosphorylated tau accumulates in a number of diseases, phosphorylation (and dephosphorylation) of tau have been closely studied. Like isoform expression, phosphorylation of tau is developmentally regulated, with phosphorylation decreasing over time.[50] A high level of phosphorylation leads to self-assembly of the protein, while the MT-binding form is more dephosphorylated.[51, 52]

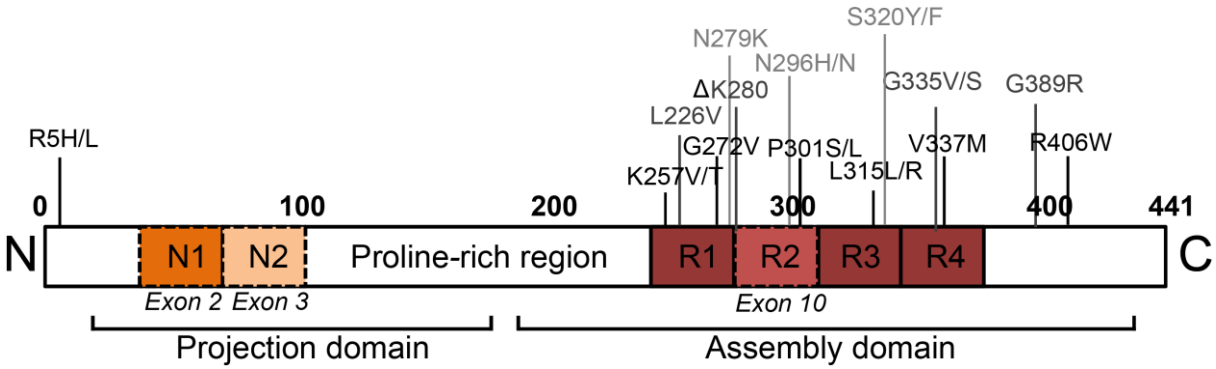

Fig. 2: Protein structure of Tau with the position of several mutations found in tauopathies. Exon 2 and exon 3 are alternatively spliced, with isoforms containing either no N-terminal insert, inserts N1, or inserts N1 and N2 in the projection domain. Exon 10 gives rise to the microtubule-binding region repeat R2 for 3R or 4R tau in the assembly domain. In between is a proline-rich region that allows for a bended conformation, where N- and C-terminus associate in a "paperclip" structure. Almost all pathological mutations are found in the repeat region. Adapted from: Gendron, T. F. and L. Petrucelli (2009). "The role of tau in neurodegeneration." Mol Neurodegener **4**: 13.[389]

Several kinases have been shown to phosphorylate tau. Phosphorylation by the kinases Glycogen synthase kinase 3 beta (GSK3β)[53] and Cyclin-dependent kinase 5 (Cdk5)[54] were shown to play an important part in the pathological phosphorylation of tau, even though GSK3β seems to have only a mild effect on hyperphosphorylated tau accumulation in the form of paired helical filaments (PHFs).[55] A similar effect was observed for mitogen-activated protein kinases (MAPKs)[55] that are activated by various stressors, including oxidative stress.[56] Phosphatases acting on tau include the protein phosphatases 2 A, B and C (PP2A, PP2B, PP2C), with PP2A being the dominant form for dephosphorylation of tau.[57]

Another posttranslational modification is acetylation by p300 acetyltransferase and CREB-binding protein (CBP)[58, 59], and deacetylation mediated by Sirtuin 1[60] and histone-deactylase 6 (HDAC6)[58]. Acetylation of tau seems to play a role in autophagy-mediated removal of tau; in addition, tau can undergo auto-acetylation mediated by cysteines in the second (not present in the 3R form) and third repeat domain, which enhances autophagic clearance.[61]

Other posttranslational modifications include proteolytic cleavage by caspases[62, 63] and calpains[64], and glycosylation, which in turn influences phosphorylation.[65, 66]

2.2.2 Tauopathies

Tauopathies are neurodegenerative diseases characterised by an increase in tau levels, abnormal posttranslational modifications (mainly hyperphosphorylation, but also truncations or acetylation), and tau aggregation (for a review on tauopathies, see e.g. Williams, 2006[67]). In some, but not all tauopathies, the 4R:3R tau ratio is altered. In healthy brains and AD, the ratio of 4R:3R is 1:1, while predominantly 4R tau accumulates for example in CBD and PSP; PiD, on the other hand, is marked by an excess of 3R tau[68].

Hyperphosphorylation of tau and subsequent mislocalisation of the protein from axons to the somatodendritic compartment occur early in disease[69, 70], and phospho-tau is ≈8-fold increased in brains[71] and cerebrospinal fluid (CSF)[72] from AD patients, while the levels of messenger RNA (mRNA) are comparable to those of healthy individuals[73], suggesting a block in removal.

So far, over 20 different tauopathies have been identified, with AD, frontotemporal lobar dementia and parkinsonism linked to chromosome 17 (FTDP-17), PiD, PSP

and CBD being the most prominent.[67] Furthermore, GWAS have identified variants in *MAPT* repeatedly as a risk factor for PD[74, 75] and several mutations were identified in patients with CBD,[28] FTDP-17[76-78] and PSP.[79]

In AD, 95% of total tau is found in neuropil threads and dystrophic neurites in the form of neurofibrillary tangles (NFTs) that consist either of PHFs or straight filaments,[80] and cognitive impairment and disease progression depend on NFT number.[81] Dysfunction of tau leads to defects in axonal transport, which impairs synapse function and subsequently causes neuronal cell death.[82, 83] However, tau pathology can be apparent many years before the onset of symptoms,[84] and synapse loss might precede NFT formation.[85]

Even though accumulated tau is predominantly found in neurons, tau-positive oligodendrocytes and astrocytes appear in motor neuron disease and FTD (also called globular glial tauopathies because of the globular form of tau inclusions; Fig. 3A),[86] and differences in the tau pathology of astrocytes are of high diagnostic value in CBD (astrocytic plaques, Fig. 3B),[27, 87] PiD (ramified astrocytes, Fig. 3C) and PSP (tufted astrocytes Fig. 3D)[88]. Also, the age-dependent, pathological accumulation of phospho-tau in astrocytes, named aging-related tau astrogliopathy (ARTAG), has been recently described. The two main findings in ARTAG are thorn-shaped astrocytes (TSA, Fig. 3E) and granular or fuzzy astrocytes (GFA, Fig. 3F), which also include bushy astrocytes found in a tauopathy called argyrophilic grain disease (AGD)[89].

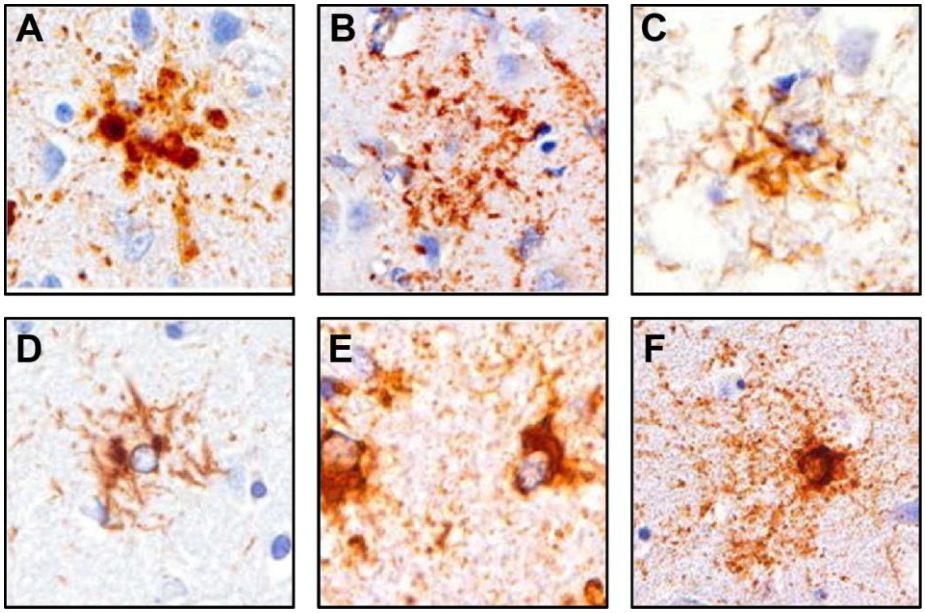

Fig. 3: Astrocytic pathology in tauopathies: **A**: Globular astroglial inclusions (globular glial tauopathies). **B**: Astrocytic plaques (CBD) **C**: Ramified astrocytes (PiD) **D**: Tufted astrocytes (PSP) **E**: Thorn-shaped astrocytes (ARTAG), **F**: Granular/fuzzy astrocytes (ARTAG), Modified from: Kovacs, G. G., et al. (2016). "Aging-related tau astrogliopathy (ARTAG): harmonized evaluation strategy." Acta Neuropathol **131**(1): 87-102.[89]

While tau accumulates in all of these diseases, there are differences in pathologies regarding the pattern of neuronal or glial pathology. Mutations can lead to a shift in 4R:3R tau ratio[90] or affect phosphorylation,[91] giving a hint for why different mutations in the same gene might give rise to different patterns of tau aggregation.

2.2.3 Dysfunctions of tau processing in disease

2.2.3.1 Tau aggregation

Tau aggregation can have a severe impact on cells, especially neurons. Overexpression of tau in rat hippocampal neurons *in vitro* and subsequent missorting of the protein into dendritic spines causes a decrease in synaptic proteins and a decline in the number of spines, followed by neurite disintegration and cell death.[92]

Cys322 is crucial for dimerisation of tau molecules because it allows for covalent binding via a disulfide bridge.[93] These dimers serve as template for fibril formation as other tau mono- and dimers bind to it, and oligomerisation from there continues in a time- and dose-dependent manner.[94] With the addition of further molecules, oligomers develop into protomers which then in turn can form fibrils in the presence of a polyanionic cofactor like heparin.[95] The core of these tau aggregates usually

contains three repeats, while the rest of the protein forms a ’fuzzy coat’ that remains unaggregated.[96]

While fibrils contain hyperphosphorylated tau, abnormal phosphorylation of tau does not result in a faster aggregation of the protein.[97] Rather, it seems as if detachment of tau from MTs leads to an accumulation of free tau, as the interaction site for both polyanion binding and tau dimerisation overlaps with that necessary for MT-binding.[44, 98]

Aggregation of tau is influenced by a number of factors that might give rise to the different phenotypes observed in tauopathies. This includes mutations, isoform balance and posttranslational modifications.

2.2.3.2 Pathologic posttranslational modifications of tau

The best studied posttranslational modification of pathological tau is hyperphosphorylation, which precedes aggregation.[99] Hyperphosphorylation can simply be caused by upregulation or overactivation of kinases,[100] or downregulation of phosphatases.[101] Also, mutations that change binding sites and motifs for (de)phosphorylation,[91] or aberrant signaling due to oxidative stress[102] can lead to abnormal phosphorylation of tau.

Both loss-of-function and gain-of-function mechanisms have been proposed to result from tau hyperphosphorylation. Detachment of tau reduces MT stability,[103] and conversely, pathologically phosphorylated tau can lead to defects in cellular transport and synaptic transmission;[104] furthermore, it changes the interaction of tau with other proteins in signalling pathways.[105]

Hyperphosphorylation of tau can also impact the removal of the protein, as phosphorylation prevents recognition by the CHIP-HSP90 complex needed for proteasomal degradation.[106] Experiments with tau modified to mimic phosphorylated forms showed that in contrast to the preferential clearance of wildtype (WT) tau by the ubiquitin-proteasome system (UPS), phospho-tau is degraded by autophagy.[107]

Another major modification of tau involved in neurodegeneration is N- and C-terminal proteolytic cleavage, as cleaved tau is found in insoluble tau fractions of PSP, CBD and FTLD cases.[26] While caspase-cleavage leads to an increase in aggregation and happens early in disease,[63, 108] calpain-cleavage reduces it.[64] Truncation seems to be connected to misfolding and accumulation of hyperphosphorylated tau,[109] and phosphorylation of tau by PKA changes calpain-cleavage of the protein.[110]

Another class of proteases involved in tau cleavage are cathepsins. Cathepsins are pH-sensitive hydrolases that are usually active in the late endosome and lysosome (see also below), and cathepsin D is involved in proteolysis of tau. Increased phosphorylation of tau accelerates cathepsin D-mediated cleavage and degradation under physical conditions, while incomplete cleavage causes aggregation.[111] Even though most active at a low pH, extralysosomal activity of cathepsin D leading to a 29kDa fragment of tau has been described,[112] while an incomplete translocation of tau across the lysosomal membrane in chaperone-mediated autophagy (CMA) caused by lysosomal disturbances might also lead to pathologic truncations.[113]

One of the causes of abnormal modifications of tau is oxidative stress. Oxidative stress leads to the formation of intermolecular disulfide bridges that changes tau conformation from an unfolded to an irreversibly folded state.[93]

Ubiquitination of tau plays an important role in tau removal, and knockout of *CHIP* (C-terminus of HSC70-interacting protein), a tau ubiquitin ligase involved in the UPS, leads to accumulation, but not aggregation of hyperphosphorylated, caspase-cleaved tau.[114] This indicates that phosphorylation and cleavage precede aggregation, while a reduction in ubiquitin-dependent removal might be relevant in tauopathies.

2.2.3.3 Removal of tau and autophagic dysfunction

The relationship between tau and the UPS is bidirectional. Tau in PHFs is ubiquitinated,[115] and NFTs and Pick bodies are positive for CHIP and ubiquitin,[116] indicating sequestration of key components of the 26S proteasome and subsequent impaired UPS function. Conversely, PHF-tau inhibits the proteasome.[117] Indeed, the levels of total, hyperphosphorylated and aggregated tau are reduced by ubiquitination by CHIP together with Hsc70 (Heat shock 70 kDa protein 8),[118] but hyperphosphorylated tau accumulating because of defective removal by the UPS can be cleared by autophagy.[119]

Inducible overexpression of tau in cells leads to accumulation of soluble and insoluble tau species and subsequent cell death that is reversible if tau expression is switched off. This, however, depends on autophagy as treatment with 3-methyladenine (3-MA) prevents clearance by inhibiting phosphatidylinositol 3-kinases (PI3K) important for autophagosome formation. Conversely, stimulation of autophagy is protective against tau accumulation.[120]

N-terminal truncation of tau can lead to a dysfunction in autophagy-lysosome degradation of the protein,[121] while tau cleaved by caspase 3 at Asp421 primes the protein for autophagic clearance,[122] probably by removing ubiquitination-sites and/or exposing motifs required for detection by the CMA machinery.[113]

2.3 The endosomal-lysosomal system

The endosomal-lysosomal system is crucial for a variety of cellular processes. It is essential for uptake of nutrients and receptors, either facilitating transport of the receptor to the PM or degradation and thereby influencing signalling processes. Furthermore, it plays a role in removal of dysfunctional proteins and organelles, effectively recycling amino acids by releasing them into the cytoplasm and clearing waste material into the extracellular space. In a similar process, pathogens can be taken up and destroyed via the endosomal-lysosomal system.[123]

Acidity increases in the different compartments of the endosomal-lysosomal system – starting from endocytic vesicles, early/sorting and recycling endosomes, late endosomes, and lysosomes – and the pH confers specificity, together with lipid content and protein composition.[124] While the exact pH of endosomal-lysosomal compartments depends on the cell type, it decreases from ≈pH6.5 and ≈pH6.0 in the recycling and early endosome, respectively, to ≈pH5.5 in late endosome and ≈pH4.5-5.0 in the lysosome[125, 126] (Fig. 4). This sequential increase in acidification is mediated by an H^+-ATPase (V-ATPase) that pumps protons into the vesicular lumen.[127]

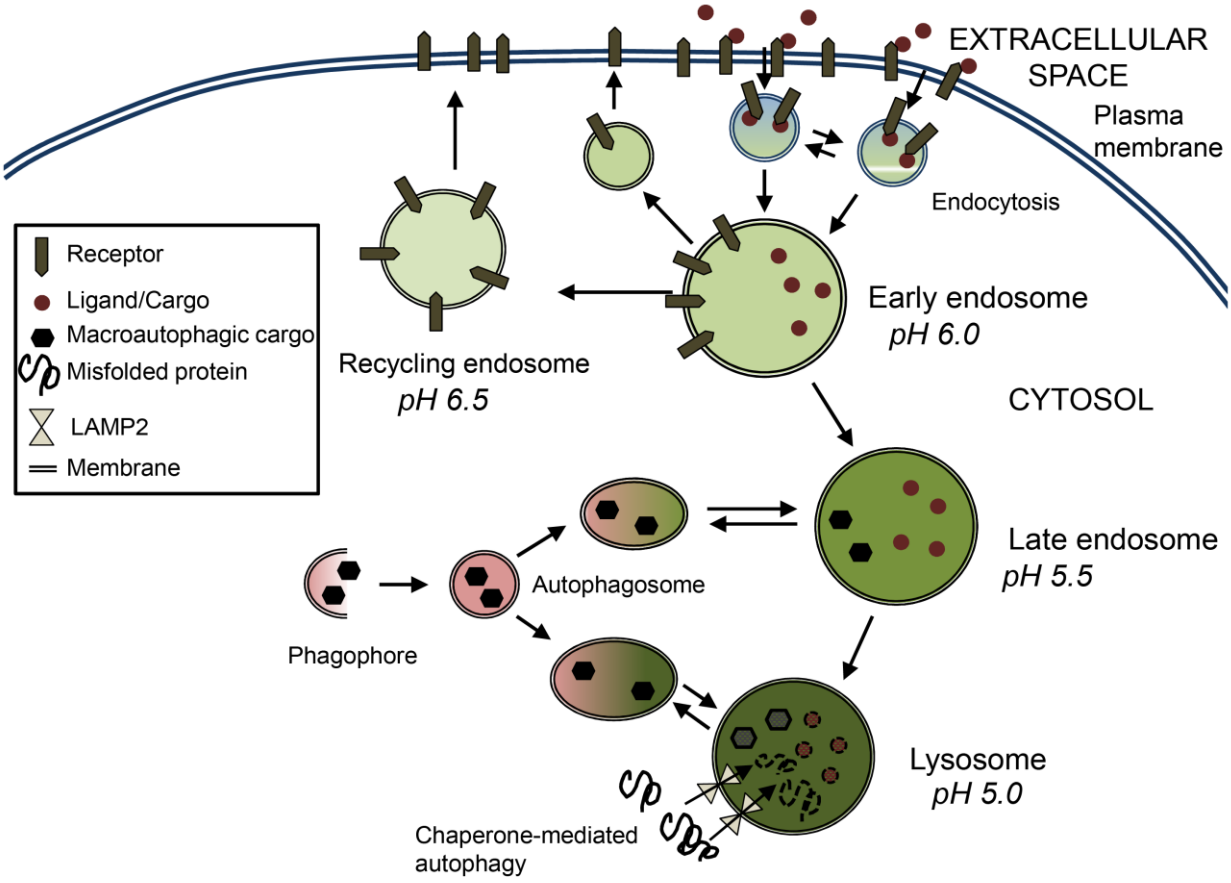

Fig. 4: Schematic of the endosomal-lysosomal system. Receptors are endocytosed after binding of their ligand by clathrin-mediated endocytosis and delivered to the early endosome after events of homotypic fusion. In the slightly acidic environment of the early endosome, ligand and receptor dissociate. Cargo can take two ways from the early endosome: Either back to the plasma membrane via the recycling endosome, that is further alkalised compared to the early endosome, or via the late endosome to the lysosome, where it is degraded. Late endosome and lysosomes also receive cargo from autophagosomes that deliver cargo from the cytosol after engulfing of cargo by a membrane, the phagophore. Furthermore, misfolded proteins can directly reach the lysosome by Chaperone-mediated autophagy that transports the proteins into the lysosome through LAMP2 in the lysosomal membrane.

There are several ways to bring cargo into the endo-lysosomal system. One is by endocytosis at the PM, another by vesicle transport from the trans-Golgi network (TGN). Autophagic processes can deliver defective proteins by CMA, or defective organelles and accumulated proteins for degradation by macroautophagy to the lysosome.[128]

2.3.1 Endocytosis, early and recycling endosome

The most common form of endocytosis is clathrin-mediated endocytosis[129], where invaginations of the membrane are formed by clathrin binding to adaptor proteins[130], leading to the formation of vesicles that then bud off into the cytoplasm. There, the clathrin coat is rapidly disassembled and vesicles fuse with each other or already existing endosomes[131]. This process depends on pH, binding and activity of Rab-GTPases (guanosine triphosphate) and recruitment of the SNARE (Soluble *N*-ethylmaleimide-sensitive factor attachment protein receptor) complex generally involved in membrane fusion[132].

Clathrin-mediated endocytosis is the main pathway for internalisation of bound ligands and receptors. One characteristic receptor endocytosed via the clathrin pathway that is often used in studies is the transferrin receptor (Tfn-R), with iron-bound Tfn as a ligand[133]. After internalisation, the decreased pH of the early endosome leads to a dissociation of receptor, Tfn and iron, effectively transporting iron into the cell. Tfn and the Tfn-R are then recycled back to the PM[134]. The low-density lipoprotein receptor (LDL-R) transporting lipids into the cell is equally recycled back to membrane while its cargo is transported to the lysosome for further processing after pH-dependent dissociation in the early endosome; however, it can also be marked for lysosomal degradation[135]. The epidermal growth factor (EGF), binding to the EGF-receptor (EGF-R), on the other hand, gets directly sorted to late endosomes and for subsequent degradation via the lysosome[136].

Recycling back to the PM is mediated by the recycling endosome. It has a tubular shape, higher pH of ≈6.4-6.5 compared to the early endosome (pH6.0) [137] and leads to rapid recycling of PM-destined cargo[138].

In addition to clathrin-dependent endocytosis, material can enter the cell via clathrin-independent pathways, for example by the formation of caveolae mediated by caveolins. While recruitment of clathrin to the PM depends on binding of an adaptor protein to activated receptors[130], this pathway is not initiated by receptors, but caveolins interacting with lipids, namely cholesterol and sphingolipids[139].

Endocytosed cargo is collected and sorted in the early or sorting endosome. Already at the PM, the Rab GTPase Rab5 quickly binds to the endocytic vesicles[140] and recruits further effector proteins that in turn activate PI3K/vacuolar sorting protein (VPS) 34 for PI3P production.[141] These pre-endosomes then fuse and quickly

acquire proteins characteristic for the endosomal compartment, for example the early endosome antigen 1 (EEA1) that is recruited by local PI3P production and then forms membrane subdomains together with Rab5.[142] EEA1 serves as a bridging protein between the two components, as it can bind to both Rab5 and PI(3)P. The binding of Rab5 leads to a conformational change of EEA1, effectively bending the protein until it collapses into an energetically more favourable conformation, thereby pulling the two membranes closer to each other.[143] After the cargo is endocytosed and in the early endosome, effector proteins bind for protein sorting, a process requiring actin polymerisation, most likely for the physical separation of cargo into early endosomal subdomains.[144]

Sorting into the late endosome – lysosome pathway is mediated by the endosomal sorting complex required for transport (ESCRT) machinery.[145] The ESCRT machinery consists of four complexes (ESCRT-0, ESCRT-I, ESCRT-II and ESCRT-III) that act sequentially. ESCRT-0 is important for cargo recognition and binding,[146] while ESCRT-I plays a role in cargo recognition[147] and recruitment of ESCRT-II,[148] which then serves as an adapter for ESCRT-III[149] that facilitates the early steps of intraluminal vesicle formation[150] which is completed by Vps4, resulting in multivesicular bodies (MVBs).[151]

Cargo that is not sorted into the degradation pathway by the ESCRT machinery can be recycled back to the PM via two different mechanisms: a fast, Rab4- and clathrin-dependent recycling pathway directly to the PM,[152] or a slow pathway that involves Rab11-positive recycling endosomes.[153] There is also a third recycling system depending on Rab8a, that recycles cargo endocytosed via clathrin-independent ways back to the PM.[154]

Some overlap exists between those pathways. Rab4 and Rab11 colocalise at the endosome during the formation of tubular structures that then bud off to become recycling endosomes; however, Rab4 is no longer present when Rab11-positive vesicles fuse with the PM, and there is evidence suggesting that the structure positive for both Rab4 and Rab11 segregates into two domains.[155]

Dynein and MTs mediate the step of separating cargo between recycling and degradation. This happens via recruitment of the dynein effector dynactin by sorting nexins (SNX) 5 and 6 that mediate both elongation and fission of the forming recycling endosome, while another SNX protein plays a role in the cargo sorting.[156]

However, the actin cytoskeleton is also involved in recycling by forming subdomains on the early endosomal membrane[157]. Similarly, cargo transport or budding off from the early to the late endosome is mediated by the actin cytoskeleton[158, 159]. Actin assembly at the early endosome in general is facilitated by the Wiskott-Aldrich syndrome protein and Scar homologue (WASH) complex, whether for formation of recycling or late endosomes[160], or in endosome-to-TGN transport via the retromer complex[161]. The process is facilitated by a factor that allows the nucleation of actin polymerisation, actin-related proteins 2 and 3 (Arp2/3)[157] (for an overview over the cargo transport through the endosomal system, see Fig. 5).

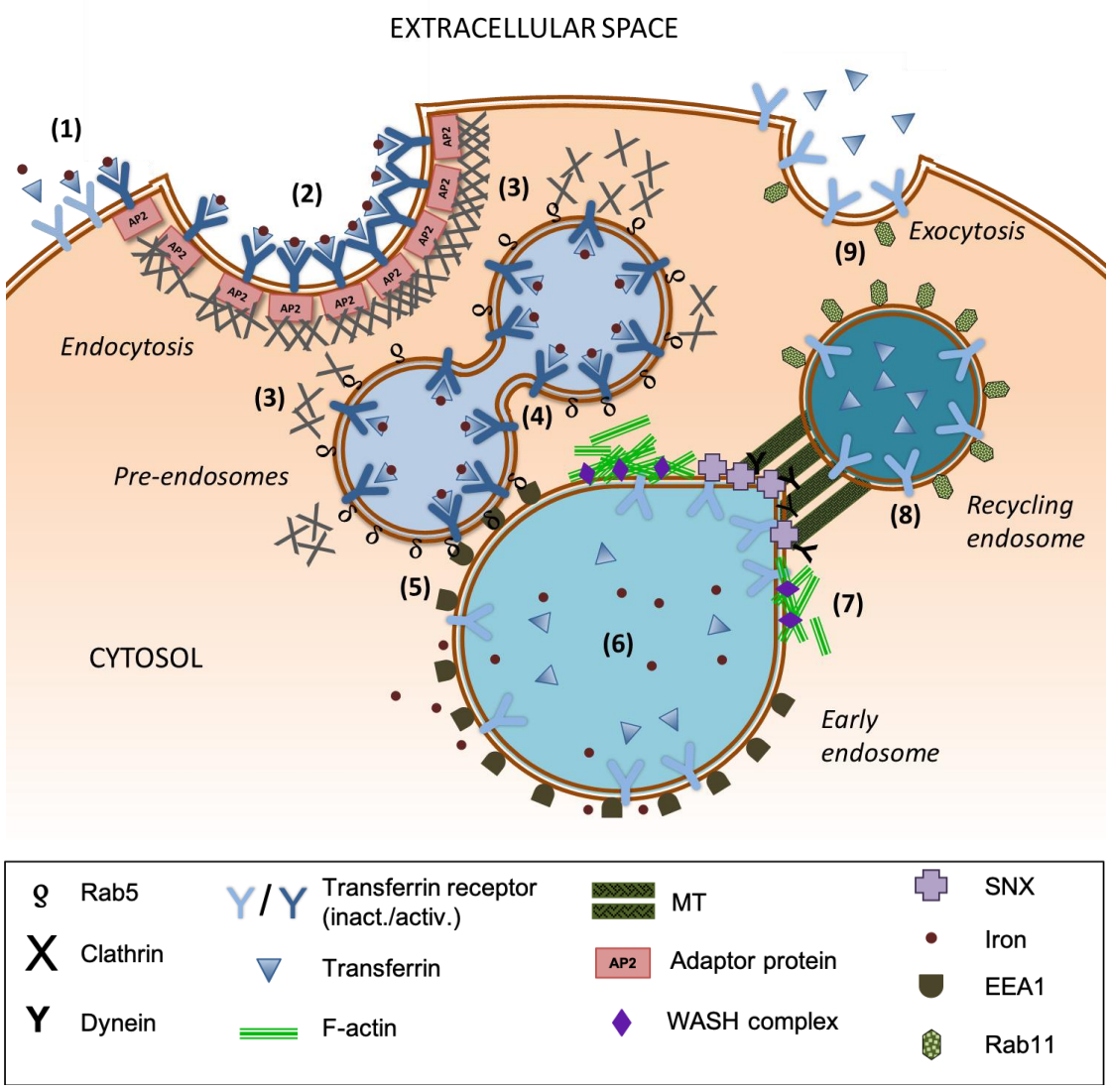

Fig. 5: Cargo transport through endocytosis, the early and the recycling endosome with Transferrin as an example. **(1)** Transferrin binds to iron and the Transferrin receptor, activating it. **(2)** The activated receptor binds to the adaptor protein complex 2 that recruits Clathrin to the membrane. Clathrin binding leads to an invagination of the membrane and eventually budding of pre-endosomes**. (3)** Clathrin dissociated from pre-endosomes, and the Rab GTPase Rab5 binds to the vesicle. **(4)** Pre-endosomes can undergo homotypic fusion before **(5)** fusing with an early endosome via Rab5-EEA1

interaction. **(6)** In the acidic lumen of the early endosome, iron, Transferrin and Transferrin receptor dissociate. The free iron is then released into the cytosol. **(7)** Recruitment of the WASH complex leads to the formation of F-actin structures at the early endosomal membrane, leading to tubulation and fission of recycling endosomes in a process supported by dynein activation via SNXs.**(8)** Dynein-mediated transport along microtubules leadings to the scission of a Rab11-positive recycling endosome that carriers the transferrin receptor and transferrin to the plasma membrane. **(9)** The recycling endosome fuses with the plasma membrane, thereby exocytosing transferrin and its receptor.

Apart from its task in the sorting of cargo, endosomes also play a role in signalling, either by terminating receptor signalling through receptor-ligand dissociation and/or degradation, or by facilitating additional or even different signalling cascades. If the EGF-R, for example, cannot be endocytosed, cell proliferation is increased as a result of enhanced signalling at the PM, but subsequent MAPK activation by phosphorylation is decreased, as it requires trafficking of the EGF-R through the endosomal system.[162]

For the transforming growth factor β (TGF-β) receptor, two pathways exist: If it gets endocytosed via clathrin, it signals from the endosome. However, if it is internalised via caveolar mechanisms, the receptor is directed into the degradation pathway via the late endosome.[163]

2.3.2 The late endosome

Late endosomes are the final product of the early endosomal sorting step, collecting cargo for degradation, but are also crucial in lysosomal biogenesis as they provide a site for acidification and enzyme delivery, and serve as an entry point for autophagosomes into the degradative pathway.

Cargo from the early needs to reach the late endosome, most likely through a conversion, where an early endosome becomes the late endosome after going through a number of transformations (for a review, see e.g. Huotari, 2011[164]). This is the case in the formation of MVBs as described above. Furthermore, a switch between Rab5 and Rab7 happens during endosomal maturation when Rab5 recruits Rab7 to the early endosomal membrane.[165] Rab7 in turn inhibits the guanosine exchange factor that activates Rab5, detaching Rab5, and leading to a replacement by Rab7[166]. Rab7 can then bind to dynein which facilitates transport into the perinuclear region, during which the endosome is further acidified.[167, 168]

While early endosomes are primarily located in the periphery of the cell, late endosomes are generally found in the perinuclear area.[169] MVBs that have reached the perinuclear area show several indicators for late endosomes, for example increased acidification (to pH 5.0-5.5) and internal membranes typical for late endosomes.[170]

This process seems to depend on pH, as treatment with the V-ATPase inhibitor Bafilomycin A1 (BafA1) blocks transport of cargo by causing defective detachment of late from early endosomes.[168] Acidity in turn depends on Rab7, as Rab7 influences the assembly of the V-ATPase and it has been shown that the two subunits, V0 and V1, interact more efficiently in the late endosome, enhancing activity of the enzyme and thereby decreasing luminal pH.[171]

Apart from acidification, Rab7 and its interaction partners play a crucial role in almost all aspects of late endosome biology and subsequent lysosomal function. This is evident from a study where overexpression of a dominant-negative form of Rab7 lead to dysfunctional transport of endosomes, an increase in lysosomal pH, and blocked transport to the lysosome, including cargo for degradation and lysosomal hydrolases.[172] Newly synthesised hydrolases leave the TGN bound to either cation-dependent (CD-) or cation-independent mannose-6-phosphate receptors (CI-MPR) in clathrin-coated vesicles that go on to fuse with the endosomes.[173] In the acidic environment of the late endosome (and, maybe, already the early endosome), hydrolases detach from their receptors[174]. From there, they are transported to the lysosome, but pH-specific activation can already occur earlier[175]. Similarly, trafficking of the MPRs back to the TGN by the retromer complex depends on interaction with Rab7.[176]

The retromer complex is involved in retrieval of proteins from the endosome and transport to other cellular compartments, including the sorting of CD-MPR and CI-MPR to the TGN and other receptors to the PM.[177] It consists of a cargo-selective complex that includes Vps35, Vps29 and Vps26, and transiently binds to a dimer of SNX proteins (SNX1 or 2 with SNX5 or 6).[178, 179] Recognition of cargo by the retromer might depends on a cytoplasmic tail motif,[180] or at least in some cases, involve reversible palmitoylation.[181]

Defects in retromer-trafficking lead to an enhanced degradation of MPRs, followed by insufficient removal of material in the lysosome due to a lack of lysosomal hydrolases[175]. After delivery of hydrolases and retrieval of receptors, late endosomes

in the perinuclear region can undergo homotypic fusion, either to form larger organelles or to exchange content in a 'kiss-and-run' type of transient fusion.[182]

Finally, late endosomes and lysosomes fuse together, a process that depends on Ca^{2+}, resulting in an intermediate organelle that then again requires separation or lysosomal restoration[182] in a pH-dependent process, for which the release of Rab7 is important.[183]

2.3.3 The lysosome

Lysosomes were first discovered by de Duve in 1955 as a membrane-separated part of the cell that played a role in acidic enzyme activity.[184] Later, they were found to be part of the cell's waste removal and recycling machinery, and crucial for many cellular processes.

Apart from removal of defective proteins and organelles, lysosomes are involved in the response to nutrient starvation,[185] lipid metabolism[186] and programmed cell death.[187]

As described above, lysosomal function depends on endosomal delivery of necessary proteins for acidification and degradative enzymes, and even their perinuclear localisation is given up if the endosomal pathway is interrupted.[172]

The lysosomal membrane contains a number of receptors and transport proteins, among them several that allow amino acids and lipids from degraded material to reach the cytoplasm, where they can be used again.[188] Furthermore, misfolded proteins that are subject to CMA can be delivered directly to the lysosome by Lysosome-Associated Membrane Protein 2 (LAMP2)-facilitated transport through the lysosomal membrane.[189, 190]

As mentioned above, the main proteases of the lysosome are cathepsins, with cathepsin D being the major aspartic protease. Cathepsins operate at an optimal pH of below 5 and are almost exclusively active in the lysosome.[191] Apart from proteases, enzymes degrading lipids, nucleic acids, and carbohydrates operate in the lysosome.[192]

Another role of the lysosome is in regulated cell death, accordingly termed lysosome-mediated cell death (LCD). LCD occurs by permeabilisation of the lysosomal membrane (LMP) that then leads to a release of cathepsins and changes in cytosolic pH.[187] Limited LMP leads to apoptosis, as cathepsins cleave pro-apoptotic members

of the Bcl-2 protein family involved in apoptosis regulation. Those translocate then to the mitochondria, where they initiate mitochondrial membrane permeabilisation and caspase-dependent cell death.[193]

Extensive LMP, on the other hand, causes necrosis as the pH of the cytosol changes and cathepsins act as effector proteins, cleaving proteins indiscriminately.[194]

A number of insults can lead to LMP, including the accumulation of toxic molecules (lysosomotropic agents)[195, 196] or a small amount of extralysosomal cathepsins that then cleave cytosolic proteins important for lysosomal integrity.[197] Similarly, μ-calpain can translocate to the lysosome after glucose or oxygen deprivation, where it might cleave Hsp70, leading to a destabilisation of lysosomes.[198]

The major activator of LCD, however, is oxidative stress. During oxidative stress, H_2O_2 diffuses through the lysosomal membrane. Since lysosomes are rich in iron retrieved from iron-containing proteins,[199] Fe(II) catalyses the formation of hydroxyl radicals from H_2O_2 that damage lipids and proteins, thereby disrupting lysosomal membrane integrity.[200]

Lysosomal biogenesis, on the other hand, is stimulated by transcription factor EB (TFEB) which induces expression of a variety of lysosomal proteins, thereby increasing waste removal by the lysosome.[201, 202] For example, TFEB regulates the expression of the V-ATPase, facilitating lysosomal acidification.[203] It also is tied to autophagy, as starvation results in arrest of phosphorylation of TFEB by mTOR complex 1 (mTORC1) and translocation from the lysosome to the nucleus where it activates transcription.[204] Consequently, overexpression of TFEB increases autophagic flux and degradation of long-lived proteins, while k.d. of TFEB reduces it.[204]

Together with TFEB, the kinase-containing mTORC1 is an important regulator of autophagy at the lysosome. During times of high cytosolic amino acids concentration and growth factor stimulation, mTORC1 is localised to the late endosome and lysosome where it phosphorylates TFEB, thereby prohibiting TFEB translocation to the nucleus.[205] This depends on endosomal maturation, as disruption of early to late endosomal conversion by constitutively active Rab5 inhibits mTORC1 activation[206]. mTORC1 inhibition by amino acid starvation in turn leads to an increase in autophagic activity to provide nutrients for the cell.[207]

2.3.4 Autophagy

Autophagy sums ups several processes that lead to the digestion of cellular components by the lysosome, hence the name (’self-eating’). During macroautophagy, organelles and macromolecules are delivered to the lysosome for the recycling of nutrients and amino acids via an intermediate structure, the autophagosome (for a review, see e.g. Mizushima, 2007[208]). Microautophagy describes the direct delivery of material to the lysosome at the lysosomal membrane,[209] while the delivery of misfolded proteins directly to the lysosome by chaperones is termed chaperone-mediated autophagy (CMA).[210]

Autophagy can be selective[211] (receptor-mediated) or non-selective (bulk autophagy, where membranes engulf portions of the cytosol indiscriminately, for example during starvation[212]). Selective autophagy depends on signals recognised by special adaptors such as p62[213] and the neighbor of BRCA1 gene 1 protein (NBR1).[214] The most common signal is ubiquitination, with polyubiquitination at lysine 63 targeting proteins for autophagic/lysosomal degradation, compared to polyubiquitination at K48 that leads to degradation by the UPS.[215] While ≈80% of proteins are degraded by the UPS, ubiquitinated aggregated proteins are removed by autophagy.[216] This ubiquitination is recognised by p62[217] and NBR1, which are both cargo receptors and substrates of autophagy themselves, being constantly turned over.[218]

CMA is an example for selective autophagy, but it does not require autophagosome formation; rather, misfolded proteins are transported directly through the lysosomal membrane by LAMP2.[219] Recognition of cargo for CMA is mediated by Hsc70[220] by identification of a KFERQ-motif that in correctly folded proteins is not exposed, but might be in misfolded proteins.[221] Macroautophagy, on the other hand, requires the formation of a phagophore, during which a membrane is formed, elongates and then engulfs the autophagic cargo. This process is initiated by Autophagy-related Gene (Atg) proteins.[222] Even though phagophore formation happens close to the ER,[223] the specific origin of the membrane remains unclear. A number of organelles have been proposed to give rise to the phagophore, including the mitochondria,[224] recycling endosomes,[225] the Golgi apparatus,[226] PM,[227] ER-mitochondria contact sites,[228] and the ER itself.[229]

During starvation-induced autophagy, mTORC1 is blocked and no longer associates with the lysosomal membrane,[230] leading to the activation of a downstream cascade after Atg1 is no longer phosphorylated.[231] During this cascade, PI3P is generated[232]

and binds to PI3P-interacting proteins such as members of the WD-repeat protein interacting with phosphoinositides (WIPI) protein family.[233] These recruit Atgs, which then conjugate the Microtubule-associated proteins 1A/1B light chain 3A (MAP1ALC3 or simply LC3-I) to phosphatidylethanolamine (PE), leading to the formation of LC3-II, a step that is important for the elongation of the forming membrane.[234]

Fully formed autophagosomes are transported via MTs to the perinuclear area,[235] a process during which they can already interact in an ESCRT-dependent manner with endosomes for acidification.[236] In the perinuclear area, they undergo fusion with the late endosome, forming the so-called amphisome, before the content is delivered to the lysosome for removal.[237] After fusion with the lysosome resulting in a structure called autolysosome, the lysosome is then recovered in a tubulation and fission process.[238]

Another form of autophagy is the autophagic removal of mitochondria, called mitophagy. Mitophagy is triggered by a loss of mitochondrial membrane potential because of mitochondrial dysfunction, which causes the Phosphatase and tensin homolog-induced putative kinase 1 (PINK1) to accumulate at the mitochondrial membrane. Phosphorylation by PINK1 activates the E3 ubiquitin ligase Parkin, which in turn ubiquitinates a number of substrates on the outer mitochondrial membrane, targeting the defective mitochondrion for autophagic removal.[239]

2.3.5 The endosomal-lysosomal system in neurodegeneration

In neurons, the endosomal-lysosomal system is especially important since neurotransmitters need to be packed in vesicles for transport, release[240] and uptake.[241] Neurotransmitter receptor signaling might depend on endocytosis[242] and membrane cycling of glutamate receptor subunits, for example, determines long-time potentiation or depression, thereby controlling synaptic strength.[243] Furthermore, neurons are especially vulnerable to toxic effects from protein aggregation, as the post-mitotic cells cannot ’dilute’ aggregates by cell division.[244]

Evidence for a dysfunction of the endosomal-lysosomal system was found in a number of neurodegenerative diseases; for example, p62, which is usually constantly turned over by autophagy, accumulates together with ubiquitin in familiar forms of AD, in CBD, and PSP, similar to LC3 puncta, both of which colocalised with hyperphosphorylated tau.[245] This has led to the idea that in neurodegeneration, an age-related reduction in endo-lysosomal function[246, 247] is further exacerbated by

additional factors and crosses a disease-causing threshold. Also, expression levels of Atg5, Atg7 and Beclin-1, proteins important for autophagic processes, are reduced in the aging brain.[248]

Dysfunction of the retromer system is linked to neurodegenerative diseases as well, as the retromer component *VPS35* is mutated in familial forms of PD.[249] But other proteins of the endosomal-lysosomal system have been implied in disease progression of PD as well. For example, mutations in *LRRK2*, which are a common cause of familial PD,[250] impair the autophagic-lysosomal system by decreasing the lysosomal pH.[251]

Mutations in the lysosomal ATPase gene *ATP13A2* can cause PD[252] but also Kufor-Rakeb syndrome,[253] a rare form of parkinsonism with dementia; also, ATP13A2 is upregulated by LRRK deficiency.[251] A loss of ATP13A2 causes an increase in lysosomal pH as well as defects in protein removal in cells,[254] and animal models of Kufor-Rakeb syndrome show brain atrophy, aging-related motor deficits, cognitive decline, gliosis and accumulation of ubiquitinated proteins and lipofuscin.[255-257]

Heterozygous mutations in the *GBA1* gene coding for β-Glucocerebrosidase (GCase) strongly increase the risk for PD,[258] and homozygous mutations are found in Gaucher's disease, a lysosomal storage disorder, where symptoms can also include parkinsonism in one of the subtypes.[259] Also, GCase activity was found to be decreased in idiopathic PD, a phenotype mimicking that of *GBA1* mutations.[260] Mutations in *GBA1* lead to decreased lysosomal function with a lack of proper acidification and defects in autophagy, resulting in enlarged lysosomes, increased oxidative stress, defects in lysosomal reformation from autophagolysosomes, and accumulation of p62 and α-synuclein in both Gaucher's disease and PD.[261-263]

In AD, both mutations in familial forms of the disease and risk variants found in GWASs point to an involvement of the endosomal-lysosomal system in the disease.[264-266] Presenilin-1 mutations increased lysosomal pH by interfering with maturation of the V0a1 subunit of the V-ATPase[267], and risk factor variant apolipoprotein E4 upregulates endocytosis by Rab5, increasing uptake of endocytosed cargo.[268] This challenges lysosomal degradation while at the same time binding to phospholipids in a process that destabilises the lysosomal membrane.[269]

Apart from genetic evidence, the endosomal-lysosomal system is involved in both APP processing and removal, and amyloid β (Aβ), which accumulates in extracellular

plaques in AD, is partially generated by β-secretase cleavage in the early endosome.[270] Dystrophic neurites with a large number of autophagosomes, lysosomes and amphisomes are found around these plaques,[271] suggesting that the exocytosed Aβ stems from neurons with autophagic-lysosomal dysfunctions.

Apart from neurons, there are studies pointing at the involvement of lysosomal dysfunction in glia cells and especially neuroinflammatory processes that accompany neurodegenerative processes. While microglia are capable of taking up amyloid β[391, 392], they do not have the ability to sufficiently degrade it[393]. Furthermore, amyloid β oligomers also disrupt lysosomal biogenesis in microglia by preventing the translocation of TFEB to the nucleus[393, 394], and decrease levels of OSTM1 which is involved in acidification of the lysosome upon activation of microglia[393].

Autophagy also plays an important role in the polarization of microglia. There are two different phenotypes for microglia: an M1 phenotype, that releases toxic nitric oxygen species and pro-inflammatory interleukins (IL-1β, IL-6), and a neuroprotective M2 form that is marked by IL-10 release[395]. An impairment of the autophagic flux in microglia led to an increase in markers for the M1 phenotype in microglia, while the stimulation of autophagy increased M2 markers[395]. Similarily, the autophagy-enhancing drug rifampicin can reduce the release of pro-inflammatory interleukins in microglia treated with rotenone[396], an inhibitor of the electron transport chain complex I that is also commonly used to model mitochondrial dysfunction in Parkinson's disease. Furthermore, treatment with rapamycin, an inhibitor of the autophagy-suppressing mTOR-pathway, was able to prevents an activation of the innate immune system in a mouse model overexpressing human tau carrying the P301L mutation related to frontotemporal dementias[397]. In the same model, a protective effect of rapamycin on synapses and neurons usually affected by P301L-tau was noted[397].

Exogenous α-synuclein fibrils, on the other hand, induced autophagy in microglia to an extend that lead to mitochondrial damage and microglial cell death[398], and a similar effect was seen in a mouse model overexpressing the AD and PSP-related A152T mutation in human tau[399]. This shows the need for a fine-tuned autophagic response to neurodegeneration-related proteins in microglia and for a resulting neuroinflammatory response.

A number of other neurodegenerative diseases have been linked to the endosomal-lysosomal system and autophagic dysfunction, both by mutations and functional evidence. A recurring finding in all of these diseases, however, is defective pH regulation in the endosomal-lysosomal system.

2.3.6 pH regulation in the endosomal-lysosomal system

The pH of the different compartments of the endosomal-lysosomal system is finely tuned and the correct pH crucial for the proper function of the system.

The acidic luminal pH of the endosomal compartments is generated through proton import by the H^+-ATPase/V-ATPase, during which the V1 subunit hydrolyses ATP and thereby provides the energy for the V0 subunit to pump H^+ across the membrane.[127, 272] The efficiency of this process differs for different compartments of the endosomal-lysosomal system and is depended on subunit composition, explaining the pH gradient from early endosome to lysosomes.[171, 273] Also, the position of lysosomes has an effect on V-ATPase subunits, leading to the observation that peripheral lysosomes are less acidic than those close to the nucleus.[274]

Since the import of protons generates a positive charge, chloride antiporters exchanging one H+ for two Cl- are required to reduce the electric potential for further acidification (Fig. 6). Chloride channel 7 (ClC-7) mediates this transport in endosomes and lysosomes.[275]

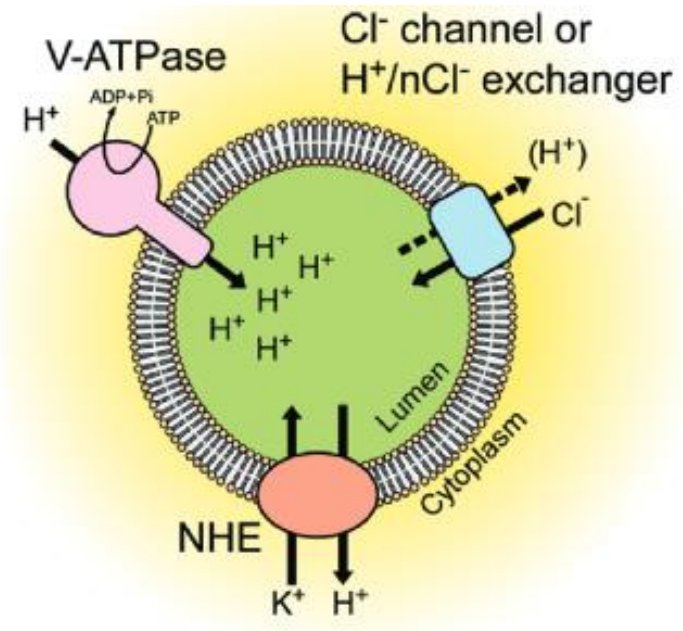

Fig. 6: Endosomal-lysosomal pH regulation. The V-ATPase transports H+ into the vesicular lumen in an ATP-dependent step. A chloride channel functions to compensate for the chemoelectric gradient that is generated by the V-ATPase, thereby aiding acidification. The pH is further regulated by an Na^+/H^+ exchanger that alkalises the lumen. From: Ohgaki (2011), Organellar Na+/H+ exchangers: novel players in organelle pH regulation and their emerging functions, Biochemistry 50(4):443-50[390]

The activity of the V-ATPase is further regulated by cellular nutrient requirements. High levels of glucose lead to a PI3P-dependent increase in V-ATPase assembly,[276] while increased amounts of amino acids induce disassembly.[277]

An elevation of pH in the lysosome because of insufficient ATPase activity, as it can occur during aging, leads to Ca^{2+} efflux into the cytosol,[278] increasing the activity of Ca^{2+}-binding proteins such as calpains.[279] As a higher pH in the lysosome has a negative impact on lysosomal transporter proteins crucial for export of amino acids into the cytosol[280] and hydrolase function, it is not surprising that pH is altered in many lysosomal storage disorders and aging-related diseases such as AD.[184]

Apart from enzyme activity, cargo dissociation from carriers in lysosomes (for example, of lipids or metal ions from proteins) is, as ligand-receptor dissociation in the endosome, dependent on the correct pH.[281-283] Furthermore, acidification of synaptic vesicles important for neurotransmitter packaging requires the activity of the V-ATPase.[284]

Fine-tuning of the endosomal pH is achieved by electroneutral H^+/cation exchange that alkalises the endosome and is mediated by Na^+/H^+ Exchangers (NHE) 6 and 9.

2.4 The solute carrier family 9 subfamily A member 6 (*SLC9A6*)/Na^+/H^+-Exchanger 6 (NHE6)

2.4.1 The Na^+/H^+ exchanger (NHE) protein family

The Na^+/H^+ exchanger (NHE) protein family consists of currently nine known members (*SLC9A1-9*, see https://www.genenames.org for official nomenclature) involved in cation exchange and pH regulation. NHE1-5 are usually found at the plasma membrane (even though NHE3 and NHE5 are constantly cycled from the recycling endosome to the PM),[285, 286] while NHE6-9 localise to intracellular organelles and might have a higher preference for K^+ than for Na^+[287] (for a table including subcellular and tissue distribution of the exchangers, see Zhao et al. 2016).[288]

Ion exchange is mediated by the highly conserved transmembrane region, while the cytosolic tails are specific for the respective isoforms and have a regulatory function.[289] For example, deletion of the cytosolic domain alters pH-sensing of NHE1, and NHE1 is phosphorylated at the C-terminus under basal conditions.[290] NHEs have

12 predicted transmembrane domains, of which the first was found to be cleaved in NHE3 and the yeast cation exchanger Nhx1, serving as a signal peptide,[291, 292] and similar processing might happen in other NHEs. Studying NHE3 topology, Zizak et al. suggest that a loop entering and exiting at the same side of the lipid bilayer between transmembrane domains 9 and 10 might confer the difference in ion transport specificity between NHE1-5 and NHE6-9.[291] Further data on NHE1 and NHE3 suggests that these isoforms might form homodimers for function by binding in the transmembrane domain.[293]

The transport of ions itself does not depend on ATP hydrolysis and is therefore passive, but the activity of the exchangers can be reduced by ATP depletion to varying degrees,[294] This, however, might be a secondary effect, as ATP depletion results in dephosphorylation of phosphatidylinositol 4,5-bisphosphate (PIP_2), which binds at the C-terminal and is, at least in NHE1, needed for transport activity.[295]

Of the intracellular exchangers, NHE6, 7 and 9 share the greatest homology, while NHE8 has the lowest similarity to the others.[296] NHE6 localises to the early endosome and transiently to the PM, while NHE7 is found in the TGN and NHE8 in the mid-to-trans Golgi compartment[296] (Fig. 7). NHE9 functions in recycling endosomes, and this isoform has been identified to play a role in autism spectrum disorder with epilepsy,[297-299] addiction,[300] and attention deficit hyperactivity disorder (ADHD).[301, 302]

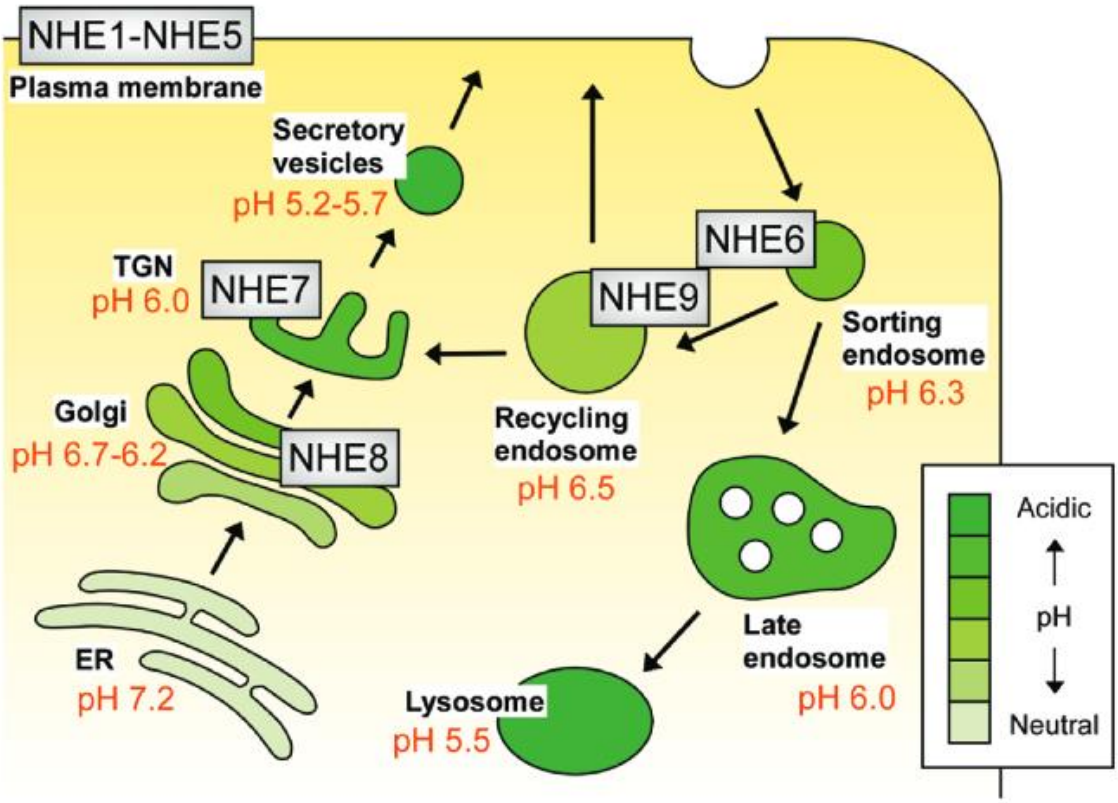

Fig. 7: The organellar Na+/H+ exchangers. While NHE1-5 are at the plasma membrane, NHE6 is found at the sorting/early endosome, while NHE9 functions at the recycling endosome. NHE8 localises to the mid-Golgi-department, while NHE7 is found in the Trans-Golgi-Network. All organellar NHEs alkalise the lumen of the respective organelle by exchange of H^+ with K^+. From: Ohgaki (2011), Organellar Na+/H+ exchangers: novel players in organelle pH regulation and their emerging functions, Biochemistry 50(4):443-50[390]

This might be due to defects in glutamate clearance, as NHE9 colocalises with the astrocytic glutamate aspartate transporter essential for glutamate uptake after synaptic release.[303] Accordingly, NHE9 is more expressed in astrocytes than in neurons, and variants associated with autism reduce, while NHE9 overexpression increases glutamate uptake into astrocytes.[303] As all four intracellular NHEs alkalise the respective compartments where they are situated, overexpression of NHE9 increases, while k.d. of NHE9 decreased the pH of endosomes in human glioma cells and, to some extent, in mouse astrocytes. However, a compensatory upregulation in NHE6 might attenuate the phenotype, suggesting that these NHEs have overlapping functions, even though a NHE6 k.d. is not met by an upregulation of NHE9.[303]

2.4.2 *SLC9A6*/NHE6

NHE6 is encoded by the *SLC9A6* gene that is located on the X-chromosome at Xq26.3 and consists of 17 exons. The protein has four isoforms with lengths of 617, 649, 669 and 701 amino acids (Ensembl gene ID: ENSG00000198689, UniProt ID: Q92581) and shows an exchange activity with K^+ instead of Na^+ as a counterion for H^+[304].

After being reported to localise to the mitochondria at first[305] and then suggested to play a role in secretory organelles between ER and PM,[306] Brett et al. detected the protein in early and recycling endosomes, and only transiently at the PM,[307] and the colocalisation of NHE6 with EEA1 was later confirmed.[296] The protein is N-glycosylated, and Western blot analysis suggests that it forms multimers.[306]

NHE6 is ubiquitously expressed, but by far the highest expression is in the brain (http://biogps.org/#goto=genereport&id=10479).

The Na^+/H^+ exchanger Nhx1 is the yeast orthologue of NHE6 and similarly localises to endosomes for sorting of cargo to the vacuole.[307, 308] Nhx1 serves as a leak for protons in the endosomal system, thereby regulating both pH in the endosome and the cell[308]. Loss of this protein causes hyperacidification of the vacuole, makes the yeast strain more susceptible for growth inhibition by weak acids, and leads to missorting of the usually vacuole-destined carboxypeptidase Y to the PM.[309]

An important binding partner of NHE6 is the receptor for activated C kinase 1 (RACK1).[310] RACK1 is a scaffolding protein involved in anchoring of activated protein kinase C (PKC) at the PM,[311] but was also shown to interact with NHE6, NHE7 and NHE9. RACK1 k.d. elevated endosomal pH and NHE6 was found to be reduced at the PM, suggesting a role of RACK1 in positioning of NHE6 at the PM. Similarly, uptake and cell surface levels of Tfn-R were diminished after RACK1 k.d., presumably because of involvement of NHE6 in endocytosis.[310] Previous data had suggested that PKC activity is needed for the activation of NHE6, and k.d. of PKC resulted in increased trafficking of cargo to the lysosome.[312] Furthermore, increased PKC activity after hypoxia in cancer cells led to an increase in NHE6 at the PM by increased interaction with, and anchoring by, RACK1.[313] The increase in endosomal pH after RACK1 k.d. can therefore be explained by the loss of NHE6 at the PM and increased levels of NHE6 in the early endosome.[310]

Since NHE6 is predominantly expressed in the brain, it is not surprising that it plays a role in synaptic function. Deane and colleagues could show that NHE6 localises to

dendritic spines and the presynapse in developing hippocampal neurons, but can also be found in astrocytes.[314] NHE6 colocalised with the AMPAR subunit GluR1 in dendrites and dendritic spines, and its postsynaptic location strongly increased after stimulation by chemical-induced NMDAR activation.[314]

Furthermore, another study could show that NHE6 localises to endosomes found in growing axons and dendrites, and less in mature axons.[315] Hippocampal neurons of a NHE6 null mice line showed decreased axonal branching and a reduction in dendrite, dendritic spine and synapse numbers, and the authors found hyperacidic endosomes that did not follow the gradient in endosomal acidification usually found along the axon[315] (with endosomes with a higher pH at the growth cone or axonal branch points, and low-pH endosomes closer to the soma[316]). The reduction in synapse number might be the result of reduced signalling of the TrkB receptor after binding of brain-derived neurotrophic factor (BDNF), as it usually continues to signal after internalisation, but is turned over quickly in NHE6 deficient cells, probably by ectopic activity of hydrolases in endosomes.[315]

The fact that k.d. of NHE6 in HeLa cells decreased endosomal pH and Tfn uptake suggests that NHE6 plays a role in clathrin-dependent endocytosis, and Tfn was shown to quickly travel from clathrin-positive to NHE6-positive vesicles via an intermediate that is positive for both.[317] However, EGF uptake is not changed by NHE6 k.d., but EGF also does not colocalise with NHE6 and its internalisation is mediated by a different adaptor protein complex from Tfn, which might lead to different involvement of NHE6 in endocytosis of EGF.[317]

2.4.3 *SLC9A6* mutations in Christianson syndrome

In 1999, Christianson et al. described a South African family with a form of X-linked mental retardation.[318] Males in this family presented with severe intellectual disability and had microcephaly, epilepsy, truncal ataxia and, if ever acquired, lost the ability to walk by the end of the first decade of life. Similarly, they were unable to speak despite normal hearing, failed to gain weight and had a reduced life expectancy (5-39 years). Cerebellar and brain stem atrophy was found both by magnetic resonance imaging (MRI) in one and autopsy in another case. During the autopsy, widespread neuronal loss and demyelination was found especially in the cerebellum and in the hippocampus but was not as evident in cortex and brain stem. No

immunohistochemical assessment of the brain pathology was mentioned in this report, so that it remains unclear if pathological protein aggregation was present in these cases.[318]

Genetic analysis at the time linked the disease to Xq24-q27.3,[318] and reanalysis of the DNA samples at a later time found a 2 base pair (bp) deletion that introduced a frameshift and 59 amino acids of nonsense sequence (p.H171fs) in the *SLC9A6* gene.[319] The same study found another 6bp deletion in a Norwegian family that caused an in-frame deletion of two amino acids in the ion exchanger domain of the NHE6 protein (E255_S256del), and another mutation that truncated the protein, leading to a loss of the final transmembrane domain and the C-terminus (R468X).[319] MRI analysis of one of the Norwegian patients at several timepoints showed progressive cerebellar atrophy, and proton magnetic resonance spectroscopy (MRS) suggested an increase in glutamate-glutamine complex in the basal ganglia (the R468X mutation was later discovered in another family with a similar phenotype, confirming also MRI and MRS findings[320]). However, investigation with the pH-sensitive dye LysoTracker, ubiquitin and EEA1 antibodies in fibroblasts from one patient did not find any large-scale aberrations in the endosomal-lysosomal system.[319] A splice-site mutation in another family included in the study causes skipping of exon 3 (V144_R169del), removing the fourth transmembrane domain and potentially strongly influencing folding of NHE6 in the membrane.[319] The patients in this study showed a phenotype similar to that found by Christianson, with X-linked mental retardation, epilepsy, microcephaly and ataxia, and a happy demeanour resulting in unprovoked laughter, a symptom not described by Christianson and characteristic of Angelman syndrome.[319] However, this mutation was later found in two patients of another family with a comparably mild phenotype, with only mild intellectual disability, microcephaly, ADHD, delayed acquisition of motor skills and speech difficulties; the mutism and persistent epilepsy observed in other patients was not found in this family, suggesting that other factors might influence the severity of the disease as well.[321]

An in-frame deletion of three amino acids (Trp338_Thr340del) adjacent to a potential transmembrane domain caused mental retardation, autistic behaviour, seizures, lack of speech, progressive motor deterioration and ataxia in the forth to fifth decade of life in six males.[322] Neither unprovoked laughter nor pronounced microcephaly was found in these patients. Upon autopsy of two cases, there was wide-spread neuronal

degeneration and a moderate general atrophy of the brain, different from the autopsy cases in the previous studies. Also, cerebellar atrophy was not as pronounced, and cortex and hippocampus were only mildly affected by neuronal loss and gliosis.[322]
However, there was diffuse tau pathology in the white matter, with filamentous tau aggregates in the cortex, the SN, locus coeruleus, basal ganglia, thalamic and cranial nerve nuclei, and hippocampus. Furthermore, tau accumulated in coiled bodies in glial cells, however, the severity of tau pathology did not correlate with the amount of neuronal loss.[322] Biochemical analysis revealed that insoluble tau consisted of hyperphosphorylated 4R tau and the authors noted that the pathology was reminiscent of that found in CBD, albeit without ballooned neurons and slight differences in affected regions.[322]
A number of other mutations were found in *SLC9A6*, with different clinical phenotypes, but always related to intellectual disability, epilepsy and inability to speak in the male members of the families.[323, 324] Protein truncation mutations in *SLC9A6* were found in one study in ≈1% of all cases with X-linked mental retardation, making it one of the most commonly mutated genes in these disabilities.[325]
Female carriers of the respective mutations were clinically affected to varying degrees. While the initial study reported mild mental retardation in a small subset of female carriers (25%),[318] the E255_S256del female mutation carriers showed no clinical symptoms,[319] while the R468X mutation was connected to severe dyslexia in one case,[319] and speech disorder, learning and schooling problems in two others from another family.[320] Similar variable phenotypes were observed in females with the V144_R169del, which had no symptoms in one family,[319] and learning disability and speech difficulties in another.[321] Other studies reported neuropsychiatric illness as a common clinical feature in female carriers, usually behavioural problems like aggression, ADHD, depression, anxiety and psychosis in families where males showed symptoms of Christianson syndrome (CS).[324,326] One study reported a case of CBS/CBD in an obligate carrier, while other carriers in this family were mainly affected by psychiatric disorders including depression, anxiety, psychosis and self-injurous behavior.[326]

A number of functional studies have started to elucidate the effect of NHE6 mutations in cellular models. The E255_S256del mutation was shown to be mostly degraded by

ER-associated protein degradation (ERAD), and protein that escaped removal was partially retained in the ER and partially located in ubiquitin-accumulation EEA1/Tfn positive early endosomes, from where it was trafficked to the lysosome in an ESCRT-dependent manner.[327]

Another study on this mutation confirmed the degradation of the mutant protein by the proteasome via ERAD and the lysosome, and showed that even though Tfn-uptake was impaired by overexpression of the mutant, EGF-uptake was not.[328] Furthermore, endosomes in mutant overexpression lead to failed to alkalise and apoptosis was increased in AP-1 cells, a chinese hamster ovarian cell line that is deficient in NHE1.[328]

Overexpression of Trp338_Thr340del NHE6 in AP-1 and HeLa cells showed that this mutant protein is retained in the ER in a monomeric, immature core-glycosylated form.[329] Full glycosylation of the protein might be important for PM localisation; still, a small fraction of Trp338_Thr340del NHE6 was transported to the PM, but could not be internalised to the same extend as WT NHE6. Similarly, while uptake of Tfn was increased in cells overexpressing WT NHE6, this was not observed in cells overexpressing the mutant, arguing for a loss of function.[329] In mouse primary hippocampal neurons, a similar overexpression experiment led to a diffuse instead of punctate distribution of NHE6 and a strong reduction in neuronal process formation, with no further branching like that observed in WT overexpression or control transfection.[329]

An *SLC9A6* knockout mouse was described in 2011, where monosialic ganglioside 2 (GM2) accumulated in homozygous females.[330] The lipid was found in late endosomes and lysosomes initially in the basolateral amygdala and in older mice in hippocampus, hypothalamus, and piriform cortex, caused by dysfunction in the lysosomal β-hexosaminidase that degrades GM2. Similar, aggresomes or storage bodies comparably to those found in lysosomal storage disorders and cells with an abnormal number or shape of nuclei were observed in the cortex. Neurons that showed GM2 accumulation also had higher levels of unesterified cholesterol, a finding reminiscent to that of the lysosomal storage disorder Niemann-Pick disease where a defect in retrograde trafficking leads to lysosomal accumulation of unesterified cholesterol.[330]

In the hippocampus, LAMP2 and cathepsin D staining was increased, suggestive of a higher number of lysosomes in the homozygous females.[330] As accumulation of

hyperphosphorylated tau in CS had previously been described,[322] tau phosphorylation was assessed but only slightly increased in the *SLC9A6* knockout mouse model.[330]

Similar to the situation in CS patients, no obvious cell loss could be detected in the cerebrum of *SLC9A6* knockout mice; however, there were extensive Purkinje cell loss in the cerebellum of hemizygous male mice and axonal spheroids similar to those found in Niemann-Pick disease.[330] Still, brain regions most affected by *SLC9A6* knockout are not those expressing the highest level of the protein, suggesting secondary factors or compensatory mechanisms that cause selective vulnerability.[330]

On a behavioural level, male animals showed modest hyperactivity, motor coordination deficits, and gross ataxia but no memory dysfunction suggestive of a mental retardation-like phenotype.[330]

Separate investigation of the heterozygous females of this mouse line showed that the lacZ-reporter used to generate the knockout by replacing exon 6 was expressed in a mosaic pattern in neurons, oligodendrocytes and astrocytes, and GM2 accumulation followed this pattern.[331] Compared to hemizygous males, Purkinje cell loss and secondary gliosis were not as pronounced, and the progressive motor phenotype observed in males was similarly not as strong, as none of the female mice displayed ataxia even at an older age. In this study, the authors found cognitive impairment in both males and females which is in contrast to the findings in male mice in the original study; however, cognitive impairment might be age-dependent and mice included in this experiment could be older than in the previous study.[331]

2.4.4 NHE6 in other diseases

Apart from CS, NHE6 dysfunction has been implied in a number of other brain-related diseases. Deletion of the NHE6 yeast orthologue Nhx1 enhanced the toxicity of the ALS and FTLD related RNA-binding protein TDP-43 (transactive response DNA binding protein 43kDa)[332].

An analysis of microarray data on autism revealed that NHE1 and NHE6 are significantly downregulated in brains from patients with autism, while NHE9 is upregulated,[298] and SNPs in the *SLC9A6* gene have been linked to autism spectrum disorder,[297] and, in one case, to schizophrenia in a heterozygous female.[333]

NHE6 was found to be downregulated in the SN of PD patients,[334] and a functional study suggests a potential role for NHE6 in AD.[335] The study found that the pattern of APP expression resembles that of NHE6 in both development and distribution in the brain, and NHE6 colocalises with APP. Furthermore, overexpression of NHE6 and monensin-treatment both lead to a relocalisation of APP from the TGN to EEA1 and Rab11-positive endosomes.[335] In cells stably expressing the APP isoform APP695, overexpression of NHE6 reduced cleavage of APP and thereby Aβ levels, while a k.d. had the opposite effect with increased levels of a C-terminal fragment and Aβ. Lastly, the author showed that NHE6 expression and protein levels were downregulated in brains of idiopathic AD patients, indicating a role for NHE6 in AD.[335]

2.4.5 The c.1464_1465insT/p.T489YfsX23 mutation and c.G1703A/p.R568Q variant in *SLC9A6*/NHE6

In 2013, Riess and colleagues identified a novel mutation in *SLC9A6* in a family with CS in males.[336] The T insertion between cDNA positions 1464 and 1465 (ENST00000370701) in a conserved region of exon 12 causes an amino acid exchange, a frameshift leading to 23 amino acids of nonsense sequence, and a premature stop codon in exon 13 (p.T489Y_fsX23, Fig. 8A). The mutation affects the last transmembrane domain and truncates the protein, removing the C-terminus important in localisation and regulation of NHE6[336] (Fig. 8B).

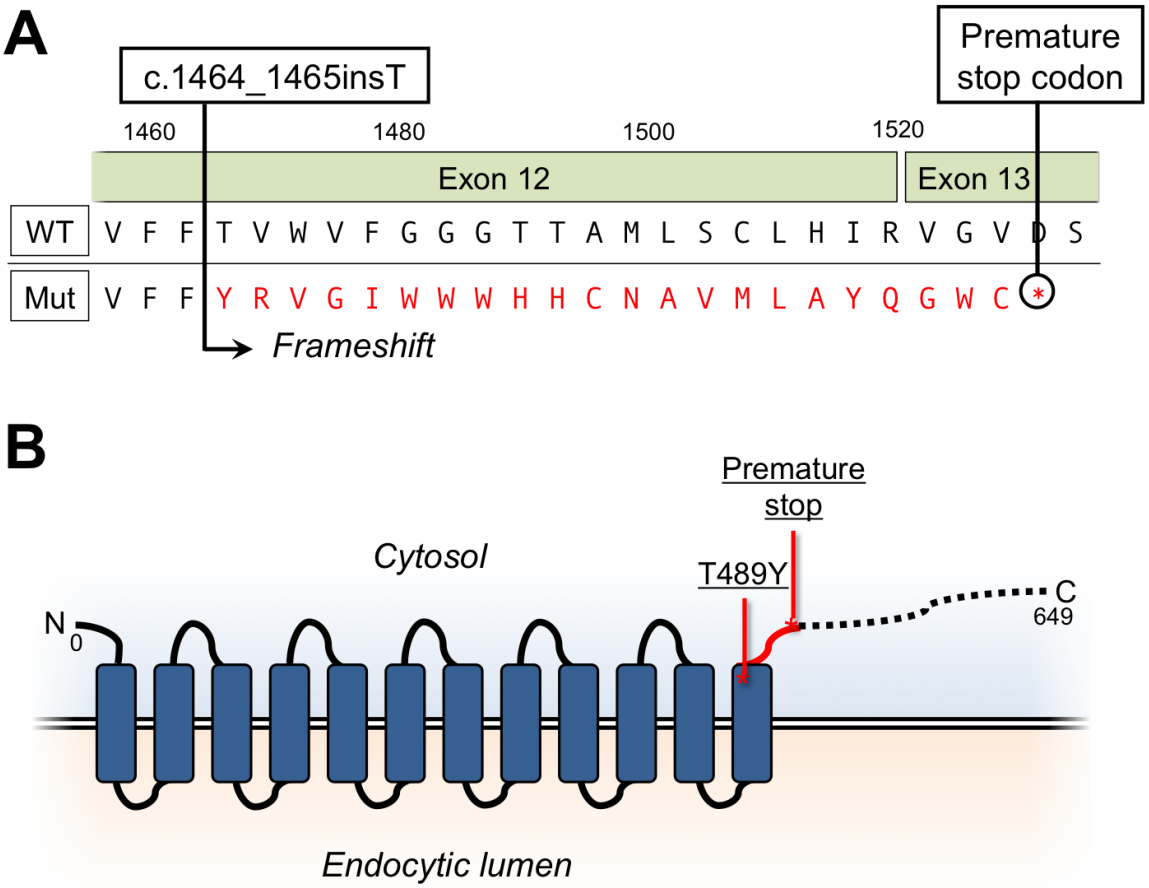

Fig. 8: Position of the c.1464_1465insT/pT489Y_fsX23 mutation in the 649 amino acid transcript used in the original paper (ENST00000370701). **A**: The T insertion between positions 1464 and 1465 leads to a T>Y amino acid exchange, a frameshift and 23 amino acids of nonsense sequence before a premature stop codon in exon 13. **B**: The T489Y exchange in the last transmembrane domain of NHE6 is followed by a nonsense sequence until a premature stop codon truncates the c-terminal of the protein.

The grandmother of the index patient, an obligate carrier, developed neurological symptoms with rigidity, slowness of movements, and depression. An MRI revealed mild general brain atrophy.[336] While she was first given a diagnosis of possible PD, it was later changed to CBS (Fig. 9A, patient #1.1). Her mother, also an obligate carrier, had shown similar symptoms in her 70s (Fig. 9A, patient. #1.2). In the mother of the index patient, a confirmed carrier, testing of X-inactivation revealed a random distribution of the two alleles, suggesting that there is no skewed X-inactivation of the mutant allele.[336]

The finding of CBS in females in this patient together with the previous description of a CBD-like pathology in male Christianson syndrome patients initiated a targeted

screen for *SLC9A6* variants in a large cohort of CBS and CBD patients. This screen identified the c.G1703A/p.R568Q variant (ENST00000370695) in a family with two CBS patients. Whereas one of these carriers showed pathology in line with CBD (Fig. 9B, patient #2.1), the other displayed a mixed pathology after autopsy (Fig. 9B, patient #2.2).

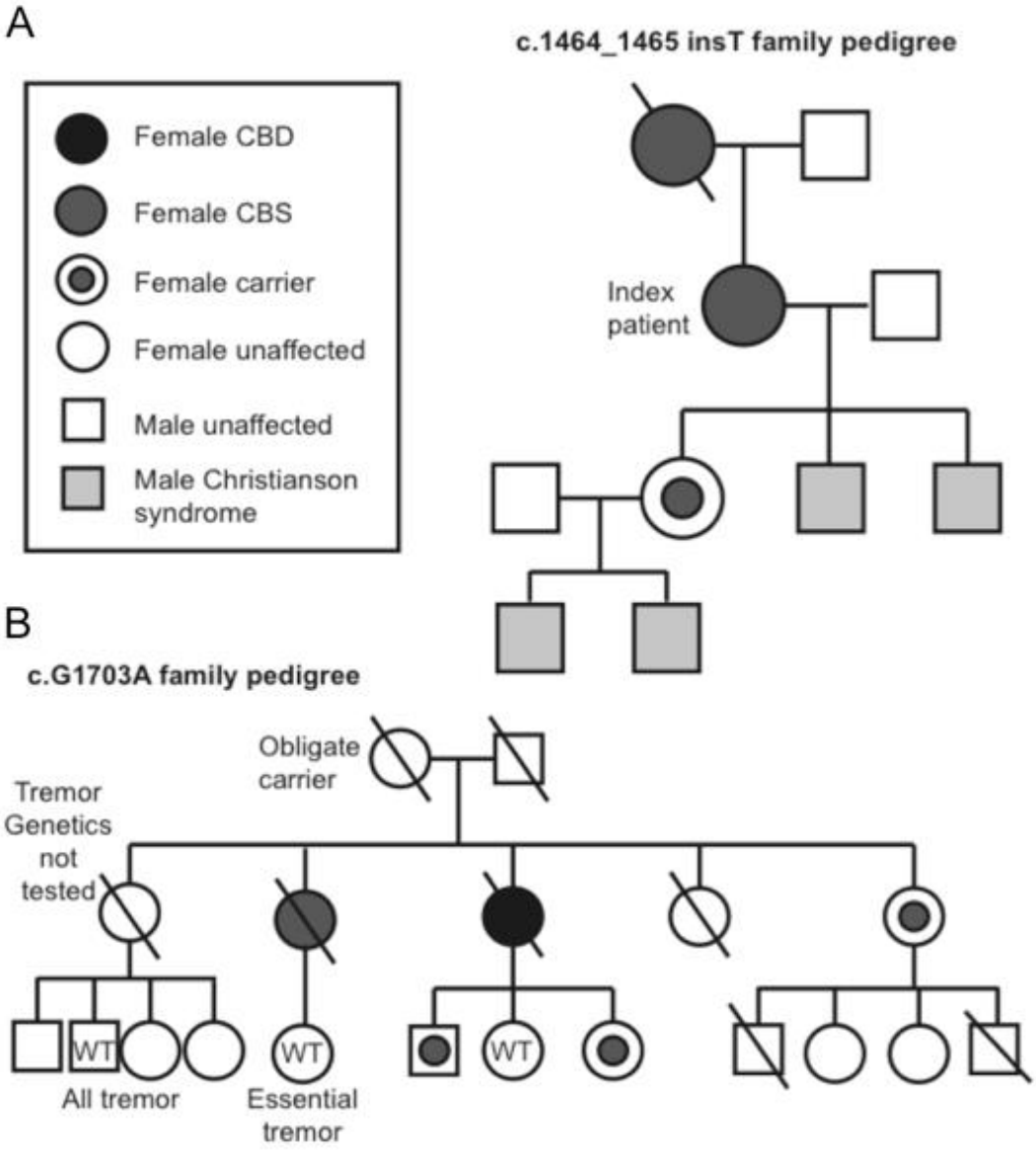

Fig. 9: Pedigrees of the two families included in this study. **A**: The family carrying the c.1464_1465insT/p.T489Yfs23X mutation. Several males in the family have Christianson syndrome, two female carriers have CBS. The unaffected female carrier was at the time of this study a lot younger than her mother or grandmother at the onset of disease. **B**: The family with the c.G1703A/p.R568Q variant in NHE6. One patient with the variant had autopsy-confirmed CBD, while her sister had CBS with an underlying mixed pathology. Several carriers in the family are unaffected, and an essential tremor in members without the R568Q variant suggests the presence of a second mutation that might play a role in the observed phenotypes.

Both patients were female, and the males in the family did not show any clinical features of CS. The c.G1703A variant in exon 14 causes the exchange of a highly conserved amino acid and is predicted to affect an adjacent splice site (Fig. 10A). It is also the last amino acid before the start of a putative RACK1-binding domain (Fig. 10A), but outside of the region that plays a role in localisation of the protein.[337] The p.R568Q is located in the C-terminal cytosolic tail of the NHE6 protein (Fig. 10B).

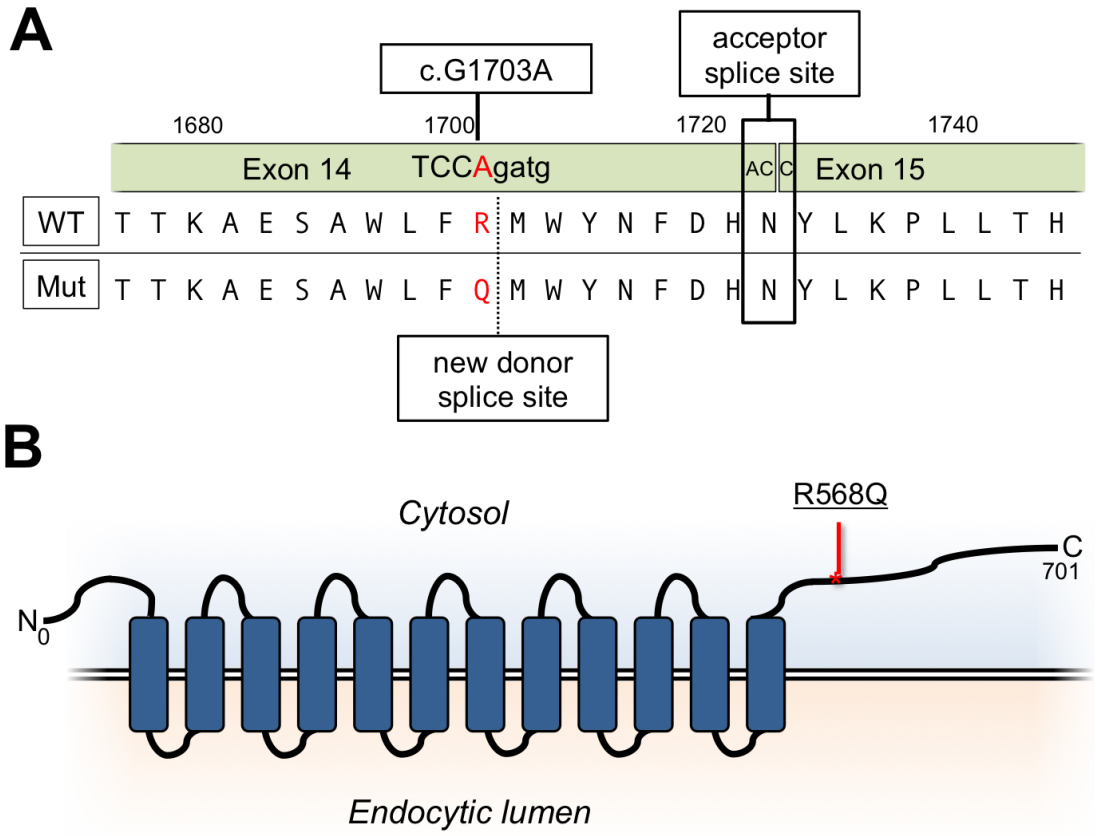

Fig. 10: Position of the c.G1703A/p.R568Q variant in the longest transcript with 701 amino acids (ENST00000370695). **A**: The G>A variant causes an R>Q amino acid exchange and is predicted to affect a nearby splice site between exon 14 and 15 by creating a new donor splice site. **B**: Approximate position of the p.R568Q variant in the c-terminus of the NHE6 protein. A putative RACK1 binding domain begins directly after the R568 residue.

The p.R568Q variant was also found in one healthy female control and one female with mild parkinsonian symptoms, and had been previously described in X-linked intellectual disability and schizophrenia,[325, 333, 338] suggesting that while the amino acid exchange might impair protein function or regulation, it is not as severe as in mutations causing a childhood disorder like CS. In the family described here, several family members were diagnosed with some form of tremor, of which at least two did

not carry the R568Q variant, suggesting additional or alternative factors involved in the two CBS cases. The importance of protective or aggravating secondary factors is underscored by the presence of the R568Q variant in another family, where two male carriers showed severe mental retardation and ataxia, while another male carrier was unaffected.[338]

2.5 Aim of this study

While CBS and CBD are both rare disease, protein accumulation and endosomal-lysosomal dysfunction occur in the vast majority of neurodegenerative diseases. Causative treatment is not available for any of the diseases at the moment, and since the etiology remains largely unclear, development of new drugs is difficult.

From control of nutrient availability, removal of toxic waste, and organellar quality control to receptor uptake, recycling and signalling, and intracellular trafficking of proteins crucial for correct cellular function, the endosomal-lysosomal system is involved in many essential processes. A number of studies have linked defective endosomal-lysosomal pH regulation to neurodegenerative diseases. Dysfunction or loss of NHE6 was previously shown in both age-related neurodegenerative and early-onset neurodevelopmental diseases, with mutations in *SLC9A6* causing CS.

This study aims to (1) functionally characterise the T489YfsX23 mutation and the R568Q variant in NHE6, and their consequences on protein function *in vitro* and *post mortem*; (2) to elucidate the consequences of loss of NHE6 function in a neuronal cell model on the endosomal-lysosomal system, and (3) to show downstream effects of a dysfunction of this system caused by NHE6 loss in terms of organellar quality control and tau pathology.

Taken together, this work investigates the dysfunction of pH regulation in the endosomal-lysosomal system in a model of neurodegenerative disease.

3. Results

3.1 Effects of the T489Yfs mutation and R568Q variant on NHE6 protein expression, stability and multimerisation

The T489Yfs mutation is disease-causing in hemizygous males[336], and the online tool MutationTaster2, which can be used to indicate the consequences and severity of a sequence change (disease causing or polymorphism)[339], predicts nonsense-mediated mRNA decay (NMD), in addition to the amino acid exchange, frameshift and premature stop codon that truncates the last 159 amino acids[1].

The T489 residue and the downstream sequence altered by the frameshift are highly conserved (Fig. 11), further explaining the severity of the mutation.

The R568Q variant, on the other hand, is a known polymorphism (dbSNP: rs146263125), even though the R568 residue is highly conserved between species (Fig. 12).

The SNP is found in 143 datasets in the Exome Aggregation Consortium (ExAC) database, which features the sequenced exomes of 60,706 individuals from different ethnicities.[340] Of these 143, 50 are hemizygous and none are homozygous, meaning 93 were found in heterozygous females. The overall allele frequency is very low (0.001631), and allele frequencies in the general population might indicate how well a certain exchange is tolerated, as alleles detrimental to survival or reproduction will be negatively selected during evolution[341]. It has to be kept in mind that the ExAC database includes a large set of exomes from Swedish schizophrenia and bipolar studies,[340] and the R568Q variant has previously been linked to schizophrenia,[333] leaving the possibility that at least a part of the alleles reported were found in psychiatric patients.

Analysis by MutationTaster2 predicted, apart from the change in the amino acid sequence, an additional donor splice site created by the G>A exchange with a

[1] (last retrieved on 25.04.2018 from *http://www.mutationtaster.org/cgi-bin/MutationTaster/MutationTaster69.cgi?sequence_snippet=TTCTGATTGTGTTTTTT[-/T]ACCGTGTGGGTATTTG&transcript_stable_id_text=ENST00000370695&gene=SLC9A6&transcript_stable_id_radio=ENST00000370695&sequence_type=cDNA&alteration_name=T489Yfs23X).*

confidence score of 0.81[2]. The creation of an additional splice site could result in a loss of 24 base pairs/eight amino acids (R568-H575) and a exchange in another one (N576H), as the AAC codon for N576 spans the exon 14-15 boundary (Fig. 13).

[2] Last retrieved on 25.04.18 from *http://www.mutationtaster.org/cgi-bin/MutationTaster/MutationTaster69.cgi?sequence_snippet=GTGCTTGGCTTTTCC[G/A]GATGTGGTACAACTTTG&transcript_stable_id_text=ENST00000370695&gene=SLC9A6&transcript_stable_id_radio=ENST00000370695&sequence_type=cDNA&alteration_name=R568Q*

Organism	Gene name	Start	Sequence	End
Homo sapiens	SLC9A6	485	MFAGLRGAMAFALAIRDTATYARQMMFSTTLLIVFFTVWVFGGGTTAMLS	534
Pan troglodytes	SLC9A6	314	MFAGLRGAMAFALAIRDTATYARQMMFSTTLLIVFFTVWVFGGGTTAMLS	363
Macaca mulatta	SLC9A6	485	MFAGLRGAMAFALAIRDTATYARQMMFSTTLLIVFFTVWVFGGGTTAMLS	534
Canis lupus	SLC9A6	487	MFAGLRGAMAFALAIRDTATYARQMMFSTTLLIVFFTVWVFGGGTTAMLS	536
Bovis taurus	SLC9A6	486	MFAGLRGAMAFALAIRDTATYARQMMFSTTLLIVFFTVWVFGGGTTAMLS	535
Mus musculus	SLC9A6	486	MFAGLRGAMAFALAIRDTATYARQMMFSTTLLIVFFTVWVFGGGTTAMLS	535
Rattus norvegicus	SLC9A6	486	MFAGLRGAMAFALAIRDTATYARQMMFSTTLLIVFFTVWVFGGGTTAMLS	535
Gallus gallus	SLC9A6	519	MFAGLRGAMAFALAIRDTATYARQMMFSTTLLIVFFTVWVFGGGTTAMLS	568
Xenopus tropicalis	slc9a6	495	MFAGLRGAMAFALAIRDTATYARQMMFSTTLLIVFFTVWVFGGGTTAMLS	544
Danio rerio	slc9a6	473	MFAGLRGAMTFALSIRDTATYARQMMFSTTLLVVFFTVWICGGGTTQMLS	522
Drosophila melanogaster	Nhe3	461	FFAGLRGAMSFALAIRNTVSDERQTMLTATSLIVIFTVVIQGGAANFLLN	510
Anopheles gambiae	AgaP_AGAP008718	485	FFAGLRGAMSFALAIRNTVSDARQAMLTTTSLIVITTVIIQGGAANFLLN	534
Caenorhabditis elegans	nhx-5	456	LFAGLRGAMAFALAGRNTSTENRQMIFATTTAVVIVTVLVNGGLTSWMID	505

Fig. 11: Alignment of the amino acids from the human SLC9A6 region containing the T489 residue altered by the c.1464_1465insT/p.T489YfsX23 mutation with several mammalian, vertebrate and invertebrate organisms. The T489 residue is conserved in all species and the overall region is highly conserved as well, especially in vertebrates. (Numbers correspond to the longest human NHE6 isoform and not to the isoform used for the inital description of the mutation by Riess et al.). Red indicates the amino acids changed by the mutation.

Organism	Gene name	Start	Sequence	Stop
Homo sapiens	SLC9A6	548	----------H-LGVPENERRTTKAESAWLFRMWYNFDH	575
Pan troglodytes	SLC9A6	377	----------H-LGVPENERRTTKAESAWLFRMWYNFDH	404
Mus mulatta	SLC9A6	548	----------H-LGIPENERRTTKAESAWLFRMWYNFDH	575
Canis lupus	SLC9A6	550	----------H-LGIPENERRTTKAESAWLFRIWYNFDH	577
Bovis taurus	SLC9A6	549	----------H-LGIPESERRTTKAESAWLFRMWYNFDH	576
Mus musculus	SLC9A6	549	----------H-LGVPDNERRTTKAESAWLFRMWYNFDH	576
Rattus norvegicus	SLC9A6	549	----------H-LGVPDNERRTTKAESAWLFRMWYNFDH	576
Gallus gallus	SLC9A6	582	----------N-VGVPESERRSTKAESAWLFRMWYNFDH	609
Xenopus tropicalis	slc9a6	558	----------Q-MAIPENERRSTKAESAWIFRLWYNFDH	585
Danio rerio	slc9a6	536	----------NSIGPDGVERRSTKQESAWLFRIWYNFDH	564
Drosophila melanogaster	Nhe3	560	NKMRLSGGTDTNLDTPVDGTNGSLGGASGGRRRNSHEKAILARIWGNFDT	609
Anopheles gambiae	AgaP_AGAP008718	585	SIKRCLASVTRRIQQSDLENPDSEGATTPGGTRRGHEKAVLARLWGNFDS	634
Caenorhabditis elegans	nhx-5	519	-GQRLENSMSSSPADQHSDLDESVPVTMSPG-LNPWDKAFLPRKWYHFDA	566

Fig. 12: Alignment of the amino acids from the human SLC9A6 region containing the R568 residue altered by c.G1703A/p.R568Q variant with several mammalian, vertebrate and invertebrate organisms. The R568 residue is conserved in all species, while the region is mostly conserved in vertebrates, with a higher level of conservation in mammals. The R568 residue altered by the c.G1703A/p.R568Q variant is marked in red.

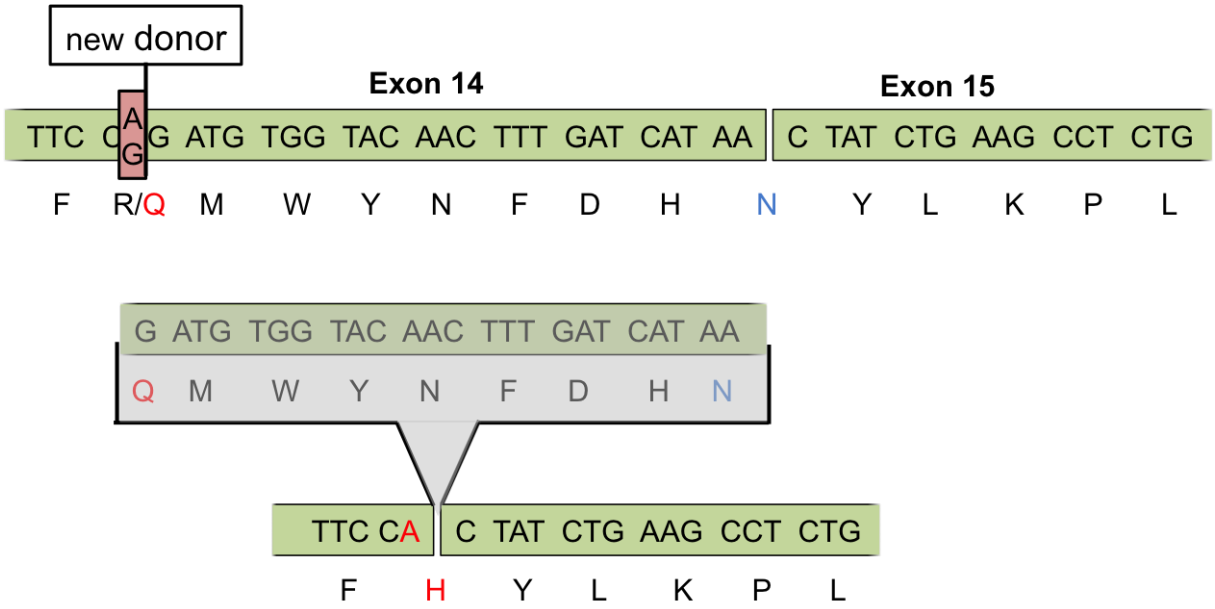

Fig. 13: Depiction of the predicted splice site change by the c.G1703A variant. The is c.G1703A exchange in exon 14 (bases in red) produces a new splice donor that would lead to an omission of amino acids 569-575 (shown in grey above exons 14 and 15). The omission of the base 1704 (G) and of the first two bases (AA) coding for N576 (in blue) at the new splice site would result in a CAC codon and a histidine at position 568 (shown in red in the lower schematic).

To test whether the splice site is affected, RNA was extracted from the medical frontal cortex of two R568Q carriers: one with autopsy-confirmed CBD and one with CBS and a mixed pathology. The pathological examination was carried out by Dennis W. Dickson, Department of Neuroscience, Mayo Clinic Florida, Jacksonville, Florida, USA. Samples used for controls were matched to the pathologies and consistent of an autopsy-confirmed CBD patient and a patient with a mixed Lewy body pathology which both had no known variant or mutation in *SLC9A6*. All samples of different brain regions used for experimental procedures in this work were prepared by Michael A. DeTure, Department of Neuroscience, Mayo Clinic Florida, Jacksonville, USA. After reverse transcription into cDNA, a polymerase chain reaction (PCR) was performed with a forward primer binding in exon 13, and a reverse primer in exon 16 (Fig. 14A) The product would encompass the splice site predicted to be influenced by the G1703A variant. However, the size of the PCR products on an agarose gel did not differ between R568Q carriers and controls, as all bands appeared at the expected size of approx. 480bp and not the approx. 450bp expected if the splice site was affected (Fig. 14B). Sequencing of the PCR product revealed only the wildtype allele, which might suggest that the variant is not expressed in the medial frontal cortex of the two patients (Fig. 14C). While the possibility exists that only the wildtype

allele is expressed, a persistent contamination with the T489Yfs NHE6 expression construct that was also present in the H_2O control in the PCR used for the sequencing run complicates the interpretation of this finding (Fig. 14D). Since the contamination occurred after replacing all reagents and changing equipment, it would be necessary to find the source before the possibilities of a splicing defect or the sole expression of the wildtype allele could be confirmed or rejected.

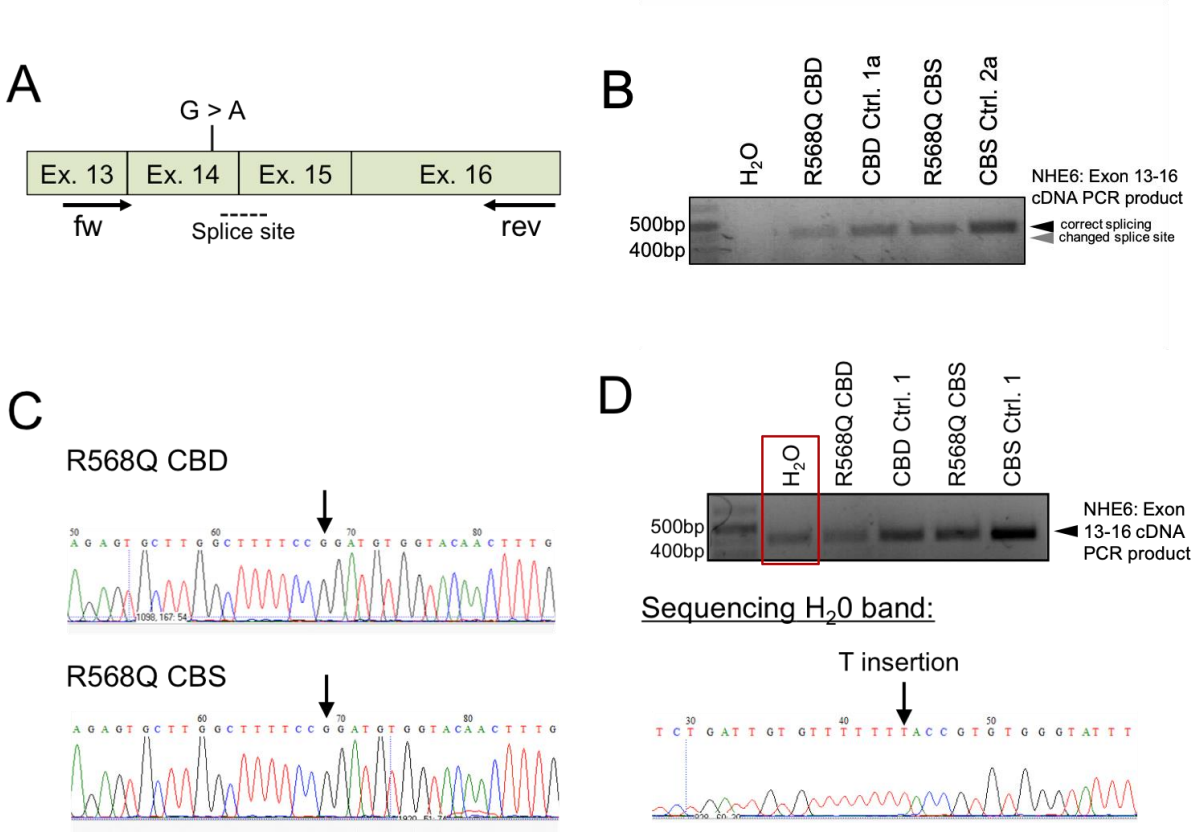

Fig. 14: Results of a qualitative reverse-transcription PCR (RT-PCR) for the potential splicing defect in brain samples from two R568Q carriers and pathology-matched controls. **A**: Schematic of forward and reverse primer positions in exon 13 and 16, respectively, resulting in a PCR product that contains the region of the predicted splice site change between exon 14 and 15. **B**: Results of a PCR using the primers shown in (A) on cDNA isolated from the medial frontal cortex of two R568Q carriers and pathology-matched controls. Expected size of the PCR product: approx. 480bp (black arrowhead). The predicted additional splice site would result in a product of approx. 450bp (grey arrowhead). **C:** Results from sequencing of the cDNA-derived PCR product from medial frontal cortex samples of the two R568Q carriers. Only the wildtype base (G) is present (arrow). **D**: Contamination in the H_2O control (red square) that was also present in the PCR for the sequencing run. Sequencing of the contamination (below) revealed it to be the T489Yfs NHE6 cDNA expression construct (arrow indicates the inserted T). The PCR was conducted three times using the same samples.

3.1.1 T489Yfs and R568Q NHE6 are expressed and partially removed via the proteasome

As a premature stop codon often results in nonsense-mediated mRNA decay, there was the possibility that the T489Yfs mutation leads to a reduction in NHE6 mRNA. To test this, RNA was extracted from a fibroblast line of a c.1464_1465insT carrier (index patient in Fig. 9) previously established by Dr. Dajana Großmann (Department of Neurodegenerative Diseases, Centre of Neurology and Hertie Institute for Clinical Brain Research, University of Tübingen, Tübingen, Germany at the time of the establishment of the cell line; now: Luxembourg Centre for Systems Biomedicine (LCSB), University of Luxembourg, Esch-sur-Alzette, Luxembourg) and Brigitte Maurer (Department of Neurodegenerative Diseases, Centre of Neurology and Hertie Institute for Clinical Brain Research, University of Tübingen, Tübingen, Germany at the time of the establishment of the cell line). After reverse transcription into cDNA, a PCR with primers against NHE6 and against Glyceraldehyde 3-phosphate dehydrogenase (GAPDH) as an input control was performed. Agarose gel electrophoresis of the semiquantitative PCR showed no difference in NHE6 cDNA levels between patient fibroblasts and a female control line (Fig. 15A), indicating that the premature stop codon caused by the T489Yfs mutation does not lead to nonsense-mediated mRNA decay. The commercial antibodies available for NHE6 usually bind in the C-terminus truncated by the T489Yfs mutation, and using an antibody directed against an N-terminal epitope did not show a specific band against the truncated protein even in an overexpression setting (Fig. 16).

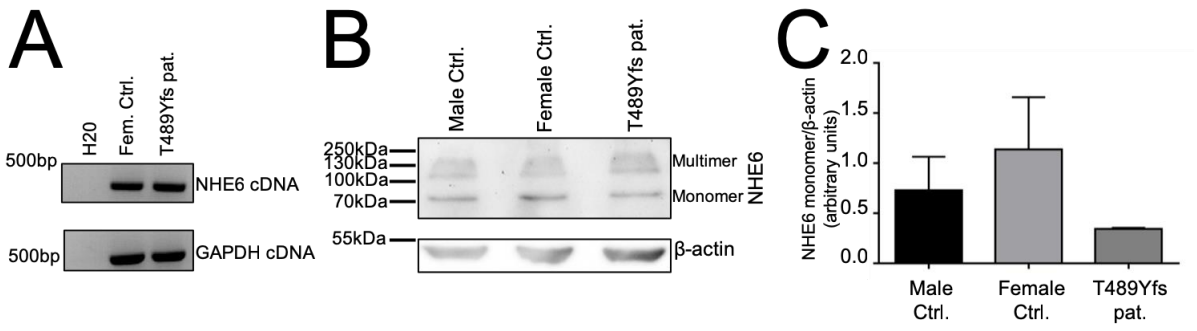

Fig. 15: mRNA and protein levels of NHE6 in fibroblasts from a patient carrying the T489Yfs23X mutation. The fibroblast line was established by Dr. Dajana Großmann and Brigitte Maurer at the Department of Neurodegenerative Diseases, Centre of Neurology and Hertie Institute for Clinical Brain Research, University of Tübingen, Tübingen, Germany. **A**: Semi-quantitative RT-PCR using primers against NHE6 and GAPDH on cDNA generated from RNA from a female healthy control and the T489Yfs23X patient firboblasts. Representative gel electrophoresis picture of three independent

experiments. **B**: Western blot with lysates from male and female healthy control fibroblasts using an antibody against the C-terminus of NHE6 (which does not detect the truncated T489YfsX23 form) and β-actin as a loading control. Representative blot of n=3. **C**: Densitometry of the (full-length) NHE6 monomer band obtained by Western blot, normalised to β-actin loading control. Mean of n=3, error bars: S.D.

Therefore, only full-length NHE6 protein could be detected in cell lysates from the patient's fibroblasts on a Western blot (Fig. 15B). Densitometry performed on Western blots showed that levels of full-length protein are diminished in the patient compared to cells from a male and a female control (Fig. 15C). Together with the finding that mRNA levels are approximately equal in patient and a female healthy control, this suggests either a higher level of degradation or an equal expression of WT and mutant allele, from which only the WT form can be detected.

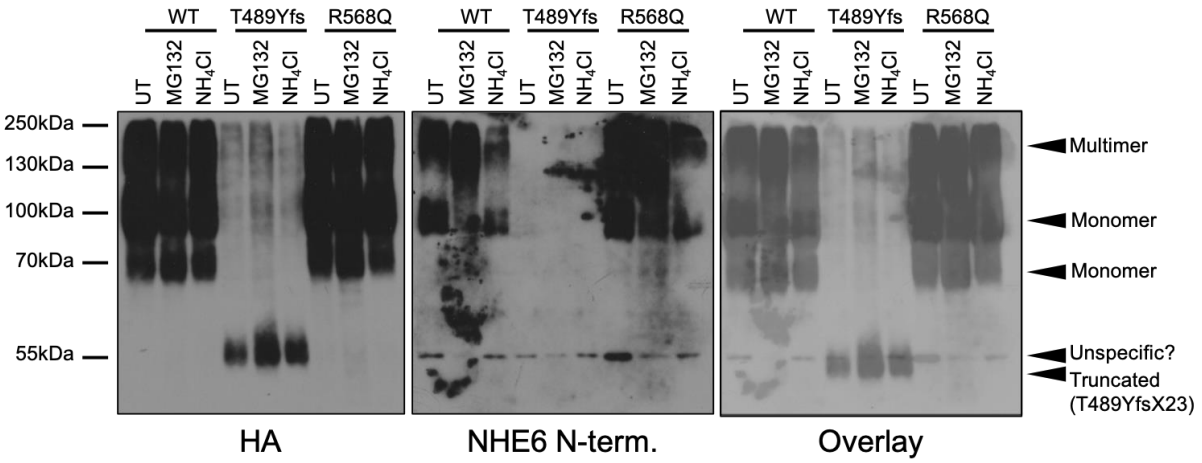

Fig. 16: Test of a commercial N-terminal NHE6 antibody (NHE6 N-term.) using in cell lysates from M17 neuroblastoma cells overexpressing either WT, T489Yfs or R568Q NHE6. Cells were transfected for 48h and either treated with normal growth medum (untreated, UT), 10µM MG132 (proteasomal inhibition) or 10mM NH_4Cl (lysosomal inhibition) for 24h before lysis. The antibody directed against the N-terminus of NHE6 does not show the truncated form detected by the antibody directed against the HA-tag in the N-terminus of the overexpressed cDNA. A band at approximately 55kDa is apparent in all conditions and potentially unspecific as the HA-antibody does not detect it. No further experiments were conducted apart from the blot shown.

To test for the possibility of degradation, a cDNA construct expressing the longest isoform of NHE6 was mutated by site-directed mutagenesis. The construct carries an haemaglutinin (HA)-tag in the first extravesicular loop of the protein and a C-terminal enhanced green fluorescent protein (eGFP); the tags were previously shown not to

affect location of the protein.[329] The HA-tag makes it possible to detect even the C-terminally truncated protein resulting from the T489Yfs mutation.

The NHE6 WT control expressing construct, as well as plasmids expressing NHE6 cDNA with the T489Yfs mutant or R568Q variant, were transfected into M17 neuroblastoma cells. To test for the possibility that the variant and mutant proteins were removed via the proteasome or the lysosome, cells were either treated with 10µM MG132 for 24 hours before lysis to inhibit the proteasome, or with 10mM NH_4Cl for inhibition of the lysosomal pathway. 48h after transfection cells were lysed and proteins separated by sodium dodecyl sulfate–polyacrylamide gel electrophoresis (SDS-PAGE) before blotting and detection with an antibody against the HA-tag in the N-terminus of the protein (Fig. 17A).

Analysis of the Western blot revealed that the T489Yfs is present in very low levels but accumulates significantly after inhibition of the proteasome with MG132 (Fig. 19B). A similar trend was observed for the R568Q variant, but the effect did not reach statistical significance (Fig. 17B). The change from untreated to MG132 treated conditions did not lead to a strong accumulation of WT NHE6 protein, indicating that the protein is not rapidly turned over under normal conditions. Treatment with the lysosomal inhibitor NH_4Cl did not lead to increased levels of any of the NHE6 forms, but to a small, yet significant decrease in T489Yfs NHE6 levels (Fig 17A, B). A similar minor reduction was also observable in wildtype and R568Q overexpressing cells, but effects for all three constructs were small and might be explained by a mild compensatory upregulation of the proteosomal pathway after lysosomal inhibition.

Overall levels of T489Yfs NHE6 protein on Western blot were strongly decreased compared to NHE6 WT and R568Q overexpressing conditions. This would be in line with a predicted NMD of the mRNA, and the existence of a protein could be explained by some mRNA escaping degradation. However, levels of protein in an overexpression system depend on a number of factors, including possible differences in secondary structure of the cDNA construct or differences in transfection efficiency. It is also possible that the overexpression of a mutant protein might influence the number of cells surviving transfection.

Overexpression of NHE6 WT, T489Yfs and R568Q NHE6 cDNA constructs without an eGFP, but with the HA-tag in SH-SY5Y neuroblastoma cells transfected for 48h and immunostained for the HA-tag showed that both the T489Yfs mutation and the R568Q variant are expressed and detectable in untreated cells (Fig. 17C).

Staining against HA also showed accumulation of WT and R568Q NHE6 in puncta that partially colocalised with the early endosomal marker protein EEA1, while the overexpression of T489Yfs NHE6 resulted in a more uniform staining that does not overlap with EEA1 staining (Fig. 18 and Appendix Fig. 40). Not enough transfected cells could be observed for a more detailed analysis of colocolasation between the different NHE6 constructs and EEA1, but differences in localisation of the protein could further influence the phenotype even if ion exchanger function is partially preserved after alterations in the amino acid sequence of the protein.

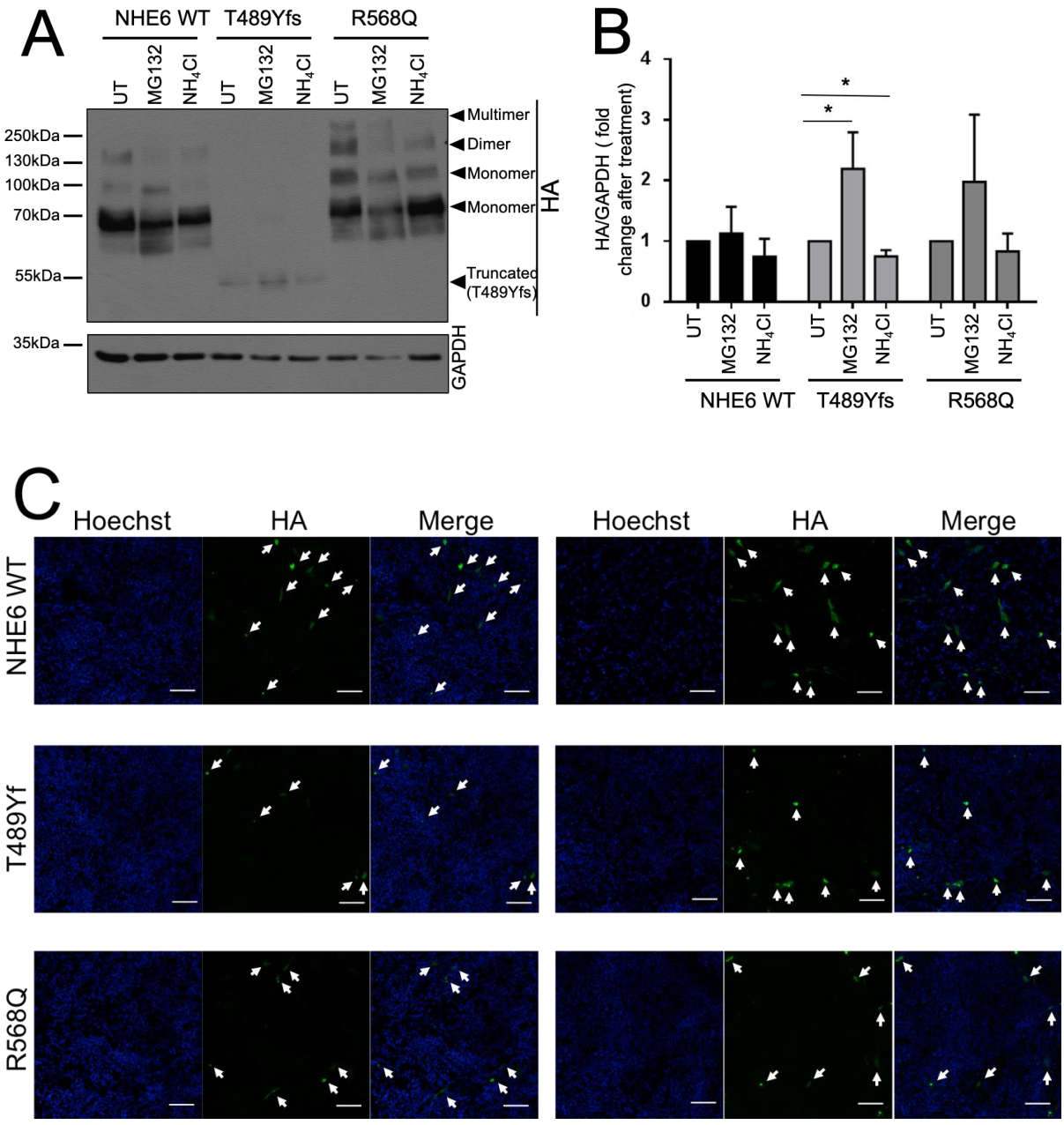

Fig. 17: Proteasomal and lysosomal removal of overexpressed WT, T489Yfs or R568Q NHE6. **A**: Western blot showing changes in NHE6 protein levels in lysates from M17 neuroblastoma cells overexpressing WT, T489Yfs or R568Q cDNA. M17 neuroblastoma cells were transfected for 48h and

either treated with normal growth medium (untreated, UT), 10µM MG132 (proteasomal inhibition) or 10mM NH_4Cl (lysosomal inhibition) for 24h before lysis. An antibody directed against the N-terminal HA-tag in the cDNA was used for detection of the protein. Blot representative of n=3. **B**: Densitometry results of Western blot bands in (A) and two further experiments. Levels of overexpressed HA-tagged NHE6 (HA) were normalised to GAPDH loading control and are shown as change in protein levels after treatment (normalised to the untreated condition for each overexpression condition). Mean of n=3, error bars: S.D., *$p<0.05$ **C**: Immunostaining of SH-SY5Y neuroblastoma cells transfected for 48h with NHE6 WT, T489Yfs or R568Q NHE6 using an antibody directed against the HA-tag in the N-terminus of the overexpression construct (green). Arrows indicate cells positive for HA. Hoechst was used as a nuclear stain (blue). Scale bar: 100µM. Pictures representative of n=3.

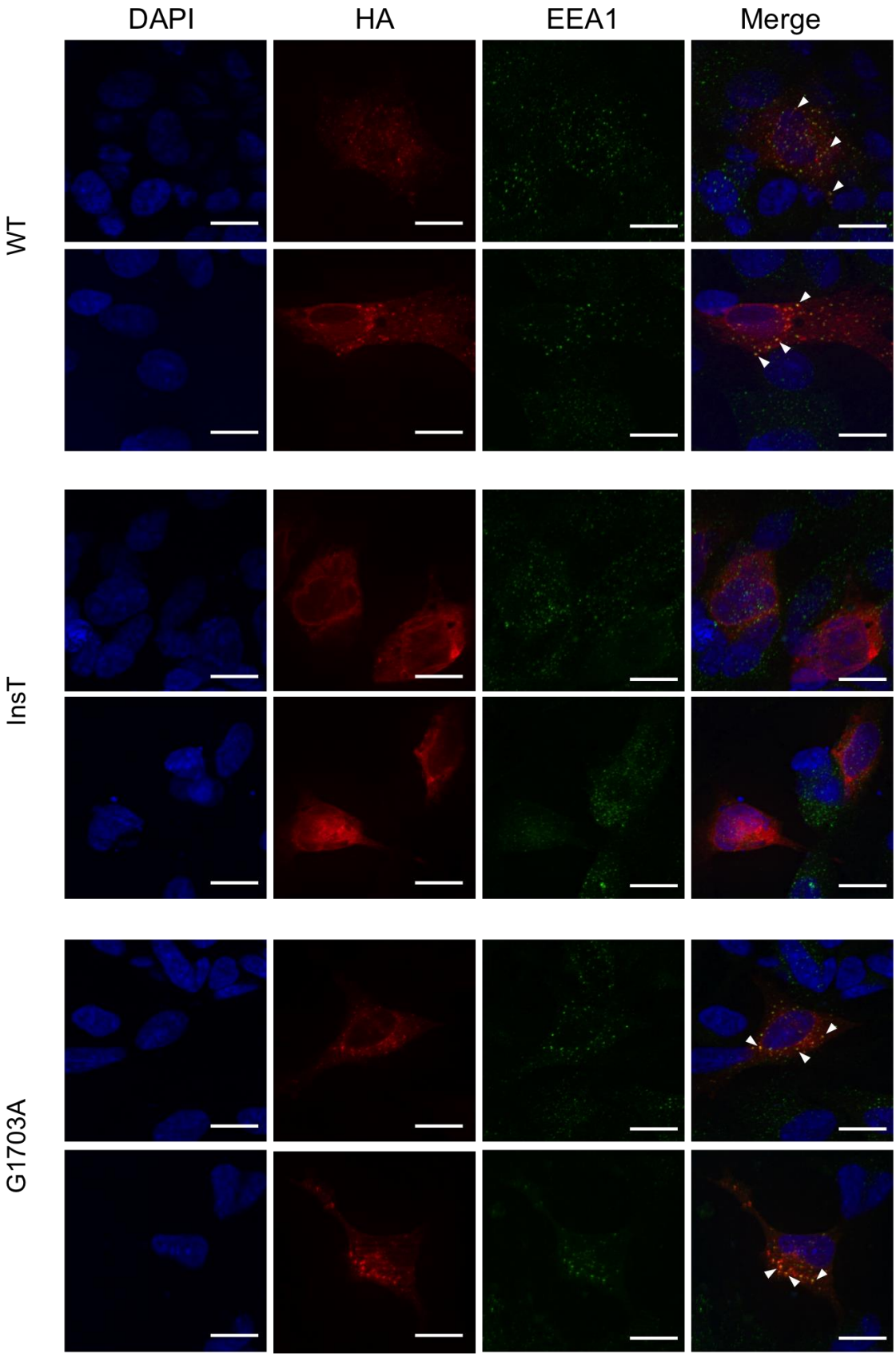

Fig. 18: Immunostaining for HA (red) and EEA1 (green) in SH-SY5Y neuroblastoma cells overexpressing WT, T489Yfs and R568Q HA-tagged NHE6 cDNA. Hoechst 33258 was used to stain the nucleus (blue). Arrowheads indicate overlap in HA and EEA1 staining; no overlap was detected for T489Yfs NHE6-HA and EEA1. Scale bar: 16µM. Pictures representative of n=3.

3.1.2 Multimerisation of NHE6 is defective in the T489Yfs mutant, but unaffected by the R568Q variant

To further analyse the effect of the T489Yfs mutation and R568Q variant, both constructs were overexpressed in M17 neuroblastoma cells along with a transfection control (the vector without an insert) and a NHE6 WT construct. 48h after transfection, cells were lysed and lysates treated with 0.025% glutaraldehyde for 5 minutes, a crosslinker that keeps proteins in their multimeric form even under denaturing conditions during SDS-PAGE and Western blotting. Because NHE6 had previously been shown to form dimers for function[329], the question of multimerisation is of special interested. While the R568Q variant did not show any effect on multimerisation as higher molecular weight bands resembled that of the WT protein, the T489Yfs protein showed a main band at approx. 55kDa, which would be the molecular weigth expected for a monomeric truncated protein of 512 amino acids. Thus, it is likely that the T489Yfs mutant leads to a failure to multimerise, suggesting that a functional protein complex cannot be formed (Fig. 19A).

A similar experiment performed on fibroblasts revealed reduced levels of functional multimers in the T489Yfs carrying patient compared to controls (Fig. 19B), which is in line with the lower full-length protein level observed by standard Western blotting. Unfortunately, it was again not possible to answer the question of an endogenous expression of the T489Yfs NHE6 protein and the effects on multimerisation as the NHE6 antibody only detects the full-length wildtype form.

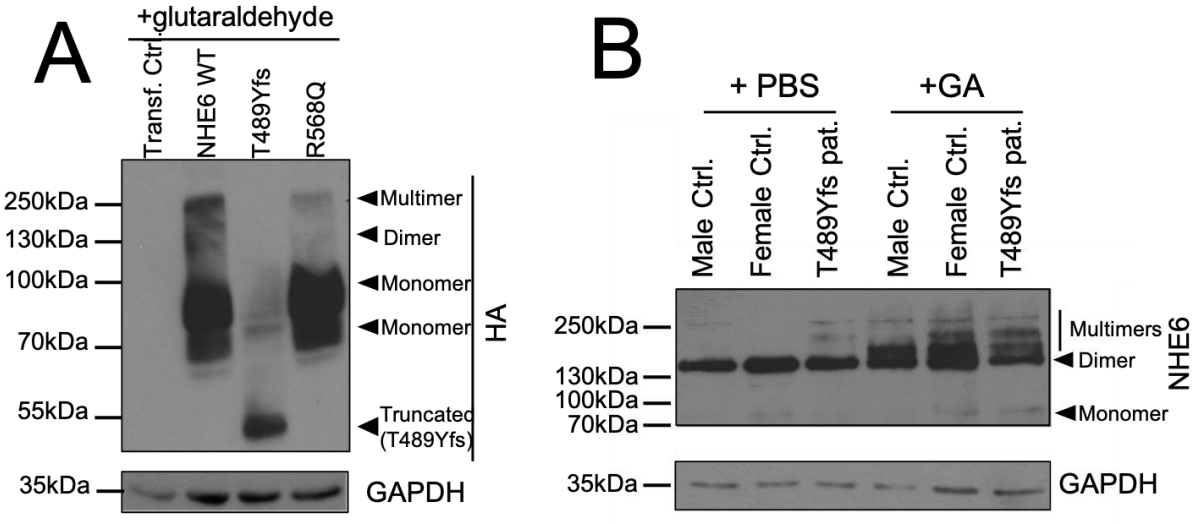

Fig. 19: Western blots showing multimers of NHE6 after cross-linking of lysates. **A**: Western blot for HA in M17 neuroblastoma cells overexpressing a transfection control (vector only), WT, T489Yfs or R568Q HA-tagged NHE6 cDNA for 48h. Lysates were treated with glutaraldehyde for the cross-linking

of protein complexes. GAPDH was used as a loading control. Representative blot of n=3. **B**: Western blot for endogenous NHE6 in fibroblast samples from a healthy male, healthy female or the T489Yfs CBS patient after crosslinking. Samples were either incubated with glutaraldehyde (GA) or PBS and the Western blot probed for NHE6. GAPDH was used as a loading control. Representative blot of n=3.

3.1.3 The chaperone Binding immunoglobulin protein/78 kDa glucose-regulated protein (BiP/GRP78) involved in unfolded protein response and ERAD is upregulated in cells overexpressing T489Yfs or R568Q NHE6

Since the T489Yfs mutation and the R568Q variant could affect the folding of the protein, levels of the chaperone BiP/GRP78 were determined by Western blot.
BiP/GRP78 is a protein involved in the ER-associated degradation of misfolded proteins, and is upregulated during the unfolded protein response (UPR).[342]
Levels of BiP were assessed by Western blotting 48h after transfection of M17 cells with a transfection control, NHE6 WT and T489Yfs and R568Q NHE6 overexpressing vectors. BiP levels were significantly elevated in the T489Yfs overexpressing cells compared to the transfection control, and strongly elevated in the R568Q variant expressing cells, even though this did not reach statistical significance if densitometry results are compared (Fig. 20A). The higher levels of BiP after overexpression of T489Yfs NHE6 are in line with the proteasomal degradation of the protein observed earlier. T489Yfs NHE6 might elicit UPR with an upregulation of BiP, which in turn initiates ERAD and protein removal via the proteasome.
Conversely, the significant increase in BiP in NHE6 WT overexpressing cells (Fig. 20A) is in contrast to the unchanged levels of WT NHE6 after inhibition of the proteasome as shown in Fig. 17A and Fig. 17B. There is the possibility that the overexpression of the protein leads to an excess of protein in the ER and elicits an unfolded protein response without significant levels of ERAD as the protein can be folded by the increased levels of chaperone.
To test whether the fibroblast cell model from the T489Yfs patient showed a similar increase of BiP, cell lysates were analysed using Western blot. A moderate increase of BiP in patient fibroblasts could be observed (Fig. 20B); however, this was not statistically significant and variable. For the interpretation of these results, it should be taken into account that NHE6 expression is very low in fibroblasts in general. This is especially true compared to an overexpression setting, so it is not unexpected to

see a strong ERAD or UPR response to potentially un- or misfolded T489Yfs NHE6 in these cells.

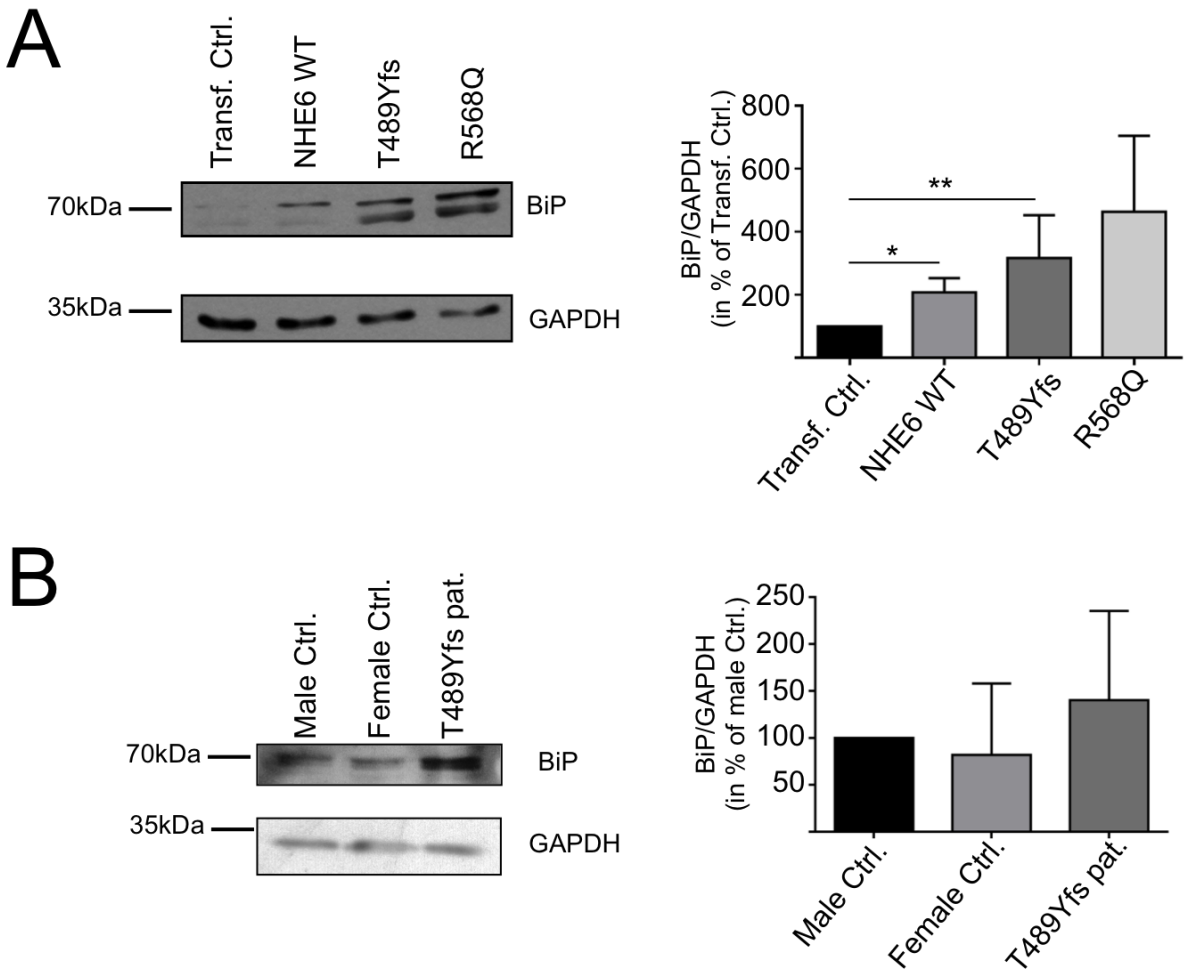

Fig. 20: Protein levels of the ER-associated chaperone BiP/GRP78 in response to the T489Yfs mutation or R568Q variant in the M17 overexpression model or fibroblasts. **A**: Western blot for BiP/GRP78 in protein samples from M17 neuroblastoma cells transfected with an empty vector as transfection control, NHE6 WT and T489Yfs or R568Q NHE6 for 48h before lysis. GAPDH was used as a loading control. Representative blot of n=3. (*Right*) Densitometry for BiP bands on the Western blot normalised to GAPDH expressed in percent of transfection control levels. Mean of n=3, error bars: S.D. *p<0.05, **p<0.01 **B**: Western blot for BiP/GRP78 levels in lysates from healthy male, healthy female or T489Yfs CBS patient fibroblasts. GAPDH was used as a loading control. Representative blot of n=3. (*Right*) Densitometry for BiP bands on Western blots normalised to GAPDH expressed in percent of healthy male control levels. Mean of n=3 error bars: S.D.

3.2 Inducible NHE6 knockdown model in M17 neuroblastoma cells

Since the results obtained from both the T489Yfs overexpression models and T489Yfs patient fibroblasts suggest a loss of NHE6 protein through proteasomal

degradation, an inducible NHE6 k.d. model in M17 neuroblastoma cells was created. To this end, an microRNA (miRNA) directed against the 3'UTR of the NHE6 mRNA was cloned into a vector with a cytomegalovirus (CMV) promoter containing Tetracycline (Tet)-repressor binding sites. This vector was then transfected into the cells along with a vector expressing a Tet-repressor that silenced expression of the construct. Treatment with 1µM Tetracycline was used to release the Tet-repressor from the Tet-binding site in the promoter, thereby facilitating expression of the miRNA and knockdown of NHE6. As a control, a similar construct carrying a non-targeting, commercial miRNA was used (supplied with the BlockIT kit used). First, the induction of miRNA expression was confirmed by treatment of cells expressing EmGFP together with the miRNA using 1µM Tetracycline. Cells showed a strong expression of EmGFP for both non-targeting and NHE6 knockdown miRNA vectors at 72h and 96h after the start of the induction (Appendix Fig. 41). For further experiments, the EmGFP was removed using DraI restrictions sites to avoid difficulties in experiments measuring any kind of fluorescence. In all cases, cells were selected for the pT-REx-DEST30 expression vector, and the pcDNA6/TR vector that expresses the Tet-repressor element until untransfected control cells had died.

In M17 neuroblastoma cells transfected with the pT-REx-DEST30 expression vector without EmGFP along the Tet-repressor vector, Western blot analysis showed reduced levels of multimeric NHE6 compared to cells with the non-targeting control miRNA after 72h of induction 1µM Tetracycline (Fig. 21A). A second band detectable at around 140kDa was not reduced by the miRNA but was also not increased by NHE6 WT overexpression in SH-SY5Y cells on Western blot (Fig. 22). Therefore it might be speculated that the observed band is not a specific detection of NHE6.

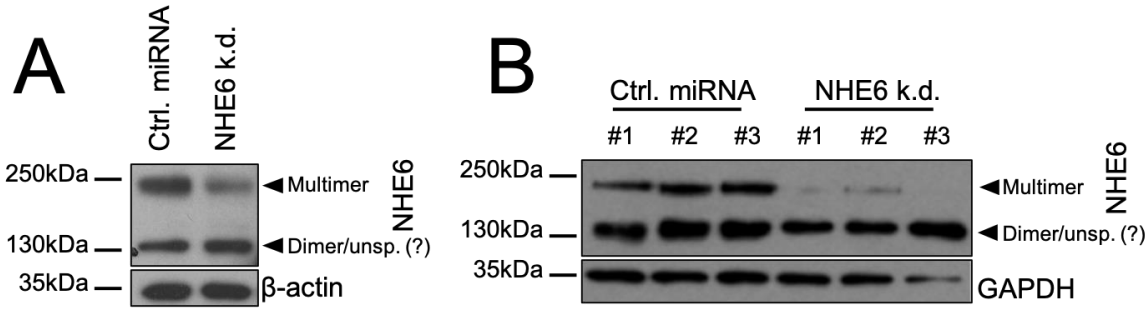

Fig. 21: NHE6 levels in lysates from M17 cells inducibly expressing a non-targeting control miRNA or a knockdown miRNA directed against the 3'UTR of the NHE6 mRNA. **A**: Western blot showing NHE6 levels in polyclonal inducible NHE6 knockdown or control miRNA lines 72h after inducting with 1µM Tetracycline. Western blot against NHE6, β-actin was used as a loading control. Representative blot of

n=3. **B**: Western blot for NHE6 levels in three monoclonal lines per condition (NHE6 knockdown or control miRNA, #1-#3). The lines were induced for 96h using 1µM Tetracycline. Monoclonal lines were generated by single-cell seeding. Representative blot of n=3.

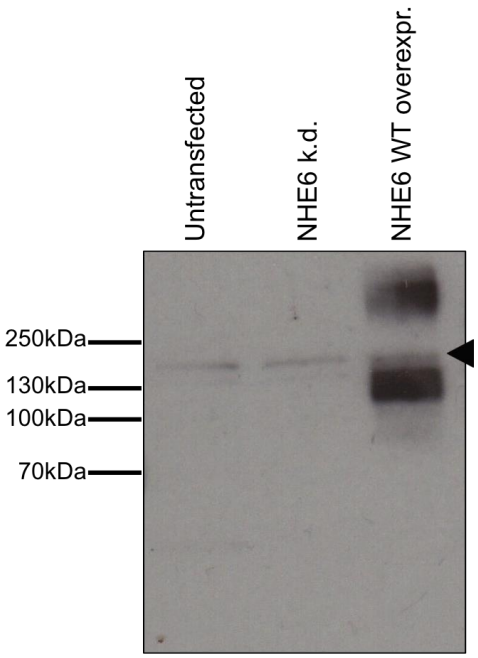

Fig. 22: Western blot NHE6 protein levels in SH-SY5Y neuroblastoma cells that were either untransfected, transfected with a NHE6 knockdown miRNA, or transfected with a cDNA-construct overexpressing WT NHE6. The Western blot was probed using the MBL NHE6 antibody. The antibody detects a band at around 140kDa in all three conditions (arrow head), however, the band is not increased in the overexpression setting. It is possible that the detected band is not specific for NHE6.

Since the amount of vectors transfected into cells can vary highly, polyclonal cells are difficult to use for quantitative microscopy experiments as the level of miRNA expression, and therefore the level of NHE6 k.d., differs greatly between single cells. In quantitative analyses, this can create a high intraexperimental error that is not due to natural variation, but rather variation in k.d. levels. To rule out this effect and to be able to more correctly assess the consequences of loss of NHE6 protein, monoclonal lines were created from a single mother cell, thereby leading to a more homogenous k.d. level in all cells of the population. For experiments, three different monoclonal lines that showed the strongest k.d. of NHE6 as shown by Western blot were used, along with control lines that were created using the same conditions. The NHE6 k.d. lines showed a strong decrease in NHE6 protein 96h after induction with 1µM Tetracycline compared to cells expressing the control miRNA, and levels of NHE6 knockdown were comparable between the three lines used (Fig. 21B). While 72h of induction showed a k.d. effect in polyclonal cells, 96h of induction were needed in the monoclonal setting, possibily due to differences in levels of the co-transfected Tet-repressor expression vector.

3.3 Marker proteins of the endosomal-lysosomal system are altered in NHE6 knockdown M17 neuroblastoma cells

Because NHE6 is involved in the correct function of the endosomal-lysosomal system, the levels of marker proteins for various compartments of the pathway were assessed in polyclonal M17 cells after k.d. of NHE6. 72h after induction cell lysates were collected and subjected to Western blotting. Analysis of levels of marker proteins showed a strong and highly significant reduction of clathrin (Fig. 23A), a protein involved in clathrin-dependent, receptor-mediated endocytosis. NHE6 has previously been shown to play a role in some, but not all modes of clathrin-dependent endocytosis as it is transiently found at the plasma membrane[317], and NHE6 seems to have a strong effect on clathrin levels in M17 neuroblastoma cells, either directly or through an interaction.

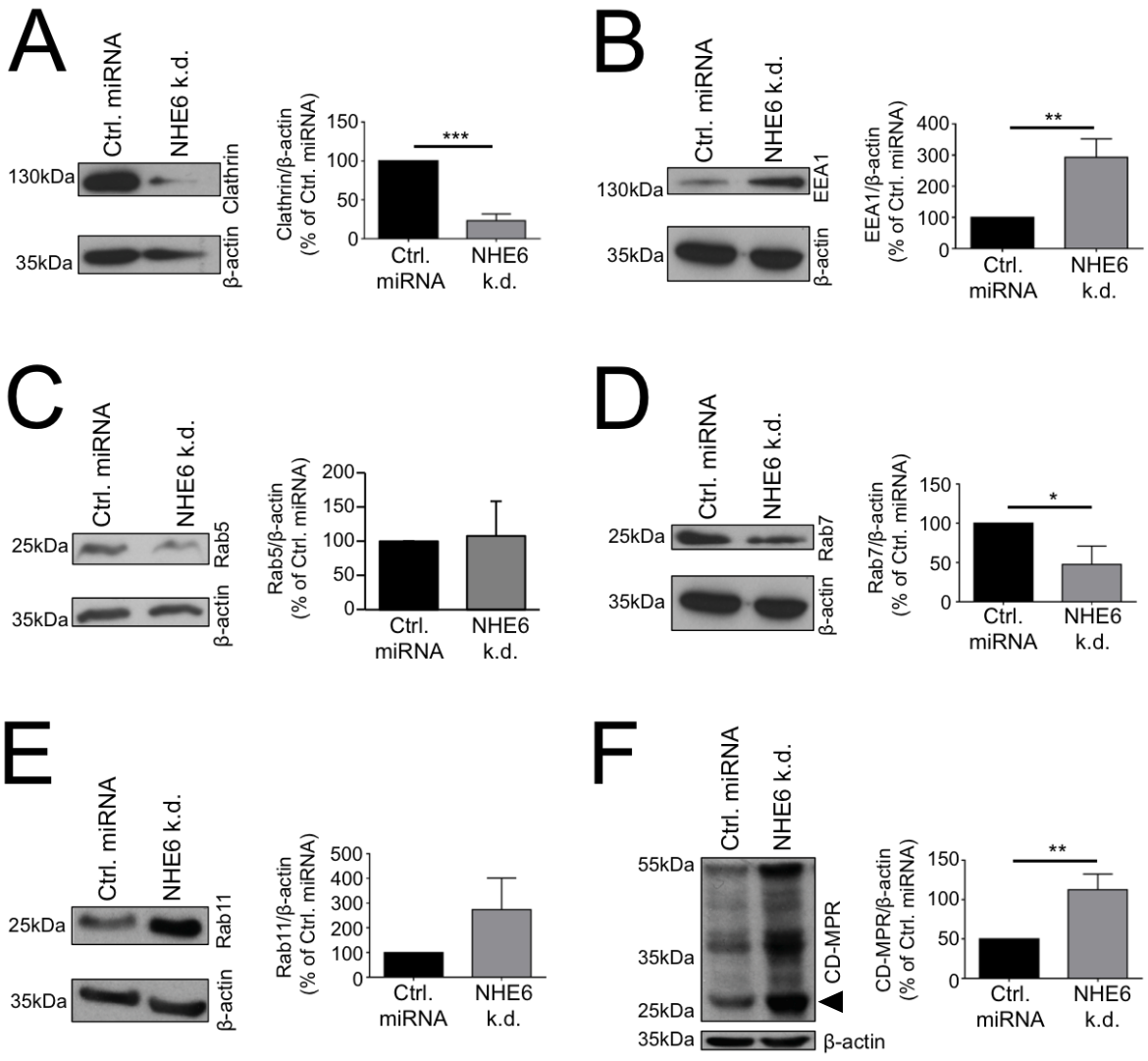

Fig. 23: Western blot and quantification of band intensity by densitometry analysis for endosomal marker proteins in M17 cells with NHE6 k.d. or a non-targeting control miRNA 72h after induction. **A**:

Western blot probed for clathrin (involved in clathrin-dependent endocytosis) and densitometry results normalised to loading control levels. **B**: Western blot probed for EEA1 (early endosome) and densitometry results normalised to loading control levels. **C**: Western blot probed for Rab5 (early endosome) and densitometry results normalised to loading control levels. **D**: Western blot probed for Rab7 (late endosome) and densitometry results normalised to loading control levels. **E**: Western blot probed for Rab11 (recycling endosome) and densitometry results normalised to loading control levels. **F**: Western blot probed for Cation-Dependent Mannose-6-Phosphate Receptor (CD-MPR) involved in Golgi-to-endosomal transport of proteins and densitometry results normalised to loading control levels. Arrow indicates predicated size (28kDa). For all Western blots, β-actin was used as a loading control. Quantifications are expressed in percent of the non-targeting control miRNA values. All graphs are mean of n=3, error bars: S.D., *p<0.05, **p<0.01, ***p<0.005, all blots are representative of n=3.

Conversely, levels of the early endosomal marker protein EEA1 were significantly increased in cells lacking despite the changes in clathrin and EEA1 levels (Fig. 23B). Rab5 acts on the intermediate structure between endocytosed vesicles and early endosome, aiding the conversion of these vesicles into or the addition to already existing early endosomes. For this, it forms a tether together with EEA1 to facilitate the fusion of pre-early and early endosomes[143]. Unlike EEA1, however, levels in Rab5 seem to be unaffected by a change in NHE6 levels (Fig. 23C). The reduction in clathrin and, potentially, vesicles originating from clathrin-dependent endocytosis on the one hand, and an increase in EEA1 and, potentially, mature early endosomes on the other, might lead to no detectable changes in the protein important for intermediate steps.

Assessment of Rab7 levels showed a decrease in the late endosomal protein (Fig. Fig. 23D). Together with the observed increase in EEA1, this suggest a defect of the endosomal maturation process from early to late ensosome in NHE6 k.d. cells.

In line with a model of defection endosomal maturation into the late endosomal pathway, levels of Rab11, a marker protein of the recycling endosome important for receptor recycling from the early endosome to the PM were increased, albeit not significantly (Fig. 23E).

Another protein found to be altered after a knockdown of NHE6 was the CD-MPR (Fig. 23F). This protein plays a role in TGN-to-endosome transport of endosomal hydrolases by binding the enzymes in the TGN and releasing them in the acidic environment of the late endosome, and to some extend also in the early endosome[173]. Increase levels of CD-MPR have been described in AD[343], and overexpression of CD-MPR leads to increase Aβ release in cell models of AD[344].

However, it is not clear whether the increase in CD-MPR protein levels in NHE6 k.d. cells is caused by an increase in expression, a decrease of degradation, or defects in retrograde trafficking that lead to an accumulation of the CD-MPR. Retrograde transport of MPRs from the endosome to the Golgi is mediated by the retromer complex[177]. However, Western blotting of samples from control and NHE6 k.d. cells did not show any change in levels of the retromer sorting complex components VPS35, VPS29 and VPS26[178] or the retromer cargo sortilin (Fig. 24).
It is therefore more likely that the accumulation of the CD-MPR is caused by another source than retrograde transport of the receptor back to the TGN.

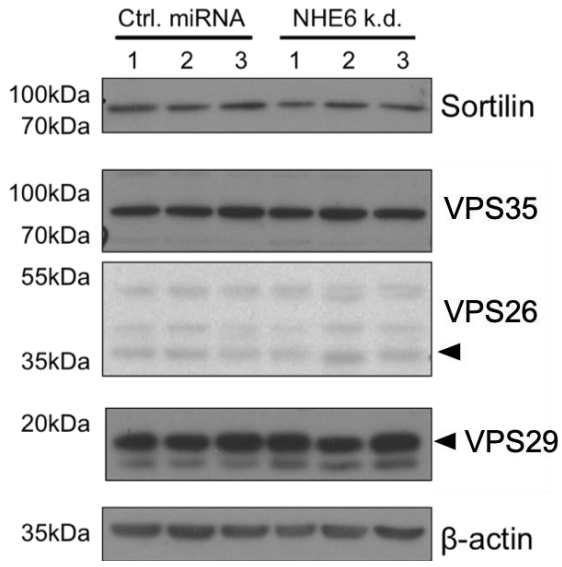

Fig. 24: Western blots for components of the retromer sorting complex (VPS35, VPS29, VPS26) and retromer cargo (sortilin) in M17 neuroblastoma cells expressing a non-targeting control or NHE6 k.d. miRNA. Brightness and contrast were adjusted on the VPS26 blot for better visibility. β-actin was used as a loading control. Arrowheads indicated expected band sizes. 1-3 denote separate experiments. Representative blot of n=3.

3.4 The pH of the endosomal-lysosomal system is affected by a loss of NHE6

As discussed above, acidification in the endosomal-lysosomal system is crucial for cellular function. To see whether differences in acidification of the endosomal-lysosomal system can be observed in both fibroblasts from the T489Yfs carrier and M17 NHE6 k.d. cells compared to controls, these cells were stained with LysoTracker dye and then subjected to microscopy analysis. LysoTracker is a dye that stains acidic vesicles below a pH of approx. 5.5, which is only found in the lysosome under physiological conditions, and is therefore used for the assessment of lysosomal phenotypes.
In fibroblasts from the T489Yfs patient, LysoTracker staining showed a distinct clustering of LysoTracker-positive vesicles around the nucleus compared to a healthy

female control which shows LysoTracker-positive stained vesicles proximal and distal from the nucleus (Fig. 25A). This appearance of a dense cluster made further analysis of size and number of these vesicles impossible. Vesicles with a higher acidity tend to be located in the perinuclear area in healthy cells as Rab7-dependent transport of the late endosome to the perinuclear area is coupled to acidification of the endosomal lumen[172]. A loss of alkalisation might therefore lead to a higher number of acidic vesicles which are then transported to this region, resulting in the observed phenotype. Analysis by flow cytometry showed in a moderate increase in LysoTracker fluorescence in T489Yfs patient fibroblasts compared to the healthy male and female control; however, this difference was not statistically significant (Fig. 25B).

In M17 NHE6 k.d. cells, the phenotype observed in fibroblasts was not as obvious in the microscopy pictures (Fig. 25C). Nevertheless, cells with reduced levels of NHE6 showed an increase in the size of the acidic vesicles that approached significance and a significant increase in the number of acidic particles when compared to the non-targeting miRNA control (Fig. 25C).

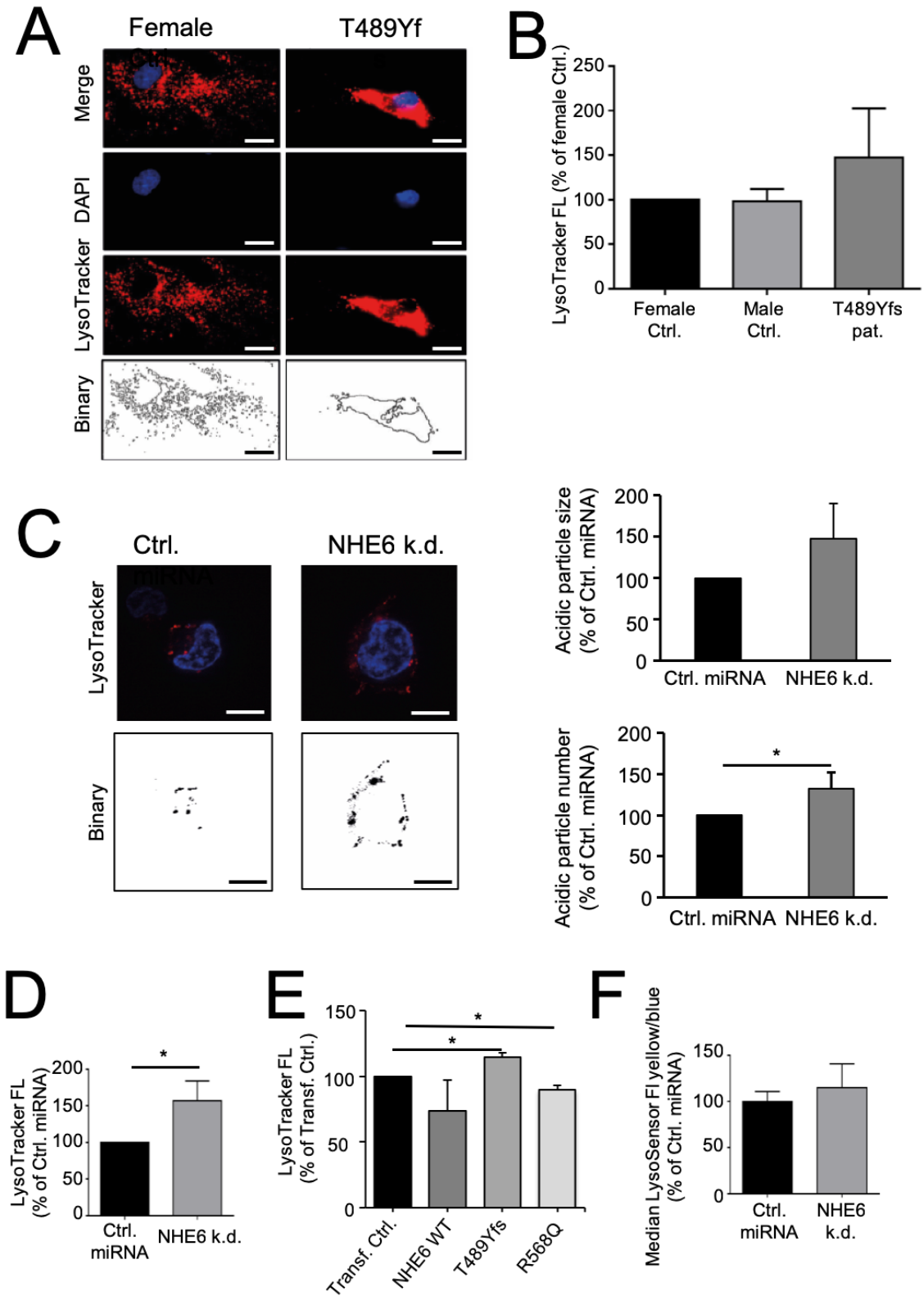

Fig. 25: Live Cell Microscopy and flow cytometry analysis for pH-sensitive dyes in M17 knockdown, overexpression and fibroblast models. **A**: Microscopy pictures of LysoTracker-stained fibroblasts from a healthy female control and the T489Yfs carrier. Binary was added to emphasize the shape of the LysoTracker-stained network. Representative pictures of n=3. Scale bar: 100µM. **B**: LysoTracker fluorescence by flow cytometry in fibroblasts from the T489Yfs patient, a healthy male and a healthy female control. Background (autofluorescence) values were subtracted from LysoTracker-stained

values and values are expressed in percent of healthy male control values. **C:** Microscopy pictures from M17 cells expressing either a non-targeting control miRNA or NHE6 k.d. miRNA and quantification of acidic particle number and size. Values are shown in percent of non-targeting control. Representative pictures of n=3. Scale bar: 10µM. **D**: LysoTracker fluorescence by flow cytometry in M17 cells expressing a non-targeting control miRNA or NHE6 k.d. miRNA. Background (autofluorescence) values were subtracted from LysoTracker-stained values. Values are shown in percent of non-targeting control. **E:** LysoTracker fluorescence by flow cytometry in M17 neuroblastoma cells overexpressing WT, T489Yfs or R568Q NHE6 compared to a transfection control (empty vector). **F**: Median LysoSensor fluorescence yellow/blue in Lysosome-RFP positive vesicles in M17 neuroblastoma cells expressing a non-targeting control or NHE6 k.d. miRNA. Microscopy images for this experiments were taken by Dr. Angelos Skodras, Department of Cellular Neurology, Hertie Institute for Clinical Brain Research, Tübingen. Values are shown in percent of non-targeting control. Unless otherwise stated, all graphs show the mean of n=3. Error bars: S.D. *p<0.05

Additionally, LysoTracker fluorescence was assessed by flow cytometry, which showed a significant increase in LysoTracker fluorescence in cells with a knockdown of NHE6 compared to the non-targeting miRNA control after subtraction of unstained background values (Fig. 25D). Furthermore, LysoTracker staining was measured by flow cytometry in M17 cells overexpressing WT, T489Yfs or R568Q NHE6 and compared to a transfection control (empty vector). Cloning of the NHE6 WT, T489Yfs and R568Q cDNA into the vector used in this experiment was performed by Manuela Kübler at the Department of Neurodegenerative Diseases, Centre of Neurology and Hertie Institute for Clinical Brain Research, University of Tübingen, Tübingen, Germany.

Overexpression of NHE6 with the T489Yfs mutation lead to significantly increased levels of LysoTracker fluorescence and thereby acidity in the endosomal-lysosomal system. NHE6 WT overexpression decreased and R568Q overexpression significantly decreased LysoTracker fluorescence compared to a transfection control (Fig. 25E), arguing for an alkalinisation expected in cells overexpressing functional NHE6.

Because the mutant protein is not detected by the NHE6 antibody available, levels of endogenous NHE6 can be assessed independently of levels of overexpressed T489Yfs NHE6. Western blotting with lysates from M17 cells overexpressing the construct showed no difference in endogenous NHE6 levels between cells transfected with a transfection control and cells transfected with T489Yfs NHE6 (Fig. 26).

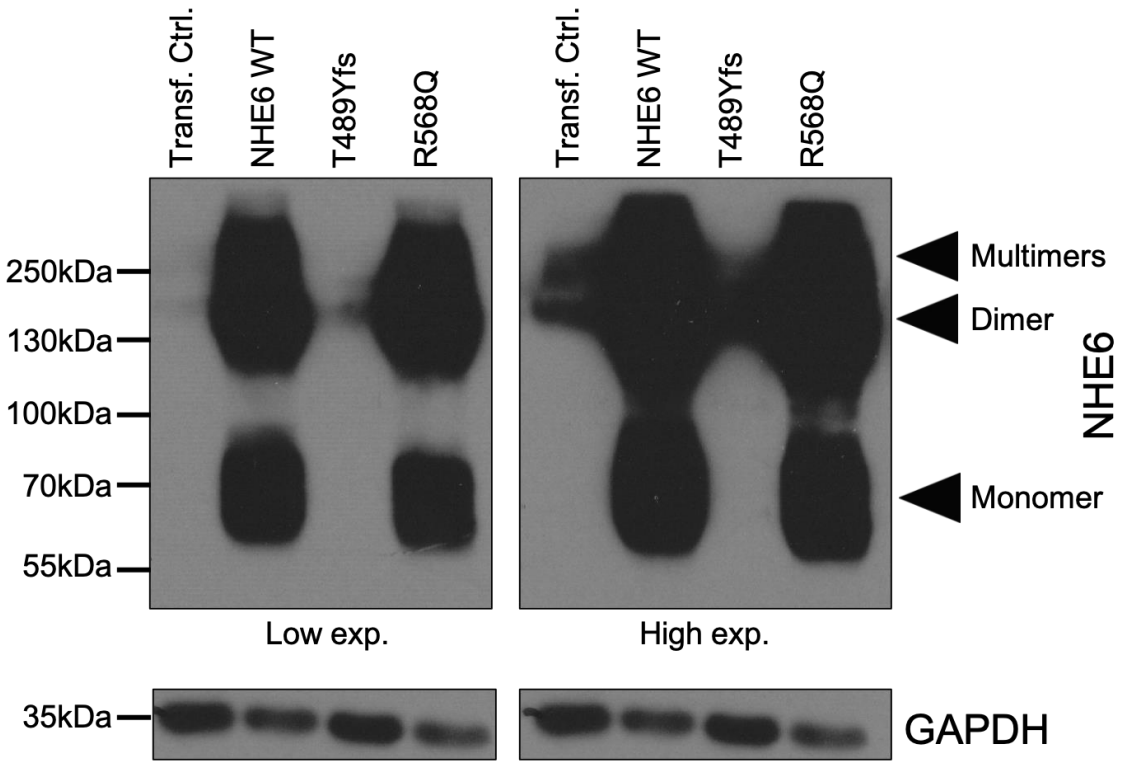

Fig. 26: Western blot for full-length NHE6 in M17 neuroblastoma cells transfected with a Transfection Control (Empty Vector), NHE6 WT, T489Yfs or R568Q NHE6 for 48h before lysis. The NHE6 antibody does not detect the truncated T489Yfs and therefore detects only endogenous NHE6 in the T489Yfs overexpressing cells. Cells transfected with T489Yfs NHE6 do not show a reduction in NHE6 protein levels when compared to the untransfectd control. GAPDH is used as a loading control. Representative blot of n=3.

Several cellular changes could lead to the increase in LysoTracker fluorescence observed in M17 NHE6 k.d. cells. A combination is possible of an increased size of fluorescent particles and an increase in the number of acidic vesicles that fall below the pH 5.5 detection threshold of the dye, especially as the LysoTracker dye does not give a graduated response to different levels in acidification. To test the hypothesis that the pH in the lysosome is reduced in M17 NHE6 k.d. cells, k.d. and control cells were transduced with a BacMam CellLight Lysosome-red fluorescent protein (RFP) construct that labels lysosomes via expression of an RFP-coupled LAMP1 protein. Cell transduced this way were then stained using the LysoSensor yellow/blue dye and the fluorescence intensity of both the acidic (yellow, 446-455nm) and the alkalic (blue, 535-544nm) component of the dye in RFP-positive vesicles measured. Microscopy images for this experiments were taken by Dr. Angelos Skodras, Department of Cellular Neurology, Hertie Institute for Clinical Brain Research,

Tübingen. Analysis of fluorescence intensity of both channels in the lysosome of the cells did not reveal a strong difference in pH (Fig. 25F). The acidic yellow fluorescence was only slightly elevated in cells with a NHE6 k.d. when expressed as a ratio to the alkalic blue fluorescence of the dye and compared to the non-targeting control miRNA. NHE6 k.d. in these cells therefore seems to have only a mild effect on acidity in the lysosome itself.

3.5 Effects on autophagy in cells with a loss of NHE6

3.5.1 Levels of LC3 are affected in cells with a loss of NHE6

Since the endosomal-lysosomal system plays a crucial role in autophagy, the levels of an autophagic marker protein, LC3, were assessed in NHE6 k.d. cells and T489Yfs fibroblasts. LC3-I is converted to LC3-II by lipidation after the induction of autophagy, and levels of LC3-II are an indicator for both the initiation of autophagy and the removal of autophagosomes, as LC3-II accumulates if degradation by the lysosome is impaired.

Autophagy can be initiated by amino acid starvation, therefore M17 NHE6 k.d. and control miRNA cells were treated either with serum-free medium (amino acid starvation) or with BafA1, a toxin that inhibits lysosomal acidification and thereby removal of autophagic cargo. Under untreated conditions, NHE6 k.d. cells show a reduction in both LC3-I and LC3-II that does not increase after amino acid deprivation, in contrast to control miRNA expressing cells (Fig. 27A). However, LC3-II accumulates if removal by the lysosome is blocked in these cells. If LC3-II levels are normalised to the loading control and compared between k.d. and control, they are lower in k.d. cell than in control. If LC3-II levels are normalised to LC3-I levels, though, it is strongly increased because of the lower LC3-I levels in k.d. cells. It therefore seems that even though the response to autophagic stimuli is decreased, there is removal of autophagic cargo, maybe even to a stronger extend than in control cells as LC3-II still accumulates under BafA1 treatment, but does not increase after starvation. This result might indicate that there is a higher turnover of autophagic vesicles under basal conditions, which would explain the increase in LC3-II levels after BafA1 treatment despite very low levels of LC3-I and low levels of LC3-II under untreated conditions.

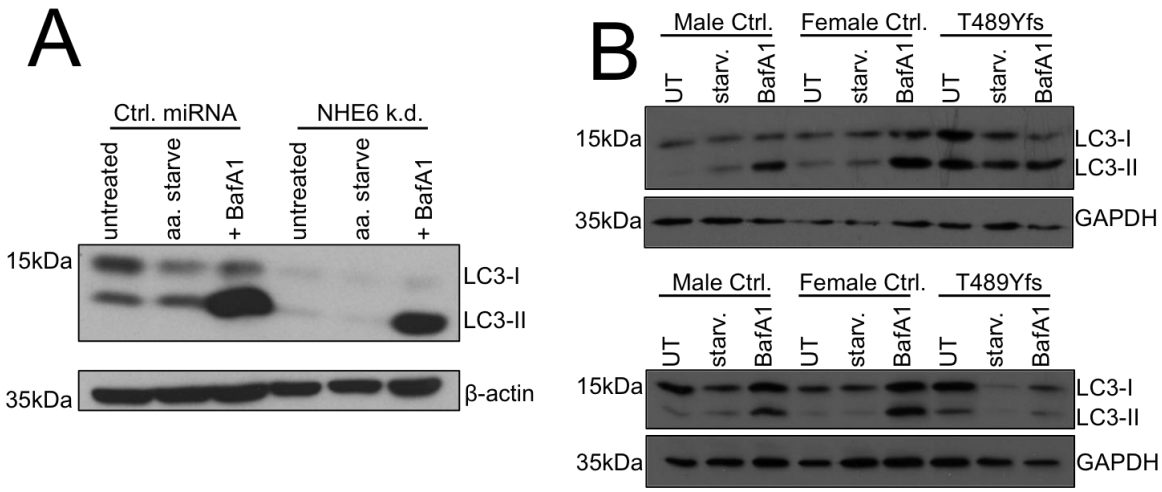

Fig. 27: Western blots for the autophagy marker protein LC3 in the M17 NHE6 knockdown and patient fibroblast model. **A**: Western blot for LC3-I and LC3-II in M17 neuroblastoma cells with a NHE6 knockdown or non-targeting control miRNA in an untreated condition, after amino acid starvation (aa. starve) of after treatment with 400nm Bafilomycin A1 for 4 hours (BafA1) to block the removal of autophagic cargo. β-actin was used as a loading control. Representative blot of n=3. **B**: Western blot for LC3-I and LC3-II in healthy male, healthy female control or T489Yfs patient fibroblasts in an untreated condition (UT), after amino acid starvation (starv.) of after treatment with 400nm Bafilomycin A1 for 4 hours (BafA1). GAPDH was used as a loading control. Of a total n=6, the upper blot is representative for n=3 results and the lower blot for the other n=3.

In fibroblasts, the results were not as clear-cut as in the M17 neuroblastoma model. Compared to male and female control cells, T489Yfs patient cells showed a constant increase in LC3-II under all conditions in three of six experiments, indicative of defective removal of autophagic vesicles (Fig. 27B, up). In the other three experiments, T489Yfs cells showed a strong reduction in LC3-II even under Bafilomycin A1 treatment, which would indicate a reduction in autophagic initiation that is mirrored by unchanged levels after amino acid starvation (Fig. 27B, down). While these results are difficult to reconcile, it should be mentioned that in fibroblasts, both passage[345] and confluency influences the activity of proteasomal and lysosomal protein degradation pathways[346]. Even if precautions are taken to keep these conditions as similar as possible between experiments, it is technically difficult to achieve as cell growing dynamics change between lines, and cell counting is not exact. All of these technical challenges might account for the pronounced difference in results between experiments regarding LC3 lipidation in fibroblasts.

3.5.2 Levels of the mitochondrial protein TOM22 are not significantly changed in M17 NHE6 k.d. cells

A specialised form of autophagy is mitophagy where defective mitochondria are removed by the autophagic pathway. To test whether mitochondria were dysfunctional in cell with a loss of NHE6, total mitochondrial content was measured in M17 inducible knockdown cells by flow cytometry of baseline levels of TOM22, an outer mitochondrial marker protein, that was coupled to a fluorescent dye. In the experiment, under NHE6 k.d. conditions an increase in TOM22 staining was observed that approached, but did not reach statistical significance ($p = 0.051$) (Fig. 28A). As an increase in mitochondrial protein under baseline conditions can be indicative of defective removal, or increased biogenesis of mitochondria, further experiments were required to determine the reason for the increase in TOM22 staining. To answer the question of whether defective mitochondria are not efficiently removed in NHE6 k.d. cells, cells were treated with Carbonyl cyanide m-chlorophenyl hydrazone (CCCP) or Valinomycin, toxins that depolarize mitochondria and thereby induce mitophagy[347]. However, the used concentrations and time points resulted in an increase of analysed mitochondrial markers on Western blot even in control miRNA expressing cells and M17 neuroblastoma not expressing any miRNA, instead of the expected decrease (Fig. 28B and Appendix Fig. 42). It was therefore impossible to use these experimental conditions to study removal of defective mitochondria in M17 neuroblastoma cells.

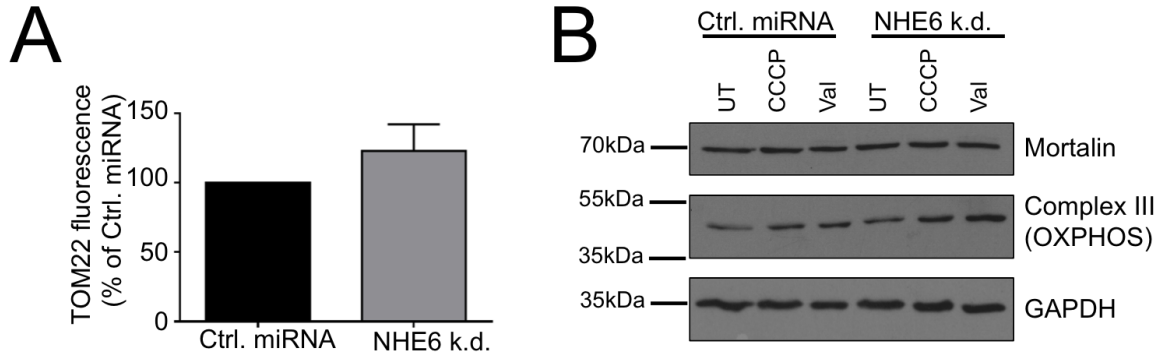

Fig. 28: Assessment of mitochondrial proteins in M17 neuroblastoma cells with a non-targeting control miRNA or NHE6 knockdown using flow cytometry and Western blot. **A**: Results of flow cytometry measurement using a GFP-coupled mitochondrial marker protein TOM22 in fixed cells. Fluorescence is expressed as percent of the non-targeting control miRNA values. Mean of n=3. Error bar: S.D. **B**: Western blot against the mitochondrial matrix protein Mortalin or using an OXPHOS antibody against subunits of mitochondrial complexes I-V, of which only complex III (47kDa) was visible. Cells were

either untreated (UT, normal growth medium) or treated with 1µM CCCP or 1µM Valinomycin (Val) for 24h before lysis to induce mitochondrial damage and mitophagy. Representative blot of n=3.

It has been shown previously that in M17 neuroblastoma cells PINK1 is stabilized on the mitochondrial membrane and that Parkin translocates to the mitochondria upon CCCP treatment[348]; however, the authors did not analyse mitochondrial removal in these cells, and CCCP treatment was shorter and in a higher concentration (2-6h and 20µM instead of 1µM for 24h as used in this study). For further studies on the removal of defective mitochondria in M17 neuroblastoma cells, optimal conditions would need to be established.

3.6 Levels of intracellular reactive oxygen species are elevated after NHE6 knowdown

Oxidative stress and reactive oxygen species (ROS) play an important role in neurodegenerative disease. To test whether levels of cellular ROS are elevated in cells with a NHE6 k.d., fluorescence of the dye Dihydroethidium (DiHET) was measured. DiHET is blue and cytosolic in its reduced state, but becomes red and translocates to the nucleus upon oxidiation. Measuring blue fluorescence (305nm) against red fluorescence (590nm) over a time of 30 minutes, after which the signal becomes saturated, revealed a significant increase in the rate of blue-to-red conversion of the dye in NHE6 k.d. cells, indicative of higher levels of cytosolic ROS (Fig. 29A). This effect was further increased by treatment with rotenone which inhibits complex I and results in increased production of mitochondrial ROS. While the effect of rotenone was strongly significant in control miRNA cells, it was elevated in NHE6 k.d. cells, but not statistically significant. Furthermore, the treatment with rotenone abolishes the difference between non-targeting control miRNA cells and NHE6 k.d. cells. This suggests that the increase in cytosolic ROS seen in the NHE6 k.d. cells is at least partially caused by mitochondria. If the increase in cytosolic ROS in NHE6 k.d. cells was independent of mitochondrial dysfunction, the increase in ROS production after rotenone treatment would be the same between non-targeting control and NHE6 k.d. cells and the statistical difference between the two lines would remain. However, as the increase seen under baseline conditions is small, the relevance of this finding remains to be established.

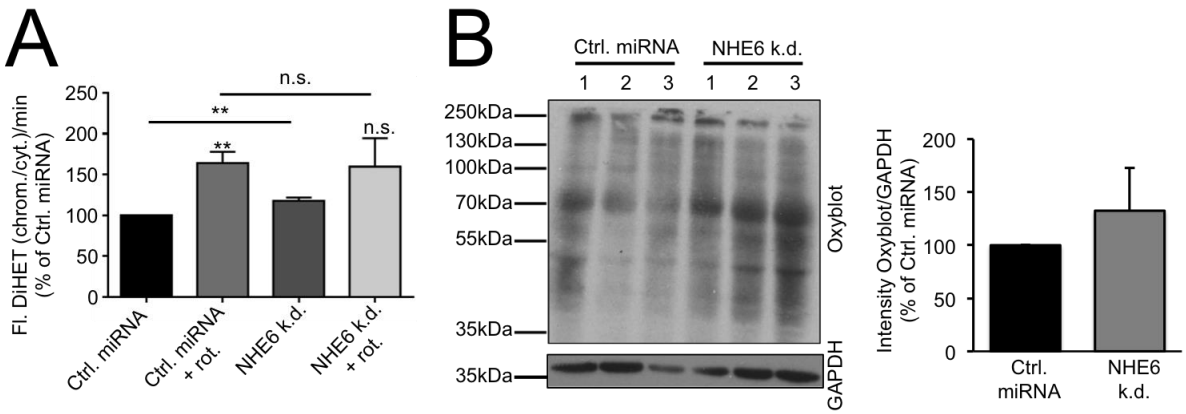

Fig. 29: Oxidative stress in the M17 neuroblastoma NHE6 k.d. model measured by dihydroethidium oxidation and protein oxdiation. **A**: Measurement of the increase in the ratio of red (chromatin-bound, oxidised) to blue DiHET fluorescence (cytosolic, not oxidised) over time in non-targeting control miRNA and NHE6 k.d. cells untreated and after rotenone treatment. Values are expressed as percent of untreated control miRNA cells. **B**: OxyBlot for the detection of oxidised proteins in control and NHE6 k.d. cells. GAPDH was used as a loading control. The quantification shows band intensity by densitometry normalised to GAPDH and expressed in percent of control miRNA values. Representative blot of n=3. Graphs are mean of n=3. Error bars: S.D. **p>0.01, n.s.=not significant

An increase in ROS is damaging to the cell as ROS can oxidate lipids and proteins and thereby influence folding and function of these macromolecules. To assess whether an increase in cellular ROS results in oxidative damage to the cells, an OxyBlot was performed. During the OxyBlot procedure, oxidated proteins are detected with a specialised antibody, allowing to assess the level of oxidative damage. While the intensity of the signal on the Oxyblot was slightly increase in NHE6 k.d. cells, no significant effect could be observed (Fig. 29B), indicating that oxidative damage by an increased ROS production in these cells is low, at least during the 96h induction time.

3.7 Effects of NHE6 k.d. and the R568Q variant on Tau

3.7.1 Tau is hyperphosphorylated in the M17 NHE6 k.d. model

Another consequence of ROS and defects in the endosomal-lysosomal system can be the accumulation of abnormally modified, especially hyperphosphorylated tau. Insoluble, hyperphosphorylated tau is found in both CBD patients and in patients with

mutations in *SLC9A6* leading to Christianson syndrome, so it was of interest to investigate the amount of phosphorylated tau in the M17 NHE6 k.d. model. Separation of phosphorylated proteins by PhosTag blots revealed a strong increase in phosphorylated tau as phosphorylated proteins bind to resins inside the PhosTag gel and appear as higher-molecular weight bands after detection with an antibody directed against total tau (Fig. 30A). This in part mirrored by an increase in overall tau levels in these cells when run on a standard Western blot, partially with a change in migration patterns (Fig. 30B). A trial with two antibodies directed at specific phosphorylation sites commonly involved in paired helical filaments involved in Alzheimer's disease (AT8 directed against pSer202 and pThr205 and AT270 against pThr181) did not yield any results (Appendix Fig. 43), and the question which sites of tau are hyperphosphorylated in the M17 neuroblastoma NHE6 k.d. model remains open. However, the strong increase in both phosphorylated tau and overall tau levels suggest a defect of tau removal in NHE6 k.d. cells rather than an increase in phosphorylation or defects in dephosphorylation.

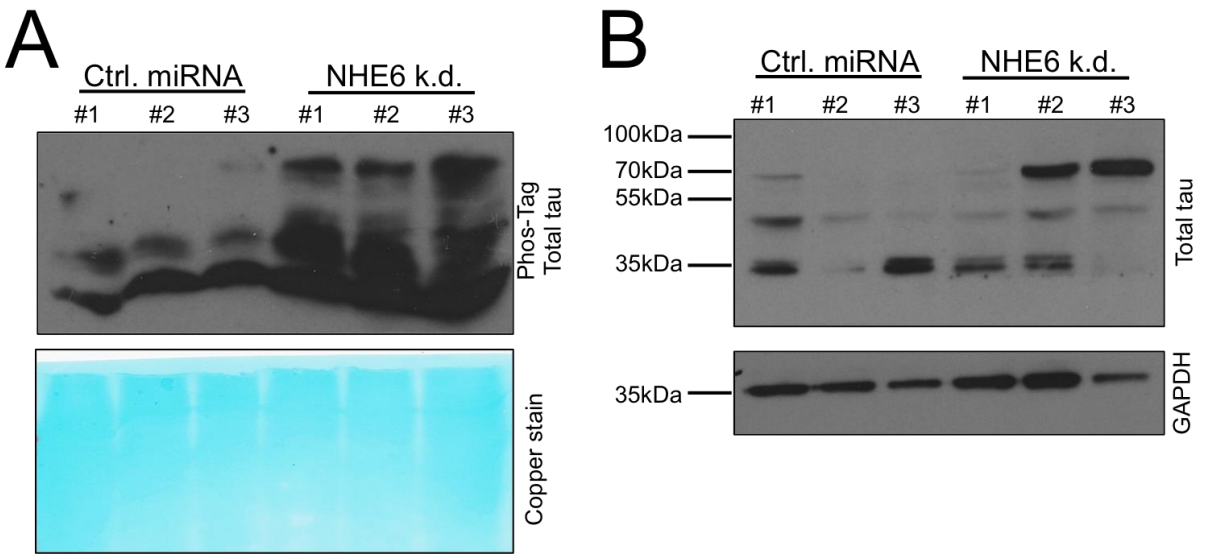

Fig. 30: Western blots for tau levels in non-targeting control miRNA and NHE6 k.d. M17 neuroblastoma cells. **A**: PhosTag gel with samples from control miRNA or NHE6 k.d. cells probed for total tau. Higher phosphorylated proteins migrate slower in a PhosTag gel and are increased in the NHE6 k.d. condition. Copper staining was used as a loading control. Representative blot of n=3. **B**: Western blot of total tau in control miRNA or NHE6 k.d. cells using the same samples as in A. The banding pattern results from different tau isoforms and posttranslational modifications of the protein. #1-#3 denote different monoclonal lines. GAPDH was used as a loading control. Representative blot of n=3.

3.7.2 Differences in Tau pathology in brain samples from two R568Q carriers

Since CBD is a tauopathy and clinically diagnosed CBS is often caused by underlying tau pathologies, it was of interest to investigate the tau pathology in the brains of two R568Q variant carriers. While one patient was diagnosed with CBS in life and CBD upon autopsy by a specialist, the other patient was diagnosed with CBS, but showed a mixed pathology, including aging-related tau astrogliopathy (ARTAG; for a detailed description, see Table 10 in the Materials and Methods section). Both patients are female, but from a family where the males do not exhibit Christianson syndrome, further underlining the R568Q variant as a rather mild exchange. The R568Q carrier with autopsy-confirmed CBD is from hereon referred to as R568Q-CBD, while the patient with a mixed pathology is referred to as R568Q-CBS. Controls are referred to as CBD Ctrl. 1a-c for controls matched to the R568Q-CBD patient, and CBS Ctrl. 2a-c for the R568Q-CBS patient.

First, sarkosyl-insoluble tau was extracted from all four brain regions available (medial frontal cortex, caudate nucleus, occipital lobe, cerebellum). Tau solubility in the detergent sarkosyl is frequently used to distinguish soluble, native tau from pathological, insoluble forms[349] and is connected to phosphorylation status of the protein[350].

Sarkosyl soluble and insoluble fractions were from the medial frontal cortex of the two patients and three pathology-matched controls each showed high levels of sarkosyl-insoluble tau in the CBD controls (the smear is typical of pathologic tau and results from excessive posttranslational modification and aggregation of the protein) (Fig. 31). While the sarkosyl-insoluble fraction R568Q-CBD patient also exhibited an increase in sarkosyl-insoluble tau, the smear is absent and the banding pattern resembles that of sarkosyl-soluble tau. Compared to CBD samples, the amounts of sarkosyl-insoluble tau are low in the R568Q-CBS patient and pathology-matched controls (Fig. 31), which is in line with the mixed pathology and an absense of a strong tau pathology in the autopsy. Levels of soluble tau, however, are more comparable between CBD and mixed pathology cases, while levels of total tau in the input before the sarkosyl precipitation step are in line with similar amounts of soluble, but not insoluble tau (Fig. 31).

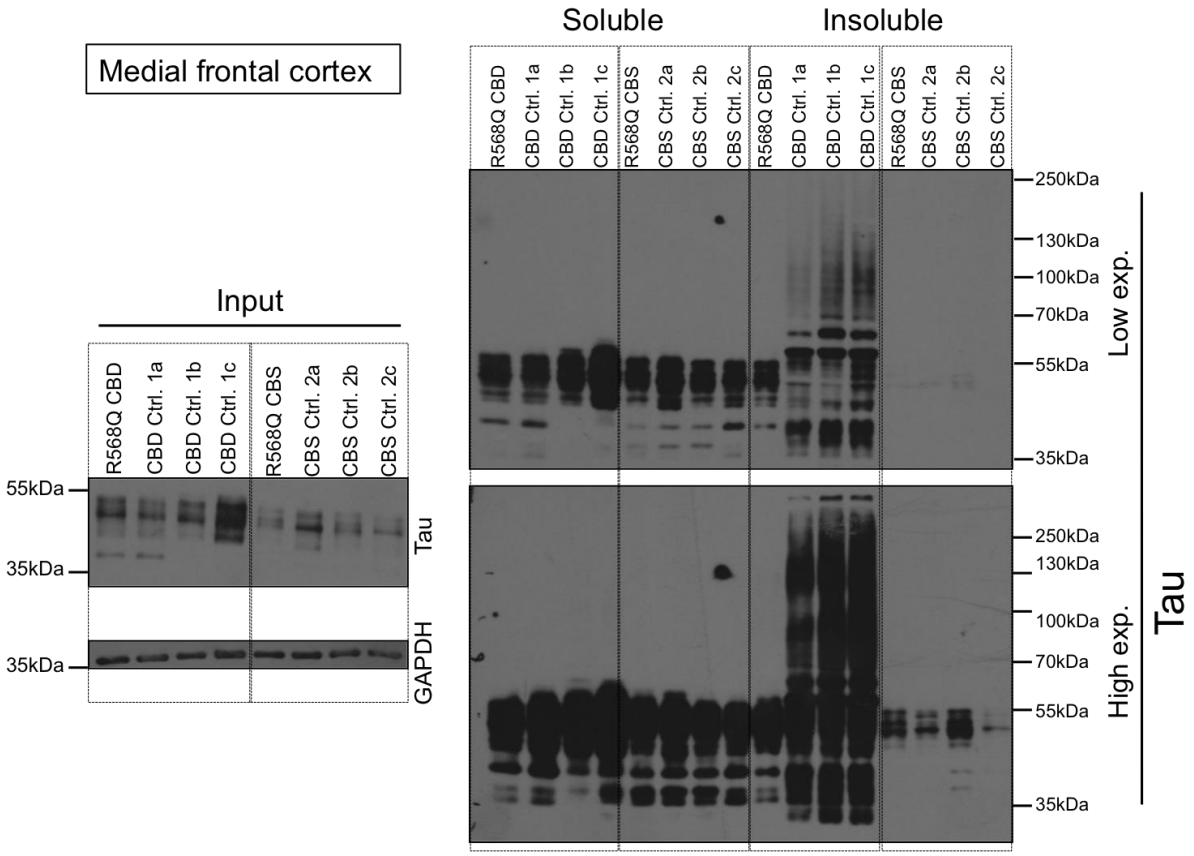

Fig. 31: Westernblot against total tau using sarkosyl soluble and insoluble tau fraction from the medial frontal cortex of two R568Q variant carriers and pathology-matched controls. An aliquot of the lysate was taken before the sarkosyl precipitation step to confirm equal input levels by immunoblotting against GAPDH and to assess levels of total tau in these samples (left). The smear observed in the CBD controls is typical for tauopathies and is caused by the accumulation of insoluble posttranslationally modified tau, different isoforms and aggregates. exp.: exposure time. This experiment was performed one time (n=1).

A similar result could be observed in the caudate nucleus (Appendix Fig. 44A). Only the CBD cases showed a strong signal for tau in the sarkosyl insolube fraction, even though the smear was less pronounced than in the medial frontal cortex. Likewise, in the R568Q-CBD patient more tau was found in the insoluble fraction, but not smear was visible even after longer exposure. In the occipital lobe, only one of the CBD controls showed the strong smear observed in the medial frontal cortex and caudate nucleus (Appendix Fig. 44B). Here, the R568Q-CBD patient did not differ from the CBS cases, while one control showed a stronger band in the insoluble fraction, but not the typical smear. In the cerebellum, all CBD cases showed a strong increase in levels of soluble, insoluble and total tau compared to CBS/mixed pathology controls (Appendix Fig. 44C). The previously observed smear was, however, absent in all cases.

When interpreting the difference between R568Q-CBD and control CBD cases in terms of a smear and, therefore, heavily modified tau, it should be kept in mind that levels of protein phosphorylation in autopsy samples depend on post mortem delay, with a decrease in phosphorylation after death, and nothing is known about the post mortem delay of the patient or the controls. Furthermore, the R568Q-CBD patient died in 1999, and storage conditions might also affect protein phosphorylation.

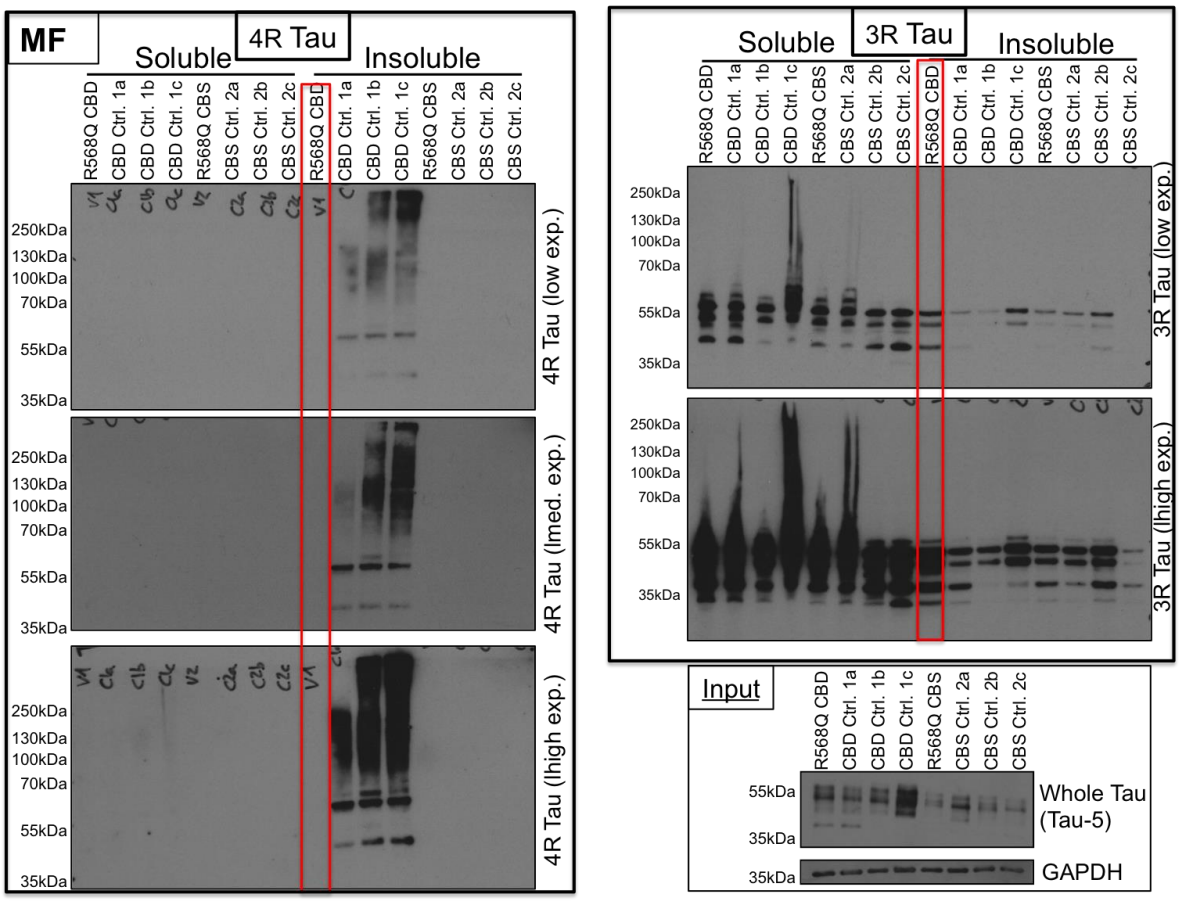

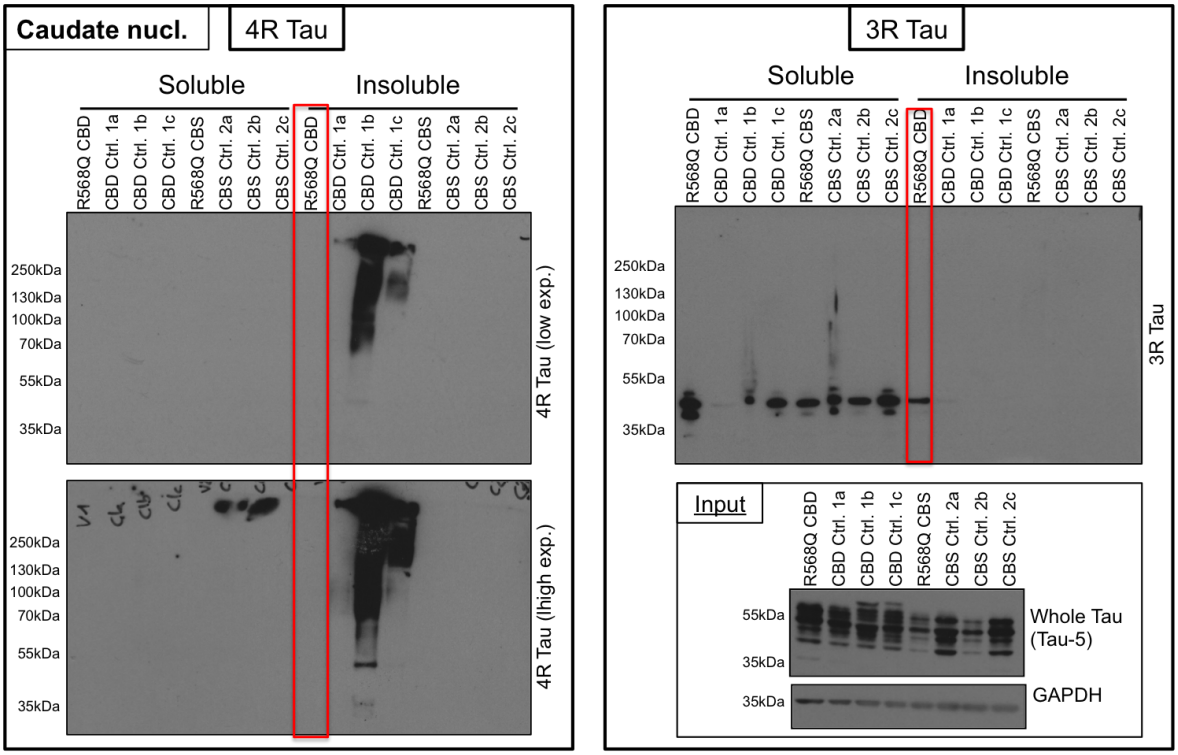

Fig. 32: Western blot for 4R and 3R tau ioforms in sarkosyl soluble and insoluble fractions from the medial frontal cortex (MF) and the caudate nucleus of two R568Q variant carriers and pathology-matched controls. In contrast to the pathology-matched controls, the R568Q CDB carrier does not show bands in the insoluble fraction on the 4R-tau probed Western blot but on the Western blot probed for 3R-tau (red rectangle). An aliquot of the lysate was taken before the sarkosyl precipitation step to confirm equal input levels by immunoblotting against GAPDH (input) and to assess levels of total tau in these samples. The samples are the same that were used in Fig. 31 and Appendix Fig. 44. Exp.: exposure. This experiment was performed one time (n=1).

CBD is a 4R-tauopathy with an increase in 4-repeat Tau isoforms. To assess the levels of different isoforms in the brain samples from R568Q carriers, 4R and 3R isoform specific antibodies can be used. A Western blot using the sarkosyl soluble and insoluble fractions from the medial frontal cortex showed that 4R-tau is mainly found in the insoluble fraction of the three CBD control cases but not of the R568Q-CBD patient. Probing the samples with an antibody against 3R tau showed a moderate increase in 3R tau in the R568Q-CBD patient compared to CBD controls in the medial frontal cortex (Fig. 32, *upper panel*). In samples from the caudate nucleus, no 4R tau was detectable in insoluble fractions of the R568Q-CBD patient, but 3R tau (Fig. 32, *lower panel*) could be detected. An attempt to detect any of the isoforms in the occipital lobe failed.

These results, however, should be interpreted with caution because the experiment was not repeated and no definite conclusion is possible from the presented data only. It would be interesting to follow up on these preliminary findings.

3.8 Cell death in models with changes in NHE6 levels

3.8.1 Early apoptosis in M17 knockdown cells is not significantly elevated

Cell death is one of the main features of neurodegeneration, and dysfunction of the endosomal-lysosomal system has repeatedly been connected to neurodegenerative diseases. One of the earliest event in programmed cell death, apoptosis, is the presentation of phosphatidylserine (PS) on the outer leaflet of the PM. This serves as a signal for immune cells to remove the dying cell and prevent necrosis and inflammation in dying tissue.

Annexin V is a protein of unknown function that can bind to PS on the cell surface. When coupled with Pacific blue, Annexin V binding can be measured by flow cytometry via quantification of fluorescence intensity, indicating the amount of cells in a population undergoing early apoptosis.

In M17 neuroblastoma cells with reduced levels of NHE6, Annexin V-Pacific blue binding was elevated, albeit not significantely, when compared to the non-targeting miRNA control (Fig. 33A). It has to be kept in mind, however, that Annexin V binding to PS only detects early stages of apoptosis, and later stages of apoptosis cannot be detected with this method.

3.8.2 Levels of general cell death in the patient fibroblast model

A measure of cell death independent of the mode of cell death (apoptosis or necrosis) is the measurement of lactate dehydrogenase (LDH) release into the medium. LDH is an enzyme that is released from the cells in cell culture after cell death and disruption of the PM, and indicates the last stage of cell death. The amount of LDH released into the medium can then be normalised to the amount of LDH released after lysis of the remaining cells, thereby giving a good indication of the amount of dying or dead cells in a population.

Staurosporine (STS) can be used as a positive control in this setting, as STS is an inducer of caspase-dependent cell death by inhibiting protein translation. In

fibroblasts, the levels of LDH release were increase in the T489Yfs patient under baseline conditions when compared to the male and female control, but not statistically significant (Fig. 33B). As expected, STS treatment lead to higher levels of cell death in all fibroblasts lines, but was the highest in the T489Yfs patient if compared to untreated female control fibroblasts. Male control fibroblasts showed a milder elevation in LDH release, however, none of the observed increases was significant (Fig. 33B).

If cell death after STS treatment is seen in relation to baseline levels of cell death, the female control shows the highest increase with double the amount of LDH release into the medium over LDH release from surviving cells, while both male control and T489Yfs patient only show an increase by 50% of the baseline (Fig. 33B).

This result suggest that in fibroblasts carrying the T489Yfs mutation, baseline levels of cell death are modestly elevated, but the cells do not show increased susceptibility to STS treatment when compared with the controls.

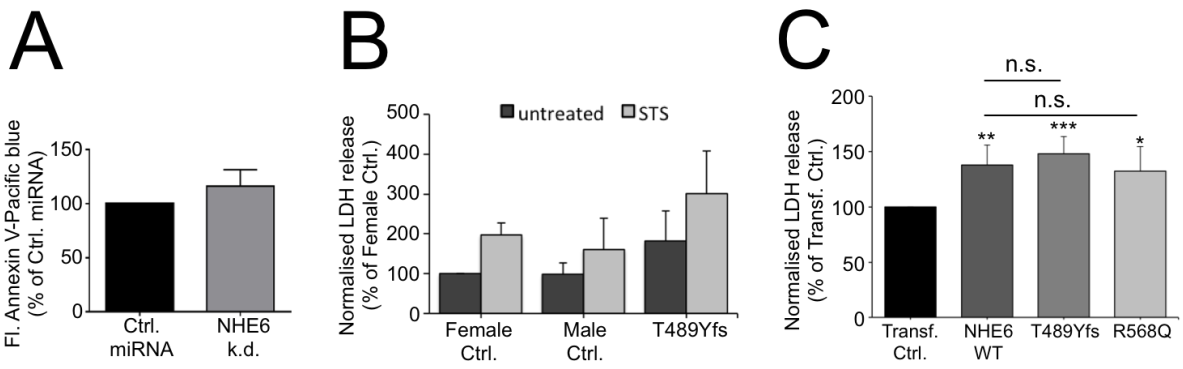

Fig. 33: Measurements of cell death-related parameter in the M17 NHE6 k.d., M17 overexpression and fibroblast model. **A**: Flow cytometry results assessing early apoptosis by binding of Annexin V coupled to a pacific blue dye in M17 neuroblastoma cells expressing either a non-targeting control miRNA or NHE6 k.d. miRNA. **B**: Total cell death measured by LDH release into the medium in fibroblasts from the female and male control or T489Yfs patient. LDH release into the medium from dying cells was normalised to LDH release from lysed, surviving cells. Fibroblasts were either left untreated or treated with staurosporine (STS) as a positive control. **C**: Total cell death measured by LDH release from M17 cells transfected for 72h either with a transfection control (empty vector) or WT, T489Yfs or R568Q NHE6. All values are expressed as percent of control conditions. All graphs show the mean of n=3, error bars: S.D. *p<0.05, **p<0.01, ***p<0.005, n.s.=not significant

3.8.3 Levels of general cell death in M17 cells overexpressing T489Yfs

Since overexpression of NHE6 T489Yfs mutant cDNA seems to influence LysoTracker signal in a gain-of-function mode and the involvement of the T489Yfs mutation in severe diseases (Christianson syndrome and CBS), there was the possibility that overexpression of T489Yfs NHE6 also affects other parameters such as cell death.

To assess the effect of overexpression of NHE6 WT, NHE6 T489Yfs and NHE6 R568Q cDNA constructs, LDH release into the medium in the last 24h of a total time of 72h after transfection was measured. Normalisation of LDH release into the medium over LDH relased from surviving cells showed an increase in all NHE6 overexpressing conditions if compared to the transfection control (Fig. 33C). While overexpression of the T489Yfs NHE6 mutation showed the strongest effect, transfection with the R568Q variant resulted in slightly lower levels of cell death than overexpression of NHE6 WT, but overall levels of cell death are similar between the lines. Again, a loss of function mutation or variant should lead to comparable levels of cell death between transfection control and protein overexpressing cell lines, which is not the case in T489Yfs mutant or R568Q variant lines.

The increase even after wildtype NHE6 overexpression is not surprising, as overexpression of this protein should heavily interfere with cellular function by alkalisation of the endosomal-lysosomal pathway. Indeed, overexpression of NHE6 WT protein had previously been shown to result in neurodegeneration and cell death after defective acidification in the endosomal-lysosomal pathway.[335]

Taken together, cell death is not significantly increased in the NHE6 k.d. model and patient fibroblasts, but in cells overexpressing NHE6 WT protein, the T489Yfs mutant or R568Q variant.

3.9 Generation of T489Yfs iPSCs and NPCs

Since NHE6 is predominantely expressed in the brain and plays a major role at the synapse, it is of interest to investigate the consequences of the T489Yfs mutation in neuronal cells. Compared to fibroblasts, neurons also express higher levels of the

protein tau, and tau is crucial for axonal function, which cannot be investigated in skin cells.

To be able to compare neuronal cells expressing T489Yfs NHE6 and WT NHE6 without the pitfalls created by overexpression, and at a physiological level, it is possible to reprogramm fibroblasts into iPSCs that then can be differentiated again into NPCs and from there into neurons. Reprogramming of fibroblasts is achieved by transfection with plasmids carrying the stem cell transcription factors cMyc, Klf4, Oct 3/4 and Sox2. After reprogramming, iPSC lines grow from single cells.

The T489Yfs patient fibroblasts were reprogrammed episomally by transfection. After isolation of stem cell clones, the clones were tested for plasmid integration by PCR and cell lines with any integration discarded. DNA extractions and PCRs for some lines were performed by Manuela Kübler at the Department of Neurodegenerative Diseases, Centre of Neurology and Hertie Institute for Clinical Brain Research, University of Tübingen, Tübingen, Germany. As reprogramming can lead to chromosomal abberations, four integration-free clones were sent for analysis of the karyotype by DNA microarray (performed by Life&Brain GENOMICS, Bonn, Germany) (clones #5.1, #6, #19 and #23) and the absence of large-scale chromosomal aberrations confirmed (Appendix Fig. 45).

In a next step, three of the four iPSC clones were characterised in regard to their pluripotent stem cell characteristics. Clone #19 was successfully differentiated into NPCs after confirmation of the karyotype, but could later on not be evaluated as an iPSC line, as a persistant contamination with cancer-like cells made them unsuitable for further use. Therefore, the T489Yfs iPSC clone #19 could not be characterised in terms of pluripotency properties.

The three clones characterised showed expression of the three endogenous stem cell transcription factors Sox2, Oct4 and SSEA4 in immunocytochemistry (ICC) (Fig. 34A, B and C). In addition to ICC, the expression of stem cell specific transcription factors was assessed using quantitative real time PCR (qRT-PCR) and compared to the expression of pluripotency markers in human embryonic stem cells (hES) and the original fibroblast line. The qRT-PCR experiment was performed by Benedikt Höglinger at the Department of Neurodegenerative Diseases, Centre of Neurology and Hertie Institute for Clinical Brain Research, University of Tübingen, Tübingen, Germany. With the exception of Klf4, qRT-PCR showed an upregulation of stem cell

transcription factors in all three T489Yfs iPSC clones compared to fibroblasts, and levels of these stem cell markers were comparable to hES (Fig. 35).

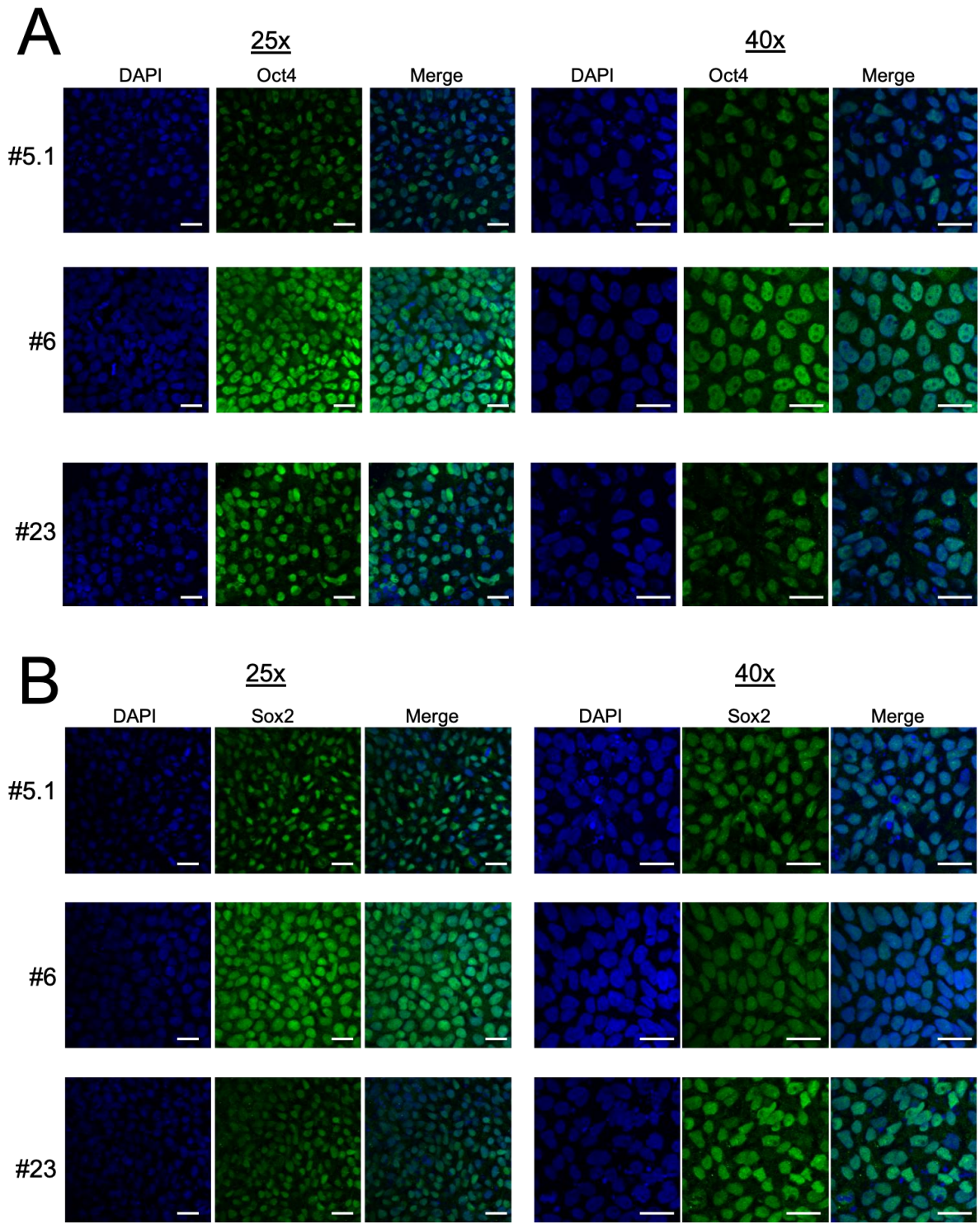

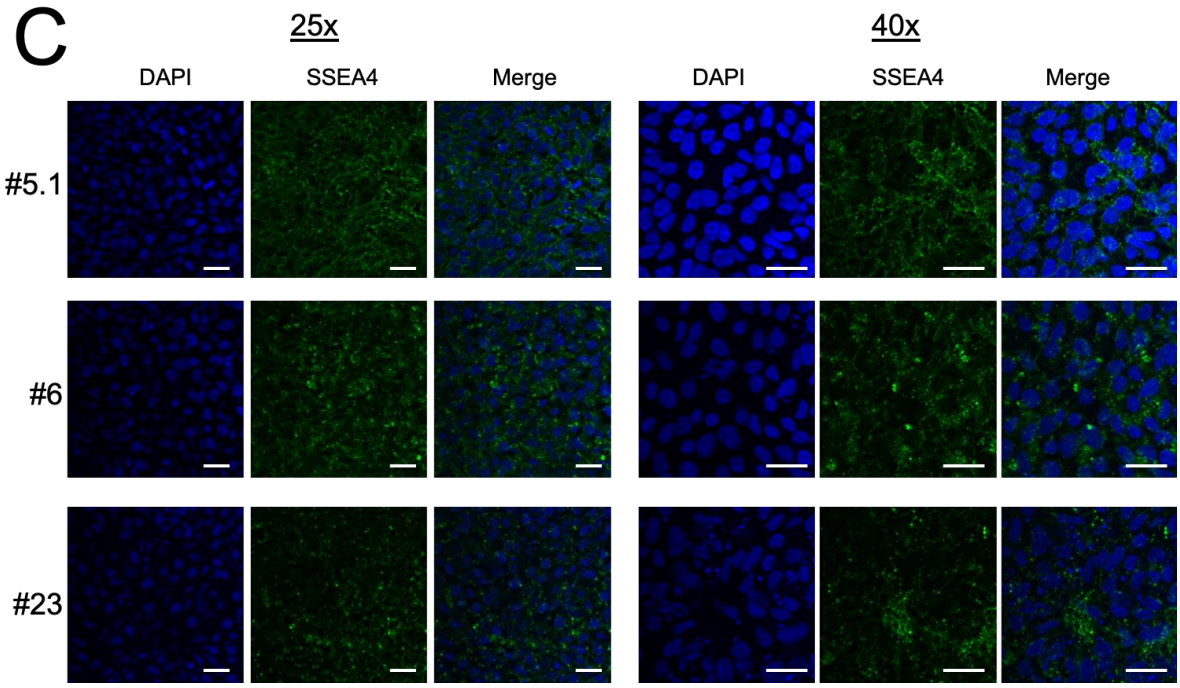

Fig. 34: Microscopy images of immunostainings for endogenous Oct4, Sox2 and SSEA4 expression in the three surviving iPSC lines (#5.1, #6, #23) from the T489Yfs23X carrier. DAPI was used as a nuclear staining. Shown two different magnifications (25x or 40x). **A**: Immunostaining for Oct4 (green) in the three lines. **B**: Immunostaining for Sox2 (green) in the three lines. **C**: Immunostaining for SSEA4 (green) in the three lines. Pictures representative for n=3. Scale bars: 25µM.

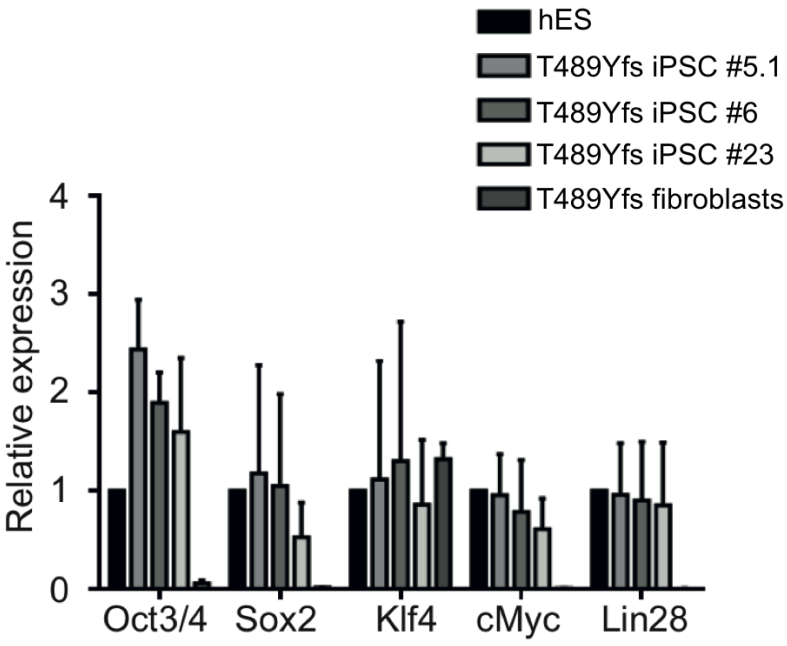

Fig. 35: qRT-PCR values for endogenous expression of Oct3/4, Sox2, Klf4, cMyc and Lin28 using RNA from three iPSC lines of the T489Yfs carrier, fibroblasts from the same carrier and RNA from human embryonic stem cells (hES) as a control. Graphs show the expression relative to RNA levels in hES cells. Mean of n=2. Error bars: S.D. Experiment by Benedikt Höglinger, Department of Neurodegenerative Diseases, Centre of Neurology and Hertie Institute for Clinical Brain Research, University of Tübingen, Tübingen, Germany.

After the analysis of the karyotype, iPSCs were used for the generation of NPCs. NPCs are precursor cells than can differentiate into different types of neurons and glia cells.

NPCs were first dorsalised for a higher yield of neurons and then differentiated in maturation medium using neuronal factors and neurotrophins such as BDNF and Glial cell-derived neurotrophic factor (GDNF). After 10 days of treatment with maturation medium, neurons are considered mature and are then kept in maturation medium, and T489Yfs. T489Yfs lines were differentiated along with an already established female and a male control line (control iPSC and NPC cell lines were generated by Christine Bus, Department of Neurodegenerative Diseases, Centre of Neurology and Hertie Institute for Clinical Brain Research, University of Tübingen, Tübingen, Germany) from NPCs, but in all attempts at differentiation, T489Yfs cells with a neuronal morphology started to detach approximately at the time of reaching maturity. A Western blot against the neuronal marker βIII-tubulin shows similar levels of the protein at 10 days after the start of maturation, but a strong decrease in the protein after 20 days in all four T489Yfs lines (Fig. 36) where the differentiation contains predominantly other cells types. It could not be established what the cause of the detachment was in the T489Yfs cells, but most likely intrinsic factors played a role as the control lines did not show similar detachment.

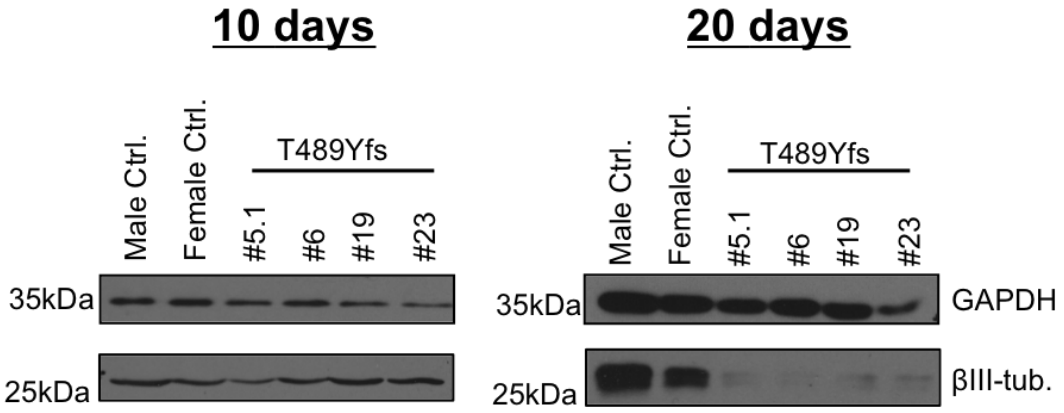

Fig. 36: Western blot for the neuronal marker βIII-tubulin in differentiated from NPCs from a healthy male or female control (established by Christine Bus at the Department of Neurodegenerative Diseases, Centre of Neurology and Hertie Institute for Clinical Brain Research, University of Tübingen, Tübingen, Germany), or the four lines from the T489Yfs carrier (#5.1., #6, #19, #23). Lysates were taken at 10 days and 20 days after the start of maturation medium. GAPDH was used as a loading control. This experiment was performed one time (n=1).

Because it might be possible that reprogramming affects X-inactivation, cell lysates from iPSCs, NPC and a differentiation from day 10 and day 20 after the start of maturation (the same samples that showed the strong reduction in neuronal content in Fig. 36) were used to assess the amount of NHE6 present in these cells. Since the T489Yfs form cannot be detected on Western blot, only WT NHE6 can be assessed. Western blotting for NHE6 of iPSCs, NPCs and differentiations at day 10 and day 20 showed a reduction of a higher-molecular weight band in two of the clones (#5.1 and #23) from the T489Yfs patient that was already present in the iPSCs and the most pronounced in the differentiation, where the band was completely lost (Appendix Fig. 44). Because of mosaicism and possible differences in X-inactivation, it is possible that two of the four clones only express the WT mutant (#6 and #19), while two only express the T489Yfs allele. The band at 130kDa which would correspond to a dimer or the fully glycosylated form, however, is still present in all cells (Fig. 37).

Together with the fact that this band is also not reduced in NHE6 k.d. cells and not increased in WT NHE6 cDNA overexpressing cells, the question remains of how specific the band is, and an unspecific binding of the antibody cannot be excluded as mentioned above. While these findings are interesting, it would be necessary to repeat reprogramming and attempts at differentiation to see how consistent the observed reduction is before drawing any conclusions from it. RNA isolation and sequencing from iPSCs and NPCs could shed further light on the allele expressed in those cells.

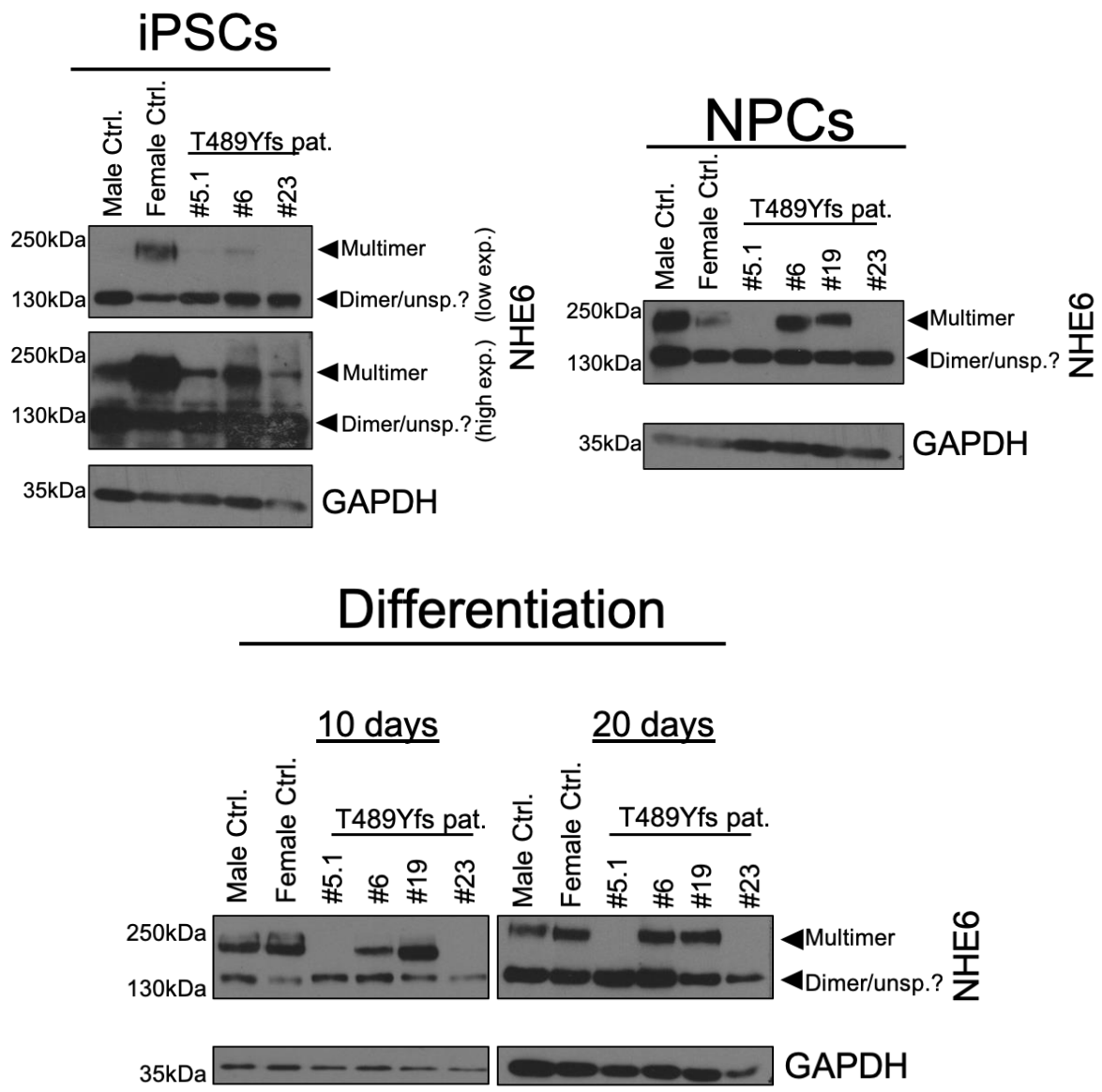

Fig. 37: Western blot for levels of full-length NHE6 in iPSCs, NPCs and a differentiation at 10 and 20 days from two healthy controls (male and female Ctrl., iPSC and NPC lines established by Christine Bus, Department of Neurodegenerative Diseases, Centre of Neurology and Hertie Institute for Clinical Brain Research, University of Tübingen, Tübingen, Germany) or the T489Yfs carrier. #5.1, #6, #19 and #23 denote the four different iPSC lines of the T489Yfs patient used for the generation of NPCs that were then differentiated into neuronal cells (differentiation). GAPDH was used as a loading control. Clone #19 was lost as an iPSC line after NPC generation and could not be used for Western blotting. Samples for the differentiations are the same used in Fig. 36. This experiment was performed one time (n=1).

Nevertheless, the use of iPSCs, NPCs and iPSC-derived neurons is worth pursuing because it allows to investigate neuronal function in a patient-derived model that is closer to the physiological condition that cellular models based on knockdown or

overexpression. Furthermore, iPSCs could be used for differentiation into other cell types affected in CBD, including astrocytes.

4 Discussion

The endosomal-lysosomal system is crucial for a number of cellular processes. Via endocytosis, nutrients enter the cells and receptors get internalised for signalling or termination of signalling. In the endosome, cargo can dissociate from its receptors for removal or transport into the cells, as it is the case with iron delivered via Tfn and receptor-mediated endocytosis. Recycling back of receptors to the plasma membrane enables to a new cycle of internalisation, cargo delivery or signalling, and several cellular processes depend on this.

Cargo in the early endosome needs to be sorted for recycling or degradation and is modified by a number of enzymes active in the endosomal lumen. Ubiquitinated cargo can be degraded via the late endosome and lysosome, thereby removing unwanted proteins, other macromolecules or pathogens. Furthermore, lipids can be processes in the lysosomes and then, together with amino acids recycled from proteins, released into the cytosol for further use. Dysfunctional organelles and protein aggregates are removed via autophagy, and the process is crucial for cell survival during starvation as is it a pathway for replenishing the amino acid pool by protein degradation and recycling.

A number of diseases have been connected to pathological changes in the endosomal-lysosomal, and the impact on the cell is severe. Especially neurons depend on this pathway for synapse function, as receptor internalisation and recycling is crucial for long-term potentiation, thereby influencing synapse strength.[351, 352] Removal of dysfunctional mitochondria and misfolded proteins is especially important as neurons cannot upregulate glycolysis to compensate for energy depletion[353] caused by mitochondrial dysfunction, and are especially vulnerable to oxidative stress and protein aggregation as they are post-mitotic and cannot ’dilute’ accumulated or misfolded proteins via cell division.

The pH in the endosomal-lysosomal system is strongly regulated as many processes depend on correct acidification and are pH-dependent, such as receptor-cargo dissociation and hydrolase activity. The V-ATPase is the key enzyme in acidification of the endosomal-lysosomal system, and finetuning of pH is achieved by alkalisation through the cation exchange function of Na^+/H^+-exchangers 6 and 9. Since NHE6 alkalises the early endosome and is also found to a lower extend in the recycling endosome and at the PM,[307] where it is involved in clathrin-mediated endocytosis,[317]

it plays a role in the sorting of cargo and works as a relay station between the recycling and the degradation pathway.

A loss of NHE6 protein function due to mutations cause a severe form of X-linked mental retardation in hemizygous males, Christianson syndrome, and mutations and variants have been associated with a range of neuropsychiatric conditions from mild intellectual disability, epilepsy to neuropsychiatric disorders in heterozygous females and carriers of milder alterations.

In the work presented here, a loss of NHE6 function due to the T489Yfs mutation was linked for the first time to corticobasal syndrome, which in almost all cases has an underlying pathology where hyperphosphorylated, insoluble tau protein accumulates. The consequences of the T489Yfs mutation and the apparently milder R568Q variant on protein structure and function were assessed, and a NHE6 knockdown model created to investigate the role of NHE6 loss in endosomal-lysosomal dysfunction, and its consequences for cellular processes. In this work, results from the NHE6 k.d. model were compared to the phenotype observed in fibroblasts from a T489Yfs carrier. Furthermore, the possibility of NHE6 dysfunction due to the R568Q variant in brain samples from two carriers and its influence on tau pathology were investigated and induced pluripotent stem cells generated from patient's fibroblasts and controls were used to generated neuronal precursor cells.

In summary, this work shows that dysfunction of the endosomal cation exchanger NHE6 can lead to changes in the endosomal-lysosomal system, influence autophagy and tau phosphorylation, and affect cellular health.

4.1 The T489Yfs mutation affects protein function to a higher degree than the R568Q variant

In an overexpression model, the T489Yfs mutation had several consequences on protein function. The protein was detected to much lower extend on Western blot than NHE6 WT or R568Q, was removed via the proteasome and failed to multimerise. While expression levels of the R568Q variant were comparable to that of the NHE6 WT constructs, levels of the protein also increased after proteasomal inhibition, which did not happen in the WT overexpressing cells. Also, multimerisation was unaffected by the R568Q variant. This shows that while the T489Yfs mutation

has a strong influence on protein stability and turnover, the effect of the R568Q variant is much milder, which is in line with the pathologies observed in the respective families carrying the T489Yfs mutation or R568Q variant, and the occurrence of the R568Q variant in healthy controls. Both the R568Q variant and T489Yfs mutation led to increases in the UPR of the ER, suggesting some influence on protein folding. Even though predicted, NMD seemed not to affect mRNA levels in fibroblasts from the T489Yfs carrier, while full-length and multimerised NHE6 were reduced.

Since the T489Yfs mutation leads to a frameshift in the last transmembrane domain and a premature stop codon, it can be expected that the protein is highly affected. Mutations previously found in Christianson syndrome showed a strong effect on protein structure, and the c.1012_1020del mutation leading to a deletion of amino acids 372-374 (p.Trp372_Thr374del) has a similar defect on multimerisation as the T489Yfs mutation.[329] As homology to other NHEs suggest that the protein is mainly functional as a homodimer or in larger multimeric complexes, a loss of multimerisation will have a strong effect on protein function. The c-terminus removed by the truncation also plays a role in regulation and localisation of the protein, and in RACK1-dependent tethering at the plasma membrane.[310, 313] Other studies had found that a reduction in PM localisation of the protein leads to defects in certain types of clathrin-dependent endocytosis, but not in others (a reduction in Tfn uptake, but not EGF was observed[317]). It is therefore conceivable that in patients carrying the T489Yfs mutation, a similar mechanism leads to a reduction in functional NHE6 by reducing multimers, a loss of protein because of ERAD and proteasomal removal, and possibly NMD, and a lack of function because of mislocalisation, missing regulation and strong dysfunction of protein folding.

Interestingly, the T489Yfs mutation does not only lead to a loss of function of the protein, but also seems to have an additional effect on intracellular pH regulation, as overexpression of this mutation resulted in increased LysoTracker fluorescence in cells expressing endogenous NHE6 that was not caused by a compensatory downregulation of endogenous NHE6. Furthermore, overexpression of T489Yfs NHE6 lead to a higher degree of cell death than overexpression of NHE6 WT or R568Q protein. This argues for a dominant-negative effect of the T489Yfs mutation beyond regulation, maybe by interfering with complex formation of WT NHE6. The

significant increase in LysoTracker fluorescence observed here is especially striking if the comparably low level of mutant protein in these cells is considered.

It is possible that mutated NHE6 can still bind to WT NHE6, leading to the degradation of both that is not detectable in cross-linking experiments because of the low level of T489Yfs and the possible transient existence before removal of these complexes. There remains, however, the question of how relevant this would be *in vivo*, as random X-inactivation in female patients should lead to either the expression of the mutant or wildtype allele, but not both at the same time, so that WT and T489Yfs NHE6 should not occur in the same cell. It also raises the question why the phenotype in females is aging-related, as the severe phenotype with neuronal loss is present at a very young age in males, and neurons expressing the T489Yfs allele in females should not differ from males and be already affected early in life, while the WT expressing cells would not be affected at all. Without the possibility to detect the mutant protein, it will be difficult to answer the question, even though distinguishing between WT or T489Yfs mRNA by fluorescence in situ hybridization (FISH) might be possible to some degree.[354]

For the R568Q variant, the overexpression model could not show a significant difference from WT protein in the parameters assessed in this study, and the presence of the amino acid exchange in non-affected members of the family and in 339 individuals (of which 125 are hemizygous) in the genome aggregation database (GnomAD) would point to high tolerance for this exchange, even though the residue is highly conserved.

Furthermore, no differences were found in the banding pattern of the protein on Western blot, suggesting the absence of a splicing defect *in vivo*. Overexpression of the R568Q variant led to similar results as obtained from wildtype overexpression and might be at most considered very moderately ameliorated. Localisation of the protein does not seem to be affected on a larger scale but further experiments (e.g. co-localisation of the R568Q protein with EEA1, Tfn, PM markers and possibly other intracellular and organellar markers) are needed for a more functional evaluation of the variant. Additionally, changes in regulation by e.g. RACK1 binding could be assessed, or responses in protein localisation after stimulation with Tfn as a paradigm for NHE6 translocation from the PM to early endosomes and for clathrin-dependent endocytosis. It is therefore possible that the R568Q variant has only a very mild effect on ion exchange activity, if any, and may play only a minor role in

causing the observed phenotypes in the patients with CBD and CBS. Another finding supporting this is the presence of an essential tremor that does not segregate with the R568Q variant in the family.

The only finding suggesting a mild effect of the R568Q variant is a not statistically significant upregulation of BiP, which is a sign of an unfolded protein response, and which was stronger than in cells overexpressing the NHE6 T489Yfs mutant or WT NHE6. Substitution of an arginine with glutamine constitutes a moderate change in amino acid properties; arginine is positively charged basic amino acid, with a basic polar side chain, while glutamine is an amide and polar with a neutral charge. Mutationtaster gives a score of 43 out of 215 for the amino acid exchange in terms of amino acid properties that can influence structure[3]; nevertheless, folding of the protein might be affected, which then could lead to proteasomal degradation.

While this might not cause a phenotype when overexpressed as protein is abundant, in a more physiological setting, it is conceivable that the effect leads to changes in protein levels that influence functionality. However, no clear differences between R568Q carriers and pathology-matched controls could be observed in the brain samples in regard to NHE6 levels. There is the possibility that protein levels of NHE6 are low in all of the investigated brain samples since they all come from patients with neurodegenerative diseases with pathological accumulation of proteins, and NHE6 was found to be reduced in brains of patient from AD[335] (protein) and PD[334] (mRNA), most likely in the absence of any mutations. A similar decrease of NHE6 might be therefore involved in several diseases, even though there is the possibility that this happens as a consequence rather than a cause of endosomal-lysosomal or other cellular dysfunction. For example, it would be conceivable that the observed low protein levels of NHE6 are the result of a downregulation to compensate for the increase in lysosomal pH that is commonly observed in aging. It would therefore be interesting to compare the pathological brain samples with samples obtained from healthy age-matched controls that were not available at the time of this study.

Studying effects of the R568Q variant was complicated by the fact that a possible change in splice sites is not represented in an overexpression model that uses

[3] Last retrieved on 25.04.2018 from *http://www.mutationtaster.org/cgi-bin/MutationTaster/MutationTaster69.cgi?sequence_snippet=TTGGCTTTTCC[G/A]GATGTGGTACAACTTT&transcript_stable_id_text=ENST00000370695&gene=SLC9A6&transcript_stable_id_radio=ENST00000370695&sequence_type=CDS&alteration_name=R568Q*

cDNA, but results from cDNA obtained from brain samples of two R568Q carriers suggested no splice site change. Unfortunately, the question of whether or not the R568Q variant was expressed in the investigated brain region at all could not be answered because of a persistent cDNA construct contamination that obscured detection of endogenously expressed NHE6 mRNA.

Only three of all mutations in *SLC9A6* linked to diseases are pure amino acid exchanges (five if variants A9S and R568Q are included), and all three lie in a transmembrane domain; most pathogenic mutations observed in CS have a more severe influence on the protein structure by either deleting parts of the protein (e.g. the p.V176_R201del mutation eliminating the whole fourth transmembrane domain) or by causing a frameshift and premature stop codon (Fig. 38 and Table 1).

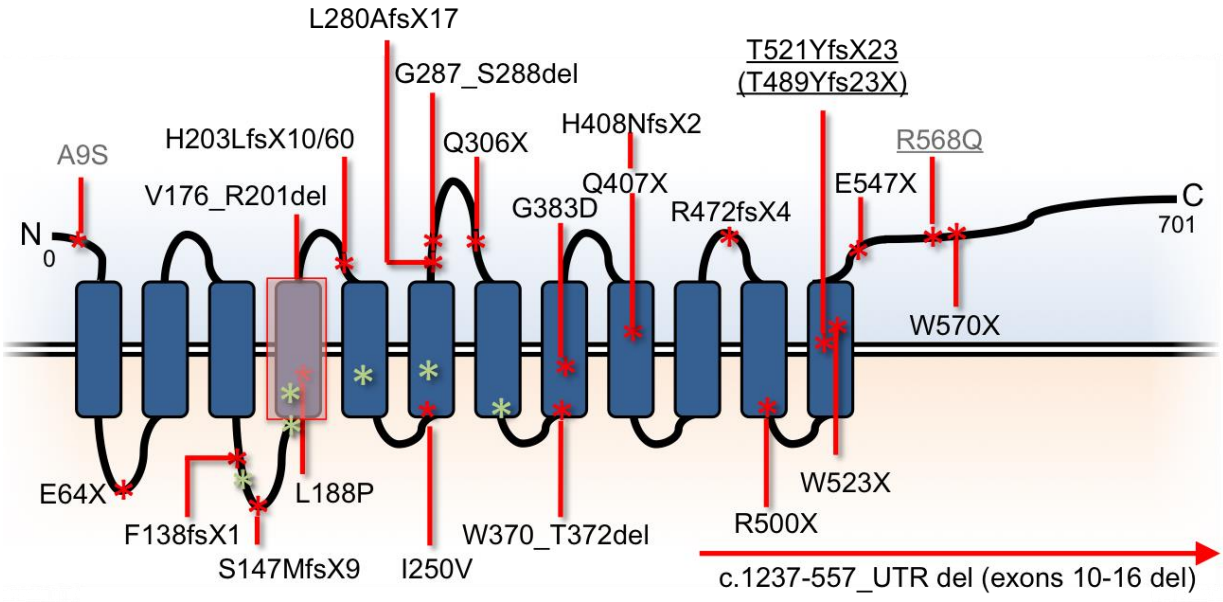

Fig. 38: Overview over disease-related mutations reported in SLC9A6 reported to date. Green asterisk indicate positions of splice site changes. The p.V176_R201del mutation eliminates the whole forth TM domain overlayed in red. All positions are according to the canonical longest transcript ENST00000370695. The two underlined changes are the ones included in this study. Grey variants indicate that a variant was found in the GnomAD database. For references, please see Table 1.

These alterations have been reported in a number of diseases, mostly in neurodevelopmental diseases, with Christianson syndrome and X-linked mental retardation or intellectual disability being the most common ones (because Christianson syndrome is a very rare disease, some of the studies might not have diagnosed a mental retardation with epilepsy and motor deficiencies as Christianson

syndrome). But also epilepsy, one of the features of Christianson syndrome, is a common finding in patients with mutations in the SLC9A6 gene (Table 1). Almost all mutations where found in males, while female patients or disorders in female family members are only rarely reported (Pescosolido et al. report mild to moderate intellectual disability and psychiatric illnesses in female family members of the Christianson syndrome patients included in their study, but do not specifiy which mutation or variant caused which phenotype in females[324]).

Table 1: Overview over disease-related mutations in SLC9A6, including information on the type of alteration and the disease it was reported in. **AA:** amino acid; **ASD**: autism spectrum disorder; **(XL)ID**: (X-linked) Intellectual disability; **XLMR**: X-linked mental retardation; **F**: female; **M**: male

Mutation	Type	Disease	Reference	Comment
p.A9S	AA exchange	Angelman-like syndrome, ASD	Fichou 2009[355], Piton 2011[333]	Frequent in GnomAD
p.E64X	Truncation	Christianson syndrome (males), CBS/CBD, learning and behavioural difficulties, psychiatric diseases, ADHD (females)	Pescosolido 2014[324], Sinajon 2016[326]	
p.F138fsX1	Frameshift, truncation	Christianson syndrome	Pescosolido 2014[324]	
c.316_325 + 28del	splice site change	early-onset epilepsy	Rim 2018[356]	Female patient
p.S147MfsX9	AA exchange, frameshift, truncation	Angelman-like syndrome	Takahashi 2011[357]	
c.526-9_526-5del	splice site change	mild ID, ASD (males), learning and speech difficulties (females)	Redin 2014[358], Masurel-Paulet 2016[321]	leads to skipping of exon 3 and 24aa deletion in TM 4
c.526+1G>A	splice site change	Christianson syndrome	Bosemani 2013[359]	
c.G526-1A	splice site change	Christianson syndrome	Pescosolido 2014[324]	
p.V176_R201del	Deletion	X-linked mental retardation/intellectual disability	Gilfillan 2008[319], Tarpey 2009[325]	
p.L188P	AA exchange	X-linked mental retardation	Hu 2009[360]	
p.H203Lfs*10	AA exchange, frameshift, truncation	Developmental delay with seizures and movement disorder	Trump 2016[361]	
p.H203LfsX60	AA exchange, frameshift, truncation	Christianson syndrome (males), mild mental retardation (females)	Christianson 1999[318]/Gilfillan 2008[319], Tarpey 2009[325]	Gilfillan sequenced the samples from Christianson 1999
c.584+5G>A	splice site change	Christianson syndrome	Mercimek-Mahmutoglu 2015[362]	
p.I250V	AA exchange	Christianson	Weitensteiner	

		syndrome	2018[363]	
c.680+1G>T	splice site change	Christianson syndrome	Riess 2013[336]	
p.L280Afs*17	AA exchange, frameshift, truncation	Cryptogenic Neonatal Infantile Epileptic Encephalopathies, severe ID, autism	Fung 2017[364]	
p.G287_S288del	Deletion	XLID, Angelman-like syndrome	Gilfillan 2008[319]	
p.Q306X	Truncation	Christianson syndrome and retinitis pigmentosa	Mignot 2013[365]	
c.1042-1C	splice site change	XLID	Piton 2013[333]	rs149044510, not in GnomAD
c.1151-1G>A	splice site change	Christianson syndrome and electrical status epilepticus during slow-wave sleep	Zanni 2014[366]	
p.W370_T372del	Deletion	XLID, ASD, stereotyped, repetitive hand movements mimicking Rett syndrome	Garbern 2010[322]	CBD-like tau deposition
p.G383D	AA exchange	Christianson syndrome	Pescosolido 2014[324]	
c.1237-557_UTR del	Truncation	Christianson syndrome	Pescosolido 2014[324]	Exons 10-16 (+3'UTR) deleted
p.Q407X	Truncation	Christianson syndrome	Schroer 2010[320]	
p.H408NfsX2	AA exchange, frameshift, truncation	early infantile epileptic encephalopathy (early-onset seizures and severe developmental delay)	Trump 2016[361]	
p.R472fsX4	Frameshift, truncation	Christianson syndrome	Pescosolido 2014[324]	
p.R500X	Truncation	XLID, Angelman-like syndrome (males), learning difficulties (females)	Gilfillan 2008[319], Tarpey 2009[319], Schroer 2010[320], Pescosolido 2014[324]	rs122461162, not in GnomAD
p.T521YfsX23 (=T489YfsX23)	AA exchange, frameshift, truncation	Christianson syndrome, CBS	Riess 2013[336], this study	
p.W523X	Truncation	Christianson syndrome	Pescosolido 2014[324]	
p.E547X	Truncation	XLID	Schuurs-Hoeijmakers 2013[367], Pescosolido 2014[324]	

p.R568Q	AA exchange	(1) Schizophrenia (F), (2) XLMR (M), (3) severe XLMR with ataxia and epilepsy (M), (4) CBS/CBD (?)	(1) Piton 2011[333], (2) Tarpey 2009[325], (3) Santoni 2014[338], (4) This study	(3): mutation in the ADSL gene as the cause of disease, but could not exclude involvement of the R568Q variant (also in a healthy uncle)
p.W570X	Truncation	Christianson syndrome	Pescosolido 2014[324]	

Since more severe mutations in SLC9A6 are often *de novo*, can only be passed on by female carriers and are therefore usually not sustained for many generations, this would argue for a higher level of tolerance against simple amino acid exchanges in the protein. It could be then expected that amino acid exchanges would be more frequent and also tolerated homozygously (as the homozygous condition in a female reflects the hemizygous condition in males). However, to date, almost no variants listed in GnomAD are found homozygously, and none of the homozygous variants is an amino acid exchange (but rather a splice, intronic or synonymous variant). This is in line with the high level of conservation of the protein, at least in vertebrates (Table 2), but rather unexpected given the severity of disease-related mutations.

Table 2: Conservation scores for the SLC9A6 gene and protein against human (Homo sapiens) from the NCBI HomoloGene Web resource[4].

Species	**Gene Symbol**	**Protein Identity (%)**	**DNA Identity (%)**
P. troglodytes	SLC9A6	100.0	99.9
M. mulatta	SLC9A6	99.3	98.9
C. lupus	SLC9A6	96.7	92.3
B. taurus	SLC9A6	97.7	93.2
M. musculus	Slc9a6	96.6	90.9
R. norvegicus	Slc9a6	96.1	89.6
G. gallus	SLC9A6	93.1	79.8
X. tropicalis	slc9a6	85.8	77.2
D. rerio	slc9a6a	79.2	71.3
D. melanogaster	Nhe3	56.0	56.8
A. gambiae	AgaP_AGAP008718	54.3	55.2
C. elegans	Nhx-5	44.5	51.1

[4] (*https://www.ncbi.nlm.nih.gov/homologene*). Last retrieved in April 30th, 2018.

One possibility for an involvement of the variant in late life neurodegeneration could be in failure to initiate any aforementioned compensatory downregulation of the protein. The R568 residue is adjacent to a regulatory region that would further be affected by the predicted splice site change[337], and a lack of binding of the NHE6 regulator RACK1 to the protein was shown to lead to an increase in endosomal pH[310]. Conversely, enhanced binding via a PKC-dependent mechanism leads to hyperacidification of endosomes in hypoxia as RACK1 binding stabilised NHE6 at the PM[313]. Thus, misregulation or failure to downregulate NHE6 function after an aging-related increase in lysosomal pH would lead to further alkalisation of the endosomal-lysosomal system and excerbate lysosomal dysfunction. This could also explain differences in the age of onset of neurodegeneration between the two sister and the pathology, as aging is a highly variable process. Furthermore, any phenotype caused by a simple reduction of ion exchanger function would make an earlier onset in a male carrier more likely due to the lack of compensation by a healthy allele, while regulatory effects would lead to neurodegeneration at an age comparable to female carriers. Additionally, the low penetrance of the variant could then be a result of environmental, genetic and epigenetic factors influencing cellular aging processes and regulatory processes influencing NHE6 function.

This, however, could not explain the fact that the R568Q variant was found in patients with early-onset diseases such as schizophrenia and X-linked intellectual disability, unless the possibility of differences in affected functions of the proteins depending on genetic and epigenetic background, and environmental factors are taken into consideration. It is, for example, possible that in interplay with disadvantageous factors involved in intracellular pH regulation, lysosomal dysfunction later in life is more pronounce, leading eventually to neurodegeneration. In an interplay with factors detrimental to synaptic function, the variant would tip the balance in the direction of diseases more affecting synaptic function, such as schizophrenia and intellectual disability, and would be benign in the absense of any of these factors.

It is necessary to emphasise that this is highly speculative, and more studies focusing on regulation of NHE6 in different conditions in general and possible effects of the R568Q variant on this regulation would be necessary to determine the involvement of the variant in the pathogenesis of neurological diseases. For this, a

model expressing the variant endogenously would be needed, as a cDNA overexpression model is not only unphysiological, but can also not be used to assess any effect of the G1703A SNP on splicing.

4.2 Loss of NHE6 leads to dysfunction of the endosomal-lysosomal system

In this study, the consequences of loss of NHE6 protein on the endosomal-lysosomal system were investigated. To this end, an inducible knockdown model in M17 neuroblastoma cells was generated and several aspects of endosomal-lysosomal function assessed, including levels of marker proteins and acidification.

Knockdown of NHE6 in M17 neuroblastoma cells led to a widespread dysregulation of the endosomal system, with a strong decrease in endocytosis-related clathrin, an increase in levels of the early endosomal marker EEA1 and, to a lower extend, the recycling endosome protein Rab11, and a decrease in Rab7, which is a marker for the late endosome. Furthermore, levels of the cation-dependent mannose-6-phosphate receptor were strongly increased, a finding that had previously been reported in AD[344].

The dysregulation of marker proteins suggests that in M17 cells with a NHE6 knockdown, the recycling pathway is somewhat favoured over the degradation pathway, as endosomal maturation is impaired. This is in contrast with previous studies that had reported an opposite effect after loss of NHE6, and a stronger acidification of the endosome would, in theory, favour the early-to-late endosomal transition, as pH decreases in the degradation pathway and increases during recycling. Still, defective acidification did not lead to an increase in the recycling of TrkA receptors in one study, but to a reduction of levels on the PM[368].

The observed phenotype might be therefore due to other factors. Whether cargo is destined for degradation or recycling is influenced by a number of factors in the early endosome. Acidification plays a role in early-to-late endosomal conversion, but also the binding of proteins and tubulation by actin-dependent factors[144]. Replacement of Rab5 by Rab7 is crucial[165, 369], as well as the formation of MVBs which is dependent on the sequential recruitment of ESCRT complexes[370]. For recycling, SNX4 is important for sorting of Tfn from the early to the recycling endosome[371], and in general the formation of subdomains on the endosomal membrane has to be intact to

facilitate discrimination between degradation and recycling cargo. Factors facilitating the accumulation of actin and the tubulation of the endosomal membrane might be affected in a way that does not depend on pH, but on the presence of the NHE6 protein, or secondarily as a result of increased EEA1 levels. The non-significant increase in Rab11 on the other hand might be a reflection of a small compensatory increase in NHE9 in reaction to a lack of NHE6, the cation exchanger of the recycling endosome. However, previous experiments have suggested that a lack in NHE9 leads to increased expression of NHE6, but the effect is much smaller vice versa, at least in the cells analysed[303]. Experiments addressing NHE9 levels and pH in Rab11-positive recycling endosomes, as well as any influence of NHE6 on the Rab4-dependent recycling pathway in the M17 NHE6 knockdown model might shed some light on the possible defects in the endosomal recycling pathway.

Loss of acidification in the endosomal-lysosomal system by defects in V-ATPase activity leads to a reduction of cargo degradation, and cargo accumulates in late endosomes and especially lysosomes. While the V-ATPase is somewhat active in the early endosome to provide for a lower pH in the endosomal lumen than in the cytosol, the activity of the V-ATPase increases from early to late endosomes and then to lysosome in an Rab7-dependent manner.[372, 373] Lysosomal pH is not affected in NHE6 knockdown cell, which argues against an involvement in pH regulation at later steps in the endosomal-lysosomal system; rather, dysregulation of the pH might be confined to the early endosome, and maybe, to some extend, to the late endosome. It is therefore conceivable that the observed increase in the number and size of acidic particles is due to overacidified endosomes that then accumulate, as would be suggested by the increase in EEA1. This is further supported by the increased LysoTracker staining in the absense of lysosomal overacidification, as LysoTracker stains vesicles with an pH of lower than approx. 5.5.
Overacidification of the early endosome could have an effect of hydrolase activity and delivery from the TGN. While the majority of hydrolases dissociate from the CD- and CI-MPRs in the late endosomes, delivery can be via the early endosome, and a lower pH there would lead to a premature detachment of hydrolases from MPRs[174]. An ectopic activity of hydrolases and destruction of cargo in the early endosome would then have strong effects on receptor signaling from the endosome, and a detrimental effect of early endosomal signaling has been observed previously in cells

lacking NHE6[315]. Also, cargo for recycling could be degraded before recycling can take place, influencing recycling delivery systems for nutrients and constant receptor signaling processes. A lack of receptors at the membrane could then influence clathrin-dependent endocytosis, and be partially causative of the low levels of clathrin observed in NHE6 k.d. cells.

Additionally, the reduction in clathrin might be caused by degradation in the early endosome, even though under normal circumstances, clathrin is removed from pre-endosomes before they fuse with the early endosome or each other to form endosomes. However, clathrin assembly and uncoating depend on pH, with a pH of 6 optimal for assembly and complex formation, while uncoating requires a neutral pH (pH 7).[374, 375] Of note, intermediate steps where clathrin-positive pre-endosomes colocalise with NHE6 exist before clathrin is removed.[317] It is therefore possible that clathrin removal from pre-endosomes is disturbed in NHE6 k.d. cells, leading to delivery of clathrin-carrying vesicles to the endosome and removal instead of recycling.

Alternatively, clathrin assembly could be affected by a lack of NHE6 and a feedback loop then lead to downregulation of expression. NHE6 is also found at the PM, where it is externalised as studies employing biotinylation of the protein in non-permeabilising conditions suggest. It is not clear whether the cation-exchange is active at the PM, but the fact that RACK1 and PKC interaction with NHE6 can lead tethering at the PM and activitation of the exchanger suggests so. Intriguingly, localisation at the PM and delivery to the endosomes by internalisation from there, as it has been observed for WT NHE6, would lead to a local acidification of the cytosol at the PM if NHE6 is active, while the lumen of the pre-endosome would be alkalised after formation of a vesicle. A similar reverse function has been proposed for NHE5 that alkalises the cytosol when places at the PM and acidifies the endosomal lumen after internalisation[376], a process important in synaptic function. It is possible that NHE6 has a similar effect in which it in contrast act to support a local acidification and then an intraluminal alkalisation. Loss of NHE6 would then rather affect acidification in the cytosol surrounding forming clathrin-positive vesicles at the early steps of endocytosis and defects in pH regulation would inhibit clathrin assembly after invagination (Fig. 39). Delivery of endocytic cargo to the early endosome seems unaffected as Rab5 levels do not change, so Rab5-EEA1 interaction and SNARE complex recruitment are still possible for fusion processes. While endosomal

maturation is somewhat inhibited as suggested by an increase in EEA1 and a reduction in Rab7, it is still possible for cargo to be removed via the lysosomal pathway, which possibly could have an effect on clathrin levels.

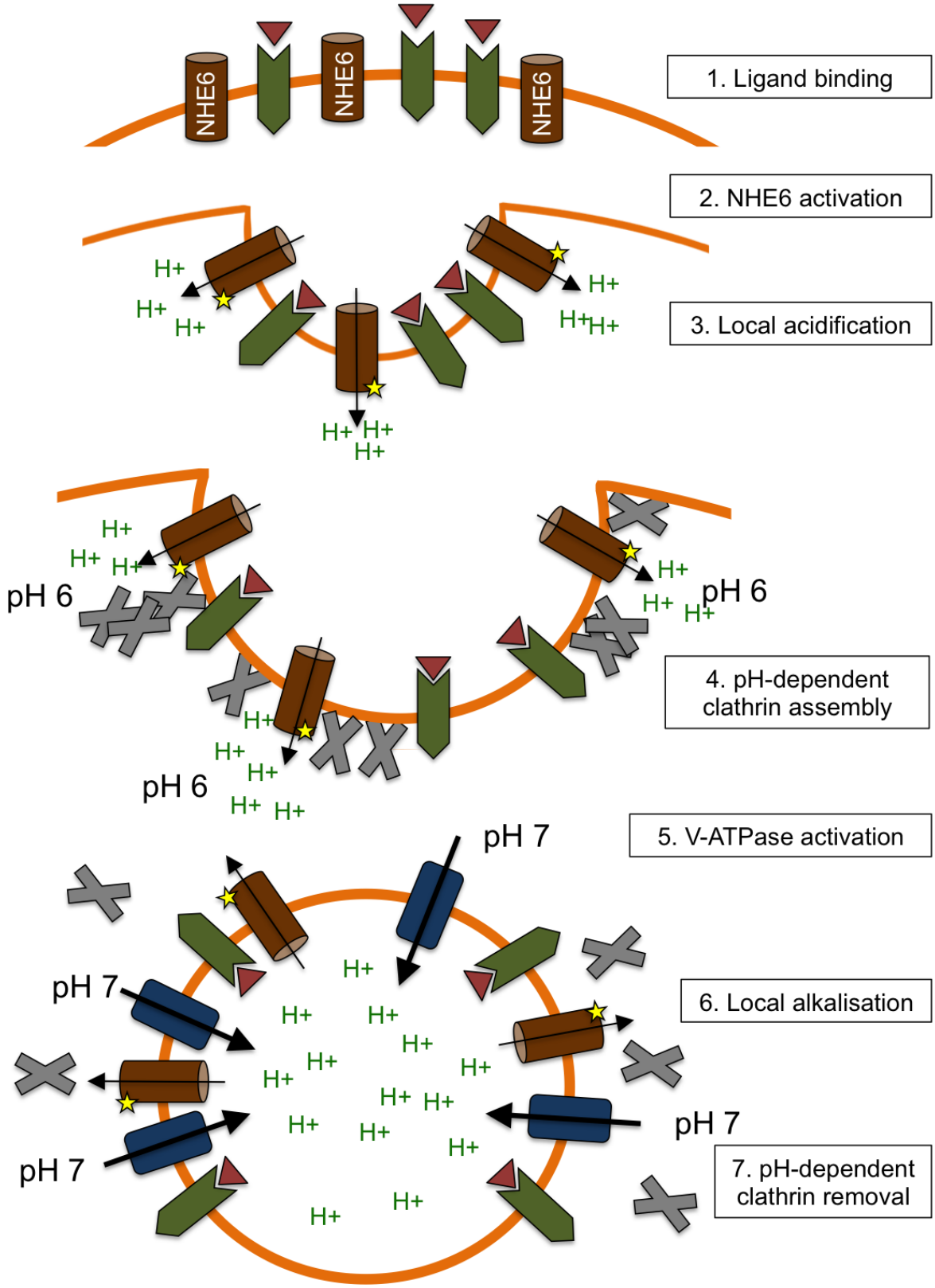

Fig. 39: Model of possible NHE6 and V-ATPase involvement in clathrin assembly by local acidification or alkalisation.

The redistribution from the degradative to the recycling pathway is surprising if pH dynamics in the endosomal-lysosomal system are taken into account. A possible explanation for this would be that simply defective removal of proteins in general via the lysosome are somewhat inhibited, leading to the observed increase in Rab11 and CD-MPR. Another possibility is a defect in cargo ubiquitination and a subsequent upregulation of proteins of the recycling pathway as it is favoured by non-ubiquitinated cargo. Similarily, the degradative pathway would be impaired as binding of the ESCRT complex and subsequent MVB formation is ubiquitin-dependent[370].

It would, however, not be entirely clear how ubiquitination could be affected by loss of NHE6. Either, active recruitment of ubiquitin ligases is impaired, or this could be a secondary effect as delivery of a number of proteins in the endosomal-lysosomal system at least in part depends on externalisation to the PM and then internalisation via clathrin-dependent endocytosis, as it is the case for LAMPs, for example. However, as recycling cargo internalisation is affected by loss of NHE6 while degradation cargo internalisation is not, the ubiquitination of cargo might not depend directly on NHE6.

CD-MPR trafficking to the endosome from the TGN is dependent on retromer. An accumulation of CD-MPR could be caused by two possible mechanisms: a defect in removal of the protein, and an increase in expression. Even though the results are not entirely conclusive, levels of the retromer cargo recognition complex seem to be unaffected by knockdown of NHE6, suggesting that trafficking of the CD-MPR back to the TGN might not be impaired. A defect in removal is therefore more likely, but the functional consequences of this are not clear. It would be interesting to see if levels of hydrolases delivered by the cation-dependent MPR are affected in cells with a loss of NHE6 as an increase in normal functioning CD-MPRs should also lead to an increase in delivered cargo.

Taken together, the dysfunction observed in the endosomal-lysosomal system on the level of marker proteins for different compartments suggest a more complex involvement of pH in the endosome than a simple model where increased acidification always favours the degradative pathway, and increase alkalisation always is in favour of recycling. A number of experiments could be conducted to further elucidate the role of different components in the observed changes in protein level. Measurements using a pH-sensitive dye for live cell imaging, such as pHrodo

coupled to Transferrin, would allow to investigate the pH in the early endosome, and at the same time the rate of internalisation and externalisation could give a further hint at differences in endo- and exocytosis. It should be kept in mind, however, that these measurements would also be affected in a model where degradation happens in the early endosome or cargo is misrouted to the degradation pathway. This could partially be avoided by using a live cell imaging compatible marker for early endosomes such as a BacMam CellLight system similar to the lysosome-RFP used in the LysoSensor experiments.

Furthermore, ICC co-staining using antibodies against EEA1 and cathepsins could help to answer the question whether cathepsins already are present in the early endosome, and data from pH measurements in the early endosome could inform whether the pH is suitable for lysosomal hydrolase activity or not. Additionally, activity of cathepsins could be measured by overexpression of cathepsin target sequences with two fluorophores using Förster resonance energy transfer (FRET) efficiency, where the signal is dependent on proximity of the two fluorophores that would be disrupted by cathepsin cleavage. This measurement would be possible in fixed cells as well, where co-staining with EEA1 would allow to specifically assess cathepsin activity in early endosomes.

In addition to the endosomal pathway markers, a marker protein for autophagy was affected. In M17 cells with a loss of NHE6, levels of the autophagic marker proteins LC3-I and LC3-II were reduced under both baseline and starvation conditions, and the upregulation of LC3-II observed in the control was not seen in NHE6 k.d. cells, indicating an impairment in the initiation of starvation-dependent autophagy. Nevertheless, inhibition of removal of autophagosomes by BafA1 led to an accumulation of LC3-II, suggesting that autophagy is induced under normal conditions and effectively cleared. LC3-II accumulation in BafA1 treatment was increased compared to control when normalised to levels of LC3-I, but reduced if normalised to total protein content. A lower amount of LC3-I protein might be due to an increased conversion into LC3-II and removal of the protein, which then could lead to an effect where autophagic acitivity is already at the highest level possible and that can no longer be increased by amino acid starvation. One explaination for a constantly activated starvation reponse would be that mTORC1-dependent inhibition of autophagy by amino acids is dependent on endosomal maturation[206, 377]. Under

normal circumstances, abundant amino acids activate mTORC1, which then inhibits autophagy by preventing formation of the complex necessary for phagophore formation[378]. Amino acid starvation conditions lead to less mTORC1 activation and hence increased autophagophore formation. However, impaired endosomal maturation as indicated by a reduction in Rab7 levels would prevent the starvation signal from being terminated even when amino acids are abundant. Amino acid starvation related autophagy would then be constantly active, leading to a depletion of the LC3-I pool, but still accumulation of LC3-II under BafA1 treatment. Experiments addressing levels of activated mTORC1, or indirectly of phosphorylated Atg13 as Atg13 phosphorylation by mTORC1 inhibits autophagy[379]. If a decrease in endosomal maturation is responsible for the observed reduction in LC3-I with accumulation of LC3-II under BafA1 treatment, NHE6 k.d. should lead to a reduction in phosphorylated Atg13 compared to control cells under conditions where amino acids are abundant.

It is important to notice that apart from the canonical autophagy pathway of LC3 lipidation via ATG7, ATG5 and ULK1, LC3 also can be become lipidated in a non-canonical pathway related to endocytosis. This pathway can be activated by disruption of lysosomal acidification[380], which might be relevant to the situation encountered in cells with a lack of NHE6, albeit with pH changed into a different direction. Investigation of changes in a number of other proteins involved in different steps of autophagosome formation and removal, such as WIPIs, p62/SQSTM and Atgs, could therefore be of interest to explain this finding.

The picture is further complicated in fibroblasts from controls and the T489Yfs patient. While levels of LC3-II in the different conditions differed in the patient from the control in each experiment, the effect observed was oppositional in half of the experiments. Either, levels of LC3-II were elevated in baseline conditions already, which was not further exacerbated by starvation or BafA1 treatment and suggests a block in removal of autophagosomes but correct initiation of autophagy. Or LC3-II did not accumulate under amino acid starvation or BafA1 treatment, suggestive of a dysfunctional initiation of early steps of autophagy.

Since function of the endosomal-lysosomal system in fibroblasts depends on a number of additional factors such as confluency, passage and growth dynamics[346] that are difficult to control even under experimental conditions, this could lead to

differences in the effects of the T489Yfs mutation on autophagy. Also, it has to be kept in mind that NHE6 expression is rather low in fibroblasts, even though there is some evidence for hyperacidification of the endosomal-lysosomal in the T489Yfs patient cells using LysoTracker in microscopy and flow cytometry. Furthermore, while the results from the one patient line offer some interesting insights, additional lines carrying the T489Yfs mutation, and ideally isogenic controls, would be a more robust way to elucidate any phenotype caused by the defect. For this, a model closer to neuronal cells would be better, for example in the form of iPSC-derived neurons, as studying defects of the endosomal-lysosomal system proved to be associated with cell-type specific difficulties in fibroblasts. Here, both a gene corrected line from one or more T489Yfs carrier as well as a line from a healthy age-matched control with a knock-in of the T489Yfs mutation would be useful. A similar approach would also be helpful with the R568Q variant, as the influence of genetic background on the phenotype could be assessed and offer some new insights into the interplay between NHE6 and other factors exacerbating or ameliorating any phenotype.

Using such models, the question of endosomal dysfunction such as hyperacidification, trafficking defects, and possible differences in levels of marker proteins and components of the endosomal-lysosomal system, as well as any defects in autophagic removal of cargo could be addressed in a more accurate and exhaustive way.

4.3 Tau phosphorylation is increased in M17 neuroblastoma cells with reduced levels of NHE6

An important feature of both CBD and Christianson syndrome, as well as in many pathologies causing CBS, is accumulation of insoluble, hyperphosphorylated tau in neurons and astrocytes. Furthermore, dysfunction of the endosomal-lysosomal system is a common theme found in tauopathies, and posttranslational modifications of tau such as truncations originate in the endosomal-lysosomal system, for example by cathepsins[112]. Futhermore, while normal tau is removed by the proteasome, accumulated or hyperphosphorylated tau, or tau carrying other disease-related modifications such as acetylation, depends on lysosomal removal via the autophagic pathway. In turn accumulation of defective tau and a loss of function of the protein

can influence lysosomal degradation properties by overwhelming the lysosomal degradation machinery. This also has effects on the transport of compartments of the endosomal-lysosomal system to the perinuclear area, a process that is important for correct acidification and fusion of late endosomes and lysosomes.

In the M17 neuroblastoma NHE6 knockdown model, hyperphosphorylated tau accumulated, suggesting a defective removal of tau protein caused by defects in the endosomal-lysosomal system and possible defects in tau processing by lysosomal hydrolases such as cathepsins. Unfortunately, it was not possible to elucidate the effect of other posttranslational modifications, especially of proteolytic cleavage, as this requires dephosphorylation and a high amount of tau that could not be achieved in a cell culture model. Still, modification such as acetylation can be detected by specific antibodies, as well as the ratio of 4R to 3R tau in these cells, and it would be of interest to see if acetylation is affected by a knockdown of NHE6.

While the most conceivable explanation for the observed accumulation of hyperphosphorylated tau is a defect in removal of the protein, another factors influencing the accumulation of hyperphosphorylated tau could be an increase in levels of oxidative stress. Oxidative stress is known to effect tau processing, and cytosolic oxidative stress is increased in the M17 NHE6 knockdown model. Higher baseline levels of the outer mitochondrial membrane protein TOM22 suggest that defective removal of mitochondria by mitophagy might play a role, but a further assessment of mitophagy using mitochondrial toxins as an inducer of mitophagy were not successful.

It would be interesting to investigate this in another model that allows for better testing of mitochondrial dynamics that are altered in cancer cells such as M17 neuroblastoma cells, and presumably a stronger effect might be observed in neuronal cells that heavily depend on mitochondrial function. A dysfunction of mitochondria leading to complex inefficiency and subsequent increases in ROS production would explain the observed increase in oxidative stress that was, however, only accompanied by a very modest increase in oxidative damage. An effect from higher protection in cancer cells against oxidative damage or a "dilution" effect of damaged proteins due to the high cell division rate could then be either excluded or serve as an explanation for the observed strong effect of a NHE6 knockdown on higher cellular ROS compared to the moderate effect on protein and lipid modification by the produced ROS. The influence of ROS and defective removal

could be further tested by assays using antioxidants, or trying to abolish hyperacidification by treatment with compounds such as Bafilomycin A1, chloroquine or NH_4Cl. However, titration of the correct concentration for the latter can be difficult as rises in pH will equally have a detrimental effect on endo-lysosomal function, and even in the inducible knockdown model, small variations in knockdown efficiency will further complicate any experimental rescue with compounds. This includes effects of a slow instead of an instant reduction in these cells, as mRNA knockdown only becomes effective if the protein existing at the start of the miRNA expression is removed by degradation pathways. Any concentration would then be only effective at a very specific timepoint, and time-dependent processes (e.g. tau accumulation over time) might not show up in an experiment, or be the result of increase pH in the endosomal-lysosomal system at earlier time points. The same holds true for any attempt to rescue the phenotype by overexpression of the WT NHE6 protein.

Again, a model using iPSC-derived neurons with a knockout of the gene would be useful, as a knockout would eliminate the difficulties and time-dependency of a knockdown approach. Given the severe effect of a complete lack of NHE6 proteins in human cells, however, it might be difficult to create a knockout model in cell culture where conditions are less optimal for neuronal survival, and a first attempt to do so failed. Here, a cancer cell knockout model that would be naturally more resistant to cell death could be used, albeit with different disadvantages regarding tau expression and mitochondrial function in cancer cells.

4.4 The R568Q variant does not lead to an exacerbated pathology in brain samples from two carriers with different pathologies

Brain samples from four brain regions of two patients carrying the R568Q variant were analysed in regard to tau pathology and endosomal marker proteins. One patient showed a CBD pathology at autopsy with tau accumulation in astrocytes and neurons, while the other patient was diagnosed with CBS in life, but found to have a mixed pathology with only a small influence of tau in the form of ARTAG.

When sarkosyl soluble and insoluble tau fractions of the R568Q-CBD patient were analysed, the tau phenotype seemed to be milder compared to CBD controls. While CBD controls showed a smear typical for severly modified tau in the sarkosyl

insoluble fraction, the R568Q-CBD patient had increased insoluble tau compared to CBS and mixed pathology cases, but reduced if compared to idiopathic CBD, and the smear covering a large number of molecular weights of the protein was absent. In the R568Q-CBD case, soluble tau did not differ from insoluble tau in terms of observed molecular weights. This is interesting as it would suggest that tau accumulates and becomes insoluble in the absence of the posttranslational modification usually found in the pathology, and is in contrast to the typical CBD phenotype found upon autopsy. However, an effect of storage conditions and post mortem delay cannot be excluded.
In the R568Q-CBS patient, on the other hand, insoluble tau was almost absent, as it was in pathology-matched controls.
Still, while the effect of the R568Q variant in cells overexpressing the cDNA suggested only a small, if any effect on protein activity, even though folding seemed to be impaired, this would argue for a strong effect on removal of protein while the effect on posttranslational modifications would be unremarkable. If the mixed pathology of the R568Q-CBS patient is taken into account, the R568Q variant, together with underlying genetic and environmental factors, might lead to a general defect in protein removal that then causes accumulation of several aggregation-prone proteins such as tau in the CBD, but TDP43 and α-synuclein in the CBS patient. The nature of the aggregating protein would be in this case not an important feature of the pathology, but rather a consequence of defects in the endosomal-lysosomal system. In mice with a NHE6 knockout, higher levels of unesterified cholesterol were found (but no tau accumulation)[330], suggesting that efflux from the lysosome into the cytosol is disturbed. This is a possibility for an effect on cellular function regardless of protein accumulation and protein removal.
Another finding of interest regarding soluble and insoluble tau fractions in the R568Q carrier with CBD was that, unlike in pathology-matched controls, both soluble and insoluble tau seemed to have a higher levels of 3R tau and not 4R tau. Calculation of ratio 3R and 4R is not possible because of the possibility of different binding efficiencies of the two antibodies, but the absence of 4R tau in the insoluble fraction of the R568Q-CBD carrier and the increase in 3R tau compared to control CBD cases suggests that different isoforms might accumulate in R568Q carriers. Still, overall levels were higher than in the R568Q-CBS case and mixed pathology-matched controls. Even though these findings are not exhaustive and experiments need to be repeated as well as expanded to other brain regions, the possibility

remains that the R568Q-CBD carrier shows tau accumulation that mirrors CBD in distribution and form of pathology, but where tau is biochemically distinct from that in other CBD cases. If these results could be confirmed not only in further brain samples, but also maybe in R568Q knock-in neurons with isogenic controls to rule out any influence of the genetic background in the family, it would provide interesting insights into possible effects of different origins of tau pathologies (endosomal dysfunction, oxidative stress, influence of mutations in tau, changes in kinase/phosphatase activity) on tau modifications and accumulation. There is also the fact that in many tauopathies, there is an involvement of astrocytes in the pathology, while tau phenotypes in AD and PD are restricted to neurons. Astrocytes only express very low levels of tau, so there is the possibility that any tau pathology observed in astrocytes is of neuronal origin. Furthermore, tau was found to be released physiologically via the synapse, a process which increases under lysosomal dysfunction and starvation conditions[381]. It would be of interest to find out why in some tauopathies, pathologic tau is taken up into astrocytes and cannot be removed, while in other neurodegenerative diseases tau is either not taken up or can be effciently removed by astrocytes. Differences in posttranslational modifications and accompanying biochemical factors might play a role, which in turn might be due to different origins of tau pathologies.

The R568Q variant has been found in a number of other diseases that primarily show defects in synapse function, such as epilepsy, schizophrenia and mild intellectual disability, and are not caused by pathological protein aggregation. In general, the R568Q variant seem to have only a mild effect on protein and therefore cellular function, as it is also found in healthy controls. Whether or not it is involved in any pathogenesis might depend in additional factors, such as a second mutation that is suggested by the occurance of an essential tremor in the absense of the SLC9A6 variant in the family described here. Environmental factors might also lead to the observed differences in diseases and pathologies connected to this variant, suggesting that the R568Q variant might be rather a risk factor than causative, if connected to a specific disease at all. This is further underlined by the fact that both carriers investigated here lived up to a high age, and in this model the R568Q variant confers susceptibilty to neurodegenerative diseases and protein aggregation, while secondary factors play a role in specificity of aggregating proteins and disease

phenotype in this family. However, the fact that the variant was found in diseases most in biased targeted screens (e.g. screening of synaptic or X-chromosomal genes) might skew the picture as genetic factors possibly involved in the disease are not addressed in the screen and will therefore not be described. Together with the fact that in the two families where more family members than the index patient were assessed (this study and Santoni, 2014[338]) a non-symptomatic carrier is described, it cannot be excluded that the few reports of the R568Q variant in neurodevelopmental or –degenerative diseases are simply coincidental findings (in the paper by Piton[333], the mother of a schizophrenia patient is described as carrying the mutation, but no definite statement on disease status is made. It is, however, likely that she is not affected with schizophrenia or other neurological or neuropsychiatric diseases as the authors mention the disease status of other carriers in the family in other cases). Further experiments establishing a functional effect of the variant (on splicing, folding, localisation and ion exchanger function, i.e. endosomal pH) would be needed to support any population- and prediction-derived conclusions.

4.5 Cell death in M17 neuroblastoma cell models and T489Yfs fibroblasts

Since region-specific cell death is a prominent feature of CBD and other tauopathies, it was of interest to evaluate levels of cell death in the M17 knockdown model, M17 cells overexpressing NHE6 WT, T489Yfs or R568Q, and fibroblasts from the T489Yfs patient.

In M17 NHE6 knockdown cells, binding Annexin V to the early apoptosis marker PS was increased, albeit not significantly. Even though cell death is still possible in cancer cells, apoptosis is usually inhibited, at least to a certain degree, and a marker of early apoptosis might detect only a certain subset of dying cells, therefore another measurement of cell death might shed a clearer light on the question of whether or not knockdown of NHE6 is lethal.

A non-apoptosis related way of measuring cell death is activity of LDH in the cell culture medium as it is released from the cells if integrity of the PM is impaired. In fibroblasts carrying the T489Yfs NHE6 mutation, LDH release in into the medium was slightly, but not significantly increased if compared to controls, but staurosporine treatment did not exacerbate this to a higher degree than in controls, suggesting that

T489Yfs fibroblasts are not more susceptible to apoptosis than controls, and that it is possible that cell death observed in T489Yfs fibroblasts is not programmed cell death, but rather necrosis-like. This would be in line with the finding that cells in neurodegenerative disorders often escape apoptosis and enter another mode of cell death that is less controlled and leads to inflammation; however, the findings are not substantial enough to draw any conclusions regarding mode of cell death and the extend.

Intestingly, cells overexpressing T489Yfs show a strong increase in cell death compared the transfection control, while LDH release is slightly increased if compared to WT NHE6 and R568Q NHE6 overexpressing cells. An increase in cells overexpressing functional NHE6 is not surprising, as fine regulation of the endosomal-lysosomal pH is crucial for cellular function and dysfunction can lead to lysosome-dependent cell death. The increase observed in T489Yfs overexpressing cells, however, is not in line with a simple loss of function model which would lead to an effect similar to that observed in the transfection control. Again, as suggested by LysoTracker data from overexpressing cells, this might describe a toxic gain of function where T489Yfs NHE6 has additional effects. While several pathways are possible, it should be considered that at least in cell death, it is possible that overexpression of a misfolded protein as suggested by data from BiP in these cells could lead to an overwhelmed proteasome and ER machinery, thereby exerting the toxic function. This would be, however, not in line with the data from the R568Q variant overexpression, which shows much higher levels of protein on Western blot and led to a stronger effect on BiP levels, but did not show an increase in cell death that would mirror this discrepancy between R568Q variant and T489Yfs mutation. It remains therefore unclear how this effect is caused, as data from other experiments including multimerisation and acidification of the endosomal-lysosomal system make a normal protein function of T489Yfs highly unlikely. Therefore it is not likely that the lack of a distinct difference between WT, T489Yfs and R568Q NHE6 in LDH release in overexpressing cells is due to a normal function of the T489Yfs protein.

It would be interesting to further address this question by, for example, proteasomal inhibition or a slight alkalisation of the endosomal-lysosomal system in these cells using very low concentrations of chloroquine, BafA1 or NH_4Cl. In the case of a distinct gain of function of the T489Yfs NHE6 protein, inhibition of proteasomal degradation might further increase the effect observed, and it would be further

interesting to see if there is a dose-dependent relationship between the amount of protein expressed, and cell death and hyperacidification observed when the T489Yfs mutant is overexpressed.

Because overexpression of any protein is not physiological, it would have been of great interest to study the effects of the T489Yfs mutation in neuronal cells expressing this protein. To this end, fibroblasts from the T489Yfs patient were reprogrammed into iPSC, and NPCs generated from these cells. While generation of iPSCs is possible and NPC generation was equally successful, several separated attempts at differentiation into midbrain-specific dopaminergic neurons failed because of detaching cells in all four patient lines. It is difficult to interpret this, as unsuccessful differentiation is not necessary dependent on mutations and not necessarily a phenotype. But it is interesting that the amount of neurons decreases in not dorsalised cells that would consist of a more mixed population, and that the higher molecular weight band in NHE6 that is usually observed on Western blot is decreased in two clones in iPSCs, further decrease in NPCs and absent in cells that were differentiated for 10 or 20 days. This could be the result of differential X-inactivation after reprogramming[382] or a pre-existing mosaicism in the patient fibroblasts, as iPSC lines are created from single cells.
It would be of great interest to solve the problem that leads to detachment of these cells during differentiation. It is conceivable that NHE6-dependent internalisation of the TGF-β3 receptor is disturbed by the T489Yfs mutation, therefore leading to defects in cell adhesion[163]. It might be possible to circumvent this problem if another adhesion molecule receptor is found whose internalisation and signaling are not NHE6-dependent. Additionally, it would be necessary to repeat all steps from reprogramming to differentiation to exclude possible batch effects to be able to make any conclusions regarding the question whether or not the T489Yfs mutation in NHE6 plays a role in detachment of these cells. Another possibility would be to try different protocols for differentiation, for example into cortical neurons or even astrocytes, as results of the mutation might differ depending on cell types. Differentiation into astrocytes and neurons, as well as a possible co-culture could also help to shed some light on the origin of the tau pathology observed in astrocytes. If tau aggregates in astrocytes stem from modified tau in neurons, a culture of astrocytes alone should not develop a tau phenotype, while it would still be

possible in a co-culture with neurons. Also, different modifications of tau could be assessed in regards to their potential for an astrocyte pathology.
However, the T489Yfs mutation leads to a strong phenotype in hemizygous males expressing only this mutation, including neurodegeneration and protein accumulation. It is therefore conceivable that differentiation of iPSCs or NPCs into a purely neuronal population might be difficult if in fact only the mutant allele is expressed. Since the detachment happens as well in at least one line that shows a higher molecular weight band in the NHE6 Western blot, secondary effects of another mutation that was not tested as a part of the FTLD panel, a defect acquired during reprogramming or other effects are possible explanations as well. Still, to address tau pathology, endo-lysosomal dysfunction and consequences on mitochondrial and, possibly, synaptic function, a human neuronal model would be helpful. This is especially the case as the existing NHE6 knockout mouse model does not develop tau accumulation and the phenotype in these mice only mirrors motor, but not other symptoms found in Christianson syndrome patients[330, 331].

4.6 A model of dysfunction of the endosomal-lysosomal system caused by a loss of NHE6

In this study, the effect of defective alkalisation and pH regulation in the early endosome due to loss of NHE6 was investigated using a neuronal cancer cell model with an inducible NHE6 knockdown, fibroblasts from patients carrying a mutation leading to a frameshift, premature stop codon and loss of the c-terminus of the protein, and an iPSC model was generated from fibroblasts with the T489Yfs mutation. Furthermore, tau pathology was assessed using brain samples from a CBD and a CBS patient carrying the R568Q variant that had been previously implied in several diseases but where the involvement in CBS/CBD is less clear than in the mutation.
The comparison between a severe mutation (T489Yfs) that causes Christianson syndrome in hemizygous males and is connected to CBS in two female carriers of this family and the mild R568Q variant allows to investigate different levels of possible NHE6 dysfunction. While the T489Yfs is strongly connected to the disease, the R568Q can be proposed as a risk factor whose outcome depends on several

accompanying circumstances, such as the presence of another mutation and/or environmental factors.

Loss of NHE6 function has severe consequences on several cellular processes, including endocytosis, recycling of receptors and signaling, removal of defective waste proteins and macromolecules such as lipids, removal of defective organelles via autophagy, and regulation of amino acid content in the cell in response to starvation stimuli.

In a model of cellular dysfunction caused by NHE6, the finetuning of the pH in the early endosome, and possible to a lower extend at the PM and in the recycling endosome, determine a number of steps downstream from the early endosome that serves a sorting station and initiation factor for further processes (Fig. 40). These processes include autophagic removal of protein aggregates and defective organelles such as mitochondria, that then have a further detrimental effect on cellular health and the endosomal-lysosomal system.

In this model, an increase in the pH in the early endosome because of a lack of NHE6 function influences the endosomal-lysosomal system and related processes, including endocytosis and conversion of early into late endosome which are reduced. This in turn influences levels of LC3 and thereby autophagy, leading to an accumulation of (defective) mitochondria. A defect in mitochondria and a general increase in mitochondrial mass increases ROS, that influences tau phosphorylation and aggregation. Since the removal of tau aggregates via autophagy also is disturbed, tau accumulates. The ROS itself is negatively affecting mitochondrial health, as is tau aggregation because of disturbances in mitochondrial transport along microtubule. Similiarily, transport of late endosomes necessary for perinuclear fusion with lysosomes is affected, further exacerbating the endo-lysosomal phenotype.

Lysosomal removal of cargo has not been addressed in this study, but might be affected, as well as other processes like lipid processing including cholesterol esterification, release of amino acids into the cytosol, chaperone-mediated autophagy, and possibly lysosomal cell death. The same is true for receptor and cargo recycling back to the PM via NHE9-alkalised recycling endosomes, and in general the correct transportation and processing of cargo through the endosomal-lysosomal system.

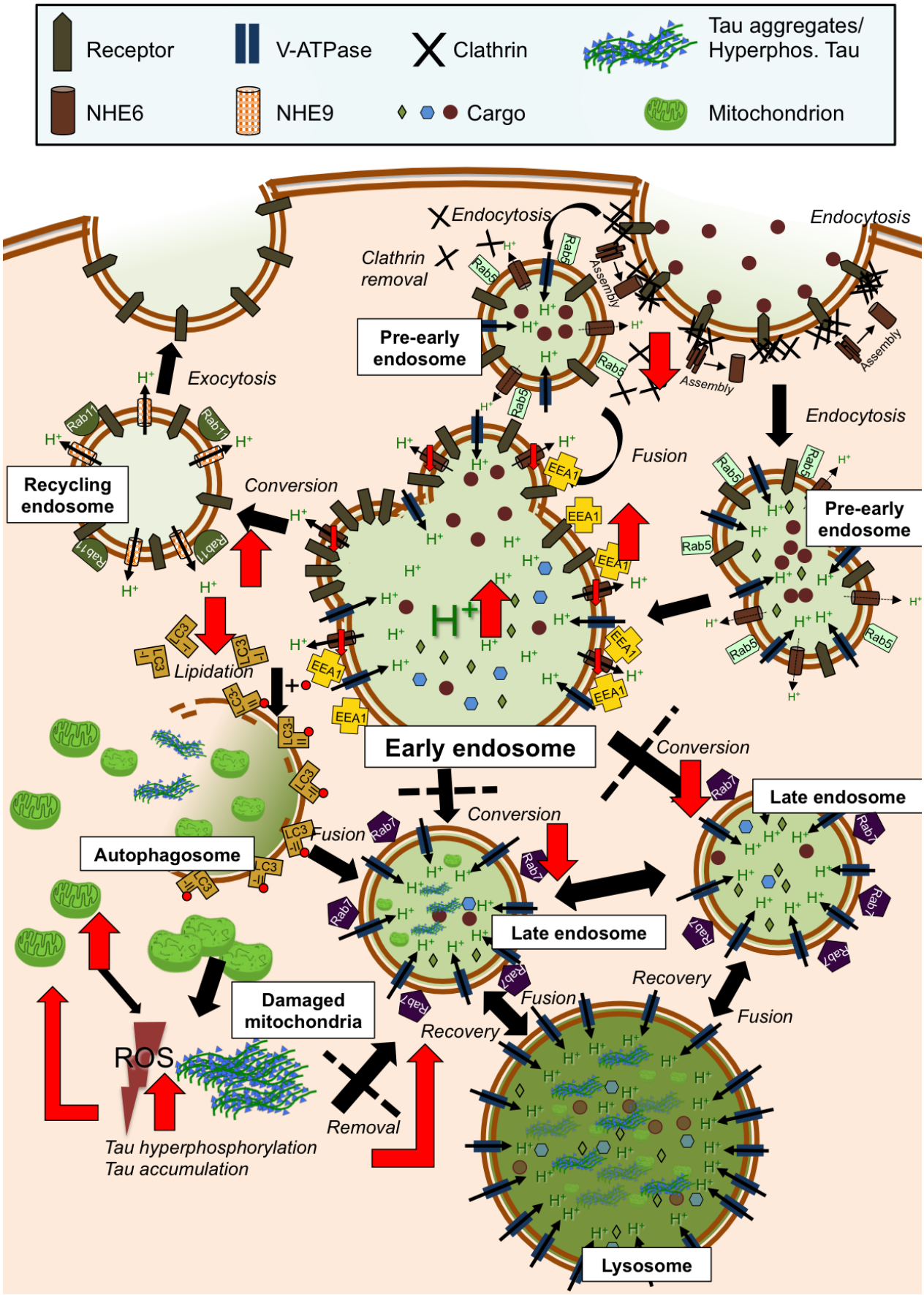

Fig. 40: Schematic of the endosomal-lysosomal system. Arrows in red indicate changes after a loss of NHE6 function.

4.7 Outlook

There are several possibilities to influence endosomal-lysosomal pH in a cell culture setting, and as overacidification of the endosomal-lysosomal system might play a substantial role not only in CBD and CS but also other neurodegenerative diseases, the development of effective regulators of endosomal-lysosomal pH could be of interest. To this end, a functional, disease-relevant model that allows for testing of several compounds in an automated fashion could be useful.

In recent years, targeted gene modifications using CRISPR/Cas9 technology have become increasingly popular due to their precision, easy generation and cost efficiency. There are several possible models that can be generated using this technology: for example, a knockout of the whole gene or certain functional features of the protein is possible by removal of exons, or replacement with resistance genes that allow for quick selection of modified cells. To study the effect of certain mutations or to model the effect of protein features changed by either a disease-related mutation, or by an artificial mutation in a regulatory or functional domain, a knock-in using cutting by CRISPR-Cas9 endonucleases and homologous recombination from a template single stranded donor oligonucleotide (ssODN) can be employed. This is especially attractive as the cell line modified can be used as an isogenic control that shares the genetic sequence of the modified cells except for the introduced mutation or knocked out gene, and allows for isolation of effects caused by this gene only. If age- and gender-matched controls are employed during studies using patient material, an additional effect by genetic variance and environmental background between controls and patient in addition to any present disease-related changes cannot be excluded. Gene correction by changing the disease-related mutation and leaving the rest of the genomic sequence untouched is therefore another good possibility, in addition to a knock-in of a mutation, to isolate effects of the mutation and circumvent the pitfalls of using heterogenous controls.

The last possibility is to tag target genes to study their endogenous expression. This would be especially interesting if a mutation such as the T489Yfs is investigated, as an endogenous expression of the protein, its localisation and interaction with possible WT NHE6 and similar properties could be elucidated without having to fall back on unphysiological overexpression of the gene. It would also reduce the need to develop an antibody that can bind to the N-terminal region of the NHE6 protein and, therefore,

a region rich in transmembrane domains, to detect the truncated T489Yfs NHE6 protein.

It would be very interesting to investigate the T489Yfs mutation in a model of gene correction or when knocked in into an iPSC cell line of a healthy control. This could maybe help to circumvent the possible difficulties during differentiation of iPSCs and NPCs from the T489Yfs carrier that were encountered during the course of this study, if they should persist in the future and factors such as an influence of the initial reprogramming can be included. Furthermore, it could be then tested whether the observed detachment is indeed connected to the T489Yfs mutation, and could then serve as a model to improve cellular function.

While the T489Yfs mutation could be of special interest because of both the strong effect that it has in patients, and the possibility of a gain of function, the much milder effect of the R568Q variant could also be investigated using similar models. This could be of special interest in another context, as the variant might play a role in other diseases than CBS/CBD. Therefore, further knowledge on its potential disease-causing properties could shed some light on cellular dysfunctions in diseases such as schizophrenia, intellectual disability, and other neuropsychiatric or neurodevelopmental diseases, where little is known so far on etiology, but which represent a high burden on patients, family and society. Since some carriers of the R568Q variant are reported as unaffected and secondary factors seem to be involved, there is at least the possibility to influence other factors to ameliorate the diseases related to the R568Q variant even if NHE6 function in itself cannot be improved, opening a road to new treatment options in these diseases. There are currently no fibroblasts from carriers available, and gene correction in one or several healthy controls could make it easier to investigate the R568Q variant, as the presence of a second mutation in the family described here is very likely. Also, cell culture of neurons could help to at least to some extend to investigate changes at the synapse that cannot be model using a neuronal cancer cell line, and as mentioned before the NHE6 knockout rodent model existing only partly resembles the phenotype observed in CS. This includes expression of synaptic marker proteins, neurotransmitter metabolism and removal and signalling pathways in neurons stimulated by the addition of glutamine. Similarly, iPSCs could be differentiated into astrocytes and co-cultured with neurons or in a purely astrocytic culture to investigate

the involvement of glial cells on disease etiology, progression, and potential ways to ameliorate the disease phenotype.

It might also be interesting to further investigate the involvement of NHE6 in other aging-related neurodegenerative diseases apart from CBS/CBD and CS, and to further investigate the previously published involvement in AD and PD. As loss of NHE6 had a severe effect in our knockdown model, even moderate changes in protein function might affect cellular health in a long-term fashion as age-dependent decreases in endosomal-lysosomal function increase. This could be done by testing for levels of NHE6 in brain samples post mortem, and even combining results with changes in the endosomal-lysosomal system observed in tissue or cerebrospinal fluid, where at least in PSP changes in endosomal proteins correlate with the disease.[383] Even though disease-related mutations in *SLC9A6* are rare, most likely because of the severe outcome that leads to evolutionary selection against such mutations, it is conceivable that protein function or levels might be affected during lifetime. A way of evaluation NHE6 function such as recovery of endosomal pH after acidification-induced stress could elucidate whether the protein function is diminished in several settings, and how potential differences in dysfunction might affect disease type and progression differently. A more diverse picture of endosomal-lysosomal dysfunction could then allow for the development of more targeted medications, or maybe serve as a tool in diagnostics.

A recent study is of particular note in this regard, as Prasad and Rao reported an epigenetic loss of NHE6 protein in astrocytes derived from a humanised mouse model carrying the AD-related ε4 allele of Apolipoprotein E (ApoE4)[384]. This lead to endosomal hyperacidification similar to that observed in this function and defective clearance of Aβ, and elevated levels of Aβ were also observed in the brain of a NHE6 knockout mouse model. Strikingly, epigenetic restoration of NHE6 expression by treatment with HDAC inhibitors reserved the effect and normalised endosomal pH and Aβ clearance[384]. Influencing NHE6 protein function might therefore be a therapeutic tool that might be valuable to further explore not only in rare forms of neurodegeneration such as CBD, but also in more common forms like AD, especially if the effect of a loss of NHE6 on both Aβ and tau clearance would be confirmed in further in-depth studies.

Taken together, the investigation of endosomal-lysosomal involvement in neurodegenerative diseases seems a path worth pursuing, since changes in this system seem to be severely detrimental to cellular health, and the endosomal-lysosomal system is heavily involved in the key processes disturbed in neurodegeneration, namely synaptic function, mitochondrial health and removal of aggregated proteins.

5. Material and Methods

5.1 Material

5.1.1 Reagents

Table 3. List of chemicals and reagents used in experimental procedures and manufacturers.

Chemical/Reagent	Manufacturer
4,6-diamino-2-pyrimidenthiol (DAPT)	Sigma-Aldrich, München, Germany
10% sodium dodecylsulfate solution (SDS)	Applichem, Darmstadt, Germany
30% Acrylamide	Applichem
Aceton	Fluka, Buchs, Switzerland
Accumax	Sigma-Aldrich
Accutase	Millipore, Temecula, USA
Agarose	Biozym, Oldendorf, Germany
Amersham ECL Select Western Blotting Detection Reagent	GE Healthcare, Buckinghamshire, UK
Amersham ECL Prime Western Blotting Detection Reagent	GE Healthcare, Buckinghamshire, UK
Ampicillin	Applichem
Ammonium Chloride (NH_4Cl)	Sigma-Aldrich
Ammonium Persulfate (APS)	Applichem
Annexin V Binding Buffer	BioLegend, San Diego, USA
Annexin V, Pacific Blue conjugated	BioLegend
Antimycin A	Sigma-Aldrich
Ascorbic Acid	Sigma-Aldrich
β-Mercaptoethanol	Fluka
B27 supplement	Gibco, Grand Island, USA
Bafilomycin A	InvivoGen, San Diego, USA
BamHi restriction enzyme	Thermo Scientific
Basic fibroblast growth factor (bFGF)	PeproTech, Rocky Hill, USA
Blasticidin	Invitrogen, Carlsbad, USA; Invivogen

Bovine Serum Albumine (BSA)	Applichem
Bradford reagent	Bio-Rad, München, Germany
Brain-derived neurotrophic factor (BDNF)	PeproTech
BrainPhys Neuronal Medium	Stem Cell Technologies, Vancouver, Canada
Bromphenole blue	Bio-Rad
Carbonyl cyanide *m*-chlorophenyl hydrazone (CCCP)	Sigma-Aldrich
CellLight Lysosomes-RFP, BacMam 2.0	Molecular Probes, Oregon, USA
CHIR 99021 - CT 99021	Axon MedChem, Groningen, Netherlands
Collagen A	Biochrom, Berlin, Germany
cOmplete, mini, EDTA-free Protease Inhibitor Cocktail	Roche Applied Science, Penzberg, Germany
Copper phthalocyanine tetrasulfonic acid	Sigma-Aldrich
D-Glucose	Sigma-Aldrich
Dako Fluorescent Mounting Medium	Dako North America, Carpinteria, USA
DAPT	Selleckchem, Houston, USA
DG1 chemically-compentent *Escherichia coli* (*E.coli)* bacteria	Eurogentec, Liege, Belgium
N^6,2'-O-Dibutyryladenosine 3',5'-Cyclic Monophosphate Sodium Salt (dbcAMP)	Applichem
Dihydroethidium (DiHET)	Santa Cruz Biotechnology, Dallas, USA
Dimethylsuloxide (DMSO)	Applichem/Sigma-Aldrich
Dithiothreitol (DTT)	Applichem
dNTPs (dATP, dCTP, dGTP, dTTP)	Invitrogen/Roche
Dorsomorphin	Sigma-Aldrich
DpnI restriction enzyme	Thermo Scientific
DraI restiction enzyme	Thermo Scientific
DreamTaq DNA Polymerase	Thermo Scientific
Dulbecco's Modified Eagle Medium (DMEM)	Biochrom, Berlin, Germany
DMEM/Ham's F12	Biochrom

DMEM/Ham's F12 + 15mM HEPES	Gibco, Paisley, USA
DMEM without phenol red	Gibco
Dulbecco's Phosphate Buffered Saline (DPBS)	Biochrom
EagI restriction enzyme	Thermo Scientific
Effectene Transfection Reagent	Qiagen, Hilden, Germany
Ethylenediaminetetraacetic acid (EDTA)	Applichem
Ethylene Glycol-bis(β-aminoethyl ether)-N,N,N',N'-Tetraacetic Acid (EGTA)	Applichem
FastAP phosphatase	Thermo Scientific
Fetal Bovine Serum (FBS)	Thermo Scientific, Rockford, USA
Fibroblast Growth Factor 2 (FGF2)	PeproTech
Fibroblast Growth Factor 8 (FGF8)	PeproTech
G418	Biochrom
Glacial Acetic Acid	Merck
Glial cell line-derived neurotrophic factor (GDNF)	PeproTech
Glycerin/Glycerol	Merck, Applichem
Glycine	Applichem
GeneRuler 1kb Plus DNA ladder	Thermo Scientific
4-(2-hydroxyethyl)-1-piperazineethanesulfonic acid (HEPES)	Fluka
Hank's Buffered Saline Solution (HBSS)	Biochrom
Heparin	Sigma-Aldrich
High Fidelity PCR enzyme mix	Thermo Scientific
Hoechst 33342 Trihydrochloride, Trihydrate 10mg/ml solution	Molecular Probes
Hoechst 33258, Pentahydrate, 10mg/ml solution	Molecular Probes
Hydrochloric acid (HCl), 25% solution	Applichem
iBlot Transfer Stack, nitrocellulose, mini/regular	Life technologies, Carlsbad, USA
Immobilon Western Blotting Reagent	Millipore
Immobilon-P Polyvenylidene difluoride (PVDF) Membrane	Millipore

Insulin-Transferrin Supplement (ITS)	Gibco
Isopropanol (2-propanol)	VWR, Darmstadt, Germany
Kanamycin	Applichem
KnockOut SR	Gibco
L-Ascorbic Acid 2-phosphate, Magnesium salt (AA2PM)	Sigma
L-Glutamine	Gibco
L-Glutamax	Gibco
Lennox Broth (LB) agar	Invitrogen, Carlsbad, USA
Lennox Broth (LB) medium	Invitrogen
LightCycler 480 SYBR Green I Master	Roche Applied Sciences
LysoSensor Yellow/Blue	Molecular Probes
LysoTracker red DND-99	Molecular Probes
Magnesium Chloride ($MgCl_2$)	Merck
Manganese Chloride ($MnCl_2$)	Applichem/Sigma-Aldrich
Matrigel Matrix	Corning
Methanol p.a.	VWR
Midori Green Advance DNA stain	Biozym Scientific, Hessisch Oldendorf, Germany
miRNA oligonucleotides, single-stranded	Invitrogen/Life technologies
Mouse embryonic fibroblasts (MEFs), mitosis-inhibited (MITC)	Gibco
mTESR1 Basal Medium	Stem Cell Technologies
N2 Supplement	Gibco
N, N, N', N'-Tetramethyl-ethylenediamine (TEMED)	Applichem
Neurobasal Medium	Gibco
Non-essential amino acids (NEAAs)	Biochrom, Gibco
Nonidet-P40 (NP40)	Fluka, Buchs, Switzerland
Normal Goat Serum (NGS)	Thermo Scientific
Normal Donkey Serum (NDS)	EMD Millipore, Billerica, USA
NuPAGE LDS 4x Sample Buffer	Novex by life technologies, Carlsbad, USA

Oligomycin A	Sigma-Aldrich
Opti-MEM 1 Reduced-Serum Medium	Gibco
PageRuler Plus Prestained Protein ladder	Thermo Scientific, Rockford, USA
Paraformaldehyde solution (PFA)	Fluka, Buchs, Switzerland
PCR primers	Metabion, Martinsried, Germany
Penicillin/Streptomycin (Pen/Strep)	Gibco
Pfu Polymerase	Thermo Scientific
Phorbol 12-myristate 13-acetate (PMA)	Sigma-Aldrich
PhosSTOP phosphatase inhibitor tablets	Roche Applied Science
Phos-tag Acrylamide	Wako chemicals, Osaka, Japan
Ponceau S	Applichem
Potassium Chloride (KCl)	Merck
RNaseZAP	Sigma-Aldrich, Steinheim, Germany
ROCK inhibitor Y-27632	Selleckchem
Rotenone	Sigma-Aldrich
Sarkosyl (Sodium N-lauroyl-sarcosinate)	Fluka
SB-431542	SelleckChem
Skim milk powder	Applichem
S.OC medium	Invitrogen
Sodium acetate (NaAc)	Merck
Sodium butyrate	Sigma-Aldrich
Sodium chloride (NaCl)	Merck
Sodium deoxycholate	Sigma-Aldrich
Spectinomycin	Sigma-Aldrich
Staurosporine (STS)	Santa Cruz Biotechnology, Dallas, USA
Sucrose	Roth
T4 DNA ligase	Promega
TeSR-E8 Basal Medium	Stemcell Technologies
Tetracycline	Invitrogen/Sigma-Aldrich
Top10 chemically competent *E.coli*	Invitrogen

TransIT-2020 Transfection Reagent	Mirus, Madison, USA
Transforming Growth Factor β-1 (TGFβ1)	PeproTech
Transforming Growth Factor β-1 (TGFβ3)	PeproTech
Trichloroacetic acid (TCA)	Roth
Tris base	Applichem
Triton X-100	Sigma-Aldrich
Trypan Blue	Sigma
Trypsin-EDTA (0.05%)	Gibco
Tween20	Roth
UltraCruz Autoradiography Film	Santa Cruz Biotechnology, Dallas, USA
Valinomycin	Sigma-Aldrich
Vectashield	Vector Laboratories, Burlingame, USA
Vitronectin (VTN)	gibco
XhoI restriction enzyme	Thermo Scientific
Z-Leu-Leu-Leu-al (MG132)	Invivogen

5.1.2 Kits

Table 4. List of kits used in experimental procedures and manufacturers.

Kit	Manufacturer
Amaxa Human Dermal Fibroblast Nucleofector Kit	Lonza, Basel, Switzerland
Micro BCA Protein Assay Kit	Thermo Scientific
BLOCK-iT Inducible Pol II miR RNAi Expression Vector Kit with EmGFP	Life technologies, Carlsbad, USA
CytoTox 96 Non-Radioactive Cytotoxicity Assay	Promega
DNeasy Blood & Tissue DNA extraction kit	Qiagen
E.Z.N.A. Endo-free Plasmid DNA Mini Kit II	Omega Bio-Tek, Norcross, USA
GeneJET RNA Purification Kit	Thermo Scientific
High Pure PCR Purification Kit	Roche Applied Science, Mannheim,

	Germany
High Pure Plasmid Isolation Kit	Roche Applied Science
High Pure RNA Isolation Kit	Roche Applied Science
iBlot Transfer Stack, nitrocellulose	Invitrogen
Inside Stain Kit	MACS Miltenyi Biotec
Maxima H Minus First Strand cDNA Synthesis Kit with dsDNase	Thermo Scientific
OxyBlot Protein Oxidation Detection Kit	Millipore
pcDNA3.1/V5-His TOPO TA kit	Invitrogen
Pierce BCA Protein Assay	Thermo Scientific
QIAfilter Plasmid Midi Kit	Qiagen, Hilden, Germany
QiaQUICK Gel extraction kit	Qiagen
Transcriptor First Strand cDNA Synthesis Kit	Roche Applied Science

5.1.3 Machines and Software

Table 5. List of machines and software used in experimental procedures and manufacturers.

Machine/Software	Use	Manufacturer
Axiovision	Microscopy software	Zeiss, Jena, Germany
AxioCamMRm	Microscopy camera	Zeiss
Beckman-Coulter Optima MAX-UP	Ultracentrifuge	Beckman-Coulter, Krefeld, Germany
Bio-Rad T100 Thermal Cycler	PCR Machine	Bio-Rad, München, Germany
CLC Main Workbench 6.9	Sequence analysis, Primer design, alignments	CLC bio, Aarhus, Denmark
CyAn ADP Analyzer	Flow cytometry	Beckman-Coulter, California, USA
FluorChem 8900/FluorChem 8900 software	Chemiluminscence detection	Protein simple, Santa Clara, USA

Prism 6	Statistical analysis	GraphPad, San Diego, USA
iBlot	Dry blotting	Invitrogen
ImageJ 1.46r and Fiji Is Just ImageJ (Fiji)	Imaging Software	Wayne Rasband, National Institutes of Health, Bethesda, USA
LightCycler	qRT-PCR	Roche
LightCycler software	qRT-PCR data acquisition and analysis	Roche
LSM 510 META Laser Scanning Microscope	Confocal Microscope	Zeiss
LSM 5 software	Software for LSM 510 confocal microscope	Zeiss
MACSQuant	Flow cytometry	Miltenyi
MACSQuantify	Software for MACSQuant Flow Cytometer	Miltenyi
Mini-PROTEAN and Trans-Blot Cell	SDS-PAGE Electrophoresis and Western blotting chamber	Bio-Rad
Mithras LB 940 Multimode Microplate Reader	Microplate Reader	Berthold Technologies, Bad Wildbad, Germany
Mithras LB 940 Multimode Microplate Reader MikroWin2000 software	Software for Mithras microplate reader	Berthold Technologies
NanoDrop Spectrophotometer ND-1000	Measurement of DNA concentration	Peqlab, Erlangen, Germany
NanoDrop ND-1000 v.3.7.1 software	Measurement of DNA concentration	Peqlab
Nucleofector 2b Device	Nucleofection machine	Lonza
PRISM 6	Statistical analysis	GraphPad Software, La Jolla, USA

SpectraMAX	Monochromatic plate reader	Molecular Devices
Summit 4.3.02b2451	FACS software	Beckman Coulter
UV gel documentation system	Agarose Gel detection	Vilber-Lourmat, Eberhardzell, Germany
Xcell 4 Surelock MidiCell	SDS-PAGE Electrophoresis chamber	life technologies
Zeiss Axiovert	Life Cell Microscope	Zeiss
Zeiss 780NLO confocal microscope	Confocal 2-photon microscope	Zeiss

5.1.4 Constructs

Table 6. List of constructs used in experimental procedures with the name used, vector name, insert and the source of the construct

Name	Vector	Insert	Source
pEGFP-HA_3-NHE6 (NHE6 WT)	pEGFP-N3	Wildtype NHE6 cDNA with an HA tag in the first extracellular loop	Gift from Rajini Rao, John Hopkins University School of Medicine, Baltimore, USA
pEGFP-HA_3-NHE6-T489Y_fsX23 (T489Yfs NHE6)	pEGFP-N3	T489Yfs NHE6 cDNA with an HA tag in the first extracellular loop	Site-directed mutagenesis from wildtype NHE6 construct
pEGFP-HA_3-NHE6-R568Q (R568Q NHE6)	pEGFP-N3	R568Q NHE6 cDNA with an HA tag in the first extracellular loop	Site-directed mutagenesis from wildtype NHE6 construct
WT NHE6 without GFP	pcDNA 3.1/V5-His TOPO TA (Invitrogen)	Wildtype NHE6 cDNA with an HA tag in the first	Cloned in using PCR-generated PolyA-overhangs from

		extracellular loop	wildtype NHE6 construct
T489Yfs NHE6 without GFP	pcDNA 3.1/V5-His TOPO TA (Invitrogen)	T489Yfs NHE6 cDNA with an HA tag in the first extracellular loop	Cloned in using PCR-generated PolyA-overhangs from T489Yfs NHE6 construct
R568Q NHE6 without GFP	pcDNA 3.1/V5-His TOPO TA (Invitrogen)	R568Q NHE6 cDNA with an HA tag in the first extracellular loop	Cloned in using PCR-generated PolyA-overhangs from R568Q NHE6 construct
Empty vector control	pEGFP-N1	None (Transfection control for pEGFP-N3)	Clontech
Empty vector control	pcDNA3.1	None (Transfection control for pcDNA3.1/V5-His TOPO TA)	Invitrogen
Tet-repressor vector	pcDNA6/TR	Tet-Repressor	Invitrogen BLOCK-iT kit
Non-targeting contro, expression vector	pcDNA 6.2-GW/miR with EmGFP	Non-targeting miRNA	Invitrogen BLOCK-iT kit
NHE6 3'UTR knockdown expression vector	pcDNA 6.2-GW/miR with EmGFP	miRNA targeting 3'UTR of NHE6 mRNA	Vector: Invitrogen BLOCK-iT kit with miR oligonucleotides from Invitrogen
Non-targeting control expression vector without EmGFP	pcDNA 6.2-GW/miR without EmGFP	Non-targeting miRNA	EmGFP removed by DraI digestion

NHE6 3'UTR knockdown expression vector without EmGFP	pcDNA 6.2-GW/miR without EmGFP	miRNA targeting 3'UTR of NHE6 mRNA	EmGFP removed by DraI digestion
Inducible non-targeting control vector	pT-REx-DEST30 (with EmGFP)	Non-targeting miRNA	Cloned in from pcDNA 6.2-GW/miR
Inducible NHE6 3'UTR knockdown vector	pT-REx-DEST30 (with EmGFP)	miRNA targeting 3'UTR of NHE6 mRNA	Cloned in from pcDNA 6.2-GW/miR
Inducible non-targeting control vector without EmGFP	pT-REx-DEST30 (without EmGFP)	Non-targeting miRNA	Cloned in from pcDNA 6.2-GW/miR
Inducible NHE6 3'UTR knockdown vector without EmGFP	pT-REx-DEST30 (without EmGFP)	miRNA targeting 3'UTR of NHE6 mRNA	Cloned in from pcDNA 6.2-GW/miR
pCXLE-hOct3/4	pCXLE	hOct3/4	Addgene (#27076)
pCXLE-hSK	pCXLE	hSK (Sox2 and KLF4)	Addgene (#27078)
pCXLE-hUL	pCXLE	hUL (L-Myc)	Addgene (#27080)

5.1.5 Used Primers

Table 7. List of primers used in experimental procedures with name, 5' to 3' sequence and purpose of the respective primer pairs.

Name	Sequence 5' to 3'	Purpose
NHE k.d. 3'UTR miRNA BLOCKiT_ top	TGC TGT TTA CTG CGT GAA GAG GCA CAG TTT TGG CCA CTG ACT GAC TGT GCC TCC ACG CAG TAA A	Inducible miRNA expression system
NHE k.d. 3'UTR miRNA	CCT GTT TAC TGC GAG GCA	

BLOCKiT_ bottom	CAG TCA GTC AGT GGC CAA AAC TGT GCC TCT TCA CGC AGT AAA C	
NHE6 mRNA/qRT-PCR fw	CTT GTT TCG TTA TTG GGT C	NHE6 cDNA detection
NHE6 mRNA/qRT-PCR rev	CCG TAA TTT GGT GAA CTT TG	
T489Yfs mutagenesis fw	GCT TCT GAT TGT GTT TTT TTA CCG TGT GGG TAT TTG GTG	Mutagenesis of NHE6 cDNA construct to introduce T489Yfs mut.
T489Yfs mutagenesis rev	CAC CAA ATA CCC ACA CGG TAA AAA AAC ACA ATC AGA AGC	
R568Q mutagenesis fw	GCA GAG AGT GCT TGG CTT TTC CAG ATG TGG TAC AAC T	Mutagenesis of NHE6 cDNA construct to introduce R568Q variant
R568Q mutagenesis rev	CAA AGT TGT ACC ACA TCT GGA AAA GCC AAG CAC TCT C	
R568Q Splice site cDNA fw	CCA AGA ACA CTT GGG TGT TCC TG	NHE6 cDNA primers to test for splicing defect in R568Q variant carriers
R568Q Splice site cDNA rev	TCA TCC ATT GGA AGA ACC AGG CG	
NHE6 TOPO cloning fw	ATG GCT CGG CGC GGC TG	Primers for cloning of the three NHE6 inserts into pcDNA 3.1/V5-His TOPO TA vector without GFP
NHE6 TOPO cloning rev	GGC TGG ACC ATG TCT CGT ATT ATC	
HMBS qRT-PCR fw	ATG CCC TGG AGA AGA ATG AAG T	Content control/ housekeeping gene for qRT-PCR
HMBS qRT-PCR rev	TTG GGT GAA AGA CAA CAG CAT C	
OCT3/4-plasmid fw	CAT TCA AAC TGA GGT AAG GG	Plasmid Oct3/4 for iPSC integration PCR
OCT3/4-plasmid rev	TAG CGT AAA AGG AGC AAC ATA G	
KLF4-plasmid fw	CCA CCT CGC CTT ACA CAT GAA GA	Plasmid KLF4 for iPSC integration PCR
KLF4-plasmid rev	TAG CGT AAA AGG AGC AAC ATA G	
SOX2-plasmid fw	TTC ACA TGT CCC AGC ACT	Plasmid Sox2 for

	ACC AGA	iPSC integration PCR
SOX2-plasmid rev	TTT GTT TGA CAG GAG CGA CAA T	
L-MYC-plasmid fw	GGC TGA GAA GAG GAT GGC TAC	Plasmid L-Myc for iPSC integration PCR
L-MYC-plasmid rev	TTT GTT TGA CAG GAG CGA CAA T	
Oct 3/4 endo qRT-PCR fw	CCC CAG GGC CCC ATT TTG GTA CC	Endogenous Oct3/4, iPSC characterisation
Oct 3/4 endo qRT-PCR rev	ACC TCA GTT TGA ATG CAT GGG AGA GC	
Sox 2 endo qRT-PCR fw	TTC ACA TGT CCC AGC ACT ACC AGA	Endogenous Sox2, iPSC characterisation
Sox 2 endo qRT-PCR rev	TCA CAT GTG TGA GAG GGG CAG TGT GC	
Nanog qRT-PCR fw	CCT GTA TTT GTG GGC CTG	iPSC characterisation
Nanog qRT-PCR rev	GAC AGT CTC CGT GTG AGG CAT	
L-myc endo qRT-PCR fw	GCG AAC CCA AGA CCC AGG CCT GCT CC	Endogenous L-myc, iPSC characterisation
L-myc endo qRT-PCR rev	CAG GGG GTC TGC TCG CAC CGT GAT G	
KLF4 endo qRT-PCR fw	ACC CAT CCT TCC TGC CCG ATC AGA	Endogenous KLF4, iPSC characterisation
KLF4 endo qRT-PCR rev	TTG GTA ATG GAG CGG CGG GAC TTG	
Rex1 qRT-PCR fw	GCA CAC TAG GCA AAC CCA CC	iPSC characterisation
Rex1 qRT-PCR rev	CAT TTG TTT CAG CTC AGC GAT G	
Lin28 qRT-PCR fw	GGA GGC CAA GAA AGG GAA TAT GA	iPSC characterisation
Lin28 qRT-PCR rev	AAC AAT CTT GTG GCC ACT TTG ACA	

5.2 Buffers and solutions

Table 8. List of buffers and solutions used in experimental procedures with their composition.

Solution/Buffer	Composition
Cell Lysis Buffer A	10mM HEPES, 1.5mM $MgCl_2$, 10mM KCl, 0.5mM DTT, 0.05% (v/v) NP-40, pH 7.9

Tris Buffered Saline (TBS) (+Tween20: TBS-T)	25mM Tris base, 140mM NaCl, pH7.5 (+0.05% (v/v) Tween20)
Tris, Acetic Acid, EDTA Buffer (TAE)	40mM Tris base, 20mM glacial acetic acid, 1mM EDTA, pH 8.5
Running Buffer SDS-PAGE	25mM Tris base, 192mM glycine, 0.1% (w/v) SDS
Transfer Buffer Western blot	25mM Tris base, 192mM glycine, 20% (v/v) methanol
Stripping Buffer Western blot	200mM glycine, 500mM NaCl, pH2.8
Homogenisation buffer sarkosyl fractionation (Buffer H)	10mM Tris pH 7.4, 1mM EGTA, 0.8M NaCl, 10% (w/v) sucrose
Radioimmunoprecipitation assay (RIPA) buffer	10mM NaPP, 150mM NaCl, 50mM Tris base, 0.5% (w/v) Natriumdesoxycholat, 0.1% (w/v) SDS, 1% (v/v) NP-40, pH 8.0
6x SDS-PAGE Sample buffer (6x Lämmli Buffer)	0.312M Tris/HCl (pH 6.8), 10% (w/v) SDS, 25% (w/v) β-Mercaptoethanol, 50% (w/v) glycerol, 0.05% (w/v) bromphenol blue
Western blot blocking solution	5% (w/v) non-fat dried milk powder or 5% (w/v) BSA in TBS-T
Copper staining solution Western blot	0.05-0.5% (w/v) Copper phthalocyanine tetrasulfonic acid in 12mM HCl
Ponceau staining solution Western blot	0.1% (w/v) Ponceau S, 5% (v/v) glacial acetic acid

5.3 Methods

5.3.1 Molecular biology

Cloning for BLOCK-iT Inducible Pol II miR RNAi Expression Vector Kit with EmGFP

Cloning of the inducible miRNA expression system was done according to manufacturer's protocol.

Top and Bottom strand DNA oligonucleotides containing an miRNA sequence targeting either the coding sequence or the 3'UTR of the NHE6 mRNA were

designed using the manufacturer's online design tool BlockiT RNAi Designer. Three sequences targeting either position 1076 or 1213 of the coding sequence, or targeting the 3'UTR of the mRNA were chosen and oligonucleotides ordered. The annealing reaction containing 50µM of top and bottom strand oligonucleotides and annealing buffer was incubated at 95°C for 4 minutes (min.) and a 10nM dilution of the reaction made. Annealing of the strands into a ≈60bp fragment was confirmed by agarose gel electrophoresis using Midori Green as detecting agent and the annealed oligonucleotides ligated into the pcDNA6.2/EmGFP-miR expression vector (Appendix Fig. 46) by using the T4 DNA ligase provided in the kit for 2 hours (h) at room temperature (RT). The product was used for transformation of chemically competent One Shot Top10 *E. coli* followed by selection on agar plates containing 50µg/ml spectinomycin at 37°C overnight (o/n), and ten clones chosen for culturing in LB medium containing 50µg/ml spectinomycin. Plasmids were isolated using the High Pure Plasmid Isolation Kit and the insertion of the correct miRNA sequence confirmed by sequencing.

The EmGFP was removed using two DraI restriction sites flanking the EmGFP sequence and annealing of the vector with T4 DNA Ligase, and the absence of the EmGFP sequence confirmed by test restriction and subsequent agarose gel electrophoresis.

Cloning into the inducible pT-REx-DEST30 vector (Appendix Fig. 47) was achieved by linearisation of 2µg of the expression vector with EagI and precipitation of the DNA with 0.1x 3M NaCl/2.5x 100% EtOH. The DNA was resuspended in TE buffer, pH 8.0, to a final concentration of 50-150ng/µl, and the sample cloned into the pDONR221 donor vector by adding BP clonase mix II to 350-1050ng of sample and 150ng pDONR221 vector at 25°C for 1h. This reaction was then mixed with 150ng of pT-REx-DEST30 vector, LR clonase II mix and incubated o/n at 25°C. Enzymes were removed by addition of Proteinase K and incubation at 37°C for 10 min. Afterwards, Top10 One Shot *E.coli* were transformed with the reaction and incubated o/n at 37°C on an agar plate containing 200µg/ml ampicillin. Bacterial clones were used to spike 5ml of LB medium containing 200µg/ml ampicillin, incubated o/n at 37°C and followed by plasmid isolation using the High Pure Plasmid Isolation kit.

Presence of the ≈200bp insert was confirmed by digestion with XhoI and BamHI and subsequent agarose gel electrophoresis.

Site-directed mutagenesis

Primers containing the desired mutation (T insertion between c.1464_1465 or c.G1703A) flanked by 10-15 bases of correct sequence and a minimum GC content of 40% were designed using CLC Workbench. A touchdown PCR using 500ng of template pEGFP-N3 vector with wildtype NHE6 insert carrying a three copies of a hemagglutinin (HA) tag between Glu55 and Glu56 (pEGFP-HA_3-NHE6, NHE6 WT vector, Appendix Fig. 48), 200µM dNTPs, 0.4nM of each primer, 1x Pfu polymerase buffer, 1 units (U) Pfu polymerase and 7% DMSO was performed with the following parameters:

Table 9. PCR parameters used for a touchdown PCR for site-directed mutagenesis of the NHE6 WT vector.

Step	Description	Temperature	Duration
1	Initial denaturing	95°C	2 min.
2	Denaturing	95°C	1 min.
3	Annealing	65-55°C	50 sec.
4	Elongation	72°C	10 min.
5	Repeat Steps 2-4 9x		
6	Denaturing	95°C	1 min.
7	Annealing	60°C	50 sec.
8	Elongation	72°C	10 min.
9	Repeat Steps 6-8 19x		
10	Final Elongation	72°C	10 min.
11	Storage	8°C	Forever

The PCR product was cleaned up by precipitation with 0.1x 3M NaAC with 2.5x 100% ethanol and the DNA pellet resuspended in ddH_2O with DpnI Buffer and 1U of DpnI enzyme. Digestion of methylated DNA by DpnI for 1h at 37°C was followed by transformation of chemically-competent *E. coli* bacteria and selection on an LB-agar plate containing 200µg/ml Kanamycin. The presence of the desired mutation and absence of additional mutations in the coding sequence were confirmed by sequencing (Microsynth SeqLab, Göttingen, Germany).

Cloning of NHE6 cDNA into the pcDNA 3.1/V5-His TOPO TA expression vector

Cloning of the NHE6 cDNA into the pcDNA 3.1/V5-His TOPO TA expression vector was performed by Manuela Kübler at the Department of Neurodegenerative Diseases, Centre of Neurology and Hertie Institute for Clinical Brain Research, University of Tübingen, Tübingen, Germany. The NHE6 WT, T489Yfs and R568Q cDNA were cloned from the pEGFP-N3 vector in to pcDNA3.1/V5-His TOPO TA expression vector according to manufacturer's instructions in the kit.

Primers leading to a product containing the whole coding sequence of the respective NHE6 variants without inclusion of the EGFP sequence were used for amplification with a Pfu polymerase. The PCR product was gel-purified and incubated at 72°C for 15 min. with 1x Taq polymerase buffer, dATP and 0.5U of Taq polymerase for additional polyA-overhangs. The PCR product was then used for ligation into the pcDNA3.1/V5-His TOPO TA expression vector in the TOPO Cloning reaction.

Transformation of chemically competent E. coli bacteria

One vial of chemically competent *E. coli* was incubated with 1-2µl of plasmid DNA on ice for 30 min., the bacteria heat shocked at 42°C for 30 sec. and the reaction cooled on ice. After addition of S.O.C LB medium, cell were pre-grown for 1h at 37°C on a shaker and the bacterial solution spread on an LB-agar plate containing the appropriate antibiotic at a concentration of 10-50µg/ml, followed by incubation o/n at 37°C.

Isolation of plasmid and preparation of bacterial stocks

For minis, 5ml LB medium containing selection antibiotics at 10-50µg/ml was spiked with a single clonal colony or from a bacterial stock, for midis 50ml and maxis 100-200ml of LB medium. Cells were grown o/n at 37°C and plasmids isolated using the appropriate High Pure Plasmid Isolation Kit or QIAfilter Plasmid Midi/Maxi Kit, resuspended in ddH_2O and DNA concentration estimated using NaNoDrop.

For bacterial stocks, a mix of 700µl bacterial solution and 300µl 50% sterile glycerol was stored at -80°C.

RNA isolation from cells (GeneJET RNA Kit) and cDNA generation (Maxima First Strand cDNA Kit)

Cells were pelleted and resuspended in lysis buffer containing 40mM DTT followed by addition of 100% EtOH for RNA precipitation. RNA was bound to the membrane of a column by addition of the lysate and centrifugation. After washing of the membrane with EtOH containing washing buffers, nucleic acids were eluted using ddH_2O and the concentration of eluted RNA measured by NaNoDrop absorbance at 260nm.
For cDNA generation, 500ng-1µg RNA solution was digested with 1U dsDNA to remove residual DNA for 2 min. at 37°C. After addition of 1x Reaction mix and Maxima enzyme mix, RNA was reverse transcribed into cDNA by incubation at 25°C for 10 min., followed by 15 min. at 50°C (65°C for NHE6) and termination of the reaction at 85°C for 5 min.

Semi-quantitative Reverse Transcriptase PCR (RT-PCR) and qualitative Real-Time PCR (qRT-PCR)

Semi-quantitative RT-PCR for NHE6 mRNA content was performed using NHE6 cDNA primers and GAPDH cDNA primers as a control. 1µg of cDNA was mixed with 400µm dNTPs, 40nM forward and reverse primers, 7% (v/v) DMSO, 1x DreamTaq buffer and 1U DreamTag polymerase. Annealing was at 65°C and elongation for 40 sec. for a 500bp fragment.
For qRT-PCR, 100ng of cDNA were mixed with 1x LightCycler 480 SYBR Green I Master and 1µM of primers and analysed using a touchdown PCR on a Roche LightCycler 480 with primers against HMBS and/or GAPDH as a content amount control. Absence of unspecific amplifications was confirmed by checking for potential peaks in the ddH_2O control using the melting temperature calling setting. Crossing point (CP) values for each condition were calculated using the LightCycler 480 Software v.1.5.1.62 and relative RNA/cDNA levels were calculated with the formula of relative cDNA levels = $2^{-(CP\ gene\ -\ CP\ HMBS\ ctrl)}$ normalised to the control.

5.3.2 Patient material

Ethical approval

All procedures performed in studies involving human participants were in accordance with the ethical standards of the institutional and/or national research committee and

with the 1964 Helsinki declaration and its later amendments or comparable ethical standards.

Generation of a patient fibroblast cell line

The T489Yfs patient fibroblast line was established by Dr. Dajana Großmann and Brigitte Maurer at the Department of Neurodegenerative Diseases, Centre of Neurology and Hertie Institute for Clinical Brain Research, University of Tübingen, Tübingen, Germany, as follows: For the generation of the T489Yfs patient fibroblast cell line, a ≈25mm^2 piece of skin was obtained from the patient after informed consent was given. Smaller fragments of the skin were kept in normal growth medium with 1% Penicillin/Streptomycin for two weeks until fibroblasts started to grow. Fibroblasts were detached using 0.05% Trypsin-EDTA, collected and grown in normal fibroblast growth medium.

Female and male control fibroblast cell lines were obtained from the Tübingen fibroblast biobank.

Brain tissue from two R568Q variant carriers and pathology-matched controls

Brain tissue from two R568Q carriers with diagnoses of CBS/CBD and CBS, and from pathology-matched controls was obtained at the Mayo Clinic, Florida, USA as part of the brain donation program (https://www.psp.org/ineedsupport/braindonation). Samples from the brains was prepared and shipped by Michael A. DeTure, PhD and the neuropathological analysis was performed by Dennis W. Dickson, both Department of Neuroscience, Mayo Clinic Florida, Jacksonville, Florida, US. Detailed information on the pathologies of the two R568Q carriers and pathology-matched controls can be found in Table 10. Braak staging is used to describe the progression and severity of alpha-synuclein pathology in Parkinson's disease. The score ranges from 1-6, with 1 describing involvement of the brain stem area and olfactory bulb, and 6 a widespread severe pathology with an involvement of the substantia nigra pars compacta and the neocortex[384]. Thal phases 1-5 describes progression and severity of Aβ-pathology in Alzheimer's disease, with phase 1 describing exclusive involvement of the neocortex, while phase 5 shows involvement of the neocortex, forebrain nuclei, brainstem and cerebellum[385].

From all patients, samples from the medial frontal cortex, caudate nucleus, occipital lobe and cerebellum were available.

Table 10. Information on brain tissue from two R568Q carriers and pathology-matched controls used in this study, including ID, age at death, sex, pathology, and Braak and Thal staging. Neuropathological examination was carried out by Dennis W. Dickson, Department of Neuroscience, Mayo Clinic Florida, Jacksonville, Florida, USA.

F: female; **M**: male; **PA**: pathological aging, **AGD**: Argyrophilic grain disease, **bLBD**: brainstem Lewy body disease, **TSA**: Thorn-shaped astrocytes, **PSD**: pigment-spheroid degeneration, **HpScl**: hippocampal sclerosis, **VaD**: vascular disease, **ARTAG**: aging-related tau astrogliopathy, **tLBD**: transitional Lewy body disease; **NFT**: neurofibrillary tangles

ID	Age	Sex	Pathology	Braak	Thal
R568Q CBD	73	F	CBD, PA, AGD	3	4
CBD Ctrl. 1a	96	F	CBD, PA, AGD, bLBD	3	3
CBD Ctrl. 1b	74	F	CBD, PA, AGD	3	3
CBD Ctrl. 1c	66	M	CBD, AGD, PA, TSA, PSD	2	3
R568Q CBS	93	F	HpScl, PA, bLBD, VaD, ARTAG	2	3
CBS Ctrl. 2a	84	M	HpScl, PA, bLBD, VaD	3	2
CBS Ctrl. 2b	85	M	tLBD, PA, VaD (clinical PSP-P)	3	3
CBS Ctrl. 2c	75	M	NFT dementia, TSA	3.5	1

5.3.3 Cell culture

Maintenance of cancer and fibroblast cell culture

Cells were kept in an incubator in a humid environment at 5% CO_2 and 37°C. Cancer cell lines (M17 neuroblastoma cells, SH-SY5Y neuroblastoma cells) were cultured in DMEM/Ham's F12 with 10% FBS and fibroblast cell lines in DMEM with 10% FBS. Cells were split at 90-100% confluency using 0.05% Trypsin-EDTA, which was quenched with medium. Cancer cells were split approx. 1:10, fibroblast cells at 1:4. Frozen stocks were prepared by collecting cells in growth medium with 10% DMSO and gradual cooling to -80°C, followed by long-term storage in liquid nitrogen. For thawing, frozen cells were resuspended in growth medium and pelleted to remove residual DMSO before seeding into cell culture flasks.

Transfection

M17 neuroblastoma cells were transfected using Mirus TransIT-2020 Transfection Reagent by adding plasmid DNA to Opti-MEM 1 Reduced-Serum Medium at 1µg/100µl and incubation with 2.5µl TransIT-2020 reagent per 100µl reaction for 30 min. at RT before addition to the cells. 0.4µg plasmid DNA and 1µl TransIT-2020 reagent were used per 1ml cell culture medium.

SH-SY5Y neuroblastoma cells were transfected using Effectene and 0.2µg plasmid DNA per 1ml cell culture medium. The plasmid DNA was incubated with Effectene Enhancer solution and Buffer EC for 5 min. at RT, followed by 8 min. incubation after addition of the Effectene Reagent. The reaction was stopped by dilution in growth medium.

Transfected cells were incubated with the transfection reagent-plasmid DNA mixture for 24h before changing to normal growth medium.

Generation of an inducible NHE6 knockdown model

For testing of the different miRNAs generated, M17 neuroblastoma cells were transfected with one of three NHE6 knockdown miRNA pcDNA6.2/GW-miR expression constructs, of which two targeted the coding sequence and one the 3'UTR. As a control, M17 cells were transfected with the same vector carrying a non-targeting sequence. After 72h of expression, cells were lysed and NHE6 mRNA content analysed by semi-quantitative RT-PCR and protein levels by Western blot. The miRNA targeting the 3'UTR had the strongest effect on NHE6 levels and was used for all subsequent experiments.

For the inducible NHE6 knockdown model, cells were transfected with an 1:1 ratio of the pcDNA6/TR Tet-repressor vector and the pT-REx-DEST30 vector carrying the NHE6 miRNA or the non-targeting control miRNA sequence and selected with 6µg/ml Blasticidin and 700µg/ml G418 and selection was completed when all untransfected selection control cells had died (after approx. 7 days).

Inducible M17 knockdown cells were cultured in the presence of 6µg/ml Blasticin and 700µg/ml G418 and induced by addition of 1µg/ml Tetracycline for 72h (polyclonal cells) or 96h (monoclonal cells). Knockdown of NHE6 after induction was confirmed by Western blotting.

For the generation of monoclonal cell lines, cells were seeded in a 96 well plate at a density of approx. 0.5 cells/well and the presence of single-cell colonies confirmed after a growth period of 14 days. NHE6 levels in monoclonal NHE6 knockdown or

non-targeting miRNA cell lines were then analysed by Western blot and three lines for each condition selected.

Treatments of cell lines

For analysis of NHE6 mutant protein removal, M17 cells were transfected with a transfection control, WT NHE6, T489Yfs NHE6 and R568Q NHE6, and the cells treated with 10µM MG132 for 24h or 20mM NH_4Cl for 4h before lysis after a total transfection time of 48h.

For induction of autophagy by amino acid starvation, cells were treated with serum-free medium for 24h, and for block of autophagic removal with 400nM BafA1 for 4h before lysis.

Induced Pluripotent Stem Cell (iPSC) generation and maintenance

The protocol used for the generation and maintenance of iPSCs was adapted from Takahashi et al. (2007)[386] and established in the laboratory by Christine Bus, Department of Neurodegenerative Diseases, Centre of Neurology and Hertie Institute for Clinical Brain Research, University of Tübingen, Tübingen, Germany.

For reprogramming, approx. 700,000 fibroblasts of the T489Yfs patient were nucleofected using the Normal Human Dermal Fibroblast Nucleofector Adult Kit with 10µg of pCXLE-hOct3/4, pCXLE-hSK and pCXLE-hUL plasmid each. Nucleofected fibroblasts were distributed on vitronectin-PBS coated 6-well plates and kept in DMEM with 10% FBS for one day, when medium was changed to DMEM supplemented with 10% FBS, 1% Pen/Strep and 2ng/ml bFGF for two additional days. Four days after nucleofection, the medium was changed to essential 8 (E8) medium (DMEM/Ham's 12 with 15mM HEPES, 1x ITS, 64mg/L AA2PM, 10µg/L FGF2, 2µg/L TGFβ1, 100ng/ml Heparin, 72ml/L TESR-E8) with 1x non-essential amino acids (NEAA), 100µM Sodium Butyrate and 0.1% Pen/Strep. The medium on nucleofected fibroblasts was changed every other day.

After 21-28 days, cellular colonies were picked, transferred to vitronectin-coated 12-well plates and kept in E8 with 1% Pen/Strep and 1x NEAA. Non-iPS cells such as cancer or differentiated cells were removed manually in regular intervals. For normal maintenance, cells were kept on vitronectin-coated plates in E8 medium with Pen/Strep and 1x NEAA and passaged at approx. 80% confluency. For passaging, cells were detached briefly with 0.1% (w/v) EDTA and directly transferred into new

plates containing E8 with 1x NEAA and 10µM Rock inhibitor Y-27632 (RI). Frozen stocks were prepared similarly with E8 medium with 1x NEAA, RI and 10% DMSO.

iPS cell line confirmation and characterisation

After generation of several iPSC lines, DNA was isolated from the cells using the Qiagen Tissue&Blood DNA kit and a PCR with primers for plasmid-specific SOX2, Oct3/4, KLF4 and L-MYC performed to exclude the possibility of integration of the plasmids into the genome. Only integration-free clonal lines were continued and tested by DNA microarray (Life&Brain GENOMICS, Bonn, Germany) for large chromosomal aberrations.

Four clones (#5.1, #6, #19, #23) without detectable changes were then kept for NPC generation, but one clone (#19) was no longer available for characterisation of the iPSCs. For characterisation, RNA was extracted from iPSCs and expression of endogenous Oct3/4, Klf4, L-myc and Sox2 as well as Nanox, Rex1 and Lin28 confirmed by qRT-PCR in relation to embryonic stem cell RNA (qRT-PCR was performed by Benedikt Höglinger). Expression of endogenous Oct4, Sox2 and SSEA4 was further confirmed by immunocytochemistry (ICC) (see 5.3.3 for details).

Generation of neuronal precursor cells (NPCs) and maintenance

The protocol used for the generation and maintenance of NPCs was adapted from Reinhardt et al. (2013)[387] and established in the laboratory by Christine Bus, Department of Neurodegenerative Diseases, Centre of Neurology and Hertie Institute for Clinical Brain Research, University of Tübingen, Tübingen, Germany.

For NPC generation, T489Yfs iPSCs were co-cultured with mitomycin-treated (non-dividing) mouse embryonic fibroblasts (MEFs) in human embryonic stem cell medium (hES) (80% DMEM/Ham's F12, 20% knockout SR, 1x NEAA, 1% Pen/Strep and 10ng/ml FGF2) for at least 5 days prior to NPC generation; if necessary, hES medium was mixed 1:1 with mTESR. iPSC colonies were then manually detached and transferred into uncoated plates with 50:50 medium (50% DMEM/Ham's F12, 50% neurobasal medium, 1x Pen/Strep, 1x L-Glutamax, 0.5x B27 supplement, 0.5x N2 supplement) containing 10µM SB-431542, 1µM Dorsomorphin, 3µM CHIR, 0.5µM PMA, 1x NEAA and 10µM RI. On uncoated plates, iPSCs form embryonic bodies which were grown under these conditions for two days. On day three, medium was exchange and on day four embryonic bodies were collected, pelleted and transferred

into plates containing NPC maintenance medium (50:50 medium with 200µM ascorbic acid, 3µM CHIR-99021-CT and 0.5µM PMA) with 1x NEAA and 10µM RI. Cells were allowed to grow in suspension until day 7, when they were plated on Matrigel with NPC maintenance medium (50:50 medium with 200µM ascorbic acid, 3µM CHIR-99021-CT and 0.5µM PMA) containing 1x NEAA and 10µM RI. Cells were then split at a 1:10 ratio and considered NPC cultures after approx. 5 times of splitting.

For NPC maintenance, cells were kept on Matrigel-covered plates with NPC maintenance medium with 1x NEAA, split at 80-100% confluency using Accutase, and transferred into medium containing 10µM RI directly after splitting. For frozen stocks, NPC maintenance medium with 1x NEAA was supplemented with 10µM RI and 10% DMSO.

NPCs were generated from the four T489Yfs patient iPSC clonal lines (#5.1, #6, #19, #23) and one an age-matched female and male control iPSC line (control lines were generated by Christine Bus, Department of Neurodegenerative Diseases, Centre of Neurology and Hertie Institute for Clinical Brain Research, University of Tübingen, Tübingen, Germany).

Differentiation of midbrain-specific dopaminergic neurons (mDANs) from NPCs

The protocol used for the differentiation of mDANs from NPCs was adapted from Reinhardt et al. (2013)[387] and established in the laboratory by Christine Bus, Department of Neurodegenerative Diseases, Centre of Neurology and Hertie Institute for Clinical Brain Research, University of Tübingen, Tübingen, Germany.

For differentiation, 100% confluent NPCs were first dorsalised for at least 7 days with NPC maintenance medium without PMA but containing 1x NEAA. For three days, cells were then treated with NPC maintenance medium with NEAA but without CHIR, followed by 7 days in 50:50 medium with 100ng/ml FGF8, 1µM PMA, 200µM ascorbic acid, 20ng/ml BDNF and 1x NEAA.

For maturation, cells were kept in BGCTA medium (50:50 medium with 10ng/ml BDNF, 10ng/ml GDNF, 1ng/ml TGF-β3, 200µM ascorbic acid, 500µM dbcAMP and 10µM DAPT) supplemented with 1x NEAA. After 10 days in BGCTA medium, cells were considered to be mature neurons.

For maintenance, neurons were kept on Matrigel-covered plates in BGCTA medium with 1x NEAAs and split with AccuMax into BGCTA medium with 1x NEAA and 10µM RI.

5.3.4 Protein biochemistry

Cell lysates, crosslinking of protein complexes and dephosphorylation

Cell lysis buffer A supplemented with 1x cOmplete Protease Inhibitor Cocktail was used for all proteins of the endosomal-lysosomal system, and RIPA buffer with protease inhibitor for most of the other samples. For phosphorylation studies, PhosSTOP phosphatase inhibitor was used in addition to protease inhibitor.

For lysis, cells were washed with PBS and collected in lysis buffer on ice. After an incubation period of >10 min. on ice, cell lysates were centrifuged at approx. 1,700xg for endosomal and approx. 20,000xg at 4°C for 10 min. to remove cellular and nuclear debris. The supernatant was used for protein estimation by Bradford assay or using a bicinchoninic acid (BCA) kit and kept at -20°C for storage.

For crosslinking, equal amounts of protein samples were treated with 0.0125% glutaraldehyde in PBS for 5 min. at room temperature and the reaction was stopped with 1µM Tris, pH 8.8.

Brain samples from R568Q carriers and controls were mechanically homogenised and proteins extracted in RIPA buffer with protease and phosphatase inhibitor. For dephosphorylation experiments, phosphatase inhibitor was omitted. Equal amounts of protein were incubated with 1x FastAP buffer and 10U FastAP for a minimum of 2h before the reaction was stopped by the addition of 6x Lämmli buffer.

If concentration of protein samples was necessary (e.g. for the detection of NHE6 in fibroblasts), equal amounts of protein were precipitated by the addition of TCA at a 1:4 ratio to the sample and incubated for 10 min. on ice, followed by centrifugation at 14,000xg for 5 min. Protein samples were washed with aceton to remove residual TCA and the pellet resuspended in loading buffer.

Insoluble tau isolation with sarkosyl[388]

Brain samples from R568Q carriers and pathology-matched controls were mechanically homogenised with an electrical homogeniser in 3x the amount Buffer H supplemented with protease and phosphatase inhibitors on ice (e.g., 150mg of brain

tissue were homogenised in 450µl Buffer H). After an incubation period of 20 min. on ice, samples were centrifuged at 27,200xg and 4°C for 20 min., and the supernatant collected. The pellet was again homogenised in 3x Buffer H and the centrifugation step repeated. The supernatant was combined with the previous collected one and the pellet discarded. 20µl of the supernatant was then mixed with 5µl of 6x Lämmli Buffer and stored at -20°C to be used as an input control later. For each sample, the same amount of remaining supernatant was then used for sarkosyl extraction by addition of 10% (w/v) sarkosyl and 100% (v/v) β-mercaptoethanol for a final concentration of 1% sarkosyl and 1% β-mercaptoethanol. The reaction was incubated at 37°C for 1h and then centrifuged at 150,000xg and 25°C for 35 min. The supernatant containing the sarkosyl-solube fraction was collected, and the pellet containing the sarkosyl-insoluble fraction was resuspended in 4x Lämmli Buffer and both stored at –20°C until further use.

Western blotting

Proteins were separated in running buffer on 10%, 12% or 15% (v/v) acrylamide SDS-PAGE with a 4% acrylamide stacking gel. Transfer was achieved either by iBlot dry transfer onto a nitrocellulose membrane, or, for proteins of the endosomal-lysosomal pathway, by wet transfer using 1x transfer buffer onto a PVDF membrane after activation of the membrane with methanol. After transfer, the membrane was blocked in 5% (w/v) milk powder/TBS-T or 5% (w/v) BSA/TBS-T depending on the antibody used. Incubation of the primary antibody in blocking solution was either o/n at 4°C or for 2h at RT, followed by 2h or 1h, respectively, of incubation with the HRP-linked secondary antibody.

The peroxidase-generated signal was developed on film using ECL, ECL prime or Immobilon chemiluminescence substrates.

Densitometry of Western blotting bands was done using the ’plot lanes’ command in ImageJ and measuring the area under the curve after the exclusion of background signal.

Table 11. List of antibodies used for Western blotting, including dilutions, blocking solution used for incubation, secondary species and the manufacturer.

Antibody	Dilution	Blocking solution	Secondary	Company
AT8 (pSer202 +	1:1000	5% milk/TBS-T	mouse	Thermo

Thr205)				Scientific
AT270 (pThr181)	1:1000	5% milk/TBS-T	mouse	Thermo Scientific
β-actin	1:5000	5% milk/TBS-T	mouse	Sigma-Aldrich
BiP/GRP78	1:1000	5% milk/TBS-T	goat	Santa Cruz
Clathrin	1:1000	5% BSA/TBS-T	rabbit	Cell Signaling Technologies
Cation-dependent Mannose-6-phosphate receptor	1:1000	5% BSA/TBS-T	mouse	Developmental Studies Hybridoma Bank Iowa, 22d4, deposited to the DSHB by Messner, D.
EEA1	1:1000	5% BSA/TBS-T	Rabbit	Cell Signaling Technologies
GAPDH	1:5000	5% milk/TBS-T	mouse	Calbiochem
HA	1:5000	5% milk/TBS-T	rabbit	Santa Cruz
LC3	1:1000	5% milk/TBS-T	rabbit	Novex
NHE6/SLC9A6	1:1000-1:5000	5% BSA/TBS-T	Rabbit	MBL
Rab5	1:1000	5% BSA/TBS-T	rabbit	Cell Signaling Technologies
Rab7	1:1000	5% BSA/TBS-T	rabbit	Cell Signaling Technologies
Rab11	1:1000	5% BSA/TBS-T	rabbit	Cell Signaling Technologies
Secondary antibody mouse, HRP-linked	1:5000	5% milk/TBS-T	n.a.	Amersham
Secondary antibody rabbit, HRP-linked	1:5000	5% milk/TBS-T	n.a.	Amersham
Secondary	1:5000-	5% milk/TBS-T	n.a.	Bio-Rad

antibody goat, HRP-linked	1:10,000			
Sortilin	1:1000	5% milk/TBS-T	Rabbit	GeneTex, Irvine, USA
Tau-5 (total Tau)	1:500	5% milk/TBS-T	mouse	Thermo Scientific
VPS26	1:1000	5% milk/TBS-T	Rabbit	GeneTex
VPS29	1:1000	5% milk/TBS-T	Rabbit	GeneTex
VPS35	1:1000	5% milk/TBS-T	Rabbit	GeneTex

PhosTag acrylamide Western blot for phosphorylated proteins

PhosTag acrylamide can be used to distinguish proteins with a higher phosphorylation from less phosphorylated forms as the PhosTag acrylamide binds to phosphorylated residues, thereby slowing down the migration of proteins in proportion to the amount of phosphorylation.

For PhosTag, a 10% acrylamide gel was supplemented with 1% (w/v) PhosTag acrylamide and 1% (w/v) $MnCl_2$ before running. The acrylamide gel was washed in running buffer with 10mM EDTA before dry transfer, or transfer buffer with 10mM EDTA before wet transfer, to remove $MnCl_2$ that could interfere with the transfer.

OxyBlot detection of carbonyl groups in proteins

OxyBlot was performed according to the manufacturer's instructions. SDS was added to equal amounts of protein sample for a final concentration of 6% SDS before the addition of an equal total amount of 2,4-dinitrophenylhydrazine (DNPH) that reacts with carbonyl groups on proteins that are created by oxidation to form 2,4-dinitrophenylhydrazone (DNP) that can be detected by specific antibodies. After incubation for 15 min at RT, the reaction was stopped by the addition of neutralisation solution and the sample loaded on a 10% acrylamide gel and the presence of DNP detected by antibodies supplied with the kit.

Immunocytochemistry for endosomal proteins

Cells were seeded on Collagen-coated coverslips and fixed with 4%PFA/PBS for 25min at RT. Permeabilisation of cells was achieved using PBS with 0.3% TritonX-100 and 0.5% BSA for 60 min at RT, followed by blocking for 60 min at RT in 10% of

appropriate serum (depending on the species the secondary antibody was raised in) in PBS. The primary antibody was incubated at a concentration of 1:250 if not otherwise specified by the manufacturer in 5% serum with 0.025% TritonX-100 in PBS for 2h at 37°C (EEA1, mouse, BD biosciences; HA, rabbit, Santa Cruz). The secondary antibody was incubated for 1h at RT in blocking solution at a concentration of 1:1000 followed by nuclear staining with Hoechst 33258 in PBS for 10 min at RT before mounting with Vectashield.

Immunocytochemistry for characterisation of iPSCs

iPSCs were seeded on Matrigel-coated coverslips and fixed with 4% PFA/PBS at RT for 20min. After permeabilisation with methanol for 5 min at -20°C, unspecific binding sites were blocked in 10% NDS/PBS-0.01% TritonX-100 for 50 min at RT. Incubation with primary antibodies (Sox2, 1:200, rabbit, abcam; SSEA4, 1:100, mouse, hybridoma bank, Oct4, 1:300, goat, abcam) was in 5% NDS/PBS-Triton o/n at 4°C. Secondary antibodies (anti-mouse, anti-rabbit, anti-goat, 1:1000, Alexa 488, molecular probes) was for 2h at RT in 10% NGS/PBS-Triton. Coverslips were mounted with DAKO after nuclear staining with Hoechst 33258 in PBS at 1:10,000 for 2min at RT.

Images from ICC were taken on an Apotome microscopy using Axiovision software.

5.3.5 Biochemical analyses

Flow cytometry

To measure acidity in the endosomal-lysosomal system, by flow cytometry, cells were stained with LysoTracker 1:10,000 (100nM) in HBSS for 15 min at 37°C. An untreated control was incubated with HBSS only. After washing out of the dye, cells were detached using Trypsin, pelleted and resuspended in 1% BSA/HBSS. The mean APC fluorescence was measured using the CyAn ADP Analyzer and background fluorescence values obtained from unstained cells was subtracted.

Levels of Tom22 were measured using the Inside Stain Kit with an GFP-coupled Tom22 antibody. To this end, cells were resuspended in PBS with 0.5% BSA and 2mM EDTA and fixed with an equal amount of Inside Fix, followed by 20 min of incubation at RT. Cells were then pelleted and after a wash resuspended in Inside Perm with a 1:10 dilution of Tom22-GFP antibody for 10 min at RT, or a mouse IgG control. The staining was stop by dilution with Inside Perm and centrifugation to

remove the staining solution. Cells were then resuspended in PBS with 0.5% BSA and 2mM EDTA and Tom22-GFP fluorescence measured on a MACSQuant Analyzer flow cytometer. Background fluorescence obtained from IgG control stained cells was subtracted for analysis.

Annexin V measurement of early apoptosis was done by detaching the cells with 2mM EDTA at 37°C for 3 min, after which the cells were collected in HBSS and pelleted. The cells were then resuspended in Annexin Binding Buffer with a 1:50 dilution of Annexin V-Pacific blue or, for a background control, in Annexin Binding Buffer only. After incubation at RT for 15 min in the dark, the staining was 4x diluted with Annexin Binding Buffer and measured with a Violet 1 channel at a CyAn ADP flow cytometer. Values obtained in the background control were subtracted from the dye condition.

Microscopy with pH-sensitive dyes

For all Live-Cell microscopy experiments, cells were seeded at a similar density on Collagen-coated 24mm coverslips and imaged in a custom-made imaging chamber. For LysoTracker analysis, cells were stained for 15 min at 37°C with LysoTracker 1:10,000 (100nM) and Hoechst 33342 1:10,000 (1µg/ml) in medium before imaging in HBSS or growth medium at Zeiss Axiovert Live Cell microscope using a red filter or the LSM 510 confocal with a 546nm laser. For particle analysis, the Analyze Particles tool from ImageJ/Fiji was used to obtain the number of particles per cell and the area.

M17 cells were induced and seeded the day before imaging for LysoSensor. Cells were transduced with CellLight Lysosomes-RFP BackMam 2.0 for 16h and stained for 5 min with 1µM LysoSensor yellow/blue in HBSS with 15mM HEPES and 20mM glucose. The same solution was used for washing out of the dye and imaging. Cells were then imaged by Dr. Angelos Skodras, Department of Cellular Neurology, Hertie Institute for Clinical Brain Research, Tübingen, on a Zeiss 780NLO confocal microscope with a spectral detector using 2-photon excitation at 750nm in a 5% CO_2 and 37°C environment. Emission was capture in a range from 410nm to 659nm in 18nm intervals. For image analysis using Fiji, the presence of a red CellLight Lysosomes-RFP was first confirmed by plotting of the signal intensity for all wavelengths for each region of interest (ROI) and the Multi Measure tool was then

used to assess the signal intensity at 446-455nm (blue) and 535-544nm (yellow) for a ratio of and yellow/blue values.
For all microscopy experiments, settings were not change between cell lines and all pictures analysed using the same settings for thresholds, background correction and the size of particles analysed.

Measurement of cellular ROS using Dihydroethidium
Cells were seeded in a black 96 well plate with clear bottom at a similar density on the day before the assay. For the Rotenone-condition were pre-treated with 5µM Rotenone in growth medium for 4h. For the measurement, the growth medium on all cells was removed and 100µM DiHET in HBSS with 20mM glucose was added to the cells and background control wells. At a monochromatic SpectraMAX reader, the fluorescence at 370nm and 535nm excitation, and 420nm emission and 610nm for cellular (blue) and chromatin-bound (red) DIHET, respectively, was measured immediately for 30 min and the rate of red to blue conversion calculated for all conditions.

LDH assay
To test for cell death independent of cell death mechanism, the CytoTox 96 Non-Radioactive Cytotoxicity Assay Kit was used according to the manufacturer's instructions. M17 cells were transfected 72h before each experiment and fibroblasts seeded at a similar density in a 96-well plate format for the measurement. 24h before the assay, the medium was changed to DMEM without phenol red supplemented with 10% FBS to avoid effects of the dye and control treatment with 1µM staurosporine (STS) was started. For each condition, triplicates were used and empty wells with the respective media as a background control.
24h after the start of STS treatment, the medium was partially taken off and cells lysed with 0.9% Triton X-100 in ddH_20 for 45 min at 37°C. 30µl of cell lysates and 30µl of medium removed before lysis, including the background controls, was then mixed with an equal amount of substrate solution solved in Assay Buffer and incubated at RT for 30 min in the dark after which 30µl of Stop Solution (1M acetic acid) was added to each well. The absorbance at 490nm was read on an ELISA reader and LDH release into the medium normalised to LDH release from lysed cells after subtraction of background values.

5.3.6 Online tools

For the design of NHE6 knockdown miRNA sequences, Invitrogen's BlockiT RNAi Designer was used and the three top hits used for cloning into the pcDNA6.2/EmGFP miRNA expression vector. (https://rnaidesigner.thermofisher.com/rnaiexpress/).

For analysis of R568Q allele frequency, the Exome Aggregation Consortium (ExAC) browser[340] version 0.3.1 at the Broad Institute, Cambridge, USA (http://exac.broadinstitute.org/) was used. For a prediction of consequences of the R568Q variant and T489Y_fs23X mutation, MutationTaster2 was used (http://www.mutationtaster.org)[339].

5.3.7 Statistical analysis

Statistical analysis and visualization of scientific data in graphs was carried out using GraphPad Prism 6. The program was used to calculate the mean of all independent experiments and to compare two conditions using a two-tailed Student's t-test. Results with a p-value <0.05 were considered to be statistically significant.

6. References

1. Levin J, Kurz A, Arzberger T, Giese A, Hoglinger GU. The Differential Diagnosis and Treatment of Atypical Parkinsonism. Deutsches Arzteblatt international. 2016 Feb 05;113(5):61-9.

2. Scholz SW, Bras J. Genetics Underlying Atypical Parkinsonism and Related Neurodegenerative Disorders. International journal of molecular sciences. 2015 Oct 16;16(10):24629-55.

3. Rebeiz JJ, Kolodny EH, Richardson EP, Jr. Corticodentatonigral degeneration with neuronal achromasia. Archives of neurology. 1968 Jan;18(1):20-33.

4. Chahine LM, Rebeiz T, Rebeiz JJ, Grossman M, Gross RG. Corticobasal syndrome: Five new things. Neurology Clinical practice. 2014 Aug;4(4):304-12.

5. Boeve BF, Lang AE, Litvan I. Corticobasal degeneration and its relationship to progressive supranuclear palsy and frontotemporal dementia. Annals of neurology. 2003;54 Suppl 5:S15-9.

6. Armstrong MJ, Litvan I, Lang AE, et al. Criteria for the diagnosis of corticobasal degeneration. Neurology. 2013 Jan 29;80(5):496-503.

7. Litvan I, Agid Y, Goetz C, et al. Accuracy of the clinical diagnosis of corticobasal degeneration: a clinicopathologic study. Neurology. 1997 Jan;48(1):119-25.

8. Boeve BF, Maraganore DM, Parisi JE, et al. Pathologic heterogeneity in clinically diagnosed corticobasal degeneration. Neurology. 1999 Sep 11;53(4):795-800.

9. Shelley BP, Hodges JR, Kipps CM, Xuereb JH, Bak TH. Is the pathology of corticobasal syndrome predictable in life? Movement disorders : official journal of the Movement Disorder Society. 2009 Aug 15;24(11):1593-9.

10. Grimes DA, Bergeron CB, Lang AE. Motor neuron disease-inclusion dementia presenting as cortical-basal ganglionic degeneration. Movement disorders : official journal of the Movement Disorder Society. 1999 Jul;14(4):674-80.

11. Grimes DA, Lang AE, Bergeron CB. Dementia as the most common presentation of cortical-basal ganglionic degeneration. Neurology. 1999 Dec 10;53(9):1969-74.

12. Lee SE, Rabinovici GD, Mayo MC, et al. Clinicopathological correlations in corticobasal degeneration. Annals of neurology. 2011 Aug;70(2):327-40.

13. Brown J, Lantos PL, Rossor MN. Familial dementia lacking specific pathological features presenting with clinical features of corticobasal degeneration. Journal of neurology, neurosurgery, and psychiatry. 1998 Oct;65(4):600-3.

14. Boeve BF. The multiple phenotypes of corticobasal syndrome and corticobasal degeneration: implications for further study. Journal of molecular neuroscience : MN. 2011 Nov;45(3):350-3.

15. Rossi G, Marelli C, Farina L, et al. The G389R mutation in the MAPT gene presenting as sporadic corticobasal syndrome. Movement disorders : official journal of the Movement Disorder Society. 2008 Apr 30;23(6):892-5.

16. Di Maria E, Tabaton M, Vigo T, et al. Corticobasal degeneration shares a common genetic background with progressive supranuclear palsy. Annals of neurology. 2000 Mar;47(3):374-7.

17. Masellis M, Momeni P, Meschino W, et al. Novel splicing mutation in the progranulin gene causing familial corticobasal syndrome. Brain : a journal of neurology. 2006 Nov;129(Pt 11):3115-23.

18. Peng G, Liu P, He F, Luo B. Posterior cortical atrophy as a primary clinical phenotype of corticobasal syndrome with a progranulin gene rs5848 TT genotype. Orphanet journal of rare diseases. 2016 Feb 06;11:13.

19. Taghdiri F, Sato C, Ghani M, Moreno D, Rogaeva E, Tartaglia MC. Novel GRN Mutations in Patients with Corticobasal Syndrome. Scientific reports. 2016 Mar 10;6:22913.

20. Baker M, Mackenzie IR, Pickering-Brown SM, et al. Mutations in progranulin cause tau-negative frontotemporal dementia linked to chromosome 17. Nature. 2006 Aug 24;442(7105):916-9.

21. Meeter LH, Patzke H, Loewen G, et al. Progranulin Levels in Plasma and Cerebrospinal Fluid in Granulin Mutation Carriers. Dementia and geriatric cognitive disorders extra. 2016 May-Aug;6(2):330-40.

22. Chen-Plotkin AS, Yuan W, Anderson C, et al. Corticobasal syndrome and primary progressive aphasia as manifestations of LRRK2 gene mutations. Neurology. 2008 Feb 12;70(7):521-7.

23. Wenning GK, Litvan I, Jankovic J, et al. Natural history and survival of 14 patients with corticobasal degeneration confirmed at postmortem examination. Journal of neurology, neurosurgery, and psychiatry. 1998 Feb;64(2):184-9.

24. Gibb WR, Luthert PJ, Marsden CD. Clinical and pathological features of corticobasal degeneration. Advances in neurology. 1990;53:51-4.

25. Taniguchi-Watanabe S, Arai T, Kametani F, et al. Biochemical classification of tauopathies by immunoblot, protein sequence and mass spectrometric analyses of sarkosyl-insoluble and trypsin-resistant tau. Acta neuropathologica. 2016 Feb;131(2):267-80.

26. Arai T, Ikeda K, Akiyama H, et al. Identification of amino-terminally cleaved tau fragments that distinguish progressive supranuclear palsy from corticobasal degeneration. Annals of neurology. 2004 Jan;55(1):72-9.

27. Dickson DW, Bergeron C, Chin SS, et al. Office of Rare Diseases neuropathologic criteria for corticobasal degeneration. Journal of neuropathology and experimental neurology. 2002 Nov;61(11):935-46.

28. Bugiani O, Murrell JR, Giaccone G, et al. Frontotemporal dementia and corticobasal degeneration in a family with a P301S mutation in tau. Journal of neuropathology and experimental neurology. 1999 Jun;58(6):667-77.

29. Spillantini MG, Yoshida H, Rizzini C, et al. A novel tau mutation (N296N) in familial dementia with swollen achromatic neurons and corticobasal inclusion bodies. Annals of neurology. 2000 Dec;48(6):939-43.

30. Kouri N, Murray ME, Hassan A, et al. Neuropathological features of corticobasal degeneration presenting as corticobasal syndrome or Richardson syndrome. Brain : a journal of neurology. 2011 Nov;134(Pt 11):3264-75.

31. Kouri N, Ross OA, Dombroski B, et al. Genome-wide association study of corticobasal degeneration identifies risk variants shared with progressive supranuclear palsy. Nature communications. 2015 Jun 16;6:7247.

32. Houlden H, Baker M, Morris HR, et al. Corticobasal degeneration and progressive supranuclear palsy share a common tau haplotype. Neurology. 2001 Jun 26;56(12):1702-6.

33. Weingarten MD, Lockwood AH, Hwo SY, Kirschner MW. A protein factor essential for microtubule assembly. Proceedings of the National Academy of Sciences of the United States of America. 1975 May;72(5):1858-62.

34. Witman GB, Cleveland DW, Weingarten MD, Kirschner MW. Tubulin requires tau for growth onto microtubule initiating sites. Proceedings of the National Academy of Sciences of the United States of America. 1976 Nov;73(11):4070-4.

35. Goedert M, Wischik CM, Crowther RA, Walker JE, Klug A. Cloning and sequencing of the cDNA encoding a core protein of the paired helical filament of Alzheimer disease: identification as the microtubule-associated protein tau. Proceedings of the National Academy of Sciences of the United States of America. 1988 Jun;85(11):4051-5.

36. Couchie D, Mavilia C, Georgieff IS, Liem RK, Shelanski ML, Nunez J. Primary structure of high molecular weight tau present in the peripheral nervous system. Proceedings of the National Academy of Sciences of the United States of America. 1992 May 15;89(10):4378-81.

37. Goedert M, Spillantini MG, Jakes R, Rutherford D, Crowther RA. Multiple isoforms of human microtubule-associated protein tau: sequences and localization in neurofibrillary tangles of Alzheimer's disease. Neuron. 1989 Oct;3(4):519-26.

38. Goedert M, Spillantini MG, Potier MC, Ulrich J, Crowther RA. Cloning and sequencing of the cDNA encoding an isoform of microtubule-associated protein tau containing four tandem repeats: differential expression of tau protein mRNAs in human brain. The EMBO journal. 1989 Feb;8(2):393-9.

39. Goedert M, Jakes R. Expression of separate isoforms of human tau protein: correlation with the tau pattern in brain and effects on tubulin polymerization. The EMBO journal. 1990 Dec;9(13):4225-30.

40. Goode BL, Feinstein SC. Identification of a novel microtubule binding and assembly domain in the developmentally regulated inter-repeat region of tau. The Journal of cell biology. 1994 Mar;124(5):769-82.

41. Vershinin M, Carter BC, Razafsky DS, King SJ, Gross SP. Multiple-motor based transport and its regulation by Tau. Proceedings of the National Academy of Sciences of the United States of America. 2007 Jan 02;104(1):87-92.

42. Drubin DG, Kirschner MW. Tau protein function in living cells. The Journal of cell biology. 1986 Dec;103(6 Pt 2):2739-46.

43. Kosik KS, Orecchio LD, Bakalis S, Neve RL. Developmentally regulated expression of specific tau sequences. Neuron. 1989 Apr;2(4):1389-97.

44. Wille H, Drewes G, Biernat J, Mandelkow EM, Mandelkow E. Alzheimer-like paired helical filaments and antiparallel dimers formed from microtubule-associated protein tau in vitro. The Journal of cell biology. 1992 Aug;118(3):573-84.

45. Schweers O, Schonbrunn-Hanebeck E, Marx A, Mandelkow E. Structural studies of tau protein and Alzheimer paired helical filaments show no evidence for beta-structure. The Journal of biological chemistry. 1994 Sep 30;269(39):24290-7.

46. Hirokawa N, Shiomura Y, Okabe S. Tau proteins: the molecular structure and mode of binding on microtubules. The Journal of cell biology. 1988 Oct;107(4):1449-59.

47. Chen J, Kanai Y, Cowan NJ, Hirokawa N. Projection domains of MAP2 and tau determine spacings between microtubules in dendrites and axons. Nature. 1992 Dec 17;360(6405):674-7.

48. Magnani E, Fan J, Gasparini L, et al. Interaction of tau protein with the dynactin complex. The EMBO journal. 2007 Oct 31;26(21):4546-54.

49. Steiner B, Mandelkow EM, Biernat J, et al. Phosphorylation of microtubule-associated protein tau: identification of the site for Ca2(+)-calmodulin dependent kinase and relationship with tau phosphorylation in Alzheimer tangles. The EMBO journal. 1990 Nov;9(11):3539-44.

50. Yu Y, Run X, Liang Z, et al. Developmental regulation of tau phosphorylation, tau kinases, and tau phosphatases. Journal of neurochemistry. 2009 Mar;108(6):1480-94.

51. Drewes G, Trinczek B, Illenberger S, et al. Microtubule-associated protein/microtubule affinity-regulating kinase (p110mark). A novel protein kinase that regulates tau-microtubule interactions and dynamic instability by phosphorylation at the Alzheimer-specific site serine 262. The Journal of biological chemistry. 1995 Mar 31;270(13):7679-88.

52. Trinczek B, Biernat J, Baumann K, Mandelkow EM, Mandelkow E. Domains of tau protein, differential phosphorylation, and dynamic instability of microtubules. Molecular biology of the cell. 1995 Dec;6(12):1887-902.

53. Hanger DP, Hughes K, Woodgett JR, Brion JP, Anderton BH. Glycogen synthase kinase-3 induces Alzheimer's disease-like phosphorylation of tau: generation of paired helical filament epitopes and neuronal localisation of the kinase. Neuroscience letters. 1992 Nov 23;147(1):58-62.

54. Baumann K, Mandelkow EM, Biernat J, Piwnica-Worms H, Mandelkow E. Abnormal Alzheimer-like phosphorylation of tau-protein by cyclin-dependent kinases cdk2 and cdk5. FEBS letters. 1993 Dec 28;336(3):417-24.

55. Schneider A, Biernat J, von Bergen M, Mandelkow E, Mandelkow EM. Phosphorylation that detaches tau protein from microtubules (Ser262, Ser214) also protects it against aggregation into Alzheimer paired helical filaments. Biochemistry. 1999 Mar 23;38(12):3549-58.

56. Son Y, Kim S, Chung HT, Pae HO. Reactive oxygen species in the activation of MAP kinases. Methods in enzymology. 2013;528:27-48.

57. Sontag E, Nunbhakdi-Craig V, Lee G, Bloom GS, Mumby MC. Regulation of the phosphorylation state and microtubule-binding activity of Tau by protein phosphatase 2A. Neuron. 1996 Dec;17(6):1201-7.

58. Cohen TJ, Guo JL, Hurtado DE, et al. The acetylation of tau inhibits its function and promotes pathological tau aggregation. Nature communications. 2011;2:252.

59. Cook C, Carlomagno Y, Gendron TF, et al. Acetylation of the KXGS motifs in tau is a critical determinant in modulation of tau aggregation and clearance. Human molecular genetics. 2014 Jan 01;23(1):104-16.

60. Min SW, Cho SH, Zhou Y, et al. Acetylation of tau inhibits its degradation and contributes to tauopathy. Neuron. 2010 Sep 23;67(6):953-66.

61. Cohen TJ, Constance BH, Hwang AW, James M, Yuan CX. Intrinsic Tau Acetylation Is Coupled to Auto-Proteolytic Tau Fragmentation. PloS one. 2016;11(7):e0158470.

62. Rissman RA, Poon WW, Blurton-Jones M, et al. Caspase-cleavage of tau is an early event in Alzheimer disease tangle pathology. The Journal of clinical investigation. 2004 Jul;114(1):121-30.

63. Horowitz PM, Patterson KR, Guillozet-Bongaarts AL, et al. Early N-terminal changes and caspase-6 cleavage of tau in Alzheimer's disease. The Journal of neuroscience : the official journal of the Society for Neuroscience. 2004 Sep 08;24(36):7895-902.

64. Park SY, Ferreira A. The generation of a 17 kDa neurotoxic fragment: an alternative mechanism by which tau mediates beta-amyloid-induced neurodegeneration. The Journal of neuroscience : the official journal of the Society for Neuroscience. 2005 Jun 01;25(22):5365-75.

65. Liu F, Zaidi T, Iqbal K, Grundke-Iqbal I, Gong CX. Aberrant glycosylation modulates phosphorylation of tau by protein kinase A and dephosphorylation of tau by protein phosphatase 2A and 5. Neuroscience. 2002;115(3):829-37.

66. Wang JZ, Grundke-Iqbal I, Iqbal K. Glycosylation of microtubule-associated protein tau: an abnormal posttranslational modification in Alzheimer's disease. Nature medicine. 1996 Aug;2(8):871-5.

67. Williams DR. Tauopathies: classification and clinical update on neurodegenerative diseases associated with microtubule-associated protein tau. Internal medicine journal. 2006 Oct;36(10):652-60.

68. Connell JW, Rodriguez-Martin T, Gibb GM, et al. Quantitative analysis of tau isoform transcripts in sporadic tauopathies. Brain research Molecular brain research. 2005 Jun 13;137(1-2):104-9.

69. Braak H, Thal DR, Ghebremedhin E, Del Tredici K. Stages of the pathologic process in Alzheimer disease: age categories from 1 to 100 years. Journal of neuropathology and experimental neurology. 2011 Nov;70(11):960-9.

70. Andorfer C, Kress Y, Espinoza M, et al. Hyperphosphorylation and aggregation of tau in mice expressing normal human tau isoforms. Journal of neurochemistry. 2003 Aug;86(3):582-90.

71. Alonso A, Zaidi T, Novak M, Grundke-Iqbal I, Iqbal K. Hyperphosphorylation induces self-assembly of tau into tangles of paired helical filaments/straight filaments. Proceedings of the National Academy of Sciences of the United States of America. 2001 Jun 05;98(12):6923-8.

72. Buerger K, Ewers M, Pirttila T, et al. CSF phosphorylated tau protein correlates with neocortical neurofibrillary pathology in Alzheimer's disease. Brain : a journal of neurology. 2006 Nov;129(Pt 11):3035-41.

73. Loring JF, Wen X, Lee JM, Seilhamer J, Somogyi R. A gene expression profile of Alzheimer's disease. DNA and cell biology. 2001 Nov;20(11):683-95.

74. Simon-Sanchez J, Schulte C, Bras JM, et al. Genome-wide association study reveals genetic risk underlying Parkinson's disease. Nature genetics. 2009 Dec;41(12):1308-12.

75. Edwards TL, Scott WK, Almonte C, et al. Genome-wide association study confirms SNPs in SNCA and the MAPT region as common risk factors for Parkinson disease. Annals of human genetics. 2010 Mar;74(2):97-109.

76. Hong M, Zhukareva V, Vogelsberg-Ragaglia V, et al. Mutation-specific functional impairments in distinct tau isoforms of hereditary FTDP-17. Science. 1998 Dec 04;282(5395):1914-7.

77. Hutton M, Lendon CL, Rizzu P, et al. Association of missense and 5'-splice-site mutations in tau with the inherited dementia FTDP-17. Nature. 1998 Jun 18;393(6686):702-5.

78. Poorkaj P, Bird TD, Wijsman E, et al. Tau is a candidate gene for chromosome 17 frontotemporal dementia. Annals of neurology. 1998 Jun;43(6):815-25.

79. Delisle MB, Murrell JR, Richardson R, et al. A mutation at codon 279 (N279K) in exon 10 of the Tau gene causes a tauopathy with dementia and supranuclear palsy. Acta neuropathologica. 1999 Jul;98(1):62-77.

80. Mitchell TW, Nissanov J, Han LY, et al. Novel method to quantify neuropil threads in brains from elders with or without cognitive impairment. The journal of histochemistry and cytochemistry : official journal of the Histochemistry Society. 2000 Dec;48(12):1627-38.

81. Arriagada PV, Growdon JH, Hedley-Whyte ET, Hyman BT. Neurofibrillary tangles but not senile plaques parallel duration and severity of Alzheimer's disease. Neurology. 1992 Mar;42(3 Pt 1):631-9.

82. Zhang B, Maiti A, Shively S, et al. Microtubule-binding drugs offset tau sequestration by stabilizing microtubules and reversing fast axonal transport deficits

in a tauopathy model. Proceedings of the National Academy of Sciences of the United States of America. 2005 Jan 04;102(1):227-31.

83. Stokin GB, Lillo C, Falzone TL, et al. Axonopathy and transport deficits early in the pathogenesis of Alzheimer's disease. Science. 2005 Feb 25;307(5713):1282-8.

84. Gauthier S, Feldman HH, Schneider LS, et al. Efficacy and safety of tau-aggregation inhibitor therapy in patients with mild or moderate Alzheimer's disease: a randomised, controlled, double-blind, parallel-arm, phase 3 trial. Lancet. 2016 Dec 10;388(10062):2873-84.

85. Yoshiyama Y, Higuchi M, Zhang B, et al. Synapse loss and microglial activation precede tangles in a P301S tauopathy mouse model. Neuron. 2007 Feb 01;53(3):337-51.

86. Ahmed Z, Bigio EH, Budka H, et al. Globular glial tauopathies (GGT): consensus recommendations. Acta neuropathologica. 2013 Oct;126(4):537-44.

87. Dickson DW. Neuropathologic differentiation of progressive supranuclear palsy and corticobasal degeneration. Journal of neurology. 1999 Sep;246 Suppl 2:II6-15.

88. Hauw JJ, Daniel SE, Dickson D, et al. Preliminary NINDS neuropathologic criteria for Steele-Richardson-Olszewski syndrome (progressive supranuclear palsy). Neurology. 1994 Nov;44(11):2015-9.

89. Kovacs GG, Ferrer I, Grinberg LT, et al. Aging-related tau astrogliopathy (ARTAG): harmonized evaluation strategy. Acta neuropathologica. 2016 Jan;131(1):87-102.

90. Minoura K, Yao TM, Tomoo K, et al. Different associational and conformational behaviors between the second and third repeat fragments in the tau microtubule-binding domain. European journal of biochemistry. 2004 Feb;271(3):545-52.

91. Alonso Adel C, Mederlyova A, Novak M, Grundke-Iqbal I, Iqbal K. Promotion of hyperphosphorylation by frontotemporal dementia tau mutations. The Journal of biological chemistry. 2004 Aug 13;279(33):34873-81.

92. Thies E, Mandelkow EM. Missorting of tau in neurons causes degeneration of synapses that can be rescued by the kinase MARK2/Par-1. The Journal of neuroscience : the official journal of the Society for Neuroscience. 2007 Mar 14;27(11):2896-907.

93. Schweers O, Mandelkow EM, Biernat J, Mandelkow E. Oxidation of cysteine-322 in the repeat domain of microtubule-associated protein tau controls the in vitro assembly of paired helical filaments. Proceedings of the National Academy of Sciences of the United States of America. 1995 Aug 29;92(18):8463-7.

94. Friedhoff P, Schneider A, Mandelkow EM, Mandelkow E. Rapid assembly of Alzheimer-like paired helical filaments from microtubule-associated protein tau monitored by fluorescence in solution. Biochemistry. 1998 Jul 14;37(28):10223-30.

95. Goedert M, Jakes R, Spillantini MG, Hasegawa M, Smith MJ, Crowther RA. Assembly of microtubule-associated protein tau into Alzheimer-like filaments induced by sulphated glycosaminoglycans. Nature. 1996 Oct 10;383(6600):550-3.

96. Novak M, Kabat J, Wischik CM. Molecular characterization of the minimal protease resistant tau unit of the Alzheimer's disease paired helical filament. The EMBO journal. 1993 Jan;12(1):365-70.

97. Hasegawa M, Crowther RA, Jakes R, Goedert M. Alzheimer-like changes in microtubule-associated protein Tau induced by sulfated glycosaminoglycans. Inhibition of microtubule binding, stimulation of phosphorylation, and filament assembly depend on the degree of sulfation. The Journal of biological chemistry. 1997 Dec 26;272(52):33118-24.

98. Mukrasch MD, Biernat J, von Bergen M, Griesinger C, Mandelkow E, Zweckstetter M. Sites of tau important for aggregation populate {beta}-structure and bind to microtubules and polyanions. The Journal of biological chemistry. 2005 Jul 01;280(26):24978-86.

99. Braak H, Braak E. Staging of Alzheimer's disease-related neurofibrillary changes. Neurobiology of aging. 1995 May-Jun;16(3):271-8; discussion 8-84.

100. Mazanetz MP, Fischer PM. Untangling tau hyperphosphorylation in drug design for neurodegenerative diseases. Nature reviews Drug discovery. 2007 Jun;6(6):464-79.

101. Kimura T, Tsutsumi K, Taoka M, et al. Isomerase Pin1 stimulates dephosphorylation of tau protein at cyclin-dependent kinase (Cdk5)-dependent Alzheimer phosphorylation sites. The Journal of biological chemistry. 2013 Mar 15;288(11):7968-77.

102. Su B, Wang X, Lee HG, et al. Chronic oxidative stress causes increased tau phosphorylation in M17 neuroblastoma cells. Neuroscience letters. 2010 Jan 14;468(3):267-71.

103. Lindwall G, Cole RD. Phosphorylation affects the ability of tau protein to promote microtubule assembly. The Journal of biological chemistry. 1984 Apr 25;259(8):5301-5.

104. Hoover BR, Reed MN, Su J, et al. Tau mislocalization to dendritic spines mediates synaptic dysfunction independently of neurodegeneration. Neuron. 2010 Dec 22;68(6):1067-81.

105. Hanger DP, Anderton BH, Noble W. Tau phosphorylation: the therapeutic challenge for neurodegenerative disease. Trends in molecular medicine. 2009 Mar;15(3):112-9.

106. Dickey CA, Kamal A, Lundgren K, et al. The high-affinity HSP90-CHIP complex recognizes and selectively degrades phosphorylated tau client proteins. The Journal of clinical investigation. 2007 Mar;117(3):648-58.

107. Rodriguez-Martin T, Cuchillo-Ibanez I, Noble W, Nyenya F, Anderton BH, Hanger DP. Tau phosphorylation affects its axonal transport and degradation. Neurobiology of aging. 2013 Sep;34(9):2146-57.

108. Gamblin TC, Chen F, Zambrano A, et al. Caspase cleavage of tau: linking amyloid and neurofibrillary tangles in Alzheimer's disease. Proceedings of the National Academy of Sciences of the United States of America. 2003 Aug 19;100(17):10032-7.

109. de Calignon A, Fox LM, Pitstick R, et al. Caspase activation precedes and leads to tangles. Nature. 2010 Apr 22;464(7292):1201-4.

110. Johnson GV. Differential phosphorylation of tau by cyclic AMP-dependent protein kinase and Ca2+/calmodulin-dependent protein kinase II: metabolic and functional consequences. Journal of neurochemistry. 1992 Dec;59(6):2056-62.

111. Kenessey A, Nacharaju P, Ko LW, Yen SH. Degradation of tau by lysosomal enzyme cathepsin D: implication for Alzheimer neurofibrillary degeneration. Journal of neurochemistry. 1997 Nov;69(5):2026-38.

112. Bednarski E, Lynch G. Cytosolic proteolysis of tau by cathepsin D in hippocampus following suppression of cathepsins B and L. Journal of neurochemistry. 1996 Nov;67(5):1846-55.

113. Wang Y, Martinez-Vicente M, Kruger U, et al. Tau fragmentation, aggregation and clearance: the dual role of lysosomal processing. Human molecular genetics. 2009 Nov 01;18(21):4153-70.

114. Dickey CA, Yue M, Lin WL, et al. Deletion of the ubiquitin ligase CHIP leads to the accumulation, but not the aggregation, of both endogenous phospho- and caspase-3-cleaved tau species. The Journal of neuroscience : the official journal of the Society for Neuroscience. 2006 Jun 28;26(26):6985-96.

115. Morishima-Kawashima M, Hasegawa M, Takio K, Suzuki M, Titani K, Ihara Y. Ubiquitin is conjugated with amino-terminally processed tau in paired helical filaments. Neuron. 1993 Jun;10(6):1151-60.

116. Petrucelli L, Dickson D, Kehoe K, et al. CHIP and Hsp70 regulate tau ubiquitination, degradation and aggregation. Human molecular genetics. 2004 Apr 01;13(7):703-14.

117. Keck S, Nitsch R, Grune T, Ullrich O. Proteasome inhibition by paired helical filament-tau in brains of patients with Alzheimer's disease. Journal of neurochemistry. 2003 Apr;85(1):115-22.

118. Shimura H, Schwartz D, Gygi SP, Kosik KS. CHIP-Hsc70 complex ubiquitinates phosphorylated tau and enhances cell survival. The Journal of biological chemistry. 2004 Feb 06;279(6):4869-76.

119. Kruger U, Wang Y, Kumar S, Mandelkow EM. Autophagic degradation of tau in primary neurons and its enhancement by trehalose. Neurobiology of aging. 2012 Oct;33(10):2291-305.

120. Hamano T, Gendron TF, Causevic E, et al. Autophagic-lysosomal perturbation enhances tau aggregation in transfectants with induced wild-type tau expression. The European journal of neuroscience. 2008 Mar;27(5):1119-30.

121. Bondulich MK, Guo T, Meehan C, et al. Tauopathy induced by low level expression of a human brain-derived tau fragment in mice is rescued by phenylbutyrate. Brain : a journal of neurology. 2016 Aug;139(Pt 8):2290-306.

122. Dolan PJ, Johnson GV. A caspase cleaved form of tau is preferentially degraded through the autophagy pathway. The Journal of biological chemistry. 2010 Jul 16;285(29):21978-87.

123. Xu H, Ren D. Lysosomal physiology. Annual review of physiology. 2015;77:57-80.

124. Krauss M, Haucke V. Shaping membranes for endocytosis. Reviews of physiology, biochemistry and pharmacology. 2011;161:45-66.

125. Yamashiro DJ, Maxfield FR. Acidification of morphologically distinct endosomes in mutant and wild-type Chinese hamster ovary cells. The Journal of cell biology. 1987 Dec;105(6 Pt 1):2723-33.

126. Maxfield FR. Measurement of vacuolar pH and cytoplasmic calcium in living cells using fluorescence microscopy. Methods in enzymology. 1989;173:745-71.

127. Fuchs R, Schmid S, Mellman I. A possible role for Na+,K+-ATPase in regulating ATP-dependent endosome acidification. Proceedings of the National Academy of Sciences of the United States of America. 1989 Jan;86(2):539-43.

128. Lamb CA, Dooley HC, Tooze SA. Endocytosis and autophagy: Shared machinery for degradation. BioEssays : news and reviews in molecular, cellular and developmental biology. 2013 Jan;35(1):34-45.

129. Pearse BM. Clathrin: a unique protein associated with intracellular transfer of membrane by coated vesicles. Proceedings of the National Academy of Sciences of the United States of America. 1976 Apr;73(4):1255-9.

130. Robinson MS. 100-kD coated vesicle proteins: molecular heterogeneity and intracellular distribution studied with monoclonal antibodies. The Journal of cell biology. 1987 Apr;104(4):887-95.

131. McMahon HT, Boucrot E. Molecular mechanism and physiological functions of clathrin-mediated endocytosis. Nature reviews Molecular cell biology. 2011 Jul 22;12(8):517-33.

132. Maxfield FR, McGraw TE. Endocytic recycling. Nature reviews Molecular cell biology. 2004 Feb;5(2):121-32.

133. Harding C, Stahl P. Transferrin recycling in reticulocytes: pH and iron are important determinants of ligand binding and processing. Biochemical and biophysical research communications. 1983 Jun 15;113(2):650-8.

134. Harding C, Heuser J, Stahl P. Receptor-mediated endocytosis of transferrin and recycling of the transferrin receptor in rat reticulocytes. The Journal of cell biology. 1983 Aug;97(2):329-39.

135. Goldstein JL, Brown MS. The LDL receptor. Arteriosclerosis, thrombosis, and vascular biology. 2009 Apr;29(4):431-8.

136. Wells A, Welsh JB, Lazar CS, Wiley HS, Gill GN, Rosenfeld MG. Ligand-induced transformation by a noninternalizing epidermal growth factor receptor. Science. 1990 Feb 23;247(4945):962-4.

137. Yamashiro DJ, Tycko B, Fluss SR, Maxfield FR. Segregation of transferrin to a mildly acidic (pH 6.5) para-Golgi compartment in the recycling pathway. Cell. 1984 Jul;37(3):789-800.

138. Thilo L, Stroud E, Haylett T. Maturation of early endosomes and vesicular traffic to lysosomes in relation to membrane recycling. Journal of cell science. 1995 Apr;108 (Pt 4):1791-803.

139. Maldonado-Baez L, Williamson C, Donaldson JG. Clathrin-independent endocytosis: a cargo-centric view. Experimental cell research. 2013 Nov 01;319(18):2759-69.

140. Bucci C, Parton RG, Mather IH, et al. The small GTPase rab5 functions as a regulatory factor in the early endocytic pathway. Cell. 1992 Sep 04;70(5):715-28.

141. Stack JH, DeWald DB, Takegawa K, Emr SD. Vesicle-mediated protein transport: regulatory interactions between the Vps15 protein kinase and the Vps34 PtdIns 3-kinase essential for protein sorting to the vacuole in yeast. The Journal of cell biology. 1995 Apr;129(2):321-34.

142. Clague MJ, Jones AT, Mills IG, Walker DM, Urbe S. Regulation of early-endosome dynamics by phosphatidylinositol 3-phosphate binding proteins. Biochemical Society transactions. 1999 Aug;27(4):662-6.

143. Murray DH, Jahnel M, Lauer J, et al. An endosomal tether undergoes an entropic collapse to bring vesicles together. Nature. 2016 Sep 01;537(7618):107-11.

144. Ohashi E, Tanabe K, Henmi Y, Mesaki K, Kobayashi Y, Takei K. Receptor sorting within endosomal trafficking pathway is facilitated by dynamic actin filaments. PloS one. 2011;6(5):e19942.

145. Hurley JH, Emr SD. The ESCRT complexes: structure and mechanism of a membrane-trafficking network. Annual review of biophysics and biomolecular structure. 2006;35:277-98.

146. Shields SB, Oestreich AJ, Winistorfer S, et al. ESCRT ubiquitin-binding domains function cooperatively during MVB cargo sorting. The Journal of cell biology. 2009 Apr 20;185(2):213-24.

147. Bilodeau PS, Winistorfer SC, Kearney WR, Robertson AD, Piper RC. Vps27-Hse1 and ESCRT-I complexes cooperate to increase efficiency of sorting ubiquitinated proteins at the endosome. The Journal of cell biology. 2003 Oct 27;163(2):237-43.

148. Mageswaran SK, Johnson NK, Odorizzi G, Babst M. Constitutively active ESCRT-II suppresses the MVB-sorting phenotype of ESCRT-0 and ESCRT-I mutants. Molecular biology of the cell. 2015 Feb 01;26(3):554-68.

149. Babst M, Katzmann DJ, Estepa-Sabal EJ, Meerloo T, Emr SD. Escrt-III: an endosome-associated heterooligomeric protein complex required for mvb sorting. Developmental cell. 2002 Aug;3(2):271-82.

150. Howard TL, Stauffer DR, Degnin CR, Hollenberg SM. CHMP1 functions as a member of a newly defined family of vesicle trafficking proteins. Journal of cell science. 2001 Jul;114(Pt 13):2395-404.

151. Babst M, Wendland B, Estepa EJ, Emr SD. The Vps4p AAA ATPase regulates membrane association of a Vps protein complex required for normal endosome function. The EMBO journal. 1998 Jun 01;17(11):2982-93.

152. Pagano A, Crottet P, Prescianotto-Baschong C, Spiess M. In vitro formation of recycling vesicles from endosomes requires adaptor protein-1/clathrin and is regulated by rab4 and the connector rabaptin-5. Molecular biology of the cell. 2004 Nov;15(11):4990-5000.

153. Baetz NW, Goldenring JR. Rab11-family interacting proteins define spatially and temporally distinct regions within the dynamic Rab11a-dependent recycling system. Molecular biology of the cell. 2013 Mar;24(5):643-58.

154. Xie S, Naslavsky N, Caplan S. Diacylglycerol kinase alpha regulates tubular recycling endosome biogenesis and major histocompatibility complex class I recycling. The Journal of biological chemistry. 2014 Nov 14;289(46):31914-26.

155. Ward ES, Martinez C, Vaccaro C, Zhou J, Tang Q, Ober RJ. From sorting endosomes to exocytosis: association of Rab4 and Rab11 GTPases with the Fc receptor, FcRn, during recycling. Molecular biology of the cell. 2005 Apr;16(4):2028-38.

156. Driskell OJ, Mironov A, Allan VJ, Woodman PG. Dynein is required for receptor sorting and the morphogenesis of early endosomes. Nature cell biology. 2007 Jan;9(1):113-20.

157. Derivery E, Sousa C, Gautier JJ, Lombard B, Loew D, Gautreau A. The Arp2/3 activator WASH controls the fission of endosomes through a large multiprotein complex. Developmental cell. 2009 Nov;17(5):712-23.

158. Morel E, Parton RG, Gruenberg J. Annexin A2-dependent polymerization of actin mediates endosome biogenesis. Developmental cell. 2009 Mar;16(3):445-57.

159. Mayran N, Parton RG, Gruenberg J. Annexin II regulates multivesicular endosome biogenesis in the degradation pathway of animal cells. The EMBO journal. 2003 Jul 01;22(13):3242-53.

160. Gomez TS, Gorman JA, de Narvajas AA, Koenig AO, Billadeau DD. Trafficking defects in WASH-knockout fibroblasts originate from collapsed endosomal and lysosomal networks. Molecular biology of the cell. 2012 Aug;23(16):3215-28.

161. Gomez TS, Billadeau DD. A FAM21-containing WASH complex regulates retromer-dependent sorting. Developmental cell. 2009 Nov;17(5):699-711.

162. Vieira AV, Lamaze C, Schmid SL. Control of EGF receptor signaling by clathrin-mediated endocytosis. Science. 1996 Dec 20;274(5295):2086-9.

163. Di Guglielmo GM, Le Roy C, Goodfellow AF, Wrana JL. Distinct endocytic pathways regulate TGF-beta receptor signalling and turnover. Nature cell biology. 2003 May;5(5):410-21.

164. Huotari J, Helenius A. Endosome maturation. The EMBO journal. 2011 Aug 31;30(17):3481-500.

165. Rink J, Ghigo E, Kalaidzidis Y, Zerial M. Rab conversion as a mechanism of progression from early to late endosomes. Cell. 2005 Sep 9;122(5):735-49.

166. Del Conte-Zerial P, Brusch L, Rink JC, et al. Membrane identity and GTPase cascades regulated by toggle and cut-out switches. Molecular systems biology. 2008;4:206.

167. Jaber N, Mohd-Naim N, Wang Z, et al. Vps34 regulates Rab7 and late endocytic trafficking through recruitment of the GTPase-activating protein Armus. Journal of cell science. 2016 Dec 01;129(23):4424-35.

168. Clague MJ, Urbe S, Aniento F, Gruenberg J. Vacuolar ATPase activity is required for endosomal carrier vesicle formation. The Journal of biological chemistry. 1994 Jan 07;269(1):21-4.

169. Rocha N, Kuijl C, van der Kant R, et al. Cholesterol sensor ORP1L contacts the ER protein VAP to control Rab7-RILP-p150 Glued and late endosome positioning. The Journal of cell biology. 2009 Jun 29;185(7):1209-25.

170. Luzio JP, Hackmann Y, Dieckmann NM, Griffiths GM. The biogenesis of lysosomes and lysosome-related organelles. Cold Spring Harbor perspectives in biology. 2014 Sep 02;6(9):a016840.

171. Lafourcade C, Sobo K, Kieffer-Jaquinod S, Garin J, van der Goot FG. Regulation of the V-ATPase along the endocytic pathway occurs through reversible subunit association and membrane localization. PloS one. 2008 Jul 23;3(7):e2758.

172. Bucci C, Thomsen P, Nicoziani P, McCarthy J, van Deurs B. Rab7: a key to lysosome biogenesis. Molecular biology of the cell. 2000 Feb;11(2):467-80.

173. Pohlmann R, Boeker MW, von Figura K. The two mannose 6-phosphate receptors transport distinct complements of lysosomal proteins. The Journal of biological chemistry. 1995 Nov 10;270(45):27311-8.

174. Runquist EA, Havel RJ. Acid hydrolases in early and late endosome fractions from rat liver. The Journal of biological chemistry. 1991 Nov 25;266(33):22557-63.

175. Arighi CN, Hartnell LM, Aguilar RC, Haft CR, Bonifacino JS. Role of the mammalian retromer in sorting of the cation-independent mannose 6-phosphate receptor. The Journal of cell biology. 2004 Apr;165(1):123-33.

176. Press B, Feng Y, Hoflack B, Wandinger-Ness A. Mutant Rab7 causes the accumulation of cathepsin D and cation-independent mannose 6-phosphate receptor in an early endocytic compartment. The Journal of cell biology. 1998 Mar 09;140(5):1075-89.

177. Seaman MN. Cargo-selective endosomal sorting for retrieval to the Golgi requires retromer. The Journal of cell biology. 2004 Apr;165(1):111-22.

178. Seaman MN, McCaffery JM, Emr SD. A membrane coat complex essential for endosome-to-Golgi retrograde transport in yeast. The Journal of cell biology. 1998 Aug 10;142(3):665-81.

179. Seaman MN, Marcusson EG, Cereghino JL, Emr SD. Endosome to Golgi retrieval of the vacuolar protein sorting receptor, Vps10p, requires the function of the VPS29, VPS30, and VPS35 gene products. The Journal of cell biology. 1997 Apr 07;137(1):79-92.

180. Seaman MN. Identification of a novel conserved sorting motif required for retromer-mediated endosome-to-TGN retrieval. Journal of cell science. 2007 Jul 15;120(Pt 14):2378-89.

181. McCormick PJ, Dumaresq-Doiron K, Pluviose AS, Pichette V, Tosato G, Lefrancois S. Palmitoylation controls recycling in lysosomal sorting and trafficking. Traffic. 2008 Nov;9(11):1984-97.

182. Bright NA, Reaves BJ, Mullock BM, Luzio JP. Dense core lysosomes can fuse with late endosomes and are re-formed from the resultant hybrid organelles. Journal of cell science. 1997 Sep;110 (Pt 17):2027-40.

183. Yu L, McPhee CK, Zheng L, et al. Termination of autophagy and reformation of lysosomes regulated by mTOR. Nature. 2010 Jun 17;465(7300):942-6.

184. Stoka V, Turk V, Turk B. Lysosomal cathepsins and their regulation in aging and neurodegeneration. Ageing research reviews. 2016 Dec;32:22-37.

185. Cang C, Zhou Y, Navarro B, et al. mTOR regulates lysosomal ATP-sensitive two-pore Na(+) channels to adapt to metabolic state. Cell. 2013 Feb 14;152(4):778-90.

186. Chu BB, Liao YC, Qi W, et al. Cholesterol transport through lysosome-peroxisome membrane contacts. Cell. 2015 Apr 09;161(2):291-306.

187. Aits S, Jaattela M. Lysosomal cell death at a glance. Journal of cell science. 2013 May 01;126(Pt 9):1905-12.

188. Settembre C, Fraldi A, Medina DL, Ballabio A. Signals from the lysosome: a control centre for cellular clearance and energy metabolism. Nature reviews Molecular cell biology. 2013 May;14(5):283-96.

189. Cuervo AM. Chaperone-mediated autophagy: selectivity pays off. Trends in endocrinology and metabolism: TEM. 2010 Mar;21(3):142-50.

190. Kon M, Cuervo AM. Chaperone-mediated autophagy in health and disease. FEBS letters. 2010 Apr 02;584(7):1399-404.

191. Bohley P, Seglen PO. Proteases and proteolysis in the lysosome. Experientia. 1992 Feb 15;48(2):151-7.

192. Shen D, Wang X, Li X, et al. Lipid storage disorders block lysosomal trafficking by inhibiting a TRP channel and lysosomal calcium release. Nature communications. 2012 Mar 13;3:731.

193. Kagedal K, Zhao M, Svensson I, Brunk UT. Sphingosine-induced apoptosis is dependent on lysosomal proteases. The Biochemical journal. 2001 Oct 15;359(Pt 2):335-43.

194. Kagedal K, Johansson U, Ollinger K. The lysosomal protease cathepsin D mediates apoptosis induced by oxidative stress. FASEB journal : official publication of the Federation of American Societies for Experimental Biology. 2001 Jul;15(9):1592-4.

195. Groth-Pedersen L, Ostenfeld MS, Hoyer-Hansen M, Nylandsted J, Jaattela M. Vincristine induces dramatic lysosomal changes and sensitizes cancer cells to lysosome-destabilizing siramesine. Cancer research. 2007 Mar 01;67(5):2217-25.

196. Li W, Yuan X, Nordgren G, et al. Induction of cell death by the lysosomotropic detergent MSDH. FEBS letters. 2000 Mar 17;470(1):35-9.

197. Taha TA, Kitatani K, Bielawski J, Cho W, Hannun YA, Obeid LM. Tumor necrosis factor induces the loss of sphingosine kinase-1 by a cathepsin B-dependent mechanism. The Journal of biological chemistry. 2005 Apr 29;280(17):17196-202.

198. Yamashima T, Saido TC, Takita M, et al. Transient brain ischaemia provokes Ca2+, PIP2 and calpain responses prior to delayed neuronal death in monkeys. The European journal of neuroscience. 1996 Sep;8(9):1932-44.

199. Kurz T, Terman A, Gustafsson B, Brunk UT. Lysosomes in iron metabolism, ageing and apoptosis. Histochemistry and cell biology. 2008 Apr;129(4):389-406.

200. Hwang JJ, Lee SJ, Kim TY, Cho JH, Koh JY. Zinc and 4-hydroxy-2-nonenal mediate lysosomal membrane permeabilization induced by H2O2 in cultured hippocampal neurons. The Journal of neuroscience : the official journal of the Society for Neuroscience. 2008 Mar 19;28(12):3114-22.

201. Polito VA, Li H, Martini-Stoica H, et al. Selective clearance of aberrant tau proteins and rescue of neurotoxicity by transcription factor EB. EMBO molecular medicine. 2014 Sep;6(9):1142-60.

202. Xiao Q, Yan P, Ma X, et al. Neuronal-Targeted TFEB Accelerates Lysosomal Degradation of APP, Reducing Abeta Generation and Amyloid Plaque Pathogenesis. The Journal of neuroscience : the official journal of the Society for Neuroscience. 2015 Sep 02;35(35):12137-51.

203. Sardiello M, Palmieri M, di Ronza A, et al. A gene network regulating lysosomal biogenesis and function. Science. 2009 Jul 24;325(5939):473-7.

204. Settembre C, Di Malta C, Polito VA, et al. TFEB links autophagy to lysosomal biogenesis. Science. 2011 Jun 17;332(6036):1429-33.

205. Pena-Llopis S, Vega-Rubin-de-Celis S, Schwartz JC, et al. Regulation of TFEB and V-ATPases by mTORC1. The EMBO journal. 2011 Jul 29;30(16):3242-58.

206. Flinn RJ, Yan Y, Goswami S, Parker PJ, Backer JM. The late endosome is essential for mTORC1 signaling. Molecular biology of the cell. 2010 Mar 01;21(5):833-41.

207. Settembre C, De Cegli R, Mansueto G, et al. TFEB controls cellular lipid metabolism through a starvation-induced autoregulatory loop. Nature cell biology. 2013 Jun;15(6):647-58.

208. Mizushima N. Autophagy: process and function. Genes & development. 2007 Nov 15;21(22):2861-73.

209. Li WW, Li J, Bao JK. Microautophagy: lesser-known self-eating. Cellular and molecular life sciences : CMLS. 2012 Apr;69(7):1125-36.

210. Kaushik S, Cuervo AM. Chaperone-mediated autophagy: a unique way to enter the lysosome world. Trends in cell biology. 2012 Aug;22(8):407-17.

211. Stolz A, Ernst A, Dikic I. Cargo recognition and trafficking in selective autophagy. Nature cell biology. 2014 Jun;16(6):495-501.

212. Takeshige K, Baba M, Tsuboi S, Noda T, Ohsumi Y. Autophagy in yeast demonstrated with proteinase-deficient mutants and conditions for its induction. The Journal of cell biology. 1992 Oct;119(2):301-11.

213. Pankiv S, Clausen TH, Lamark T, et al. p62/SQSTM1 binds directly to Atg8/LC3 to facilitate degradation of ubiquitinated protein aggregates by autophagy. The Journal of biological chemistry. 2007 Aug 17;282(33):24131-45.

214. Kirkin V, Lamark T, Sou YS, et al. A role for NBR1 in autophagosomal degradation of ubiquitinated substrates. Molecular cell. 2009 Feb 27;33(4):505-16.

215. Tan JM, Wong ES, Kirkpatrick DS, et al. Lysine 63-linked ubiquitination promotes the formation and autophagic clearance of protein inclusions associated with neurodegenerative diseases. Human molecular genetics. 2008 Feb 01;17(3):431-9.

216. Filimonenko M, Isakson P, Finley KD, et al. The selective macroautophagic degradation of aggregated proteins requires the PI3P-binding protein Alfy. Molecular cell. 2010 Apr 23;38(2):265-79.

217. Kim PK, Hailey DW, Mullen RT, Lippincott-Schwartz J. Ubiquitin signals autophagic degradation of cytosolic proteins and peroxisomes. Proceedings of the National Academy of Sciences of the United States of America. 2008 Dec 30;105(52):20567-74.

218. Rui YN, Xu Z, Chen Z, Zhang S. The GST-BHMT assay reveals a distinct mechanism underlying proteasome inhibition-induced macroautophagy in mammalian cells. Autophagy. 2015;11(5):812-32.

219. Cuervo AM, Dice JF. A receptor for the selective uptake and degradation of proteins by lysosomes. Science. 1996 Jul 26;273(5274):501-3.

220. Chiang HL, Terlecky SR, Plant CP, Dice JF. A role for a 70-kilodalton heat shock protein in lysosomal degradation of intracellular proteins. Science. 1989 Oct 20;246(4928):382-5.

221. Dice JF. Peptide sequences that target cytosolic proteins for lysosomal proteolysis. Trends in biochemical sciences. 1990 Aug;15(8):305-9.

222. Mizushima N, Yoshimori T, Ohsumi Y. The role of Atg proteins in autophagosome formation. Annual review of cell and developmental biology. 2011;27:107-32.

223. Graef M, Friedman JR, Graham C, Babu M, Nunnari J. ER exit sites are physical and functional core autophagosome biogenesis components. Molecular biology of the cell. 2013 Sep;24(18):2918-31.

224. Hailey DW, Rambold AS, Satpute-Krishnan P, et al. Mitochondria supply membranes for autophagosome biogenesis during starvation. Cell. 2010 May 14;141(4):656-67.

225. Knaevelsrud H, Carlsson SR, Simonsen A. SNX18 tubulates recycling endosomes for autophagosome biogenesis. Autophagy. 2013 Oct;9(10):1639-41.

226. Ohashi Y, Munro S. Membrane delivery to the yeast autophagosome from the Golgi-endosomal system. Molecular biology of the cell. 2010 Nov 15;21(22):3998-4008.

227. Ravikumar B, Moreau K, Jahreiss L, Puri C, Rubinsztein DC. Plasma membrane contributes to the formation of pre-autophagosomal structures. Nature cell biology. 2010 Aug;12(8):747-57.

228. Hamasaki M, Furuta N, Matsuda A, et al. Autophagosomes form at ER-mitochondria contact sites. Nature. 2013 Mar 21;495(7441):389-93.

229. Yla-Anttila P, Vihinen H, Jokitalo E, Eskelinen EL. 3D tomography reveals connections between the phagophore and endoplasmic reticulum. Autophagy. 2009 Nov;5(8):1180-5.

230. Zoncu R, Bar-Peled L, Efeyan A, Wang S, Sancak Y, Sabatini DM. mTORC1 senses lysosomal amino acids through an inside-out mechanism that requires the vacuolar H(+)-ATPase. Science. 2011 Nov 04;334(6056):678-83.

231. Noda T, Ohsumi Y. Tor, a phosphatidylinositol kinase homologue, controls autophagy in yeast. The Journal of biological chemistry. 1998 Feb 13;273(7):3963-6.

232. Kihara A, Noda T, Ishihara N, Ohsumi Y. Two distinct Vps34 phosphatidylinositol 3-kinase complexes function in autophagy and carboxypeptidase Y sorting in Saccharomyces cerevisiae. The Journal of cell biology. 2001 Feb 05;152(3):519-30.

233. Proikas-Cezanne T, Waddell S, Gaugel A, Frickey T, Lupas A, Nordheim A. WIPI-1alpha (WIPI49), a member of the novel 7-bladed WIPI protein family, is aberrantly expressed in human cancer and is linked to starvation-induced autophagy. Oncogene. 2004 Dec 16;23(58):9314-25.

234. Dooley HC, Razi M, Polson HE, Girardin SE, Wilson MI, Tooze SA. WIPI2 links LC3 conjugation with PI3P, autophagosome formation, and pathogen clearance by recruiting Atg12-5-16L1. Molecular cell. 2014 Jul 17;55(2):238-52.

235. Korolchuk VI, Saiki S, Lichtenberg M, et al. Lysosomal positioning coordinates cellular nutrient responses. Nature cell biology. 2011 Apr;13(4):453-60.

236. Fader CM, Sanchez DG, Mestre MB, Colombo MI. TI-VAMP/VAMP7 and VAMP3/cellubrevin: two v-SNARE proteins involved in specific steps of the autophagy/multivesicular body pathways. Biochimica et biophysica acta. 2009 Dec;1793(12):1901-16.

237. Filimonenko M, Stuffers S, Raiborg C, et al. Functional multivesicular bodies are required for autophagic clearance of protein aggregates associated with neurodegenerative disease. The Journal of cell biology. 2007 Nov 05;179(3):485-500.

238. Du W, Su QP, Chen Y, et al. Kinesin 1 Drives Autolysosome Tubulation. Developmental cell. 2016 May 23;37(4):326-36.

239. Nguyen TN, Padman BS, Lazarou M. Deciphering the Molecular Signals of PINK1/Parkin Mitophagy. Trends in cell biology. 2016 Oct;26(10):733-44.

240. Kokotos AC, Cousin MA. Synaptic vesicle generation from central nerve terminal endosomes. Traffic. 2015 Mar;16(3):229-40.

241. Cheung G, Jupp OJ, Cousin MA. Activity-dependent bulk endocytosis and clathrin-dependent endocytosis replenish specific synaptic vesicle pools in central nerve terminals. The Journal of neuroscience : the official journal of the Society for Neuroscience. 2010 Jun 16;30(24):8151-61.

242. May V, Parsons RL. G Protein-Coupled Receptor Endosomal Signaling and Regulation of Neuronal Excitability and Stress Responses: Signaling Options and Lessons From the PAC1 Receptor. Journal of cellular physiology. 2017 Apr;232(4):698-706.

243. Groc L, Choquet D. AMPA and NMDA glutamate receptor trafficking: multiple roads for reaching and leaving the synapse. Cell and tissue research. 2006 Nov;326(2):423-38.

244. Hara T, Nakamura K, Matsui M, et al. Suppression of basal autophagy in neural cells causes neurodegenerative disease in mice. Nature. 2006 Jun 15;441(7095):885-9.

245. Piras A, Collin L, Gruninger F, Graff C, Ronnback A. Autophagic and lysosomal defects in human tauopathies: analysis of post-mortem brain from patients with familial Alzheimer disease, corticobasal degeneration and progressive supranuclear palsy. Acta neuropathologica communications. 2016 Mar 02;4:22.

246. Vittorini S, Paradiso C, Donati A, et al. The age-related accumulation of protein carbonyl in rat liver correlates with the age-related decline in liver proteolytic activities. The journals of gerontology Series A, Biological sciences and medical sciences. 1999 Aug;54(8):B318-23.

247. Terman A. The effect of age on formation and elimination of autophagic vacuoles in mouse hepatocytes. Gerontology. 1995;41 Suppl 2:319-26.

248. Lipinski MM, Zheng B, Lu T, et al. Genome-wide analysis reveals mechanisms modulating autophagy in normal brain aging and in Alzheimer's disease. Proceedings of the National Academy of Sciences of the United States of America. 2010 Aug 10;107(32):14164-9.

249. Vilarino-Guell C, Wider C, Ross OA, et al. VPS35 mutations in Parkinson disease. American journal of human genetics. 2011 Jul 15;89(1):162-7.

250. Di Fonzo A, Rohe CF, Ferreira J, et al. A frequent LRRK2 gene mutation associated with autosomal dominant Parkinson's disease. Lancet. 2005 Jan 29-Feb 4;365(9457):412-5.

251. Henry AG, Aghamohammadzadeh S, Samaroo H, et al. Pathogenic LRRK2 mutations, through increased kinase activity, produce enlarged lysosomes with reduced degradative capacity and increase ATP13A2 expression. Human molecular genetics. 2015 Nov 01;24(21):6013-28.

252. Di Fonzo A, Chien HF, Socal M, et al. ATP13A2 missense mutations in juvenile parkinsonism and young onset Parkinson disease. Neurology. 2007 May 08;68(19):1557-62.

253. Ramirez A, Heimbach A, Grundemann J, et al. Hereditary parkinsonism with dementia is caused by mutations in ATP13A2, encoding a lysosomal type 5 P-type ATPase. Nature genetics. 2006 Oct;38(10):1184-91.

254. Dehay B, Ramirez A, Martinez-Vicente M, et al. Loss of P-type ATPase ATP13A2/PARK9 function induces general lysosomal deficiency and leads to Parkinson disease neurodegeneration. Proceedings of the National Academy of Sciences of the United States of America. 2012 Jun 12;109(24):9611-6.

255. Kett LR, Stiller B, Bernath MM, et al. alpha-Synuclein-independent histopathological and motor deficits in mice lacking the endolysosomal Parkinsonism protein Atp13a2. The Journal of neuroscience : the official journal of the Society for Neuroscience. 2015 Apr 08;35(14):5724-42.

256. Schultheis PJ, Fleming SM, Clippinger AK, et al. Atp13a2-deficient mice exhibit neuronal ceroid lipofuscinosis, limited alpha-synuclein accumulation and age-dependent sensorimotor deficits. Human molecular genetics. 2013 May 15;22(10):2067-82.

257. Wohlke A, Philipp U, Bock P, et al. A one base pair deletion in the canine ATP13A2 gene causes exon skipping and late-onset neuronal ceroid lipofuscinosis in the Tibetan terrier. PLoS genetics. 2011 Oct;7(10):e1002304.

258. Sidransky E, Nalls MA, Aasly JO, et al. Multicenter analysis of glucocerebrosidase mutations in Parkinson's disease. The New England journal of medicine. 2009 Oct 22;361(17):1651-61.

259. Sidransky E, Lopez G. The link between the GBA gene and parkinsonism. The Lancet Neurology. 2012 Nov;11(11):986-98.

260. Rocha EM, Smith GA, Park E, et al. Progressive decline of glucocerebrosidase in aging and Parkinson's disease. Annals of clinical and translational neurology. 2015 Apr;2(4):433-8.

261. Schondorf DC, Aureli M, McAllister FE, et al. iPSC-derived neurons from GBA1-associated Parkinson's disease patients show autophagic defects and impaired calcium homeostasis. Nature communications. 2014 Jun 06;5:4028.

262. Magalhaes J, Gegg ME, Migdalska-Richards A, Doherty MK, Whitfield PD, Schapira AH. Autophagic lysosome reformation dysfunction in glucocerebrosidase deficient cells: relevance to Parkinson disease. Human molecular genetics. 2016 Aug 15;25(16):3432-45.

263. Fernandes HJ, Hartfield EM, Christian HC, et al. ER Stress and Autophagic Perturbations Lead to Elevated Extracellular alpha-Synuclein in GBA-N370S Parkinson's iPSC-Derived Dopamine Neurons. Stem cell reports. 2016 Mar 08;6(3):342-56.

264. Lambert JC, Grenier-Boley B, Harold D, et al. Genome-wide haplotype association study identifies the FRMD4A gene as a risk locus for Alzheimer's disease. Molecular psychiatry. 2013 Apr;18(4):461-70.

265. Naj AC, Jun G, Beecham GW, et al. Common variants at MS4A4/MS4A6E, CD2AP, CD33 and EPHA1 are associated with late-onset Alzheimer's disease. Nature genetics. 2011 May;43(5):436-41.

266. Coffey EE, Beckel JM, Laties AM, Mitchell CH. Lysosomal alkalization and dysfunction in human fibroblasts with the Alzheimer's disease-linked presenilin 1 A246E mutation can be reversed with cAMP. Neuroscience. 2014 Mar 28;263:111-24.

267. Lee JH, McBrayer MK, Wolfe DM, et al. Presenilin 1 Maintains Lysosomal Ca(2+) Homeostasis via TRPML1 by Regulating vATPase-Mediated Lysosome Acidification. Cell reports. 2015 Sep 01;12(9):1430-44.

268. Cataldo AM, Peterhoff CM, Troncoso JC, Gomez-Isla T, Hyman BT, Nixon RA. Endocytic pathway abnormalities precede amyloid beta deposition in sporadic Alzheimer's disease and Down syndrome: differential effects of APOE genotype and presenilin mutations. The American journal of pathology. 2000 Jul;157(1):277-86.

269. Ji ZS, Miranda RD, Newhouse YM, Weisgraber KH, Huang Y, Mahley RW. Apolipoprotein E4 potentiates amyloid beta peptide-induced lysosomal leakage and apoptosis in neuronal cells. The Journal of biological chemistry. 2002 Jun 14;277(24):21821-8.

270. Whyte LS, Lau AA, Hemsley KM, Hopwood JJ, Sargeant TJ. Endo-lysosomal and autophagic dysfunction: a driving factor in Alzheimer's disease? Journal of neurochemistry. 2017 Mar;140(5):703-17.

271. Nixon RA, Wegiel J, Kumar A, et al. Extensive involvement of autophagy in Alzheimer disease: an immuno-electron microscopy study. Journal of neuropathology and experimental neurology. 2005 Feb;64(2):113-22.

272. Arai K, Shimaya A, Hiratani N, Ohkuma S. Purification and characterization of lysosomal H(+)-ATPase. An anion-sensitive v-type H(+)-ATPase from rat liver lysosomes. The Journal of biological chemistry. 1993 Mar 15;268(8):5649-60.

273. Forgac M. Vacuolar ATPases: rotary proton pumps in physiology and pathophysiology. Nature reviews Molecular cell biology. 2007 Nov;8(11):917-29.

274. Johnson DE, Ostrowski P, Jaumouille V, Grinstein S. The position of lysosomes within the cell determines their luminal pH. The Journal of cell biology. 2016 Mar 14;212(6):677-92.

275. Graves AR, Curran PK, Smith CL, Mindell JA. The Cl-/H+ antiporter ClC-7 is the primary chloride permeation pathway in lysosomes. Nature. 2008 Jun 05;453(7196):788-92.

276. Sautin YY, Lu M, Gaugler A, Zhang L, Gluck SL. Phosphatidylinositol 3-kinase-mediated effects of glucose on vacuolar H+-ATPase assembly, translocation, and acidification of intracellular compartments in renal epithelial cells. Molecular and cellular biology. 2005 Jan;25(2):575-89.

277. Stransky LA, Forgac M. Amino Acid Availability Modulates Vacuolar H+-ATPase Assembly. The Journal of biological chemistry. 2015 Nov 06;290(45):27360-9.

278. Christensen KA, Myers JT, Swanson JA. pH-dependent regulation of lysosomal calcium in macrophages. Journal of cell science. 2002 Feb 01;115(Pt 3):599-607.

279. McBrayer M, Nixon RA. Lysosome and calcium dysregulation in Alzheimer's disease: partners in crime. Biochemical Society transactions. 2013 Dec;41(6):1495-502.

280. Smith ML, Greene AA, Potashnik R, Mendoza SA, Schneider JA. Lysosomal cystine transport. Effect of intralysosomal pH and membrane potential. The Journal of biological chemistry. 1987 Jan 25;262(3):1244-53.

281. Yamashiro DJ, Maxfield FR. Acidification of endocytic compartments and the intracellular pathways of ligands and receptors. Journal of cellular biochemistry. 1984;26(4):231-46.

282. Singh R, Kaushik S, Wang Y, et al. Autophagy regulates lipid metabolism. Nature. 2009 Apr 30;458(7242):1131-5.

283. Asano T, Komatsu M, Yamaguchi-Iwai Y, Ishikawa F, Mizushima N, Iwai K. Distinct mechanisms of ferritin delivery to lysosomes in iron-depleted and iron-replete cells. Molecular and cellular biology. 2011 May;31(10):2040-52.

284. Cidon S, Sihra TS. Characterization of a H+-ATPase in rat brain synaptic vesicles. Coupling to L-glutamate transport. The Journal of biological chemistry. 1989 May 15;264(14):8281-8.

285. Janecki AJ, Montrose MH, Zimniak P, et al. Subcellular redistribution is involved in acute regulation of the brush border Na+/H+ exchanger isoform 3 in

human colon adenocarcinoma cell line Caco-2. Protein kinase C-mediated inhibition of the exchanger. The Journal of biological chemistry. 1998 Apr 10;273(15):8790-8.

286. Szaszi K, Paulsen A, Szabo EZ, Numata M, Grinstein S, Orlowski J. Clathrin-mediated endocytosis and recycling of the neuron-specific Na+/H+ exchanger NHE5 isoform. Regulation by phosphatidylinositol 3'-kinase and the actin cytoskeleton. The Journal of biological chemistry. 2002 Nov 08;277(45):42623-32.

287. Donowitz M, Ming Tse C, Fuster D. SLC9/NHE gene family, a plasma membrane and organellar family of Na(+)/H(+) exchangers. Molecular aspects of medicine. 2013 Apr-Jun;34(2-3):236-51.

288. Zhao H, Carney KE, Falgoust L, Pan JW, Sun D, Zhang Z. Emerging roles of Na(+)/H(+) exchangers in epilepsy and developmental brain disorders. Progress in neurobiology. 2016 Mar-May;138-140:19-35.

289. Hendus-Altenburger R, Kragelund BB, Pedersen SF. Structural dynamics and regulation of the mammalian SLC9A family of Na(+)/H(+) exchangers. Current topics in membranes. 2014;73:69-148.

290. Wakabayashi S, Fafournoux P, Sardet C, Pouyssegur J. The Na+/H+ antiporter cytoplasmic domain mediates growth factor signals and controls "H(+)-sensing". Proceedings of the National Academy of Sciences of the United States of America. 1992 Mar 15;89(6):2424-8.

291. Zizak M, Cavet ME, Bayle D, et al. Na(+)/H(+) exchanger NHE3 has 11 membrane spanning domains and a cleaved signal peptide: topology analysis using in vitro transcription/translation. Biochemistry. 2000 Jul 11;39(27):8102-12.

292. Wells KM, Rao R. The yeast Na+/H+ exchanger Nhx1 is an N-linked glycoprotein. Topological implications. The Journal of biological chemistry. 2001 Feb 02;276(5):3401-7.

293. Fafournoux P, Noel J, Pouyssegur J. Evidence that Na+/H+ exchanger isoforms NHE1 and NHE3 exist as stable dimers in membranes with a high degree of specificity for homodimers. The Journal of biological chemistry. 1994 Jan 28;269(4):2589-96.

294. Kapus A, Grinstein S, Wasan S, Kandasamy R, Orlowski J. Functional characterization of three isoforms of the Na+/H+ exchanger stably expressed in Chinese hamster ovary cells. ATP dependence, osmotic sensitivity, and role in cell proliferation. The Journal of biological chemistry. 1994 Sep 23;269(38):23544-52.

295. Aharonovitz O, Zaun HC, Balla T, York JD, Orlowski J, Grinstein S. Intracellular pH regulation by Na(+)/H(+) exchange requires phosphatidylinositol 4,5-bisphosphate. The Journal of cell biology. 2000 Jul 10;150(1):213-24.

296. Nakamura N, Tanaka S, Teko Y, Mitsui K, Kanazawa H. Four Na+/H+ exchanger isoforms are distributed to Golgi and post-Golgi compartments and are involved in organelle pH regulation. The Journal of biological chemistry. 2005 Jan 14;280(2):1561-72.

297. Morrow EM, Yoo SY, Flavell SW, et al. Identifying autism loci and genes by tracing recent shared ancestry. Science. 2008 Jul 11;321(5886):218-23.

298. Schwede M, Garbett K, Mirnics K, Geschwind DH, Morrow EM. Genes for endosomal NHE6 and NHE9 are misregulated in autism brains. Molecular psychiatry. 2014 Mar;19(3):277-9.

299. Cardon M, Evankovich KD, Holder JL, Jr. Exonic deletion of SLC9A9 in autism with epilepsy. Neurology Genetics. 2016 Apr;2(2):e62.

300. Vink JM, Smit AB, de Geus EJ, et al. Genome-wide association study of smoking initiation and current smoking. American journal of human genetics. 2009 Mar;84(3):367-79.

301. Franke B, Neale BM, Faraone SV. Genome-wide association studies in ADHD. Human genetics. 2009 Jul;126(1):13-50.

302. de Silva MG, Elliott K, Dahl HH, et al. Disruption of a novel member of a sodium/hydrogen exchanger family and DOCK3 is associated with an attention deficit hyperactivity disorder-like phenotype. Journal of medical genetics. 2003 Oct;40(10):733-40.

303. Kondapalli KC, Hack A, Schushan M, Landau M, Ben-Tal N, Rao R. Functional evaluation of autism-associated mutations in NHE9. Nature communications. 2013;4:2510.

304. Hill JK, Brett CL, Chyou A, et al. Vestibular hair bundles control pH with (Na+, K+)/H+ exchangers NHE6 and NHE9. The Journal of neuroscience : the official journal of the Society for Neuroscience. 2006 Sep 27;26(39):9944-55.

305. Numata M, Petrecca K, Lake N, Orlowski J. Identification of a mitochondrial Na+/H+ exchanger. The Journal of biological chemistry. 1998 Mar 20;273(12):6951-9.

306. Miyazaki E, Sakaguchi M, Wakabayashi S, Shigekawa M, Mihara K. NHE6 protein possesses a signal peptide destined for endoplasmic reticulum membrane and localizes in secretory organelles of the cell. The Journal of biological chemistry. 2001 Dec 28;276(52):49221-7.

307. Brett CL, Wei Y, Donowitz M, Rao R. Human Na(+)/H(+) exchanger isoform 6 is found in recycling endosomes of cells, not in mitochondria. American journal of physiology Cell physiology. 2002 May;282(5):C1031-41.

308. Bowers K, Levi BP, Patel FI, Stevens TH. The sodium/proton exchanger Nhx1p is required for endosomal protein trafficking in the yeast Saccharomyces cerevisiae. Molecular biology of the cell. 2000 Dec;11(12):4277-94.

309. Mukherjee S, Kallay L, Brett CL, Rao R. Mutational analysis of the intramembranous H10 loop of yeast Nhx1 reveals a critical role in ion homoeostasis and vesicle trafficking. The Biochemical journal. 2006 Aug 15;398(1):97-105.

310. Ohgaki R, Fukura N, Matsushita M, Mitsui K, Kanazawa H. Cell surface levels of organellar Na+/H+ exchanger isoform 6 are regulated by interaction with RACK1. The Journal of biological chemistry. 2008 Feb 15;283(7):4417-29.

311. Ron D, Chen CH, Caldwell J, Jamieson L, Orr E, Mochly-Rosen D. Cloning of an intracellular receptor for protein kinase C: a homolog of the beta subunit of G proteins. Proceedings of the National Academy of Sciences of the United States of America. 1994 Feb 01;91(3):839-43.

312. Muro S, Mateescu M, Gajewski C, Robinson M, Muzykantov VR, Koval M. Control of intracellular trafficking of ICAM-1-targeted nanocarriers by endothelial Na+/H+ exchanger proteins. American journal of physiology Lung cellular and molecular physiology. 2006 May;290(5):L809-17.

313. Lucien F, Pelletier PP, Lavoie RR, et al. Hypoxia-induced mobilization of NHE6 to the plasma membrane triggers endosome hyperacidification and chemoresistance. Nature communications. 2017 Jun 21;8:15884.

314. Deane EC, Ilie AE, Sizdahkhani S, Das Gupta M, Orlowski J, McKinney RA. Enhanced recruitment of endosomal Na+/H+ exchanger NHE6 into Dendritic spines of hippocampal pyramidal neurons during NMDA receptor-dependent long-term potentiation. The Journal of neuroscience : the official journal of the Society for Neuroscience. 2013 Jan 9;33(2):595-610.

315. Ouyang Q, Lizarraga SB, Schmidt M, et al. Christianson syndrome protein NHE6 modulates TrkB endosomal signaling required for neuronal circuit development. Neuron. 2013 Oct 2;80(1):97-112.

316. Overly CC, Hollenbeck PJ. Dynamic organization of endocytic pathways in axons of cultured sympathetic neurons. The Journal of neuroscience : the official journal of the Society for Neuroscience. 1996 Oct 01;16(19):6056-64.

317. Xinhan L, Matsushita M, Numaza M, Taguchi A, Mitsui K, Kanazawa H. Na+/H+ exchanger isoform 6 (NHE6/SLC9A6) is involved in clathrin-dependent endocytosis of transferrin. American journal of physiology Cell physiology. 2011 Dec;301(6):C1431-44.

318. Christianson AL, Stevenson RE, van der Meyden CH, et al. X linked severe mental retardation, craniofacial dysmorphology, epilepsy, ophthalmoplegia, and cerebellar atrophy in a large South African kindred is localised to Xq24-q27. Journal of medical genetics. 1999 Oct;36(10):759-66.

319. Gilfillan GD, Selmer KK, Roxrud I, et al. SLC9A6 mutations cause X-linked mental retardation, microcephaly, epilepsy, and ataxia, a phenotype mimicking Angelman syndrome. American journal of human genetics. 2008 Apr;82(4):1003-10.

320. Schroer RJ, Holden KR, Tarpey PS, et al. Natural history of Christianson syndrome. American journal of medical genetics Part A. 2010 Nov;152A(11):2775-83.

321. Masurel-Paulet A, Piton A, Chancenotte S, et al. A new family with an SLC9A6 mutation expanding the phenotypic spectrum of Christianson syndrome. American journal of medical genetics Part A. 2016 Aug;170(8):2103-10.

322. Garbern JY, Neumann M, Trojanowski JQ, et al. A mutation affecting the sodium/proton exchanger, SLC9A6, causes mental retardation with tau deposition. Brain : a journal of neurology. 2010 May;133(Pt 5):1391-402.

323. Kondapalli KC, Prasad H, Rao R. An inside job: how endosomal Na(+)/H(+) exchangers link to autism and neurological disease. Frontiers in cellular neuroscience. 2014;8:172.

324. Pescosolido MF, Stein DM, Schmidt M, et al. Genetic and phenotypic diversity of NHE6 mutations in Christianson syndrome. Annals of neurology. 2014 Oct;76(4):581-93.

325. Tarpey PS, Smith R, Pleasance E, et al. A systematic, large-scale resequencing screen of X-chromosome coding exons in mental retardation. Nature genetics. 2009 May;41(5):535-43.

326. Sinajon P, Verbaan D, So J. The expanding phenotypic spectrum of female SLC9A6 mutation carriers: a case series and review of the literature. Human genetics. 2016 Aug;135(8):841-50.

327. Roxrud I, Raiborg C, Gilfillan GD, Stromme P, Stenmark H. Dual degradation mechanisms ensure disposal of NHE6 mutant protein associated with neurological disease. Experimental cell research. 2009 Oct 15;315(17):3014-27.

328. Ilie A, Gao AY, Reid J, et al. A Christianson syndrome-linked deletion mutation ((287)ES(288)) in SLC9A6 disrupts recycling endosomal function and elicits neurodegeneration and cell death. Molecular neurodegeneration. 2016 Sep 02;11(1):63.

329. Ilie A, Weinstein E, Boucher A, McKinney RA, Orlowski J. Impaired posttranslational processing and trafficking of an endosomal Na+/H+ exchanger NHE6 mutant (Delta(370)WST(372)) associated with X-linked intellectual disability and autism. Neurochemistry international. 2014 Jul;73:192-203.

330. Stromme P, Dobrenis K, Sillitoe RV, et al. X-linked Angelman-like syndrome caused by Slc9a6 knockout in mice exhibits evidence of endosomal-lysosomal dysfunction. Brain : a journal of neurology. 2011 Nov;134(Pt 11):3369-83.

331. Sikora J, Leddy J, Gulinello M, Walkley SU. X-linked Christianson syndrome: heterozygous female Slc9a6 knockout mice develop mosaic neuropathological changes and related behavioral abnormalities. Disease models & mechanisms. 2016 Jan;9(1):13-23.

332. Armakola M, Higgins MJ, Figley MD, et al. Inhibition of RNA lariat debranching enzyme suppresses TDP-43 toxicity in ALS disease models. Nature genetics. 2012 Dec;44(12):1302-9.

333. Piton A, Gauthier J, Hamdan FF, et al. Systematic resequencing of X-chromosome synaptic genes in autism spectrum disorder and schizophrenia. Molecular psychiatry. 2011 Aug;16(8):867-80.

334. Hauser MA, Li YJ, Xu H, et al. Expression profiling of substantia nigra in Parkinson disease, progressive supranuclear palsy, and frontotemporal dementia with parkinsonism. Archives of neurology. 2005 Jun;62(6):917-21.

335. Prasad H, Rao R. The Na+/H+ Exchanger NHE6 Modulates Endosomal pH to Control Processing of Amyloid Precursor Protein in a Cell Culture Model of Alzheimer Disease. The Journal of biological chemistry. 2015 Jan 5.

336. Riess A, Rossier E, Kruger R, et al. Novel SLC9A6 mutations in two families with Christianson syndrome. Clinical genetics. 2013 Jun;83(6):596-7.

337. Fukura N, Ohgaki R, Matsushita M, Nakamura N, Mitsui K, Kanazawa H. A membrane-proximal region in the C-terminal tail of NHE7 is required for its distribution in the trans-Golgi network, distinct from NHE6 localization at endosomes. The Journal of membrane biology. 2010 Apr;234(3):149-58.

338. Santoni FA, Makrythanasis P, Nikolaev S, et al. Simultaneous identification and prioritization of variants in familial, de novo, and somatic genetic disorders with VariantMaster. Genome research. 2014 Feb;24(2):349-55.

339. Schwarz JM, Cooper DN, Schuelke M, Seelow D. MutationTaster2: mutation prediction for the deep-sequencing age. Nature methods. 2014 Apr;11(4):361-2.

340. Lek M, Karczewski KJ, Minikel EV, et al. Analysis of protein-coding genetic variation in 60,706 humans. Nature. 2016 Aug 18;536(7616):285-91.

341. Tennessen JA, Bigham AW, O'Connor TD, et al. Evolution and functional impact of rare coding variation from deep sequencing of human exomes. Science. 2012 Jul 6;337(6090):64-9.

342. Nishikawa S, Brodsky JL, Nakatsukasa K. Roles of molecular chaperones in endoplasmic reticulum (ER) quality control and ER-associated degradation (ERAD). Journal of biochemistry. 2005 May;137(5):551-5.

343. Cataldo AM, Barnett JL, Pieroni C, Nixon RA. Increased neuronal endocytosis and protease delivery to early endosomes in sporadic Alzheimer's disease: neuropathologic evidence for a mechanism of increased beta-amyloidogenesis. The Journal of neuroscience : the official journal of the Society for Neuroscience. 1997 Aug 15;17(16):6142-51.

344. Mathews PM, Guerra CB, Jiang Y, et al. Alzheimer's disease-related overexpression of the cation-dependent mannose 6-phosphate receptor increases Abeta secretion: role for altered lysosomal hydrolase distribution in beta-amyloidogenesis. The Journal of biological chemistry. 2002 Feb 15;277(7):5299-307.

345. Ott C, Konig J, Hohn A, Jung T, Grune T. Reduced autophagy leads to an impaired ferritin turnover in senescent fibroblasts. Free radical biology & medicine. 2016 Dec;101:325-33.

346. Fuertes G, Martin De Llano JJ, Villarroya A, Rivett AJ, Knecht E. Changes in the proteolytic activities of proteasomes and lysosomes in human fibroblasts produced by serum withdrawal, amino-acid deprivation and confluent conditions. The Biochemical journal. 2003 Oct 1;375(Pt 1):75-86.

347. Narendra D, Tanaka A, Suen DF, Youle RJ. Parkin-induced mitophagy in the pathogenesis of Parkinson disease. Autophagy. 2009 Jul;5(5):706-8.

348. Narendra DP, Jin SM, Tanaka A, et al. PINK1 is selectively stabilized on impaired mitochondria to activate Parkin. PLoS biology. 2010 Jan 26;8(1):e1000298.

349. Ren Y, Sahara N. Characteristics of tau oligomers. Frontiers in neurology. 2013;4:102.

350. Hirata-Fukae C, Li HF, Ma L, et al. Levels of soluble and insoluble tau reflect overall status of tau phosphorylation in vivo. Neuroscience letters. 2009 Jan 23;450(1):51-5.

351. Hanley JG. Endosomal sorting of AMPA receptors in hippocampal neurons. Biochemical Society transactions. 2010 Apr;38(2):460-5.

352. Park M, Penick EC, Edwards JG, Kauer JA, Ehlers MD. Recycling endosomes supply AMPA receptors for LTP. Science. 2004 Sep 24;305(5692):1972-5.

353. Bolanos JP, Almeida A, Moncada S. Glycolysis: a bioenergetic or a survival pathway? Trends in biochemical sciences. 2010 Mar;35(3):145-9.

354. Larsson C, Grundberg I, Soderberg O, Nilsson M. In situ detection and genotyping of individual mRNA molecules. Nature methods. 2010 May;7(5):395-7.

355. Fichou Y, Bahi-Buisson N, Nectoux J, et al. Mutation in the SLC9A6 gene is not a frequent cause of sporadic Angelman-like syndrome. European journal of human genetics : EJHG. 2009 Nov;17(11):1378-80.

356. Rim JH, Kim SH, Hwang IS, et al. Efficient strategy for the molecular diagnosis of intractable early-onset epilepsy using targeted gene sequencing. BMC medical genomics. 2018 Feb 1;11(1):6.

357. Takahashi Y, Hosoki K, Matsushita M, et al. A loss-of-function mutation in the SLC9A6 gene causes X-linked mental retardation resembling Angelman syndrome. American journal of medical genetics Part B, Neuropsychiatric genetics : the official publication of the International Society of Psychiatric Genetics. 2011 Dec;156B(7):799-807.

358. Redin C, Gerard B, Lauer J, et al. Efficient strategy for the molecular diagnosis of intellectual disability using targeted high-throughput sequencing. Journal of medical genetics. 2014 Nov;51(11):724-36.

359. Bosemani T, Zanni G, Hartman AL, et al. Christianson syndrome: spectrum of neuroimaging findings. Neuropediatrics. 2014 Aug;45(4):247-51.

360. Hu H, Wrogemann K, Kalscheuer V, et al. Mutation screening in 86 known X-linked mental retardation genes by droplet-based multiplex PCR and massive parallel sequencing. The HUGO journal. 2009 Dec;3(1-4):41-9.

361. Trump N, McTague A, Brittain H, et al. Improving diagnosis and broadening the phenotypes in early-onset seizure and severe developmental delay disorders through gene panel analysis. Journal of medical genetics. 2016 May;53(5):310-7.

362. Mercimek-Mahmutoglu S, Patel J, Cordeiro D, et al. Diagnostic yield of genetic testing in epileptic encephalopathy in childhood. Epilepsia. 2015 May;56(5):707-16.

363. Weitensteiner V, Zhang R, Bungenberg J, et al. Exome sequencing in syndromic brain malformations identifies novel mutations in ACTB, and SLC9A6, and suggests BAZ1A as a new candidate gene. Birth defects research. 2018 Apr 17;110(7):587-97.

364. Fung CW, Kwong AK, Wong VC. Gene panel analysis for nonsyndromic cryptogenic neonatal/infantile epileptic encephalopathy. Epilepsia open. 2017 Jun;2(2):236-43.

365. Mignot C, Heron D, Bursztyn J, et al. Novel mutation in SLC9A6 gene in a patient with Christianson syndrome and retinitis pigmentosum. Brain & development. 2013 Feb;35(2):172-6.

366. Zanni G, Barresi S, Cohen R, et al. A novel mutation in the endosomal Na+/H+ exchanger NHE6 (SLC9A6) causes Christianson syndrome with electrical status epilepticus during slow-wave sleep (ESES). Epilepsy research. 2014 May;108(4):811-5.

367. Schuurs-Hoeijmakers JH, Vulto-van Silfhout AT, Vissers LE, et al. Identification of pathogenic gene variants in small families with intellectually disabled siblings by exome sequencing. Journal of medical genetics. 2013 Dec;50(12):802-11.

368. Diering GH, Numata Y, Fan S, Church J, Numata M. Endosomal acidification by Na+/H+ exchanger NHE5 regulates TrkA cell-surface targeting and NGF-induced PI3K signaling. Molecular biology of the cell. 2013 Nov;24(21):3435-48.

369. Deinhardt K, Salinas S, Verastegui C, et al. Rab5 and Rab7 control endocytic sorting along the axonal retrograde transport pathway. Neuron. 2006 Oct 19;52(2):293-305.

370. Henne WM, Buchkovich NJ, Emr SD. The ESCRT pathway. Developmental cell. 2011 Jul 19;21(1):77-91.

371. Traer CJ, Rutherford AC, Palmer KJ, et al. SNX4 coordinates endosomal sorting of TfnR with dynein-mediated transport into the endocytic recycling compartment. Nature cell biology. 2007 Dec;9(12):1370-80.

372. De Luca M, Bucci C. A new V-ATPase regulatory mechanism mediated by the Rab interacting lysosomal protein (RILP). Communicative & integrative biology. 2014 Oct;7(5).

373. De Luca M, Cogli L, Progida C, et al. RILP regulates vacuolar ATPase through interaction with the V1G1 subunit. Journal of cell science. 2014 Jun 15;127(Pt 12):2697-708.

374. Young A, Stoilova-McPhie S, Rothnie A, et al. Hsc70-induced changes in clathrin-auxilin cage structure suggest a role for clathrin light chains in cage disassembly. Traffic. 2013 Sep;14(9):987-96.

375. Barouch W, Prasad K, Greene L, Eisenberg E. Auxilin-induced interaction of the molecular chaperone Hsc70 with clathrin baskets. Biochemistry. 1997 Apr 8;36(14):4303-8.

376. Diering GH, Mills F, Bamji SX, Numata M. Regulation of dendritic spine growth through activity-dependent recruitment of the brain-enriched Na(+)/H(+) exchanger NHE5. Molecular biology of the cell. 2011 Jul 1;22(13):2246-57.

377. Li L, Kim E, Yuan H, et al. Regulation of mTORC1 by the Rab and Arf GTPases. The Journal of biological chemistry. 2010 Jun 25;285(26):19705-9.

378. Alers S, Loffler AS, Wesselborg S, Stork B. Role of AMPK-mTOR-Ulk1/2 in the regulation of autophagy: cross talk, shortcuts, and feedbacks. Molecular and cellular biology. 2012 Jan;32(1):2-11.

379. Yeasmin AM, Waliullah TM, Kondo A, Kaneko A, Koike N, Ushimaru T. Orchestrated Action of PP2A Antagonizes Atg13 Phosphorylation and Promotes Autophagy after the Inactivation of TORC1. PloS one. 2016;11(12):e0166636.

380. Florey O, Gammoh N, Kim SE, Jiang X, Overholtzer M. V-ATPase and osmotic imbalances activate endolysosomal LC3 lipidation. Autophagy. 2015;11(1):88-99.

381. Mohamed NV, Plouffe V, Remillard-Labrosse G, Planel E, Leclerc N. Starvation and inhibition of lysosomal function increased tau secretion by primary cortical neurons. Scientific reports. 2014 Jul 17;4:5715.

382. Barakat TS, Ghazvini M, de Hoon B, et al. Stable X chromosome reactivation in female human induced pluripotent stem cells. Stem cell reports. 2015 Feb 10;4(2):199-208.

383. Boman A, Svensson S, Boxer A, et al. Distinct Lysosomal Network Protein Profiles in Parkinsonian Syndrome Cerebrospinal Fluid. Journal of Parkinson's disease. 2016 Apr 2;6(2):307-15.

384. Braak H, Del Tredici K, Rub U, de Vos RA, Jansen Steur EN, Braak E. Staging of brain pathology related to sporadic Parkinson's disease. Neurobiology of aging. 2003 Mar-Apr;24(2):197-211.

385. Thal DR, Rub U, Orantes M, Braak H. Phases of A beta-deposition in the human brain and its relevance for the development of AD. Neurology. 2002 Jun 25;58(12):1791-800.

386. Takahashi K, Tanabe K, Ohnuki M, Narita M, Ichisaka T, Tomoda K, Yamanaka S. Induction of pluripotent stem cells from adult human fibroblasts by defined factors. Cell. 2007 Nov 30;131(5):861-872.

387. Reinhardt P, Glatza M, Hemmer K, Tsytsyura Y, Thies CS, et al. Derivation and Expansion Using Only Small Molecules of Human Neural Progenitors for Neurodegenerative Disease Modeling. Plos One. 2013 Mar 22;8(3)

388. Eckermann K, Mocanu MM, Khlistunova I, et al. The beta-propensity of Tau determines aggregation and synaptic loss in inducible mouse models of tauopathy. The journal of biological chemistry. 2007 Oct 26;282(43):31755-65.

389. Gendron TF, Petrucelli L. The role of tau in neurodegeneration. Molecular Neurodegeneration. 2009 Mar 11;4:13

390. Ohgaki R, van IJzendoom SC, Matsushita M, Hoekstra D, Kanazawa H. Organellar Na+/H+ exchangers: novel players in organelle pH regulation and their emerging functions. Biochemistry. 2011 Feb 1;50(4):443-50

391. Chung H, Brazil MI, Soe TT, Maxfield FR. Uptake, degradation, and release of fibrillar and soluble forms of Alzheimer's amyloid beta-peptide by microglial cells. The journal of biological chemistry. 1999 Nov 5;274(45):32301-8

392. Wes PD, Sayed FA, Bard F, Gan L. Targeting microglia for the treatment of Alzheimer's Disease. Glia. 2016 Oct;64(10):1710-32

393. Guo X, Tang P, Chen L, Lin P, et al.. Amyloid β-induced redistribution of transcriptional factor EB and lysosomal dysfunction in primary microglial cells. Frontiers in Aging Neuroscience. 2017 Jul 19;9:228

394. Yao XC, Xue X, Zhang HT, Zhu MM, et al. Pseudoginsenoside-F11 alleviates oligomeric β-amyloid-induced endosome-lysosome defects in microglia. Traffic 2019 Jan;20(1):61-70

395. Jin MM, Wang F, Qi D, Liu WW, et al. A Critical Role of Autophagy in Regulating Microglia Polarization in Neurodegeneration. Frontiers in Aging Neuroscience. 2018 Nov 20;10:378

396. Liang Y, Zhou T, Chen Q, Lin D, et al. Rifampicin inhibits rotenone-induced microglial inflammation via enhancement of autophagy. Neurotoxicology 2017 Dec;63:137-145

397. Siman R, Cocca R, Dong Y. The mTOR Inhibitor Rapamycin Mitigates Perforant Pathway Neurodegeneration and Synapse Loss in a Mouse Model of Early-Stage Alzheimer-Type Tauopathy. PLoS One. 2015 Nov 5;10(11):e0142340

398. Bussi C, Paralta Ramos JM, Arroyo DS, Gallea JI, et al. Alpha-synuclein fibrils recruit TBK1 and OPTN to lysosomal damage sites and induce autophagy in microglial cells. Journal of Cell Science 2018 Nov 30;131(23)

399. Age-dependent neuroinflammation and cognitive decline in a novel Ala152Thr-Tau transgenic mouse model of PSP and AD. Acta Neuropathologica Communications. 2016 Feb 25;4:17

Online references

1. MutationTaster2: http://www.mutationtaster.org/
2. MutationTaster2 results for SLC9A6 c.1464_1465insT mutation, Transcript ENST00000370698:

http://www.mutationtaster.org/cgi-bin/MutationTaster/MutationTaster69.cgi?sequence_snippet=TTCTGATTGTGTTTTTT[-/T]ACCGTGTGGGTATTTGGTGGTGGC&transcript_stable_id_text=ENST00000370698&gene=SLC9A6&transcript_stable_id_radio=ENST00000370698&sequence_type=CDS&alteration_name=T489Yfs (last retrieved 06.02.2018)

3. MutationTaster2 results for SLC9A6 c.G1703A variant, Transcript ENST00000370695:

http://www.mutationtaster.org/cgi-bin/MutationTaster/MutationTaster69.cgi?sequence_snippet=TTGGCTTTTCC[G/A]GATGTGGTACAACTTT&transcript_stable_id_text=ENST00000370695&gene=SLC9A6&transcript_stable_id_radio=ENST00000370695&sequence_type=CDS&alteration_name=R568Q (last retrieved 06.02.2018)

4. Exome Aggregation Consortium database (ExAC): http://exac.broadinstitute.org/
5. ExAC Frequencies for SLC9A6 c.G1703A (rs146263125):

http://exac.broadinstitute.org/variant/X-135115628-G-A

7. Appendix

7.1 Appendix Figures

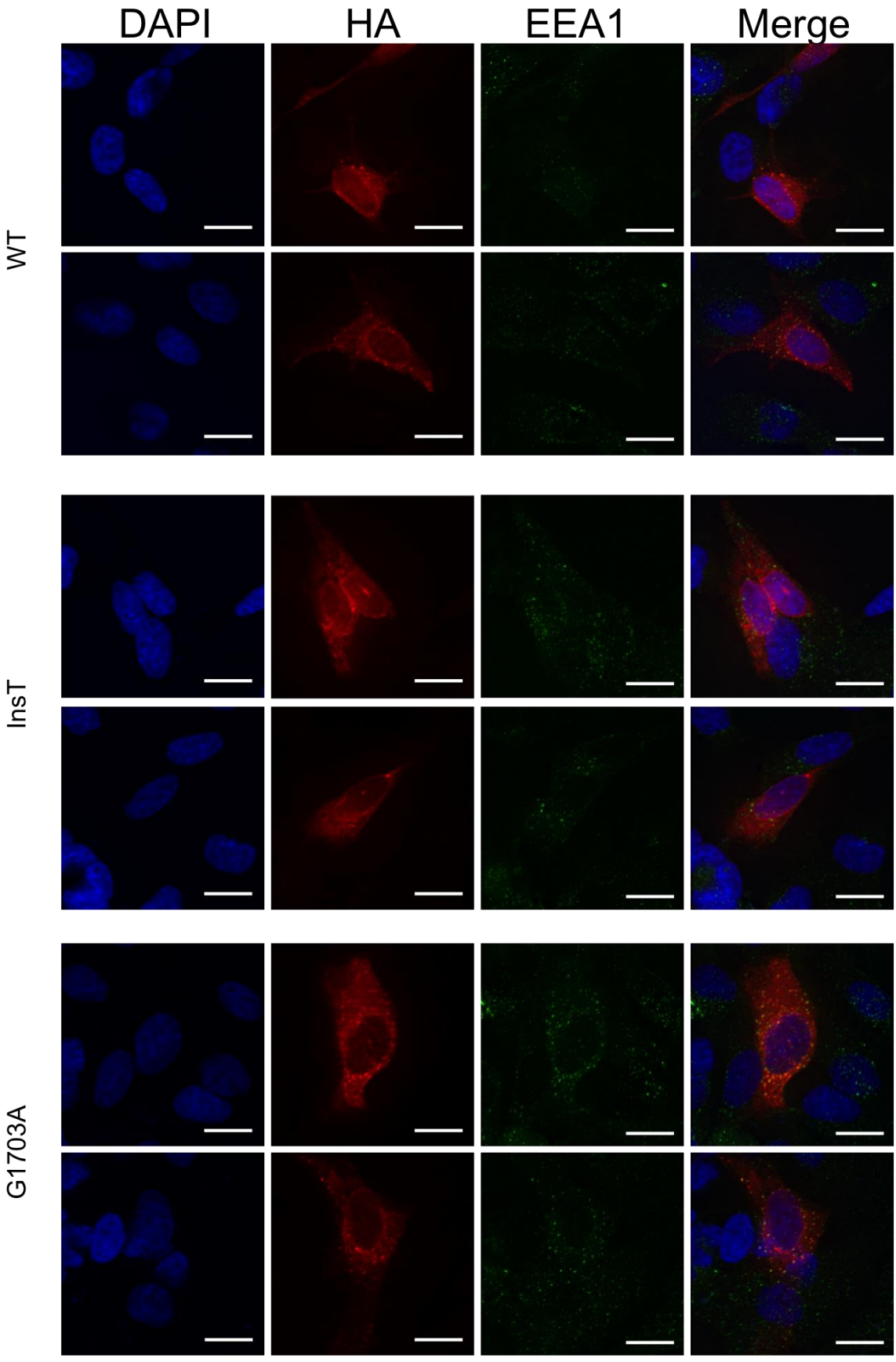
DAPI
HA
EEA1
Merge
WT
InsT
G1703A

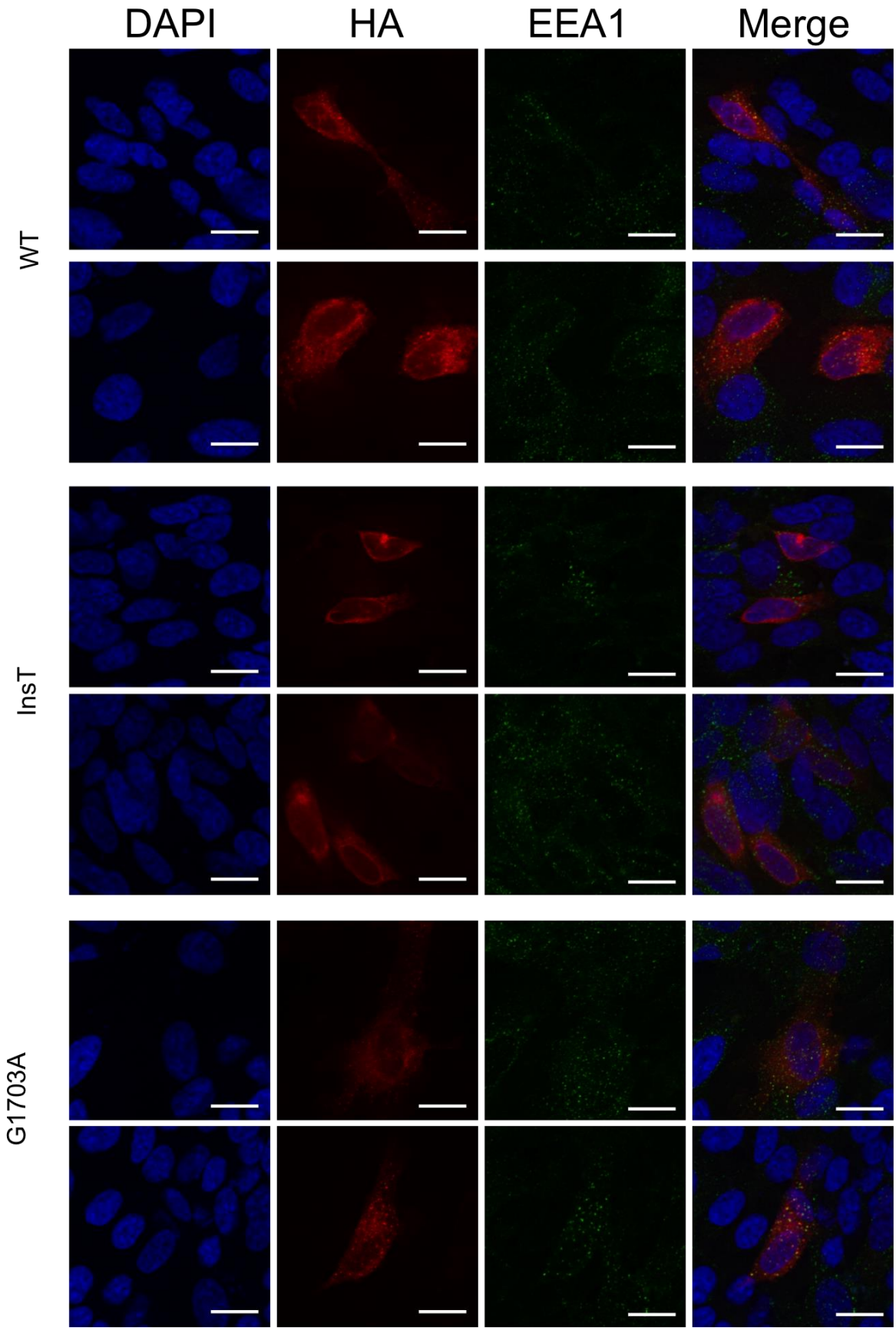
DAPI
HA
EEA1
Merge
WT
InsT
G1703A

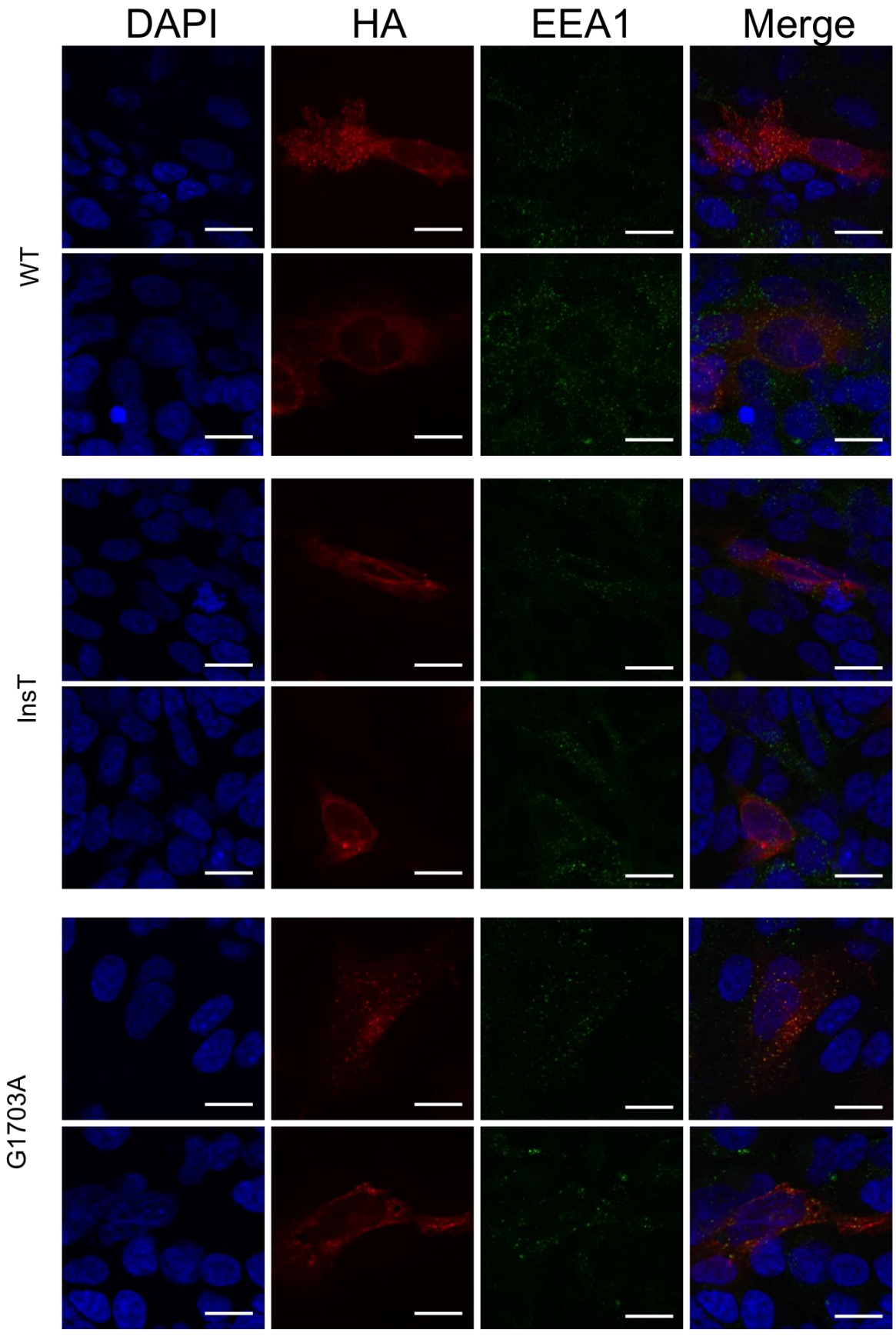

Fig. 40: Immunostaining for HA (red) and EEA1 (green) in SH-SY5Ys neuroblastoma cells overexpressing WT, T489Yfs and R568Q NHE6 cDNA with an HA-tag. Nuclear staining with Hoechst 33258. Scale bar: 16µM

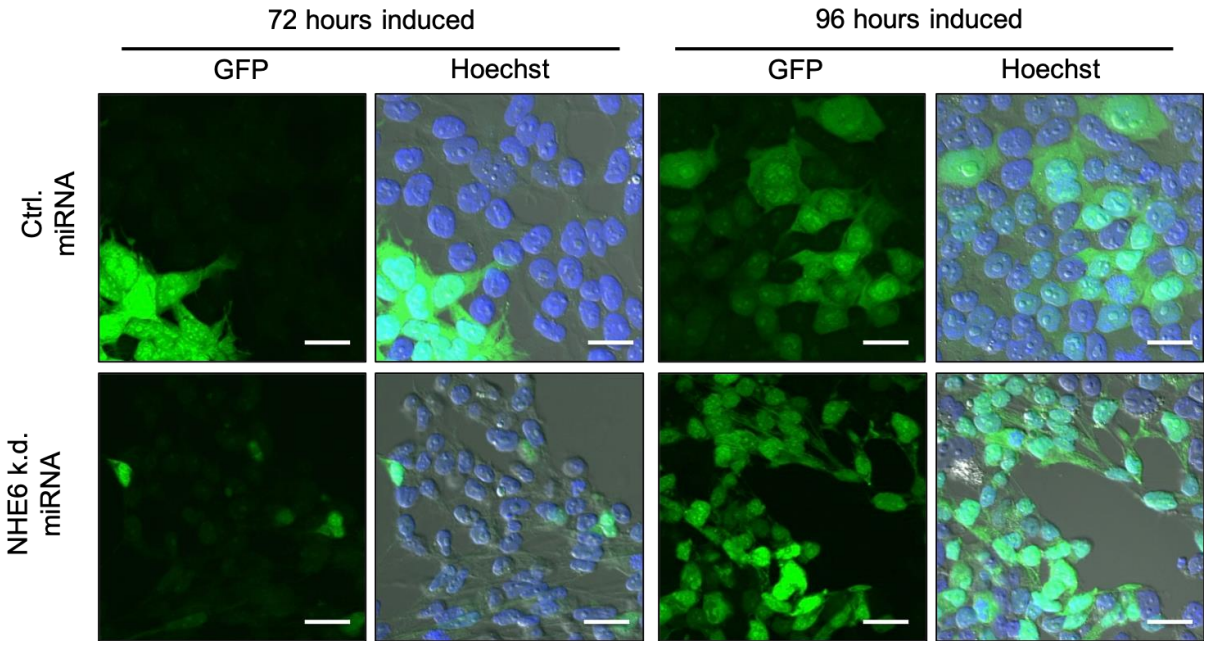

Fig. 41: Fluorescence microscopy pictures of polyclonal M17 neuroblastoma lines with inducible non-targeting control or NHE6 k.d. miRNA vectors expressing EGFP after 72h and 96h of induction. Expression varies between individual cells as transfection levels differ. Scale bar: 25µM.

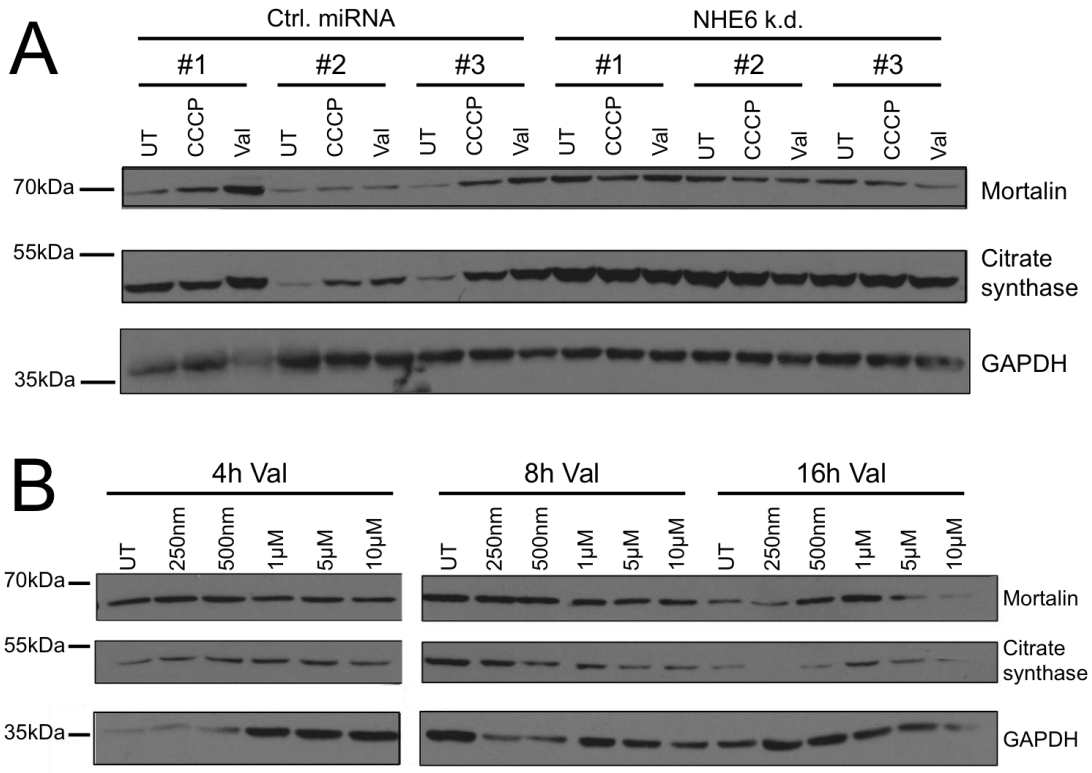

Fig. 42: Western blots for mitochondrial marker proteins in samples from cells treated with mitochondrial toxins to determine conditions for further testing of possible effects of a NHE6 k.d. on mitochondrial removal. **A**: Western blot for the mitochondrial matrix proteins Mortalin and citrate synthase in M17 neuroblastoma cells with a non-targeting control miRNA or a NHE6 k.d. miRNA. Cells were treated with either normal growth medium (untreated, UT), 1µM CCCP or 1µM Valinomycin (Val) for 24h before lysis. #1, #2 and #3 denote different monoclonal lines. Western blot representative of n=3. **B**: Western blot for mitochondrial matrix proteins Mortalin and citrate synthase in M17 neuroblastoma cells treated with different concentrations of Valinomycin for 4h, 8h or 16h before lysis. GAPDH was used as a loading control. Western blot shows the only independent experiment conducted.

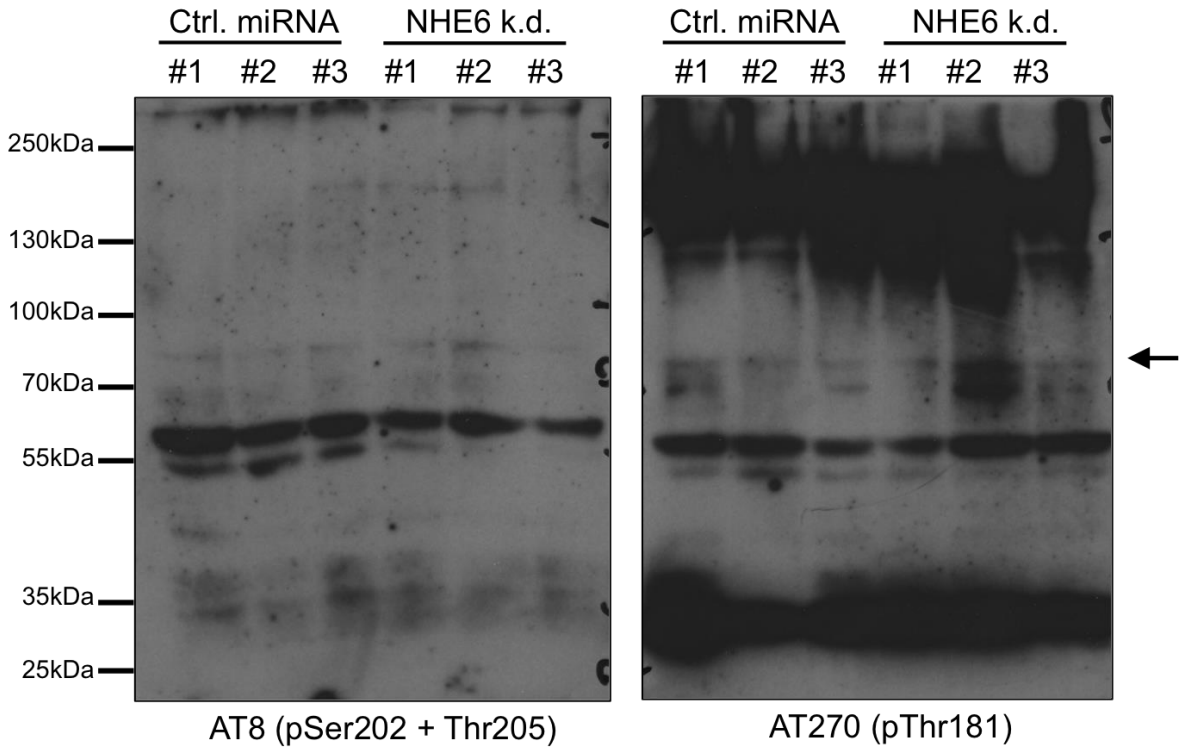

Fig. 43: Western blot using two different phospho-specific tau antibodies AT8 (pSer202+pThr205) and AT270 (pThr181) in M17 control or NHE6 k.d. cells. The expected height for both antibodies is 79kDa (arrow). #1-#3 denote different monoclonal lines.

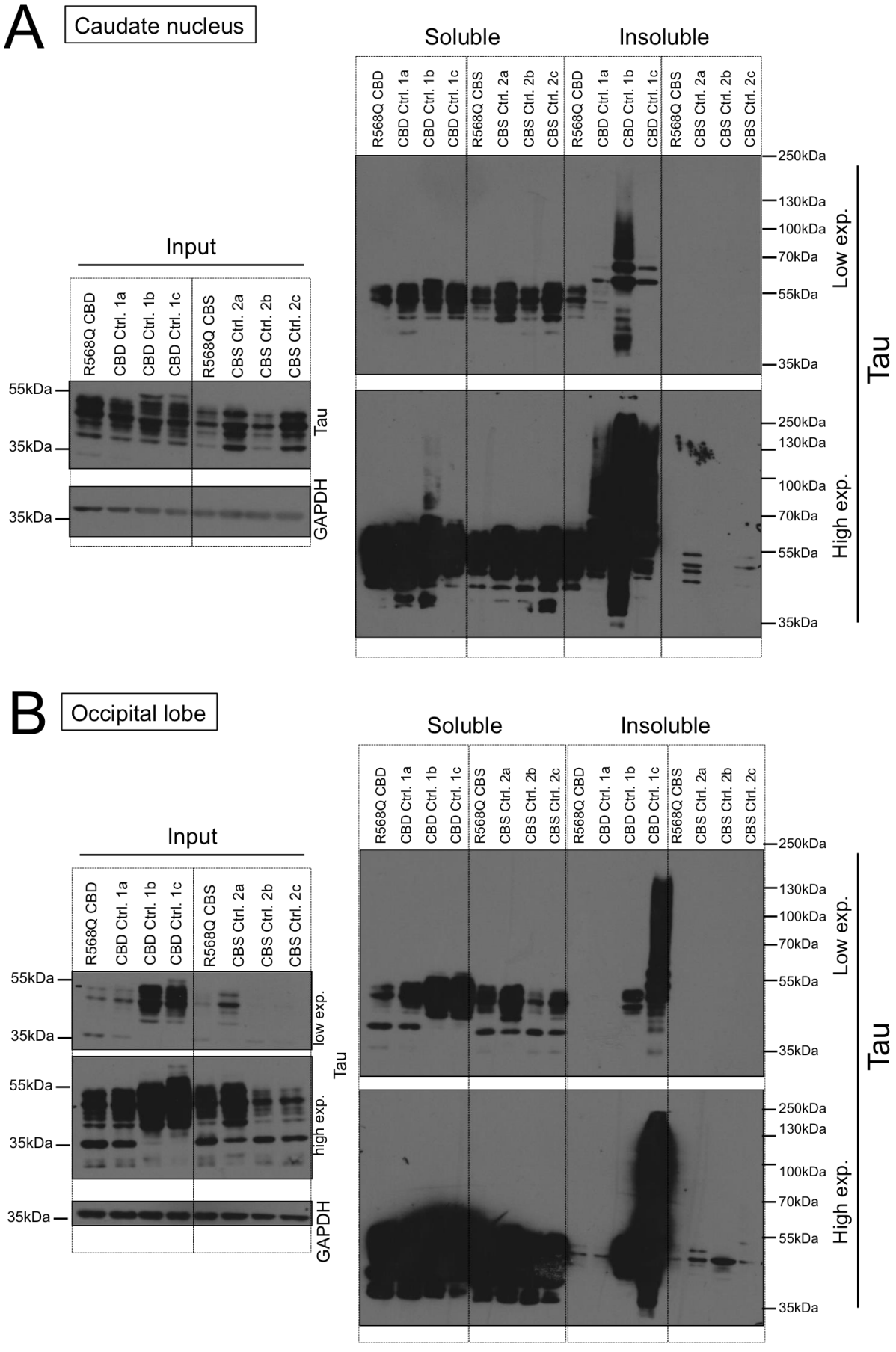
A
Caudate nucleus
Soluble
Insoluble
Input
R568Q CBD
CBD Ctrl. 1a
CBD Ctrl. 1b
CBD Ctrl. 1c
R568Q CBS
CBS Ctrl. 2a
CBS Ctrl. 2b
CBS Ctrl. 2c
55kDa
35kDa
Tau
GAPDH
250kDa
130kDa
100kDa
70kDa
55kDa
35kDa
Low exp.
High exp.
Tau
B
Occipital lobe
low exp.
high exp.

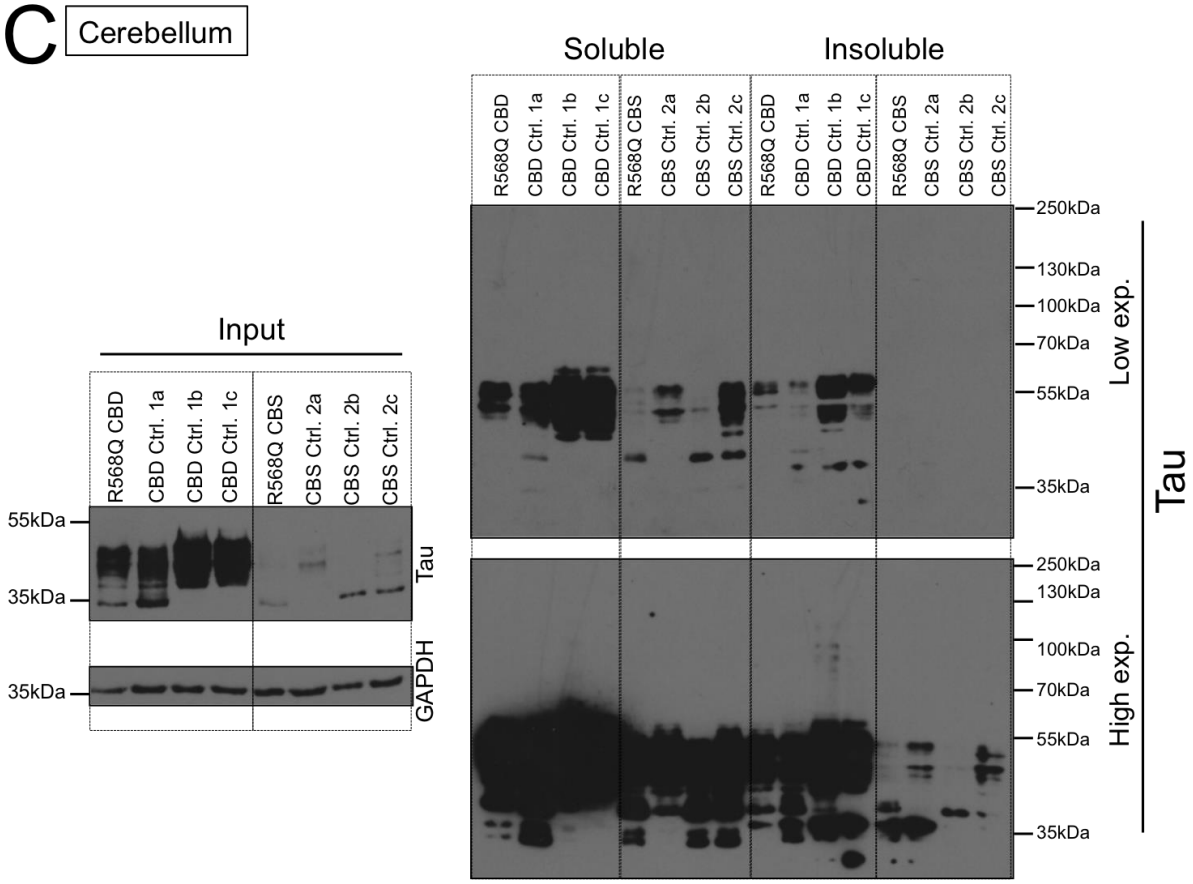

Fig. 44: Western blots for sarkosyl soluble and insoluble tau in several brain regions of two R568Q variant carriers and pathology-matched controls. An aliquot of the lysate was taken before the sarkosyl precipitation step to confirm equal input levels by immunoblotting against GAPDH and to assess levels of total tau in these samples. **A**: Western blot for tau in sarkosyl soluble and insoluble fractions in the caudate nucleus of two R568Q variant carriers (R568Q-CBD and R568Q-CBS) and pathology-matched controls (CBD Ctrl. 1a-c for R568Q-CBD and CBS Ctrl 2a-c for R568Q-CBS). **B**: Western blot for tau in sarkosyl soluble and insoluble fractions in the occipital lobe of two R568Q variant carriers and pathology-matched controls. **C**: Western blot for tau in sarkosyl soluble and insoluble fractions in the cerebellum of two R568Q variant carriers and pathology-matched controls. exp.: exposure time

A

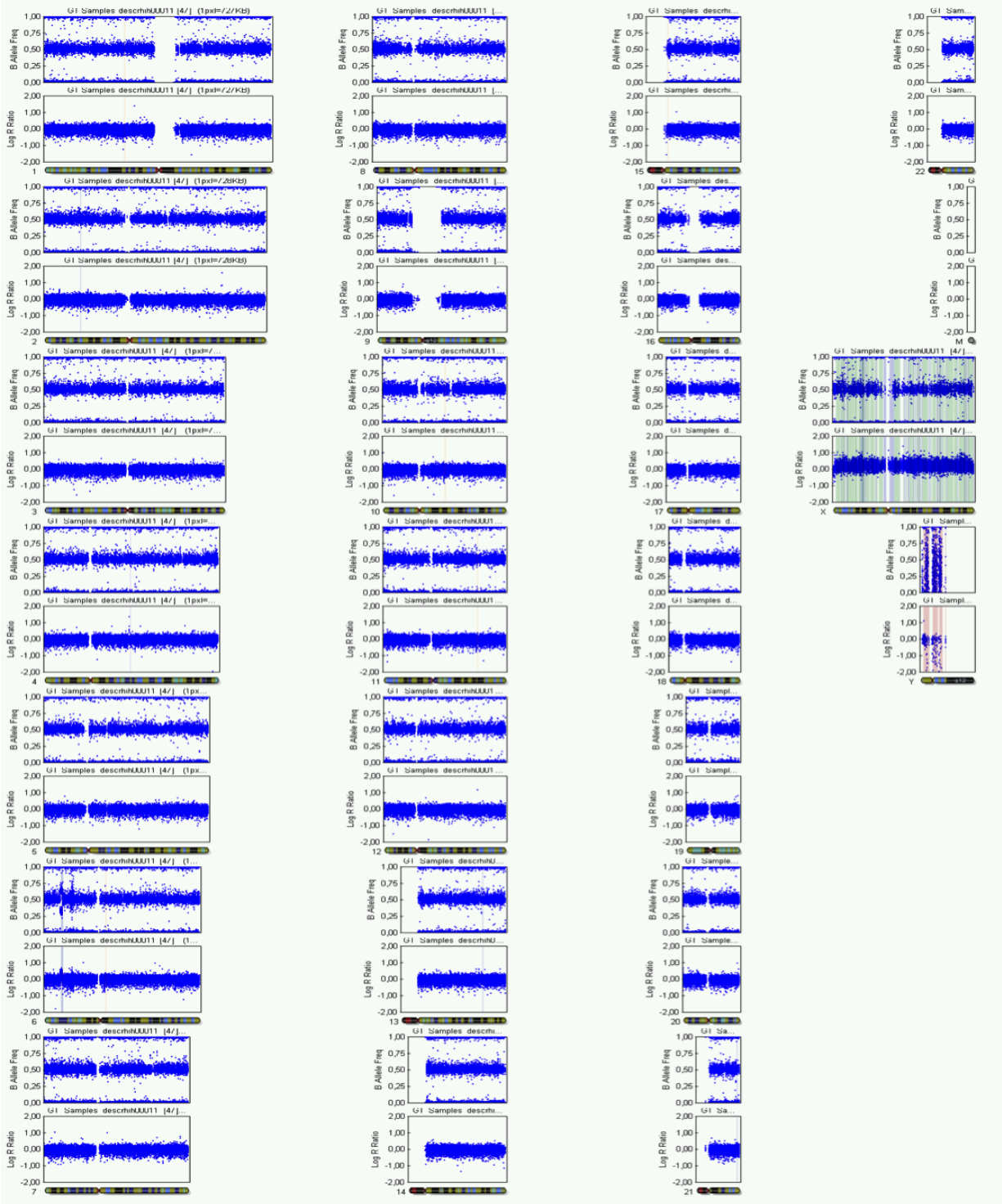

B

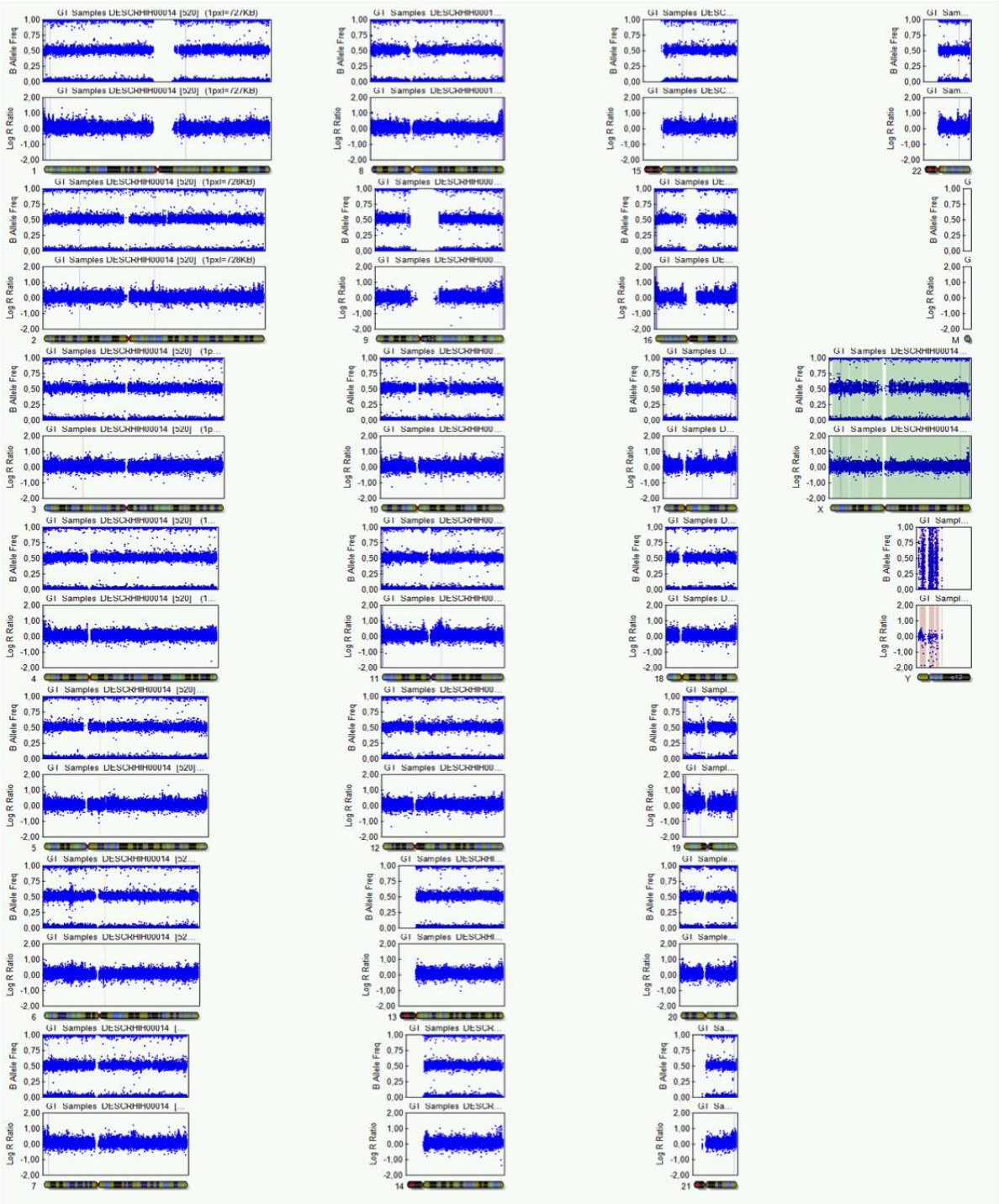

C

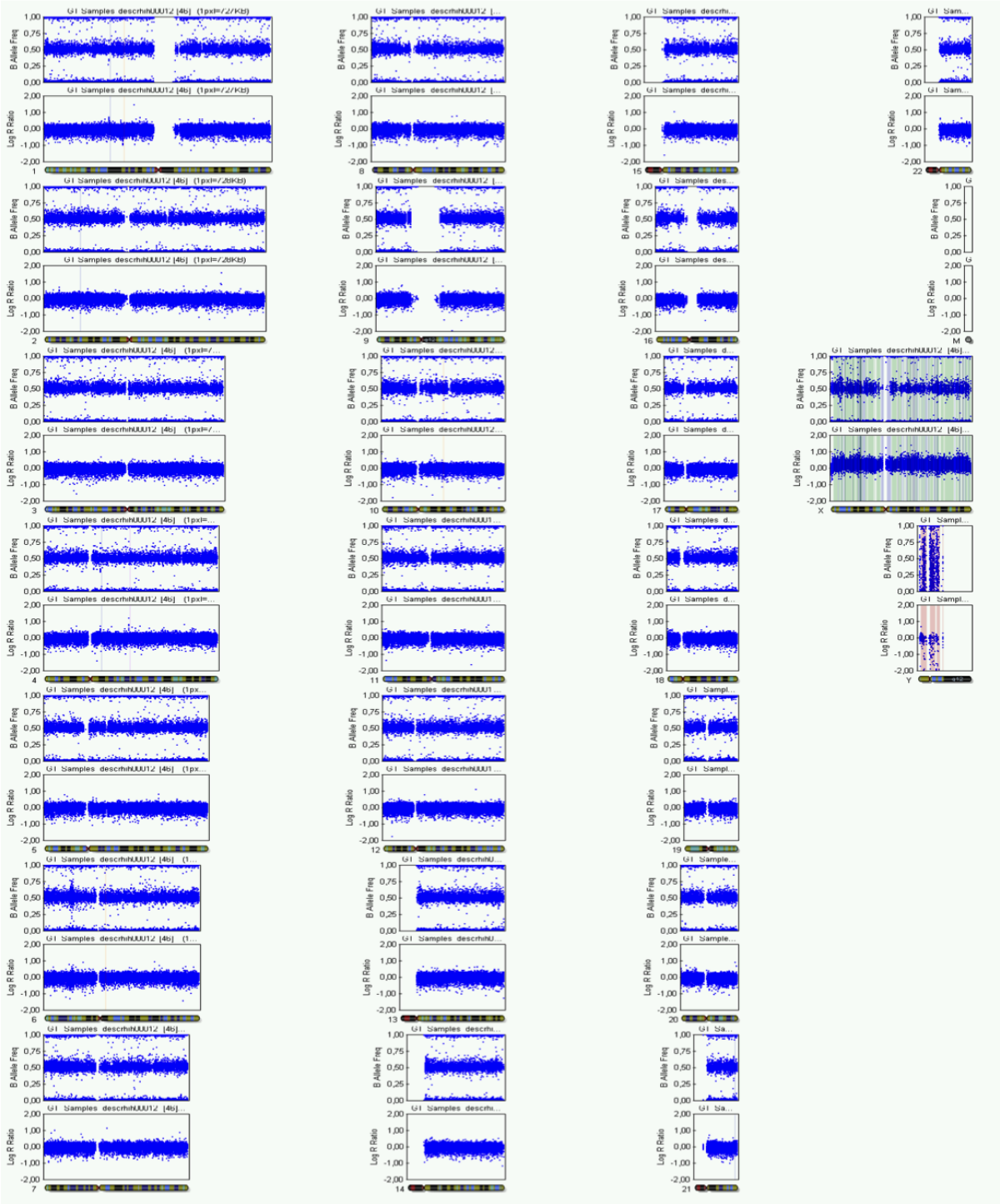

D

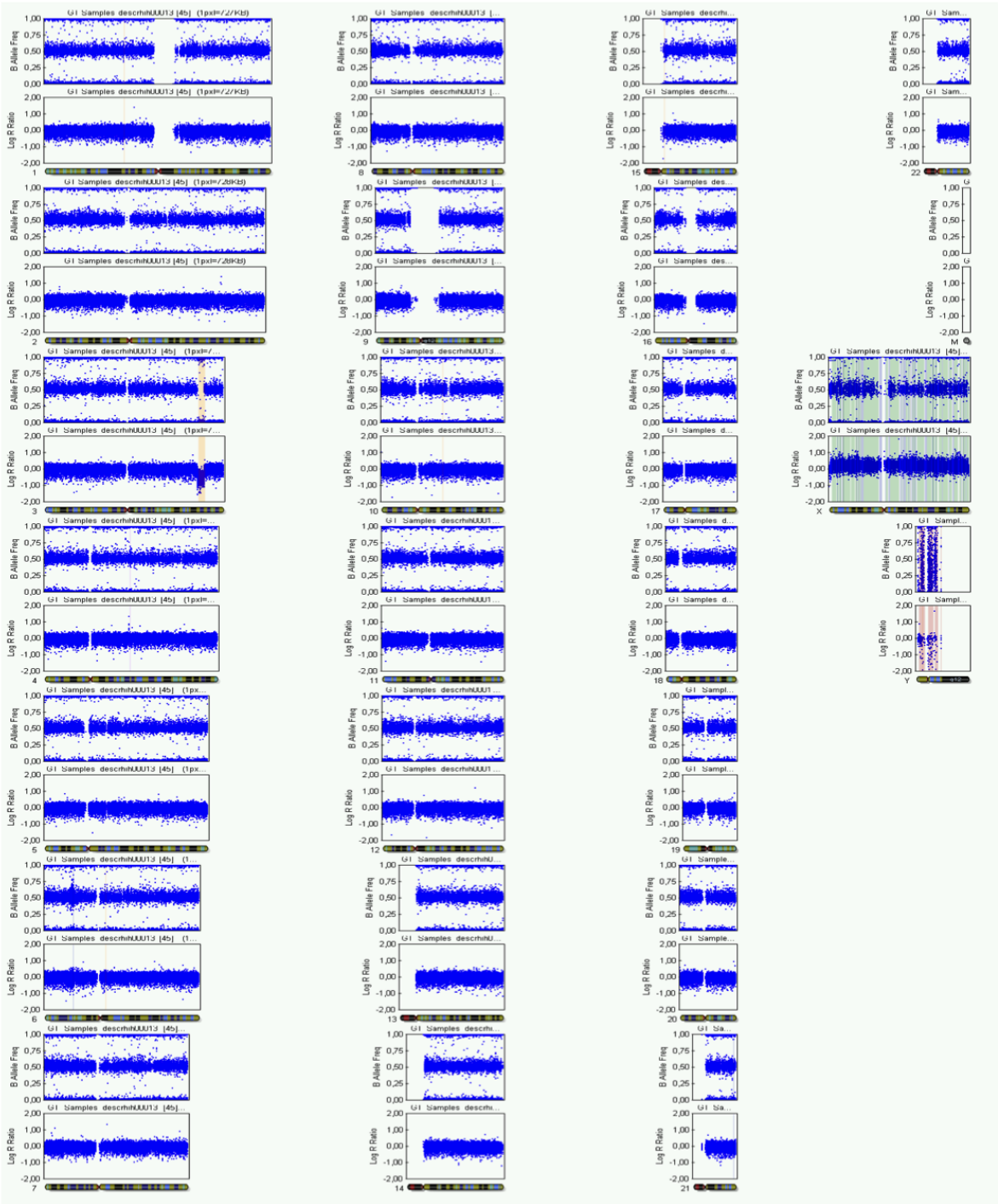

Fig. 45: Results from a DNA microarray screen (performed by Life&Brain GENOMICS, Bonn, Germany) testing for larger chromosomal aberrations in the four iPSC lines of the T489Yfs23X carrier. **A**: Results for the T489Yfs iPSC line #5.1. **B**: Results for the T489Yfs iPSC line #6. **C**: Results for the T489Yfs iPSC line #19. **D**: Results for the T489Yfs iPSC line #23.

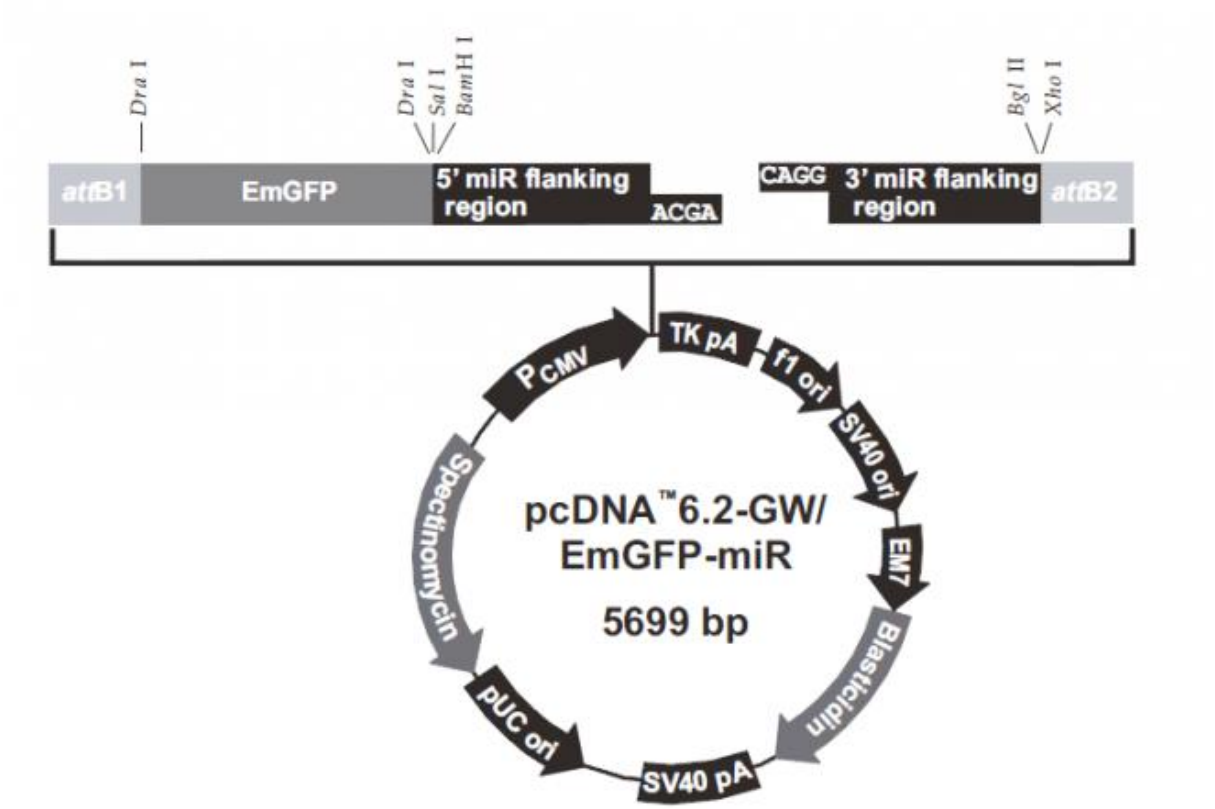

Fig. 46: Vector map of the pcDNA6.2-GW/EmGFP-miR expression vector used as an intermediate in the cloning of the inducible NHE6 miRNA constructs. The oligonucleotides containing the respective miRNA sequences were cloned in using the ACGA/CAGG overhangs between the 5‘ miR and 3‘ miR flanking regions. The EmGFP was later removed using DraI restriction sites, and *att*B1 and *att*B2 sites used to clone the EmGFP/miR sequence into the Tet-inducible pT-REx-DEST30 vector via an intermediate step.

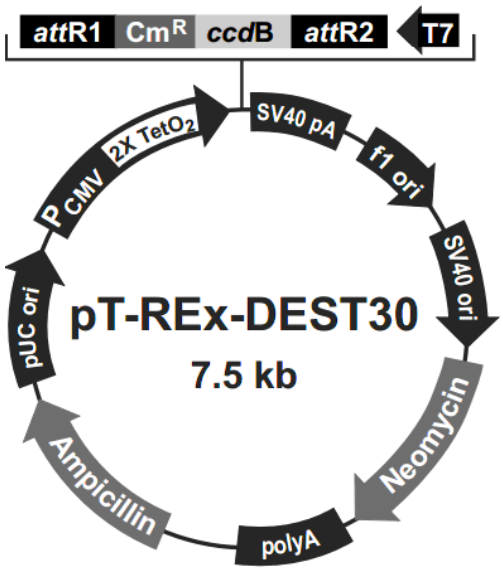

Fig. 47: Vector map of the pT-REx-DEST30 vector used for the generation of inducible NHE6 and control knockdown lines. The vector contains a cytomegalovirus (CMV) promoter with two Tet-repressor sites(2x$TetO_2$) in front of the miRNA sequence that is cloned in using the *att*R1 and *att*R2 cloning sites.

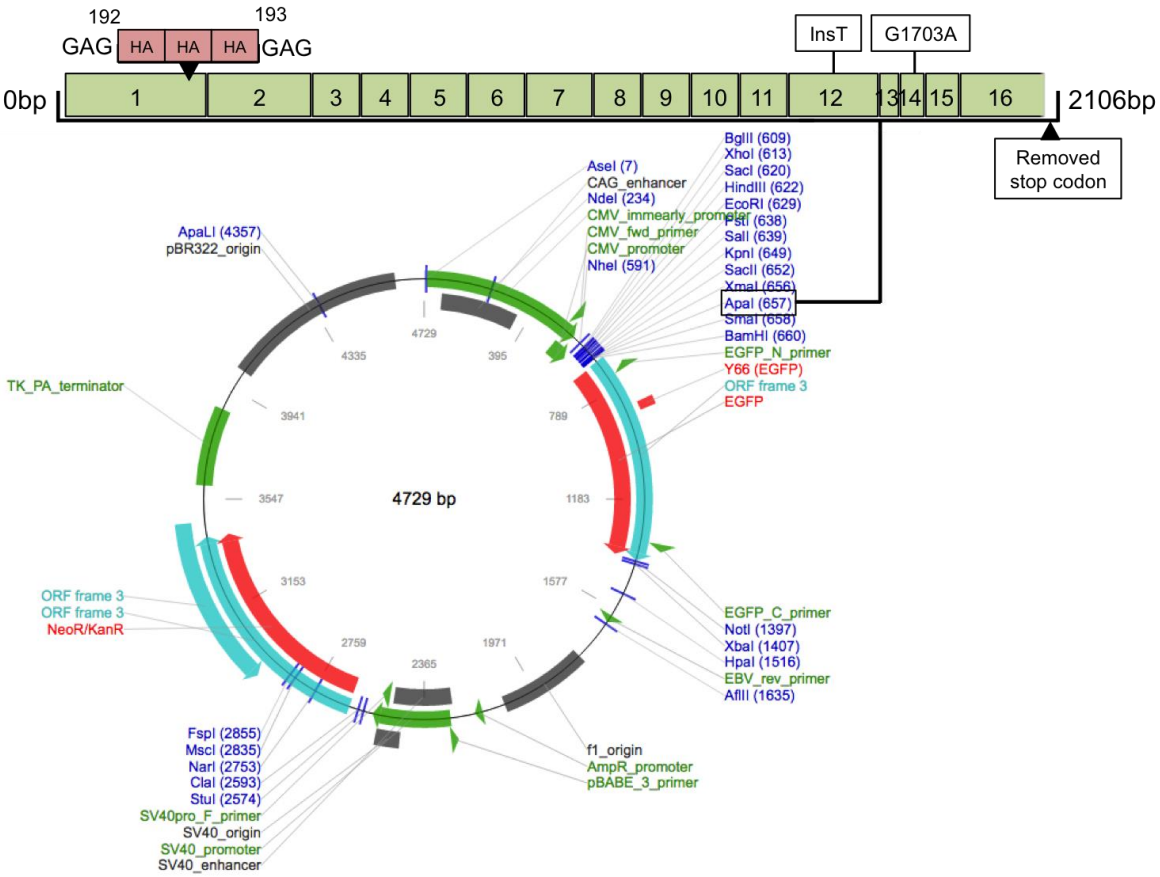

Fig. 48: Vector map of the pEGFP-N3 NHE6-HA expression vector. The ApaI restriction site was used to clone in the cDNA of the longest NHE6 isoform. An HA-tag was introduced in the first exon and the stop codon removed to allow for a EGFP fusion protein.

Source for the map of the pEGFP-N3 vector: https://www.addgene.org/vector-database/2493/

7.2 List of Figures and Tables

Figures

Tables

7.3 Abbreviations

3-MA: 3-methyladenine
3/4R: 3/4-repeat
Aβ: Amyloid β
AD: Alzheimer’s disease
ADHD: attention deficit hyperactivity disorder
AGD: argyrophilic grain disease
AMPAR: α-amino-3-hydroxy-5-methyl-4-isoxazolepropionic acid receptor
ALS: Amyotrophic lateral sclerosis
APP: amyloid precursor protein
Arp: actin-related protein
ARTAG: Aging-related tau astrogliopathy
Atg7: autophagy-related protein 7
BafA1: Bafilomycin A1
BDNF: brain-derived neurotrophic factor
BiP/GRP78: Binding immunoglobulin protein/78 kDa glucose-regulated protein
Bp: base pair
CBD: Corticobasal degeneration

CBP: CREB-binding protein

CBS: Corticobasal syndrome

CCCP: Carbonyl cyanide *m*-chlorophenyl hydrazone

Cdk5: Cyclin-dependent kinase 5

CHIP: C-terminus of HSC70-interacting protein

CD-MPR: cation-dependent mannose-6-phosphate receptor

CI-MPR: cation-independent mannose-6-phosphate receptor

ClC: Chloride channel

CMA: chaperone-mediated autophagy

CMV: cytomegalovirus

CSF: cerebrospinal fluid

DiHET: Dihydroethidium

DMEM: Dulbecco's Modified Eagle's Medium

DMSO: Dimethyl sulfoxide

DNA: Deoxyribonucleic acid

EEA1: early endosome antigen 1

EGF(-R): Endodermal growth factor (receptor)

ER: endoplasmic reticulum

ERAD: Endoplasmic-reticulum-associated protein degradation

ESCRT: endosomal sorting complex required for transport

ExAC: Exome Aggregation Consortium

FISH: fluorescence in situ hybridisation

FRET: Förster resonance energy transfer

FTDP-17: Frontotemporal dementia and parkinsonism linked to chromosome 17

FTLD: Frontotemporal lobar degeneration

GAPDH: Glyceraldehyde 3-phosphate dehydrogenase

GCase: β-Glucocerebrosidase

GDNF: Glial cell-derived neurotrophic factor

eGFP: enhanced green fluorescent protein

GLT-1: Glutamate transporter 1

GM2: monosialic ganglioside 2

GnomAD: Genome Aggregation Database

GSK3β: Glycogen synthase kinase 3 beta

GTP: guanosine triphosphate

GWAS: Genome-wide association study

HA: Haemaglutinin

HDAC6: Histone deactylase 6

HSP90: Heat shock protein 90

HSC70: Heat shock 70 kDa protein 8

ICC: immunocytochemistry

iPSC: induced pluripotent stem cells

IL: Interleukin

LAMP-2a: Lysosome-associated membrane protein type 2a

LCD: lysosome-mediated cell death

LDL(-R): low-density lipoprotein receptor

LDH: Lactate dehydrogenase

LMP: Lysosomal membrane permeabilisation

LRRK2: Leukine-rich repeat kinase

KIF13B: kinesin family member 13B

k.d.: knockdown

kDa: kilo Dalton

MAP1ALC3/LC3: Microtubule-associated proteins 1A/1B light chain 3A

MAPK: mitogen-activated protein kinase

MAPT: Microtubule-associated protein tau

MOBP: myelin-associated oligodendrocyte basic protein

MRI: Magnetic resonance imaging

MT: microtubule

MVB: multivesicular body

NBR1: neighbor of BRCA1 gene 1 protein

NFT: neurofibrillary tangles

NHE: Na^+/H^+ exchanger

NMD: Nonsense-mediated mRNA decay

NMDAR: *N*-Methyl-D-aspartate receptor

NPC: neuronal precursor cell

PAGE: Polyacrylamide gel electrophoresis

PCR: polymerase chain reaction

PD: Parkinson’s disease

PE: phosphatidylethanolamine

PiD: Pick’s disease

PI3P: phosphatidylinositol 3-phosphate

PI3K: Phosphatidylinositol 3-kinase

PINK1: Phosphatase and tensin homolog-induced putative kinase 1

PIP2: Phosphatidylinositol 4,5-bisphosphate

PHF: Paired helical filament

PKA: Protein kinase A

PKC: Protein kinase C

PM: Plasma membrane

PP2A: Protein phosphatase A

PP2B: Protein phosphatase B

PP2C: Protein phosphatase C

PS: Phosphatidylserine

PSP: Progressive supranuclear palsy

RACK1: Receptor for activated C kinase 1

RFP: red fluorescent protein

RIPA buffer: Radioimmunoprecipitation assay buffer

RNA: ribonucleic acid

mRNA: messenger RNA

miRNA: microRNA

ROS: reactive oxygen species

qRT-PCR: quantitative real time PCR

SDS: Sodium dodecyl sulfate

SLC9A6: solute carrier family 9 subfamily A member 6

SNARE: Soluble *N*-ethylmaleimide-sensitive factor Attachment Protein receptor

SNP: Single nucleotide polymorphism

SNX: sorting nexin

SOS1: Son of sevenless homolog 1

ssODN: single stranded donor oligonucleotide

STS: staurosporine

TDP-43: transactive response DNA binding protein 43kDa

Tet: Tetracycline

TGF-β: transforming growth factor β

TGN: Trans Golgi network

TFEB: Transcription factor EB

Tfn(-R): Transferrin (receptor)

mTOR(C1): mammalian target of rapamycin complex 1

Trk: tyrosine receptor kinase

UPS: Ubiquitin-proteasome system

UPR: unfolded protein response

VPS: Vacuolar sorting protein

WASH: Wiskott-Aldrich syndrome protein and Scar homologue

WIPI: WD-repeat protein interacting with phosphoinositides

WT: Wildtype

Acknowledgements

First of all, I would like to thank the patients and their families, as the work presented here would not have been possible without their cooperation.

I would also like to thank Dr. Julia Fitzgerald for her supervision and support, and for giving me guidance, but also freedom to explore and develop new ideas and approaches during my time with her. Also, I want to thank Prof. Dr. Rejko Krüger for his support and supervision and for keeping an overview over the work conducted. Furthermore, I would like to thank apl. Prof. Dr. Tassula Proikas-Cezanne for agreeing to examine the thesis.

I am also thankful to Prof. Dr. Olaf Rieß in Tübingen, and Prof. Dennis Dickson, Prof. Dr. Owen Ross and Prof. Zbigniew Wsolek in Florida who made valuable comments and provided access to the patients; Dr. Dajana Großmann and Brigitte Maurer for establishing the fibroblasts line of the T489Yfs patient, and Manuela Kübler cloned for cloning of the pcDNA3.1-TOPO constructs. Furthermore, I would like to thank Dr. Angelos Skodras for his help in taking the microscopy images for the LysoSensor experiment and for answering all questions regarding microscopy and image analysis, and in general his support.

Then, most importantly, the people from the Department of Neurodegeneration, for their great support during my time in the lab: Tine, Christine Bus, who not only helped me with everything iPSCs, NPCs and neurons, but also to have a fantastic time; Susanna Hoffmann, for your most valuable friendship; Silvia DeCicco for endless talks about life and science, and her invaluable support; Lukas Schwarz for cigarettes and wine, and his friendship; and Dr. David Schöndorf, Pascale Baden and Dr. Dina Ivanyuk; Richard Wüst and Kevin Schindler; Philipp Kahle, Sven Geissler and the cake club for all the great times (and cakes).

My friends who were so patient with me: Herr Erdbeer, Tytus, Kati, but especially Uwe, Uli and Torge. Without your support, I probaby would have quit somewhere along the line.

My parents, for all their support and for never giving up in trying to understand what I actually do, for their patience and understanding when I was too stressed out or busy or simply in my own world.

The world’s one and only Sebastian, Baschdl, der Herr Rodeit, for simply being there, and a friendship that can’t be described by words. May the triumvirate live forever.

Lastly, I want to thank my favourite human being Alex, Herr Fick: for his unwavering support, his endless patience and understanding for all my antics; for all the undeserved love and just being there, always.